Journal of Duhok University

Journal of
Duhok University

Pure and Engineering Sciences
Published biannual by Duhok University

Address:
Zakho Street 38
1006AJ
Kurdistan Region-Iraq
The Secretariat, JDU Editorial Board,

Mobile.: 00964 (0) 07508504928
www.jdu.uod.ac E-mail: jdu@uod.ac

UoD Printing Press

JOURNAL **O**F **D**UHOK **U**NIVERSITY

(Pure and **E**ngineering **S**ciences**)**

VOLUME 18 **DECEMBER**

NUMBER 1 2015

JOURNAL PAPER INSTRUCTIONS TO AUTHORS

General

The paper should be valuable and should not have been published or submitted for publication in any other Journals. The text should be complete with abstract, introduction, material and methods, results, discussion and reference. The text must not exceed 15 pages for sciences papers and 25 for the humanities

Content Text

The content text must be Normal, 10 pt., Times New Roman, at least 12 lines spaced, and justified. Each paragraph should be spaced after 6 pt. The first line of the paragraphs should not be indented.

Footnotes

Footnotes should not be used.

Page Margins

The paper size should be A-4 size and page margins must be 2.5 cm top and bottom, 3 cm left and 2 cm right.

Page Numbers

Include page numbers. The page numbers should be placed in the lower right hand corner.

Titles

The paper title must be capitalized, bold, centered, 11 pt., and spaced after 18 pt. Main titles and abstract title should be capitalized 9 pt., aligned left, bold, spaced before 12 pt., and after 6 pt., and numbered as (1., 2.,3.). Principle subtitles must be written in 10 pt, bold, aligned left.

Author(s)

The name(s) of the author(s) should be written only in the first page, capitalized, 8 pt, normal, centered, and spaced after 18 pt.
(See below).

ALI MUHAMMED1, JALAL AMEEN 2 and DLOVAN ASSAD 2

The authors' names should not cover all line and if there are more than, 3 or 4 writers the rest should be spaced to the line below, and writers also should be single spaced. The writers from the same department or the institution should be numbered by different numbers and indicated in the line below in 8 pt, as the following:

1 Department of Geography, College of Arts, University of Duhok, Kurdistan Region, Iraq
2 Department of Soil & Water Science, College of Agriculture, University of Duhok, Kurdistan Region, Iraq

Abstract

Abstract body should be 8 pt., bold, aligned left, and single spaced. The abstract must not exceed 300 words. (4-6) keywords must be provided at the end of abstract. The keywords title must be capitalized, 8 pt., aligned left, and Italic. The keywords should be written in 8 pt., Italic, and their initials should be capitalized. Paragraphs in the abstract should be spaced after 6. (See below)

KEYWORDS: *Erosivity factor, Rainfall, Fournier index, Water Quality*

Summary should be provided also in Kurdish and Arabic at the end of the paper.

Figures and Tables

Except the tables, all the graphs, maps and photographs must be named as figures. Tables and Figures should be numbered consecutively by Arabic numerals. The tables and figures must not exceed the page margins and must be on one page. All Table outline border should be (1 ½ pt.), inside border should be (½ pt.); table details should be Arial font and written with 7 pt. the figure and table names must be written with 8 pt. style. Names must be written in the middle on top for the tables with space 4 after and for the diagrams/figures, underneath on the bottom with space 4 before and 12 after. If the figure and table names have to be more than one line, the line spacing should be single spaced, and the terms of "Figures" and "Tables" must be bold. (See below)

Table (1): The effect of pepper shoot & root aqueous extract on the growth of different other plants:

	Shoot Extract					Root Extract				
Plant type	Conc. %	Root length (cm)	Shoot length (cm)	Intact plant length (cm)	Inhibition %	Conc. %	Root length (cm)	Shoot length (cm)	Intact plant length (cm)	Inhibition %
Okra	0	*25.7 a**	27.8 a	53.5a	-	0	25.7a	27.8a	53.5a	-
	5	25.00a	26.77a	51.77a	3.23	1	24.50a	27.00a	51.50a	3.73
	10	24.50a	25.95a	50.45a	5.70	2	23.87a	25.65a	49.52a	7.43
Sorghum	0	21.6a	27.2a	48.8a	-	0	21.7a	27.2a	48.9a	-
	5	13.00b	17.25b	30.25b	38.03	1	9.8b	25.5ab	35.3b	27.6
	10	6.00c	5.50c	11.50c	76.44	2	9.4b	22.6b	31.9 b	34.6

Figure (1): xxxxxxxxxxxxx

Bullets and Numbering

Bullets and numbers should be indented 1 cm from the left margin and hanging indent should be 0.5 cm. Each line of bullets and numbers should be single spaced.

References

References should be indicated in the typescript by giving the author's name, with the year of publication in parentheses, as detailed in the APA style guide. All lines after the first line of each entry in your reference list should be indented one cm from the left margin (hanging indentation). If several papers by the same author(s) and from the same year are cited, a, b, c, etc. should be put after the year of publication. The references should be listed in full at the end of the paper in standard APA format. For example:

For Books:

Ritter, D. F., Kochel, R. C., and Miller, J. R. (2002). Process Geomorphology (4th ed.). New York: McGraw-Hill.

Massey, W. R., and Jameson, W. M., Jr. (2001). Organizational behavior and the new internet logic (3rd ed.). New York: McGraw-Hill.

For articles:

- Harlow, H. F. (1983). Fundamentals for preparing psychology journal articles. *Journal of Comparative and Physiological Psychology*, 55, 893-896.
- Loughran, J., and Corrigan, D. (1995). Teaching portfolios: A strategy for developing learning and teaching in preservice education. *Teaching and Teacher Education*, 11, 565-577.

For chapters within books:

- Smith, N. (1997). Challenges and choices facing social studies teachers. In R. Case & P. Clark (Eds.), The Canadian anthology of social studies (pp. 3-9). Burnaby, BC: Simon Fraser University Field Relations.

For conference proceedings:

- Demirci, A., McAdams, M. A., Alagha, O., and Karakuyu, M. (2006). The relationship between land use change and water quality in Küçükçekmece Lake watershed. In A. Demirci, M. Karakuyu, and M. A. McAdams (Eds.). *Proceedings of 4th gis days in Türkiye* (pp. 27-35). Đstanbul, 13-16 September.
- Healey, M., Foote, K., and Hay, I. (2000). Developing the International Network for Learning and Teaching (INLT) *Geography in Higher Education. In: International Geographical Union Commission on Geographical Education* (Eds.). Geographical Education at the Cross-roads: Directions for the Next Millennium, Proceedings of the Kyongju Symposium (pp. 203-207), Korea.

For online documents:

- Standler, R. (2000). Plagiarism in colleges in the USA. Retrieved August 6, 2004, from www.rbs2.com/plag.htm
- Bernstein, M. (2002). 10 tips on writing the living Web. A List Apart: For People Who Make Websites, 149. Retrieved May 2, 2006, from http://www.alistapart.com/articles/writeliving
- Titles of journals and names of publishers, etc. should not be abbreviated. Acronyms for the names of organisations, examinations, etc. should be preceded by the title in full.

Note: Referred scientific materials such as: e-journals, e-books, etc. can be used as reference by authors.

For further information about APA reference style please visit http://owl.english.purdue.edu/owl/resource/560/01/

Submission

Four copies of the research paper with CD containing the paper in one file (Microsoft word 2003) should be submitted to the following address:

The Secretariat,
JDU Editorial Board,
Presidency of Dohuk University, Dohuk Governorate,
Kurdistan Region, Iraq.
Mobile: 07508504828
E-mail: jdu@uod.ac

CONTENTS

EFFECT OF POLYETHYLENE WASTE FIBERS ON STRENGTH OF CEMENT STABILIZED CLAYEY SOIL

ZUHEIR **M**. **S**ALIH. **A**LAFANDI
Dept.of Building and Construction,Duhok Technical Institute,Duhok Polytechnich University,Kurdistan Rrgion-Iraq

(Received: April 2, 2014 ; Accepted for publication: January 19, 2015)

ABSTRACT

This paper aims to study the possibility of using Polyethylene waste material (500 cc water bottle) in soil stabilization in form of fibers. Unconfined compressive strength (UCS) and Split tensile strength (STS) tests were carried out on natural and stabilized soils with three cement contents (3%, 6% and 9%) and three fiber contents (0.4%, 0.8% and 1.2%). In these tests, each fiber content percentage was added in three lengths ;1cm; 2cm and 3cm. The results showed that there is an optimum content of fiber which gives maximum (UCS or STS) strength. This optimum content depends on fiber length and cement content.

KEYWORDS: Soil stabilization, Soil reinforcement, Strength, Waste Material, Polyethylene, cement.

INTRODUCTION

Recently wide researches have been Performed to protect the environment. The use of waste materials in construction applications has many environmental benefits including costs saving in terms of their disposal and possible recyclability.

Waste materials such as fly ash, glass, plastics, blast furnace slag, rice husk ash, scrap tire rubber, waste iron powder, egg shells, and other pozzolanic materials have been used to improve the geotechnical characteristics of soils (Reddy et al,2001; Amu et al 2005; Alhassan,2008; Zha et al. 2008; Naeini et al. 2008; Al-Khashab et al. 2008; Okonkwo et al. 2012;Vaidyaet al.2009; Barazesh et al. 2012).

Naturally soils do not posses tensile strength. This is the reason for the need for improving the weakness of soil; researchers have done numerous attempts with augmenting elements like steel fibers, glass fibers, stainless steel, polymer textiles such as geotextile, geogrid and so on (Kalhor, 2008).

Fibers can be utilized for reinforcing soils either in continuous inserted forms (sheets woven or non woven geotextiles and strips) or as randomly orientated discrete inclusions. The first approach involves introducing oriented layers of planar sheets into soil. Whereas, in the second one, fibers are spread over the whole volume of the reinforced soil randomly by virtue of the mixing process (Mirzababaei et al. 2009).

Stabilized and reinforced soils are, in general a composite materials resulted from combination and optimization of the properties of individual constituent materials. Reinforcing of the subgrade soils or flexible pavements with short length fibers have evoked considerable interest for both highway engineers and manufacturers (Khattab et al. 2011). A number of researchers have studied the effect of using fibres in clayey soils experimentally (Kalhor, 2008; Naeini, et al. 2008; Naeini, et al. 2009; Al-Mhaidib, 2010; Chegenizadeh et al. 2012; Malekzadeh et al. 2012). Their results showed a significant improvement in soil properties after adding fibers.

The use of cement or lime with fibers for stabilization of clayey soils have attracted many researchers, such as (Limprasert, 1995 ;Kudo et al. 2001; DALL'AQUA et al. 2010; Ramesh et al. 2010; Khattab et al. 2011). Most of these researchers have studied the compressive and tensile strengths behavior of the fiber-reinforced soil-cement mixtures. Their results showed that using fibers increases the tensile strength and durability of the soils, and decreases crack appearance.

Waste fiber materials were used by some researchers for soil stabilization. Naeini et al. (2008) used polymer waste fiber material that obtained from scrap rubber tires, and added randomly to stabilize clayey soil with different

percentages. The results showed a clear significant improvement in the shear strength parameters (C and Ø) of the treated soils. Mirzababaei et al. (2009) investigated the effect of four types surplus carpet fibers on the strength and other geotechnical properties of cohesive soils. They found that the results varied widely depending on fiber type. Muntohar, (2009) studied the strength of the stabilized clay-soil reinforced with randomly distributed discrete plastic waste fibers by conducting unconfined compressive strength and tensile-split strength tests. His results showed that inclusion of the plastic waste fiber increases significantly both the unconfined compressive strength and tensile-split strength of the stabilized clay soil.

Polyethylene products are major components of waste materials in Iraq today. Since, more than 5000 ton per year of Polyethylene (500 cm³ bottle capacity) become waste material in Duhok city only (Hanna et al.2012). Therefore, this study is an attempt to examine the possibility of using these waste materials for improving the compressive and tensile soil strength. The study also includes the influence of length and amount of fibers which added as randomly oriented in cement stabilized and unstabilized clayey soils.

EXPERIMENTAL PROGRAM

The experimental program includes determination of index properties of soil, grain size analysis and standard proctor compaction tests on cement stabilized and unstabilized soil. Three percentages of cement were used (3%, 6% and 9%) of dry weight of soil. Three sizes of fibers (1cm, 2cm and 3cm) in length were added to unstabilized and stabilized clayey soil in three contents (0.4%, 0.8% and 1.2%) of dry weight of the soil. Twenty four (unreinforced) and two hundred and sixteen (reinforced) cylindrical samples were prepared of 50 mm in dia. and 100 mm height after then the unconfined compressive (UCS) and split tensile strength (STS) were found as shown in Table 1.

MATERIALS

1. SOIL

The soil used in this study was obtained from Etit area in Duhok city, North of Iraq. Some of the Physical properties of the soil are listed in Table 2. The tests were done according to the ASTM standards.

2. CEMENT

Turkish ordinary portland cement was used in the preparation of stabilized soils samples.

3. FIBERS

Polyethylene (500 ml capacity bottle) as a waste material was used in the form of fiber. Fibers were prepared by cutting waste bottles into three sizes in length (1 cm, 2 cm and 3 cm) and each of 2.5 to 3 mm in width as shown in Fig.(1).

Table (1): Test programme for UCS and STS

% of Fiber			Unconfined Compressive Strength(UCS)				Split Tensile Strength(STS)			
			% of Cement				% of Cement			
0 %			0 %	3 %	6 %	9 %	0 %	3 %	6 %	9 %
0.4%	Fiber Length (cm)	1	0 %	3 %	6 %	9 %	0 %	3 %	6 %	9 %
		2	0 %	3 %	6 %	9 %	0 %	3 %	6 %	9 %
		3	0 %	3 %	6 %	9 %	0 %	3 %	6 %	9 %
0.8%	Fiber Length (	1	0 %	3 %	6 %	9 %	0 %	3 %	6 %	9 %
		2	0 %	3 %	6 %	9 %	0 %	3 %	6 %	9 %

		3	0 %	3 %	6 %	9 %	0 %	3 %	6 %	9 %
1.2%	Fiber Length (cm)	1	0 %	3 %	6 %	9 %	0 %	3 %	6 %	9 %
		2	0 %	3 %	6 %	9 %	0 %	3 %	6 %	9 %
		3	0 %	3 %	6 %	9 %	0 %	3 %	6 %	9 %

Note: 3 samples were tested for each variable

Table (2): Physical properties of Natural soil

Liquid limit (%)	Plastic limit (%)	Plasticity index (%)	Specific Gravity Gs	Gravel (%)	Sand (%)	Silt (%)	Clay (%)	Soil Classification according to USCS
51	26	25	2.72	----	9	44	47	(CH)

Fig. (1): Fibers used in the study.

SEPECIMEN PREPERATION

Soil samples were prepared and compacted according to ASTM D- 698 for natural soil and ASTM D-558 for soil-cement mixture. The procedure used was for standard compaction method. Cement amounts of (3,6 and 9%) were used to stabilize soil. The required amount of water was added after mixing the cement with soil. The mixture was then placed in plastic bags for absorption period of (24) hours for natural soil and (10) minutes for cement stabilized soil. The mixtures were then compacted in the mould. To prepare the samples for testing unconfined compressive strength and split tensile strength a special mould was used (50 mm in dia. ,100 mm height) by compacting the soil in three layers using special hammer weighing (1452 gm) and falling from (340 mm) to obtain standard compaction energy of 593 kN-m/m^3 after (8 blows) for each layer. All samples were prepared at optimum moister (OMC) and maximum dry density (MDD) for stabilized and unstabilized soil. To obtain reinforced soil samples (stabilized or unstabilized), the fibers were added in three sizes (1,2 and 3 cm) and each size was in three percentages (0.4%,0.8% and 1.2%) of dry weight of soil.

STRENGTH TESTS

The unconfined compressive strength (UCS) and the splitting tensile strength (STS) tests were conducted on cylindrical specimens of 50 mm x 100 mm size in accordance with ASTM D-2166 and ASTM C496, respectively (see Figs. (2 and 3)). The splitting tensile strength (STS) is calculated according to the following equation:

$STS = 2p_{max}/(\pi*D*L)$ ……...…..(1)

where, P_{max} is the applied maximum load, L and D are the length and diameter of the specimen respectively. The prepared samples treated with cement, for both strength tests were sealed with aluminum foil, plastic bags and finally by paraffin to cure for the curing time (7) days at a temperature of 25 C^0.

Fig. (2): Conducting UCS on Samples.

Fig. (3): Conducting STS on Samples.

RESULTS AND DISCUSSION

Dry Density – Moisture Content Of Natural Soil And Soil Cement Mixture:

It can be observed from Fig.(4) that MDD of soil decreased from 1.57 to 1.55 (gm/cm^3) because of dissipating some of compaction efforts to broke the early cementing bonds created during the mellowing time (10min.). Also it can be noted that OMC increases with the addition of cement from 21% to 26.5% due to the addition of more fine materials, and/or to the hydration of cement (Khattab et al. 2011).

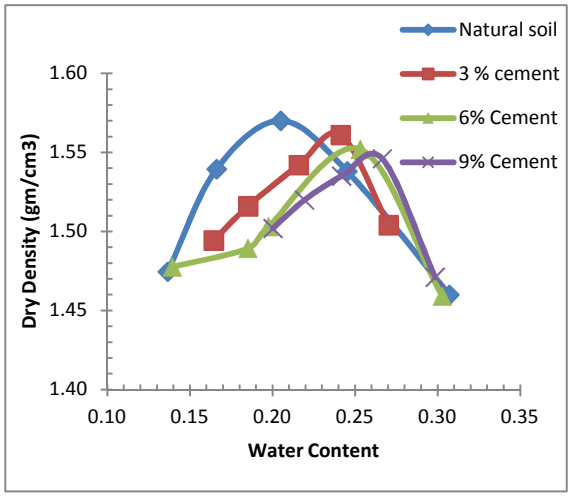

Fig. (4): Compaction Characteristics of soil- cement mixture.

1. Strength Of Natural And Stabilized Soil

Fig.(5) shows the results of unconfined compressive strength (UCS) and split tensile strength (STS) for natural and stabilized soil with cement. All values were obtained at maximum dry density (MDD) and optimum moisture content (OMC) in standard compaction method.

The values of UCS were (115.69, 487.82, 1153 and 1569.14) kPa while the STS values were (22.95, 80.34, 190.03 and 258.77) kPa both for (0%, 3%, 6% and 9%) cement content respectively.

It can be seen that there is a continuously increase in the strengths (UCS and STS) with the addition of cement**.**

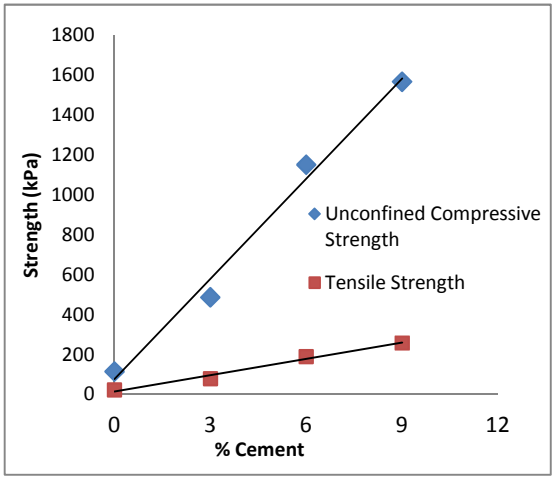

Fig. (5): Strength-Cement relationship.

3.Effect Of Fiber Length And Content On Strength Of Soil

Table (3) and Figs. (6 and 7) show the results of unconfined compressive and split tensile strengths for different cement content, fiber length and fiber amount. The unconfined compressive and tensile strengths of unreinforced soil samples were used as reference sample for comparison with different stabilized and unstabilized fibrous soil samples.

The values of strengths shown in Figs. (6 and 7) are plotted against the length of fiber for different fiber contents (0.4%, 0.8% and 1.2%) for cement contents (0%, 3%, 6% and 9%). Also, the strengths are plotted against fiber content for different fiber length (1cm, 2cm and 3cm) for each cement contents. In Figs. (6 and 7), the right hand scale represents the percentages of improvement in strength (UCS or STS).

The data in these figures and table indicated that the values of strength (UCS or STS) are increased until a specific length and then decreased. The optimum length for UCS was (2cm) for (0%,3% and 6%) cement content (see Fig.6 (a, c, e)) and (1cm) for 9% cement content (see Fig. 6g). While the optimum length for STS was (1cm) for all percentages of cement.

The influence of fiber amount on UCS and STS is shown in Figs. (6 and 7). The optimum fiber content, for UCS was 0.4% for (0% and 3%) cement content and 0.8% for (6% and 9%) cement content. For STS the optimum content was 0.8% for natural soil (0% cement content) and 0.4% for (3%, 6% and 9%) of cement content.

The UCS values at optimum fiber content as mentioned above, are increased from (115.69, 487.82, 1153, 1569.14) kPa to (220.87, 696.09, 1633.34, 2305.8) kPa causing an improvement of (90.9%, 42.69%, 41.66% , 46.94%) for cement content (0%, 3%, 6% and 9%) respectively. Whereas, the STS at optimum fiber content, are values increased from (22.95, 80.34, 190.02, 258.77) kPa to (38.88, 95.99, 229.54, 318.25) kPa with improvement of (69.38%, 19.48%, 20.79%, 22.98%) for cement content (0%, 3%, 6% and 9%) respectively.

These results are mainly due to the combined effect of cement and fiber contents. However, the addition of fiber is found to be more efficient in compressive strength than split tensile strength, and in unstabilized soil than stabilized soil.

It is observed that at small fiber contents, the (UCS) and (STS) strength were increased (Figs. (6 and 7)) because of some of the applied load is transferred from soil skeleton to fiber through the friction interface between soil-fibers system, leading to increase the strength in all cases up to certain limit. Then adding fibers above this limit causes a separation in clay particles and a formation of slippage planes which in turn reduces the strength (Naeini, et al. 2008).

As fiber content, the fiber length increases through the (UCS) and (STS) strengths (Figs. (6 and 7)) also increase up to peak value related to the force needed to pull out fibers. After that, when the length is increased from this limit, it is difficult to distribute in soil causing weak planes and leading to reduction in strengths (Muntohar, 2009).

Table (3): Results of strengths for the natural and reinforced soils.

% of Fiber		Unconfined Compressive Strength (kPa)				Split Tensile Strength (kPa)			
		% of Cement				**% of Cement**			
		0 %	3 %	6 %	9 %	0 %	3 %	6 %	9 %
0 %		115.69	487.82	1153	1569.14	22.95	80.34	190.02	258.77
0.4%	Fiber Length (cm) 1	196.78	574.66	1365.99	1997.74	37.56	95.99	229.54	318.25
	2	220.87	696.09	1460.53	1901.20	34.43	88.97	222.40	293.20
	3	206.40	556.70	1385.08	1819.75	32.86	87.74	215.32	303.64
0.8%	Fiber Length (cm) 1	189.97	495.73	1481.57	2305.80	38.88	91.04	204.56	295.29
	2	203.50	630.25	1633.34	2267.89	37.56	82.59	192.34	277.85
	3	173.75	432.87	1496.03	2207.33	37.04	80.59	189.31	280.06
1.2%	Fiber Length (cm) 1	188.81	508.64	1334.23	1965.13	38.01	88.53	203.45	298.42
	2	208.01	648.79	1412.26	1928.36	37.56	80.35	188.37	274.42
	3	173.08	448.77	1295.82	1903.77	36.76	81.16	186.73	280.04

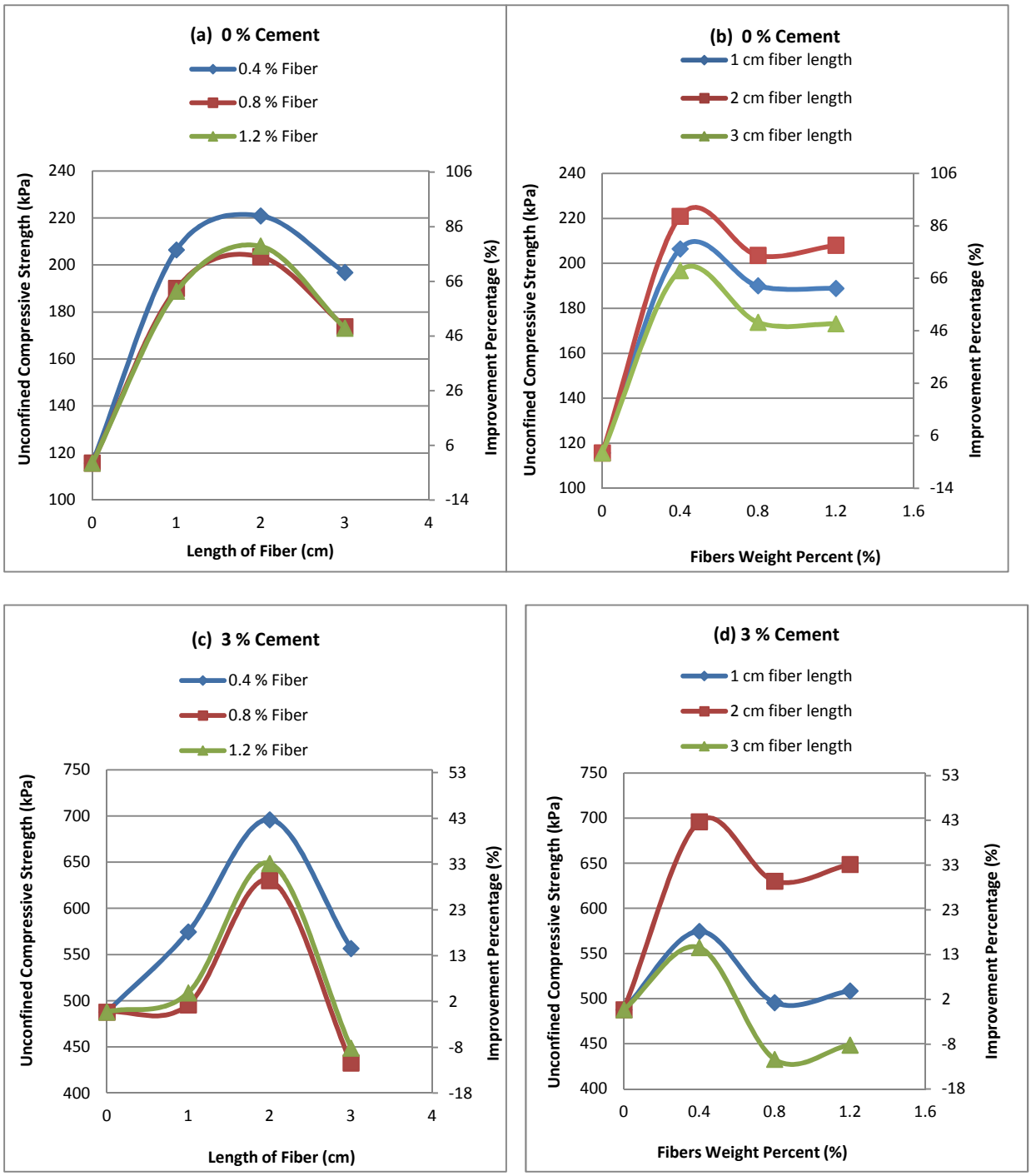

Fig.6 (a-b-c-d): Results of UCS for natural and stabilized reinforced soil.

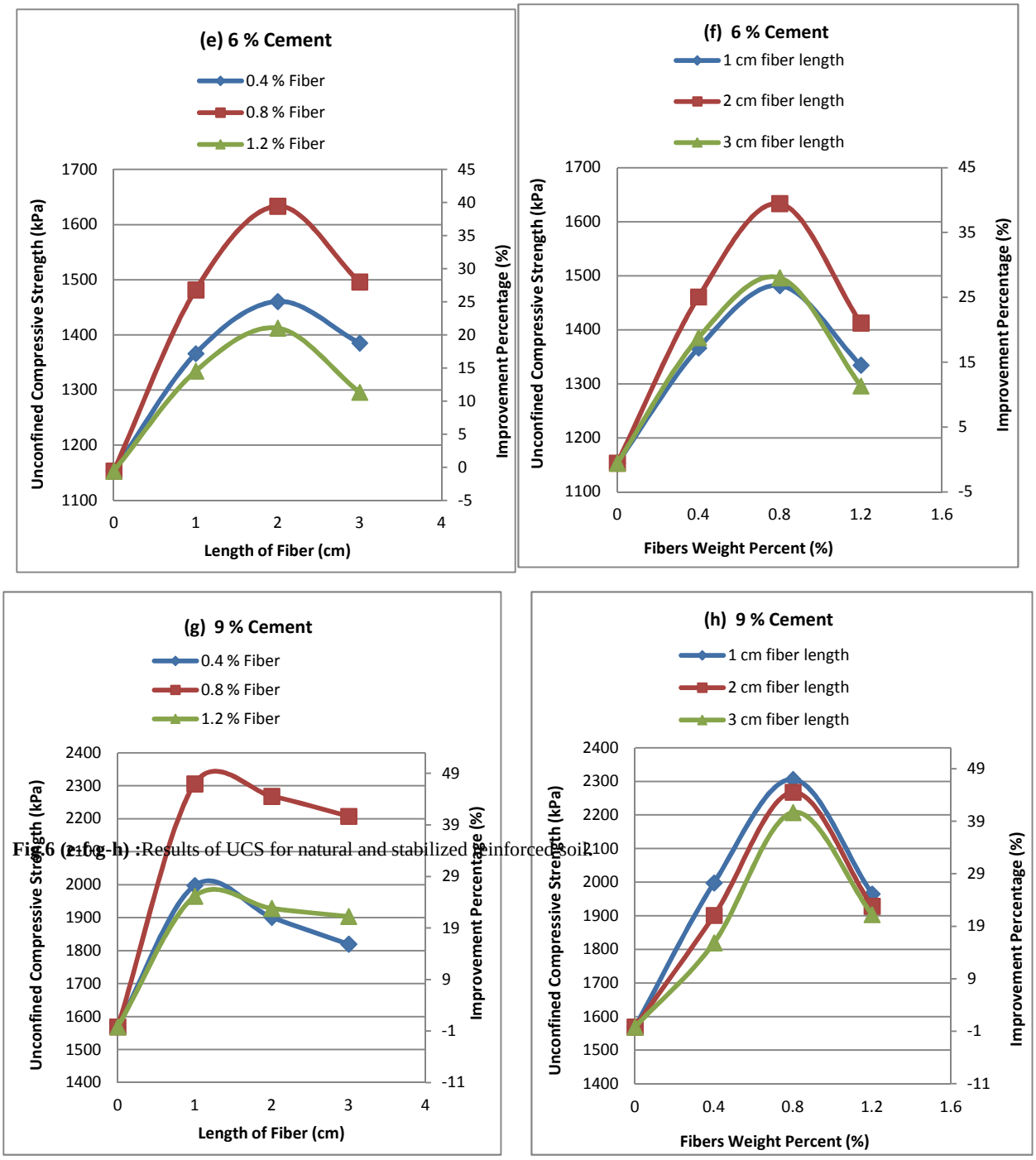

Fig.6 (e-f-g-h) : Results of UCS for natural and stabilized reinforced soil.

Fig.7 (e-f-g-h): Results of STS for natural and stabilized reinforced soil.

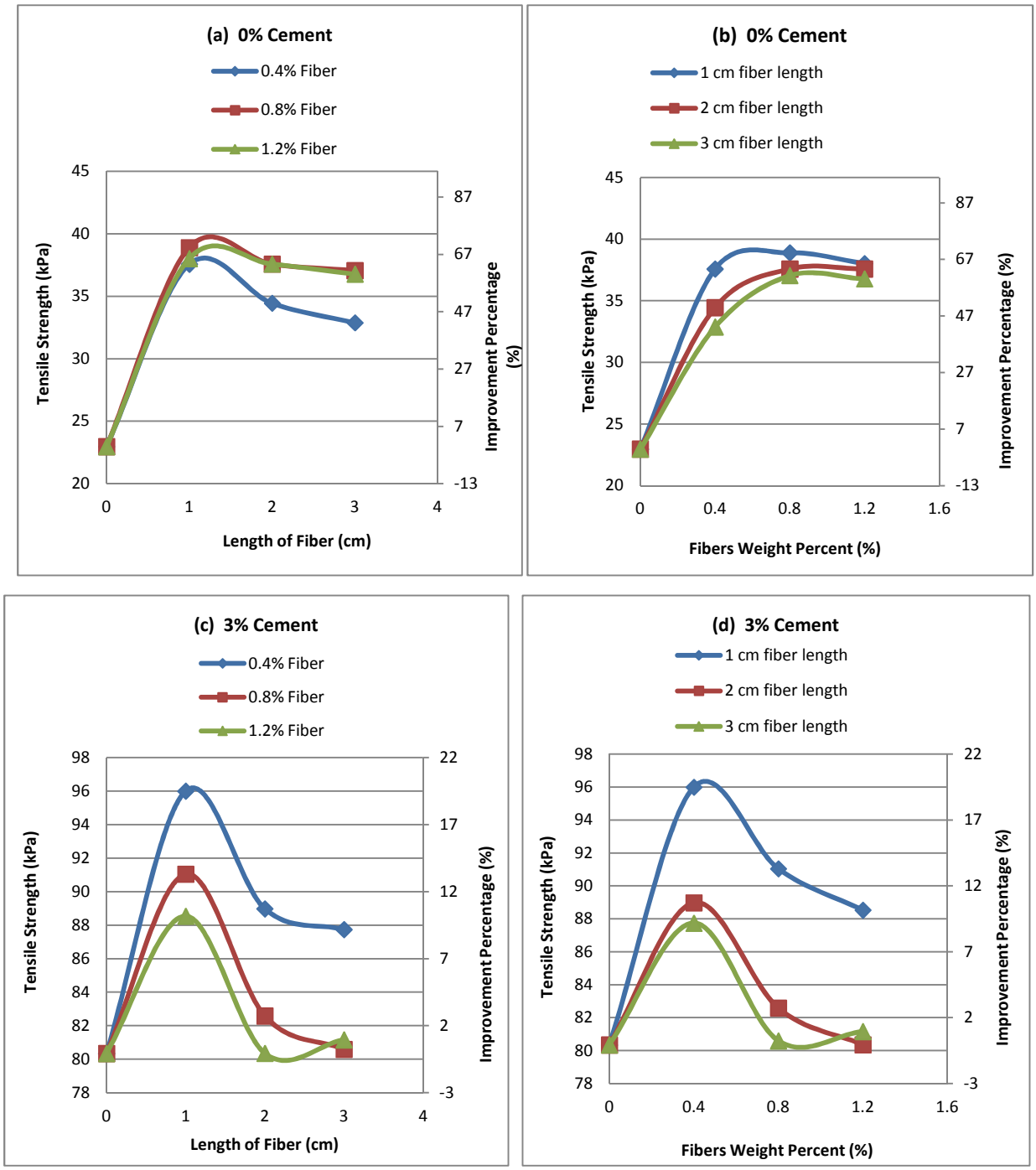

Fig. 7 (a-b-c-d) : Results of STS for natural and stabilized reinforced soil.

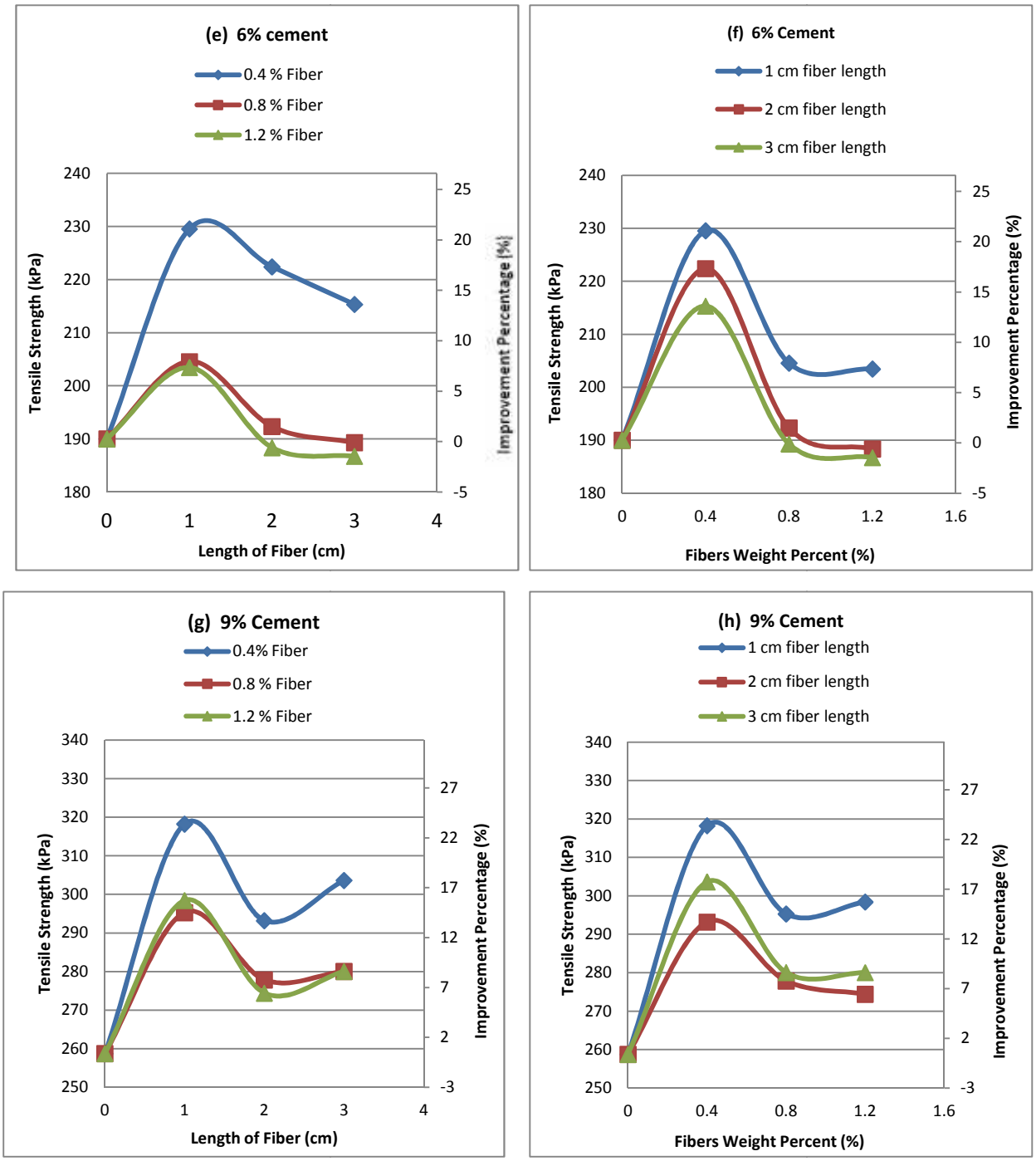

Fig.7 (e-f-g-h): Results of STS for natural and stabilized reinforced soil.

CONCLUSIONS

According to the laboratory results of this limited study, the following conclusions can be drawn:

1- The maximum dry density (γ_{dmax}) decreases and Optimum moisture content (OMC) of clayey soil increases with increasing cement content.

2- Adding cement to clayey soil increases the compressive and tensile strengths, and the improvement is proportional to the cement content up to a certain limit.

3- Reinforcing soil (Natural or stabilized soil) with polyethylene fibers is found to improve compressive strength till an optimum content which is 0.4% for 0% and 3% cement contents;

0.8% for 6% and 9% cement contents . For tensile strength, the optimum fiber content is 0.8% for natural soil and 0.4% for stabilized soil. Then after, adding more fibers decrease the compressive and tensile strengths. In compressive strength , a fiber length of 2 cm was found to be beneficial for 0% , 3% and 6% cement, whereas, 1 cm length was efficient for 9% cement content. In addition to, 1cm length of fiber is sufficient enough to reach maximum tensile strength for natural and stabilized soil.

4- Fiber addition is more effective in natural soil than stabilized soil for both compressive and tensile strength, and the efficiency of fiber addition in Compressive strength is more evident than the tensile strength.

REFERENCES

-Alhassan M.,(2008)" Potentials of Rice Husk Ash for Soil Stabilization", AU J.T. 11(4): 246-250.

-Al-Khashab, Mohammad Natheer,.and Al-Hayalee, Mohammed Thafer,(2008)," Treatment of Expansive Clayey Soil with Crushed Limestone Engineering & Technology Journal,Vol.26, Issue 3, pp. 376-386

-Al-Mhaidib A. I.,(2010)," Effects of Fiber on Swell of Expansive Soils", Proceedings of the Twentieth International Offshore and Polar Engineering Conference Beijing, China, June 20-25, 2010, pp. 663-669.

-Amu O. O., Fajobi A. B. and Oke B.,O.,(2005)" Effect of Eggshell Powder on the Stabilizing Potential of Lime on an Expansive Clay Soil", Research Journal of Agriculture and Biological Sciences 1(1): 80-84.

-Barazesh A., Saba H., and Gharib M.,(2012)," The Effect Of Adding Iron Powder On Atterberg Limits Of Clay Soils", International Research Journal of Applied and Basic Sciences, Vol, 3 (11): 2349-2354.

-Chegenizadeh A., Nikraz H.,(2012)" Laboratory Evaluation of Fibre-Composite ", International Journal of Science and Engineering Investigations vol. 1, issue 9, pp. 69-72.

-Dall'aqua G.P,(2010), Ghataora G.S. and Ling U.K.," Behaviour of Fibre-Reinforced and Stabilized Clayey Soils Subjected to Cyclic Loading",StudiaGeotechnica et Mechanica, Vol. XXXII, No. 3, pp. **3-16.**

-FushengZha. SongyuLiu .Yanjun Du and KeruiCui(2008)," Behavior of expansive soils stabilized with fly ash", Nat Hazards (2008) 47:509–523

-Kalhor A.,(2008)," Effect of Metal Fibers on Clayey Soils", EJGE, Vol. 13,Bund.K

-Khattab S. A., Al-Kiki I. M., and Al-Zubaydi A. H.,(2011)" Effect of Fibers on Some Engineering Properties of Cement and Lime Stabilized Soils",Eng.& Tech. Journal, Vol.29, No.5, 2011, pp. 886-905.

-Kudo M., Ochiai H., and Omine K., (2001),"Mechanical properties in short-fibers mixture stabilized volcanic cohesive soil", Lanmarks in Earth Reinforcement, Ochiai et al(eds), Swetz & Zeitlinger , ISBN 90 2651 852 B, pp. 73-76.

-Limprasert T.,(1995)," Behavior of Soil , Soil-Cement, and Soil-Cement-Fiber Under Multiaxial Test" M.Sc. Thesis, Ohio University, Athens, Ohio

-Malekzadeh M., and Bilsel H., (2012)"Swell And Compressibility of Fiber Reinforced Expansive Soils", International Journal of Advanced Technology in Civil Engineering, ISSN: 2231 – 5721, Volume-1, Issue-2, pp. 42-46.

-Mirzababaei M., Miraftab M., McMahon P. and Mohamed M. (2009)," Undrained Behaviour of Clay Reinforced with Surplus Carpet Fibres", proceeding of the second International Symposium on Fibre Recycling, May 2009, Atlanta, Georgia, U.S.A .

-Muntohar, A. S.,(2009)," Influence of Plastic Waste Fibers on the Strength of Lime-Rice Husk Ash Stabilized Clay Soil", Civil Engineering Dimension, Vol. 11, No. 1, 32-40.

-Naeini S. A. and Sadjadi S. M.,(2008)," Effect of Waste Polymer Materials on Shear Strength of Unsaturated Clays", EJGE, Vol. 13,Bund.K

-Naeini S. A., Moayed R. Z.,(2009)," Effect of Plasticity Index and Reinforcement on the CBR Value of Soft Clay", International Journal of Civil Engineering. Vol. 7, No. 2, pp. 124-130.**1**

-Okonkwo, U. N., Odiong, I. C., and Akpabio, E. E.,(2012)" The Effects of Eggshell Ash on Strength Properties of Cement-Stabilized Lateritic", International Journal of Sustainable Construction Engineering & Technology (ISSN: 2180-3242) Vol 3, Issue 1, pp. 18-25.

-Ramesh H.N., Krishna K.V. and Mamatha H.V.,(2010)," Compaction and strength behavior of lime-coir fiber treated Black Cotton soil", Geomechanics and Engineering, Vol. 2, No. 1 ,19-28.

-Reddy K. R. and Marella A.,(2001) " Properties of Different Size Scrap Tire Shreds: Implication on Using as Drainage Material in Landfill Cover System", The Seventeenth International Conference on Solid Waste Technology and Management, October 2001, Philadelphia, PA, USA.

-Thamer H. Hanna and Ismail H. Mosa,(2012)" Effect of Using Waste Polyethylene Production on Mechanical Properties of Concrete", J. Duhok Univ,Vol.15, No.1, pp. 37-46.

-Vaidya M.K., Chore H.S, Kousitha P., Ukrande S.K. (2009)" Geotechnical Characterization Cement - Fly Ash –Fiber Mix", Second International Conference on Emerging Trends in Engineering (SICETE), 16th to 18th December 2009 Nagpur, Maharashtra, India ISSN: 2278-1684, PP: 60-66.

كارتێكرنا ريشالێن بەرملیكێن پولی ئەسیلین ل سەر بەرگریا ئاخا چەسپاندی ب چیمەنتوین

پوختە

ئارمانجا ڤێ توێژینێ ڤەكولینا شیانێن بكارئینانا بەرمایكێن پولی ئەسیلین (بولی اپیلین) (بوتلێن ئاڤا ڤەخارنێ 500 مللم) بشێوێ رشالان بو چەسپاندنا ئاخێ. تێستا پەسارا نەدورپێچكری (UCS) و تێستا كێشانا ژێكڤەبوونێ (STS) بو ئاخا سروشتی و یا چەسپاندی ب چیمەنتوین ب رێژەیێن (3%, 6%,9%) هاتنە ئەنجام دان ژبو دیاركرنا كارتێكرنا ریشالان. تێستێن پەسار و كێشان بو نموونێن ئاخا چەسپاندی و نە چەسپاندی ب ریشالا ب رێژەیێن (0.4% , 0.8% , 1.2%) هاتنە ئەنجام دان, و هەر رێژەكا ڤان ریشالان كریە دناڤ ئاخێ دا ب درێژاهیێن جودا (1, 2, 3)سم بین. ئەنجاما دیاركرن كو زێدەكرنا ڤان جورە ریشالان ب رێژەكا دیاركری دبیتە ئەگەرێ زێدەبوونا بەرگریا (پەساریان كێشان) و ئەڤ رێژا دیاركری پەستێ ل سەر درێژیا ریشالان و رێژەیا چیمەنتوین دكەت.

تأثير الياف مخلفات البولي اثيلين على مقاومة التربة الطينية المثبتة بالاسمنت

الخلاصة

يهدف هذا البحث إلى دراسة إمكانية استخدام مخلفات البولي اثيلين (قناني الماء 500 ملل) على شكل الياف في تثبيت التربة. تم اجراء فحص الانضغاط الغير المحصور(UCS) وفحص الشد ألانفلاقي(STS) للتربة الطبيعية والتربة المثبتة بالاسمنت بثلاث نسب (3% و6% و9%).لبيان مدى تأثير الالياف, تم اجراء فحصي الانضغاط والشد على نماذج التربة المثبتة والغير المثبتة وبمحتوى الياف مختلفة (0.4% و0.8% و1.2%) ,وكل نسبة من الالياف تم اضافتها بثلاثة اطوال (1 و2 و3) سم.بينت النتائج بان هناك محتوى امثل من الالياف باضافتها يتم الحصول على اعلى مقاومة (انضغاط او شد).هذا المحتوى الامثل يعتمد على طول الالياف ومحتوى الاسمنت.

VISCOELASTIC MHD FLUID FLOW BETWEEN NONPARALLEL PLATES: ANALYTICAL INVESTIGATION

MOHAMMADHOSSEIN **S**ABOUR and **M**OHAMMADREZA **A**ZIMI
Dept. of New Sciences and Technologies, University of Tehran, Tehran-Iran

(Received: June 2, 2014; Accepted for publication: March 9, 2015)

ABSTRACT

The present study discusses the velocity profile of the steady 2-dimensional flow of a MHD Viscoelastic fluid between two nonparallel plates. Firstly, a similarity transformation is used to reduce the partial differential equations of modeling the flow, to single third-order nonlinear differential equations containing the semi angle between the plates, Reynolds number, the magnetic field strength and Weissenberg number as parameters. The analytical method used Galerkin Optimal Homotopy Asymptotic Method to solve the problem. The obtained approximate results are compared with those of numerical solution in some numerical cases.

***KEYWORDS*:** MHD, Viscoelastic Fluid, Nonparallel plates, Analytical Solution, GOHAM.

1. INTRODUCTION

Most industrial fluid processing includes non-Newtonian liquids like multi-grade oils, liquid detergents, paints, polymer solutions and polymer melts. In recent years the analysis of the effect of rotating concentric cylinders using non-Newtonian liquids is a popular area of research, not only due to its geophysical and technological importance but also in view of the interesting mathematical features presented by the equations governing the flow [1-6].

The study of flow for an electrically conducting fluid has applications in many engineering problems such as MHD power generators, MHD pumps, accelerators, plasma studies, geothermal energy extractions, the boundary layer control, aerodynamic heating, electrostatic precipitation, etc. One of the early works was done by Hughes et al. [7] performing a CFD analysis for simple parabolic and elliptic MHD flows in presence of constant magnetic field. Serizawa et al. [8] investigated the MHD effects on NaK-Nitrogen two phase flow and heat transfer in vertical round tubes. Unsteady MHD film flow over a rotating infinite disk was studied by Kumari and Nath [9]. In a study by Xu et al. [10] a series solution of unsteady three-dimensional MHD flow and heat transfer in the boundary layer for the case of impulsive stretching plate was given. Analytical solution was given to the problem of the unsteady MHD flow of a viscous fluid between moving parallel plates by Sweet et al.[11]. Li et al. [12] solved two-dimensional steady MHD flow in ducts using a numerical scheme.

Most scientific problems in fluid mechanics such as MHD Viscous fluid flow over the stretching sheet are inherently nonlinear by nature and except for a limited number of cases, most of them do not have exact solutions. Accordingly, the nonlinear equations are usually solved using other methods including numerical techniques or using analytical methods. Some of these methods are Homotopy Perturbation Method (HPM) [13, 14], Reconstruction of Variational Iteration Method (RVIM) [15], Glerkin Optimal Homotopy Asymptotic Method (GOHAM) [16] and others [17, 18].

The aim of this study is to discuss the analytic solutions of the two-demensional MHD viscoelastic flow between converging / diverging flow.

2. Problem Description

Consider a steady, incompressible and non-Newtonian fluid in a 2D converging/diverging channel flow as shown in Fig. 1

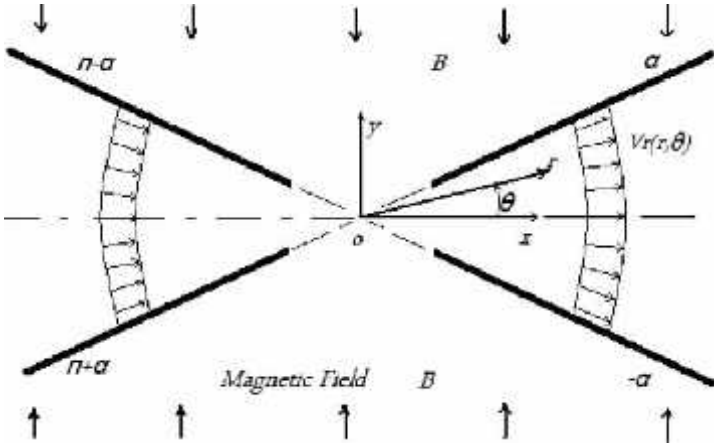

Fig.(1):- Geometry of problem.

Clearly a viscous fluid is governed by continuity and Navier Stokes equations and when the fluid is considered to be incompressible, isothermal and without gravitational force, the conservation of momentum and total mass are as follows [19]:

$$\nabla \cdot V = 0 \tag{1}$$

(2)

where ° is the fluid density, p is pressure, V is velocity vector, and, f_B denotes the force inserted by the magnetic field on the flow domain:

$$f_B = \pm \left(E + V \times B\right) \times B \tag{3}$$

in which E is the electric field. In the last term of Eq. (3) on the right-hand side is $B = B_0 + b$ the total magnetic field, ± is the electrical conductivity. For small magnetic Reynolds number the induced magnetic field is neglected and hence it can be easily written [9,10] as:

$$f_B = -\pm \left[(v_r \cos^{-}) \cos^{-} B^2 \hat{e}_r + (v_r \cos^{-}) \sin^{-} B^2 \hat{e}_r \right] \tag{4}$$

In this study purely radial flow is assumed. By rearranging the equations for polar coordinate system with no tangential velocity, the simplified equations can be obtained as:

$$\frac{1}{r}\frac{\partial}{\partial r}(r v_r) = 0 \tag{5}$$

$$\circ\left(v_r \frac{\partial v_r}{\partial r}\right) = -\frac{\partial p}{\partial r} + \left(\frac{1}{r}\frac{\partial(r^{2}{}_{rr})}{\partial r} + \frac{1}{r}\frac{\partial^{2}{}_{-r}}{\partial r} - \frac{^{2}\!-}{r}\right) - \pm v_r B^2 \cos^{2} - \tag{6}$$

$$0 = -\frac{\partial p}{\partial^{-}} + \left(\frac{1}{r^2}\frac{\partial\left(r^{2\,2}{}_{r^{-}}\right)}{\partial r} + \frac{1}{r}\frac{\partial^{2}\!-}{\partial^{-}} - \frac{^{2}{}_{-r} - ^{2}{}_{r^{-}}}{r}\right) - \pm v_r B^2 \sin^{-}\cos^{-} \tag{7}$$

In which $^{-}$ and r are the component of the polar coordinate system, and v_r is radial velocity, which in the steady state flow is just a function of $^{-}$ and r.

Stress in a non-Newtonian fluid can be considered as:

$$^{2} = \sim_1 D + \sim_2 D^{\nabla} + \sim_3 D \cdot D \tag{8}$$

Where $\sim_1, \sim_2$, and $\sim_3$ are the material modules and are considered to be functions of temperature in general. In Eq.(8) D is the deviatoric part of the velocity [19]:

$$D = \frac{1}{2}\left[\nabla V + (\nabla V)^T\right] \tag{9}$$

and upper convected time derivative (∇) is the special time derivative calculated in the form of :

$$\overset{\nabla}{D} = (V \cdot \nabla) D - (\nabla V)^T \cdot D - D \cdot \nabla V \tag{10}$$

Eliminating pressure from Eqs.(6, 7) , and using Eq.(5) the following nonlinear ODE can be obtained:

$$F''' + 2\,\mathrm{Re}\,\sim FF' + 4\sim^{2} F' + Wi\left(8\sim FF''' + 32\sim^{3} FF'\right) - H\,\mathrm{Re}\left[F'\cos(\sim\,\text{¦}) - \sim F\sin(2\sim\,\text{¦})\right] = 0 \quad (11)$$

where *Re, Wi, and H* are the Reynolds, Weissenberg and Hartman numbers respectively. With the boundary conditions as the form:

$$F(\pm 1) = 0, \quad F(0) = 1 \quad (12)$$

Eq.(11) is defined by considering the following parameters:

$$\mathrm{Re} = \frac{\circ f_0 \sim}{\ll_0}, \quad Wi = \frac{\cdot_{1,0} f_0}{r^2 \ll_0 \sim}, \quad H = \frac{\pm B^2 r^2 \sim}{\circ f_0} \quad (13)$$

$\ll_0$ and $\cdot_{1,0}$ denoting the fluid's viscosity coefficient and the first normal stress coefficient of the fluid's elasticity, respectively calculated in zero shear rate.

In Eq.(13) f_0 is a dimensional constant that can be obtained from the volumetric flow rate Q, by means of the equation:

$$f_0 = \frac{Q}{\int_{-1}^{1} \sim F(\text{¦})\,d\text{¦}} \quad (14)$$

in which $\text{¦} = \frac{—}{\sim}$ as shown in ref. [19].

3. Application of GOHAM

Following differential equation is considered:

$$L(u(t)) + N(u(t)) + g(t) = 0, \quad B(u) = 0 \quad (15)$$

where, L is a linear operator, $u(t)$ is an unknown function, $g(t)$ is a known function, $N(u(t))$ is a nonlinear operator and B is a boundary operator. By means of OHAM one first constructs a set of equations:

$$(1-p)\left[L(¤(², p) + g(²))\right] - H(p)\left[L(¤(², p)) + g(²) + N(¤(², p))\right]B(¤(², p)) = 0 \quad (16)$$

Where, ² is an independent variable, $p \in [0,1]$ is an embedding parameter, $H(p)$ denotes a nonzero auxiliary function for $p \neq 0$ and $H(0) = 0$, $¤(², p)$ is an unknown function. Obviously, when $p = 0$ and $p = 1$, it holds that:

$$¤(², 0) = u_0(²), \quad ¤(², 1) = u(²) \quad (17)$$

Ths, as *p* increases from *0* to *1*, the solution $¤(², p)$ varies from $u_0(²)$ to the solution $u(²)$, where $u_0(²)$ is obtained from Eq. (16) for $p = 0$:

$$L(u_0(²)) + g(²) = 0, \quad B(u_0) = 0 \quad (18)$$

The auxiliary function $H(p)$ can be chosen in the form:

$$H(p) = p_1 C_1 + p_2 C_2 + \cdots \quad (19)$$

Where C_1, C_2 , … are constants which can be determined later. Expanding $¤(², p)$ in a series with respect to *p*, one has:

$$¤(², p, C_i) = u_0(²) + \sum_{k>1} u_k(², C_i) p_k, \quad i = 1,2,... \quad (20)$$

Substituting Eq.(20) into Eq.(16), collecting the same powers of *p*, and equating each coefficient of *p* to zero, a set of differential equations with boundary conditions can be obtained. Solving these differential equations by boundary onditions, $u_0(²), u_1(², C_1), u_2(², C_2), ...$ are obtained.

Generally speaking, the solution of Eq.(4) can be determined approximately in the form:

$$¤(², p, C_i) = u_0(²) + \sum_{k>1} u_k(², C_i) p_k, \quad i = 1,2,...,m \tag{21}$$

$$\tilde{u}(m) = u_0(²) + \sum_{k=1}^{m} u_k(², C_i) \tag{22}$$

Note that the last coefficient C_m can be function of ². Substituting Eq.(19) into Eq.(15), results the following residual:

$$R(², C_i) = L(\tilde{u}^{(m)}(², C_i)) + g(²) + N(\tilde{u}^{(m)}(², C_i)) \tag{23}$$

If $R(², C_i) = 0$ then $\tilde{u}^{(m)}(², C_i)$ happens to be the exact solution. Generally such a case will not arise for nonlinear problems, but the functioning by Galerkin method can be minimized:

$$w_i = \frac{\partial R(², C_1, C_2, \cdots, C_m)}{\partial C_i}, \quad i = 1,2,...,m \tag{24}$$

The unknown constants $C_i\ (i = 1,2,...,m)$ can be identified from the conditions:

$$J(C_1, C_2) = \int_a^b w_i R(², C_1, C_2, ..., C_m) d² = 0 \tag{25}$$

Where *a* and *b* are two values, depending on the given problem. With these constants, the approximate solution (of order *m*) (Equation. (25)) is well determined. It can be observed that the method proposed in this work generalizes these two methods using the special (more general) auxiliary function $H(p)$.

4. Results and Discussions

In this article, an analytical solution for magnetohydrodynamic flows of viscoelastic fluids in converging/ diverging channels is presented. In figure.2.the effect of Reynolds number on velocity profile in case $~ = -\frac{®}{9}$, H=10, Wi=0.1. As it can be seen in figure.2 , increasing the Reynolds number results in a uniform increase in the velocity. Figure.2 also presents a comparison between analytical results obtained by HPM and numerical solutions achieved from forth order Runge Kutta method. According to figure, the obtained results have good agreement with numerical solutions.

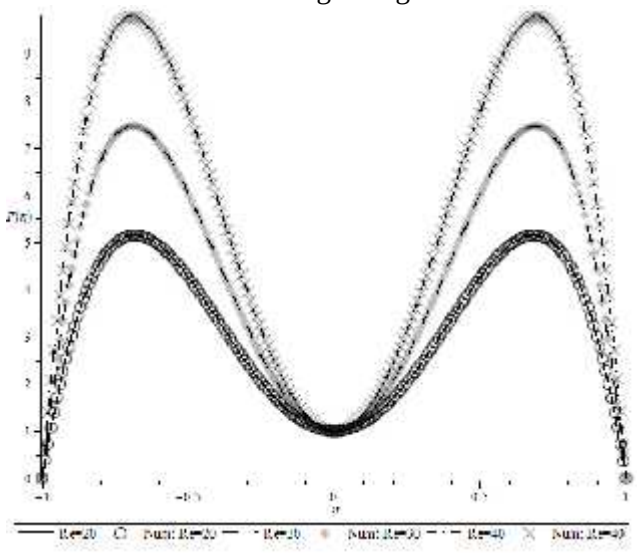

Fig.(2):-Effect of Reynolds number on Velocity profile in case $~ = -\frac{®}{9}$, H=10, Wi=0.1

(Line: GOHAM, Symbols: RK4)

In figure.3 the effect of semi angle on velocity profile in case Re=30, Wi=0.2 and H=10 has been presented for both cases converging and diverging channel. The velocity curves show that the rate of transport is considerably increased with increase of the semi-angle between the two walls especially when two plates move together.

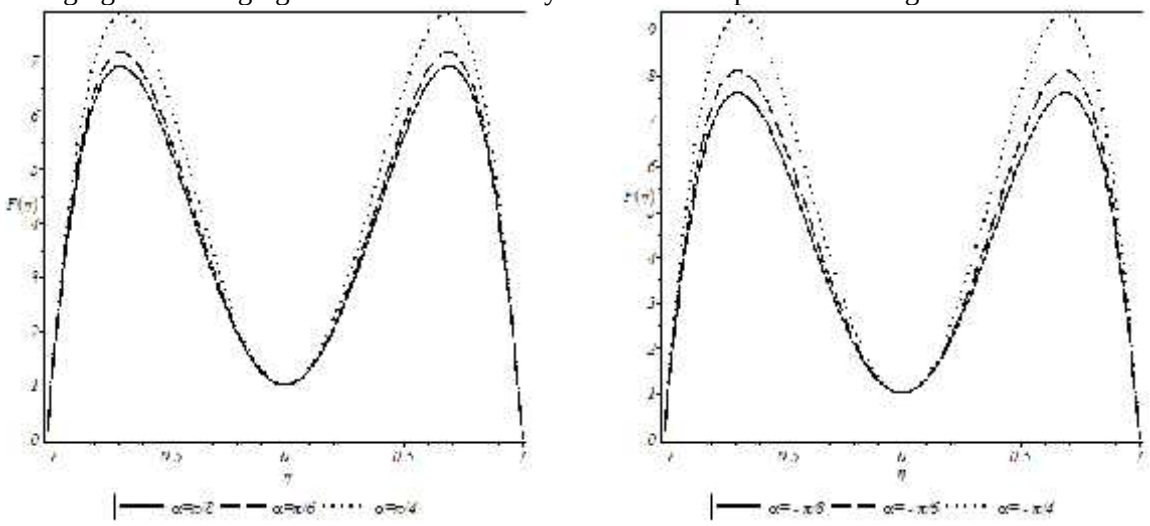

a b

Fig.(3):- Effect of semi angle on Velocity profile in case Re=30, Wi=0.2 and H=10 a- converging channel, b-diverging channel.

In Figure.4 we can see the effect of the magnetic field strength to the velocity in r direction. As it can be seen by increasing H the maximum velocity is increasing. Therefore, increasing the electrical conductivity of the fluid or increasing the magnitude of the magnetic field results in a non-uniform increase in r-direction velocity.

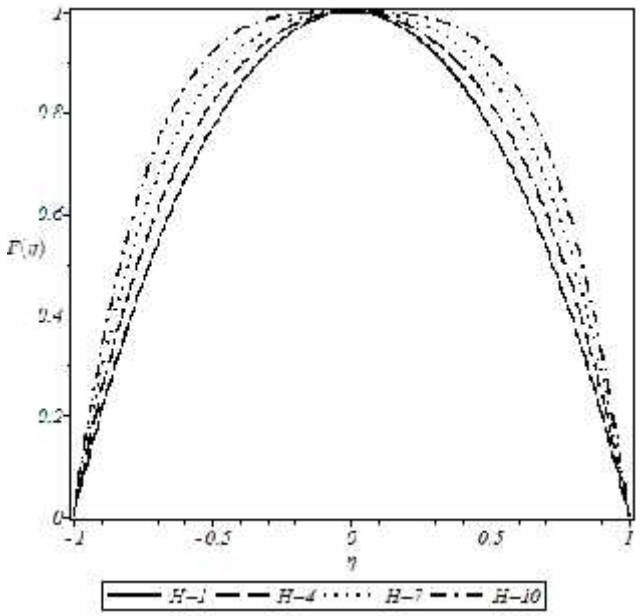

Fig.(4):- Effect of Hartman number on velocity profile in case $\sim = -\frac{®}{9}$, Re=1, Wi=0.1

Effect of Wisenberg number on the velocity profiles in a converging channel, has been presented in figure.5. As it can be illustrated by increasing Wisenberg number, an increment on velocity profile is occured.

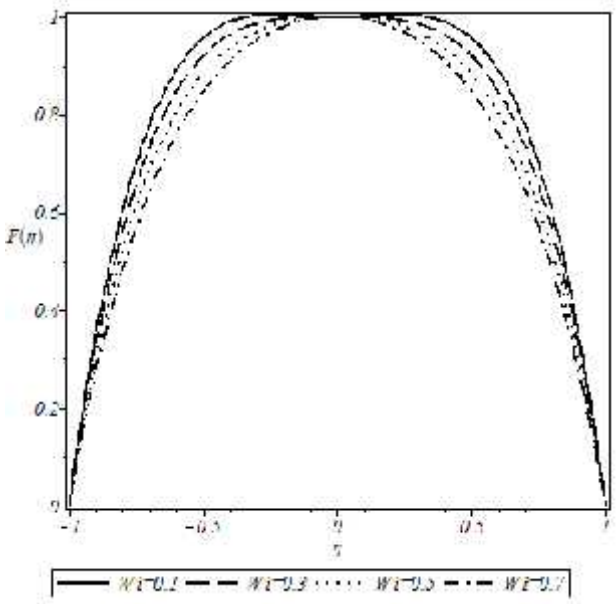

Fig.(5):- Effect of Wisenberg number on velocity profiles in case $\sim = \frac{®}{4}$, Re=4, H=4

CONCLUSIONS

In this article, an analytical solution for magnetohydrodynamic flows of viscoelastic fluids in converging/diverging channels is presented. A similarity transform reduces the Navier– Stokes and energy equations to a set of non-linear ordinary differential equations that are solved analytically by means of the GOHAM. The results obtained in this study are compared with numerical results. Close agreement of the two sets of results indicates the accuracy of GOHAM. The effect of key parameters on velocity has been also checked through some plots.

REFERENCES

- JD Jackson. A study of squeezing flow. *Appl. Sci. Res.* 1962; 11, 148–152.
- AM Siddiqui, S Irum and AR Ansari. Unsteady squeezing flow of a viscous MHD fluid between parallel plates: a solution using the homotopy perturbation method. *Math. Model. Anal.* 2008; 13(4), 565–576.
- B.Hoffner, OH.Campanella, MG.Corradini, M.Peleg, Squeezing flow of a high viscous incompressible liquid pressed between slightly inclined lubricated wide plates. *Rheol. Acta.* 2001; 40, 289-295.
- Mohammadreza Azimi, Alireza Azimi, Flow Simulation of GO nanofluid in Semi Porous Channel, Turkish Journal of Science and Technology, Vol.9, No.1, 2014, pp.67-72.
- Ganji, D.D., M. Azimi, "Application of DTM on MHD Jeffery Hamel problem with nanoparticle," *The* Scientific Bulletin *Series D*, 75, 223-230 (2013).
- M. Azimi, F. Ommi, 2013, Using Nanofluid for Heat Transfer Enhancement in Engine Cooling Process, Nano Energy and Power Research, Vol.2, pp.1-3.
- Hughes, M., K. A. Pericleous, M. Cross, "The CFD analysis of simple parabolic and elliptic MHD flows," *Appl. Math. Modelling*, 18, 150-155 (1994).
- Serizawa, A., T. Ida, O. Takahashi, I. Michiyoshi, "MHD effect on NaK-Nitrogen twp-phase flow and heat transfer in a vertical round tube," *Int. J. Multiphase flow* , 16, 761-788 (1990).
- Kumari, M., G. Nath, "Unsteady MHD film flow over a rotating infinite disk," *International Journal of Engineering Sience*, 42, 1099-1117 (2004).
- Xu, H., S. J. Liao, I. Pop, "Series solution of unsteady three-dimensional MHD flow and heat transfer in the boundary layer over an impulsively stretching plate," *European Journal of Mechanics B/Fluids*, 26, 15-27 (2007).
- Sweet, E., K. Vajravelu, R. A. Van Gorder, I. Pop, "Analytical solution for the unsteady MHD flow of a viscous fluid between moving parallel plates," *Commun. Nonlinear Sci. Numer. Simulat*. 16, 266-273 (2011).
- Li Y., Z. F. Tian, "An experimental compact difference scheme for solving 2D steady magnetohydrodynamic (MHD) duct flow

problems", *Journal of Computational Physics*, 231, 5443-5468 (2012).

- M. Azimi, A. Azimi, Investigation on the Film Flow of a Third Grade Fluid on an Inclined Plane Using HPM, Mechanics and Mechanical Engineering 18 (1) (2014) 251-256.
- F. Shakeri, D.D.Ganji, M. Azimi, Application of HPM-Pade' to Jeffery Hamel Flow Problem, International Review of Mehanical Engineering, 6 (3) (2012) 537-540.
- A. Azimi, M. Azimi, Analytical Investigation on 2-D unsteady MHD Viscoelastic flow between Moving Parallel Plates Using RVIM and HPM 11 (11) (2014) 955-963.
- M. Azimi, A. Azimi, M. Mirzaei, Investigation of the Unsteady Graphene Oxide Nanofluid Flow Between Two Moving Plates, Journal of Computational and Theoretical Nanoscience 11 (2014) 2104-2108.
- D.D. Ganji, M. Azimi, Application of Max min Approach and Amplitude Frequency Formulation to the nonlinear oscillation systems, The Scientific Bulletin Series A 3 (2012) 131-140.

J D.D. Ganji, M. Azimi, M. Mostofi, Energy Balance Method and amplitude frequency formulation based of strongly nonlinear oscillator, Indian journal of pure & applied physics 50 (2012) 670-675.

J K. Sadeghy, N. Khabazi, S. M. Taghavi, Magnetohydrodynamic (MHD) flows of viscoelastic fluids in converging/ diverging channels. Int. J. Engng Sci., 2007, 45, 923–938.

MODELING OF BEKHMA RESERVOIR SYSTEM OPERATION USING FUZZY LOGIC CONTROLLER

MAHDI **D**AWOOD*, **K**AMEL **A**. **A**LMOHSEEN** and **S**HAKER **A**. **J**ALIL*

* Dept. of Water resource Engineering, College of Engineering, University of Duhok, Kurdistan Region-Iraq
** Dept. of. Dams and Water resource Engineering, College of Engineering, University of Mosul-Iraq
* Dept. of Water resource Engineering, College of Engineering, University of Duhok, Kurdistan Region -Iraq

(Received: June 25, 2014; Accepted for publication: December 10, 2014)

ABSTRACT

A new approach is presented to obtain the operational rules for Bekhma Reservoir System (BRS) using the concept of Fuzzy Logic Controller (FLC). The technique is an attempt to introduce a mechanism that assists the operator of the reservoir system to do the job in a systematic manner. This technique has to be applied in each time step of the procedure. Thus the need of simulation model to mimic the reservoir operation procedures over a certain horizon of time is evident. In this regard, Simulation model based on Simulink technique was implemented to test the performance of BRS where FLC rules are used to operate the system. The applicability of this technique is illustrated for BRS operation where 73 years of recorded average monthly inflows are available. The monthly inflow data have been transformed into daily based data by means of disaggregation procedures. Additionally, the necessary membership functions required by the Fuzzy Logic Algorithms were built based on the inflow and the elevation of the reservoir in which they were representing the inputs. Thus the inflows and the elevations of storage in each selected simulation time step are characterized as: very low, low, moderate, high and very high respectively. While the releases have also been characterized using the same aforementioned five categories to represent the output of the fuzzy controller. The obtained results were compared to the results emerged from previous study conducted on the same system with the same set of data, except that it was using constant release from BRS. The present study reveals that there is 8.45% improvement based on hydropower generation when FCL is used compared to that resulted from the constant reservoir release operation concepts.

1. INTRODUCTION

The operating rules of any reservoir system are typically expressed as storage volume versus time of the year, and are generally derived using either optimization procedures or simulation models. Dawood et al. (2014) proposed two simulation models for operating the Bekhma Reservoir System (BRS); HEC-ResSim (Model-I) and Simulink based technique (Model-II). However, they suggested a constant release from the reservoir calculated by trial and error such that the procedures were based on reliability level in which trails values of release have been assumed, then the simulation model was run for each presumed release value until a reasonable level of reliability is achieved (in that case 100% reliability was sought, i.e. there is no failure either beyond the minimum elevation or maximum elevation of storage in the reservoir over all simulation time using the whole set of daily inflows). The performance of the system in any given period in the future depends on the compatibility

between the set of realized reservoir inflows and the adopted operating policy.

Referring to (Dawood et al. 2014) , where a constant release from the reservoir has been calculated by trial and error, but this method though it gave high level of reliability, it was unrealistic in sense it is difficult to maintain constant releases from real reservoir system over the whole period of operation. Thus, new look was needed to cope with the uncertainty usually associated with the inflow and level of storage in the reservoir. Consequently, and in order to overcome the identified shortcomings of the constant release method as discussed above, fuzzy logic based analysis was used to establish more realistic and robust operation of BRS

.2. FUZZY LOGIC APPROACH

Fuzzy logic based approach is an approximate reasoning method and is useful for coping with

uncertainties in modeling situations. A fuzzy set has a membership function that admits a degree of membership in the set from complete exclusion (0) to absolute inclusion (1) (Almohseen, 2003).

The membership represents a certain degree of belonging of the object in the fuzzy set. The transition from belonging to not belonging is gradual, and affords a means of handling ambiguity and overcomes a major weakness of crisp sets, (Yang and Soh, 2000).

Fuzzy Logic Controller (FLC) was designed as a fuzzy rule based system incorporating fuzzy linguistics described by membership functions. The triangular-shaped membership functions have been used in the present study to express the degree of membership in a fuzzy set. These membership functions are simple to implement in terms of mathematical manipulations and are also adequate for practical purposes, (Adeli and Hung, 1995).

The triangular membership function is shown in (Fig.1) below and is expressed mathematically as:

$\mu j\ (x) = 0 \quad$ if $x < a1$;

$\mu j\ (x) = \{ (x - a1)/ (a2 - a1)\}$ if $a1 \leq x \leq a2$;

$\mu j\ (x) = 1 \quad$ if $x = a2$;

$\mu j\ (x) = \{ (a3 - x) / (a3 - a2)\}$ if $a2 < x \leq a3$;

$\mu j\ (x) = 0 \quad$ if $x > a3$;

Where:

/a1, a2, and a3 are predefined parameters identified in (Fig.1).

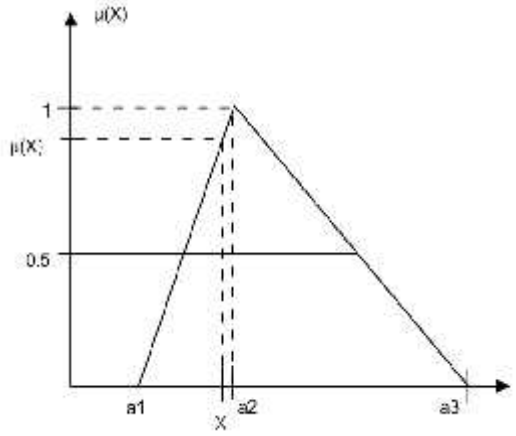

Fig. (1): Typical triangular-shaped fuzzy membership function (After Almohseen, 2003)

Fuzzy rules take the form IF (condition) then (action), where conditions and actions are linguistic labels applied to input and output variables. For example, the expected inflow in to BRS may be described with linguistic variable such as 'low', 'medium' or 'high'. The steps in designing a simple FLC have been reported by Ross, (1995), and can be summarized by Identifying the variables (inputs and outputs) of the system, partition the set of each variable into a number of fuzzy subsets assigning each subset a linguistic label, then determine a membership function of each fuzzy subset, and assign the fuzzy relationships between the input fuzzy subsets on the one hand and the output fuzzy subsets on the other hand, fuzzify the inputs to the controller and use fuzzy approximate reasoning to infer the output contributed from each rule, aggregate the fuzzy outputs recommended by each rule and finally apply defuzzification to form crisp output.

The application of fuzzy sets in water resources modeling includes the works of Bogardi et al. (1983) and Kindler (1992), Fuzzy Logic Programming has been also applied by Russel and Cambell (1996), Shrestha et al. (1996), Fontane et al. (1997), Teegavarapu and Simonovic (1999), Panigrahi and Mujumdar (2000), and Singh and Mujumdar (2002). Thus, and due to the successful application of fuzzy logic technique, the current study is an attempt to apply this approach to operate Bekhma reservoir system.

3.APPLICATION

Since the main purpose of Bekhma reservoir system is to generate hydroelectricity, therefore it is necessary to operate the system based on short

time such as one day intervals due to the fluctuation of the demand on power over this time period. However, the available inflow data for BRS is based on average monthly intervals over the period January-1932 to December-2004, i.e. (876) mean monthly flow records. Consequently, the monthly data has been subjected to disaggregation procedures to convert them into daily data (26633 days) using a disaggregation approach based in HEC-ResSim software. Table (1) shows the disaggregated inflow during the year 2002. While (Fig.2) depicts the daily inflow into Bekhma Reservoir over the period January 1st 1932 to December 1st 2004 after being disaggregated Fuzzy logic toolbox is compatible to work with Simulink in Matlab platform. The FLC uses the expected daily inflow into Bekhma reservoir and the level of storage at the reservoir as inputs and yields the daily release from the reservoir as output. The designed membership functions and the corresponding rules for operating Bekhma reservoir system are depicted in figures (3) to (7) for the FLC used in this study.

Table (1): Daily Inflow into Bekhma Reservoir (During year 2002) after disaggregation

2002	1	2	3	4	5	6	7	8	9	10	11	12	Mean
1	137.50	231.30	313.60	307.80	265.20	232.40	217.90	210.50	205.20	199.40	200.50	301.00	235.19
2	159.60	303.00	324.30	291.40	239.00	225.80	210.00	211.00	199.50	199.30	201.70	400.40	247.08
3	159.60	303.00	324.30	291.40	239.00	225.80	210.00	211.00	199.50	199.30	201.70	400.40	247.08
4	159.60	303.00	324.30	291.40	239.00	225.80	210.00	211.00	199.50	199.30	201.70	400.40	247.08
5	159.60	303.00	324.30	291.40	239.00	225.80	210.00	211.00	199.50	199.30	201.70	400.40	247.08
6	159.60	303.00	324.30	291.40	239.00	225.80	210.00	211.00	199.50	199.30	201.70	400.40	247.08
7	159.60	303.00	324.30	291.40	239.00	225.80	210.00	211.00	199.50	199.30	201.70	400.40	247.08
8	159.60	303.00	324.30	291.40	239.00	225.80	210.00	211.00	199.50	199.30	201.70	400.40	247.08
9	159.60	303.00	324.30	291.40	239.00	225.80	210.00	211.00	199.50	199.30	201.70	400.40	247.08
10	159.60	303.00	324.30	291.40	239.00	225.80	210.00	211.00	199.50	199.30	201.70	400.40	247.08
11	159.60	303.00	324.30	291.40	239.00	225.80	210.00	211.00	199.50	199.30	201.70	400.40	247.08
12	159.60	303.00	324.30	291.40	239.00	225.80	210.00	211.00	199.50	199.30	201.70	400.40	247.08
13	159.60	303.00	324.30	291.40	239.00	225.80	210.00	211.00	199.50	199.30	201.70	400.40	247.08
14	159.60	303.00	324.30	291.40	239.00	225.80	210.00	211.00	199.50	199.30	201.70	400.40	247.08
15	159.60	303.00	324.30	291.40	239.00	225.80	210.00	211.00	199.50	199.30	201.70	400.40	247.08
16	159.60	303.00	324.30	291.40	239.00	225.80	210.00	211.00	199.50	199.30	201.70	400.40	247.08
17	159.60	303.00	324.30	291.40	239.00	225.80	210.00	211.00	199.50	199.30	201.70	400.40	247.08
18	159.60	303.00	324.30	291.40	239.00	225.80	210.00	211.00	199.50	199.30	201.70	400.40	247.08
19	159.60	303.00	324.30	291.40	239.00	225.80	210.00	211.00	199.50	199.30	201.70	400.40	247.08
20	159.60	303.00	324.30	291.40	239.00	225.80	210.00	211.00	199.50	199.30	201.70	400.40	247.08
21	159.60	303.00	324.30	291.40	239.00	225.80	210.00	211.00	199.50	199.30	201.70	400.40	247.08
22	159.60	303.00	324.30	291.40	239.00	225.80	210.00	211.00	199.50	199.30	201.70	400.40	247.08
23	159.60	303.00	324.30	291.40	239.00	225.80	210.00	211.00	199.50	199.30	201.70	400.40	247.08
24	159.60	303.00	324.30	291.40	239.00	225.80	210.00	211.00	199.50	199.30	201.70	400.40	247.08
25	159.60	303.00	324.30	291.40	239.00	225.80	210.00	211.00	199.50	199.30	201.70	400.40	247.08
26	159.60	303.00	324.30	291.40	239.00	225.80	210.00	211.00	199.50	199.30	201.70	400.40	247.08
27	159.60	303.00	324.30	291.40	239.00	225.80	210.00	211.00	199.50	199.30	201.70	400.40	247.08
28	159.60	303.00	324.30	291.40	239.00	225.80	210.00	211.00	199.50	199.30	201.70	400.40	247.08
29	159.60		324.30	291.40	239.00	225.80	210.00	211.00	199.50	199.30	201.70	400.40	242.00
30	159.60		324.30	291.40	239.00	225.80	210.00	211.00	199.50	199.30	201.70	400.40	242.00
31	159.60		324.30		239.00		210.00	211.00		199.30		400.40	249.09
Sum	4925.50	8412.30	10042.60	8758.40	7435.20	6780.60	6517.90	6540.50	5990.70	6178.40	6049.80	12313.00	2901.45

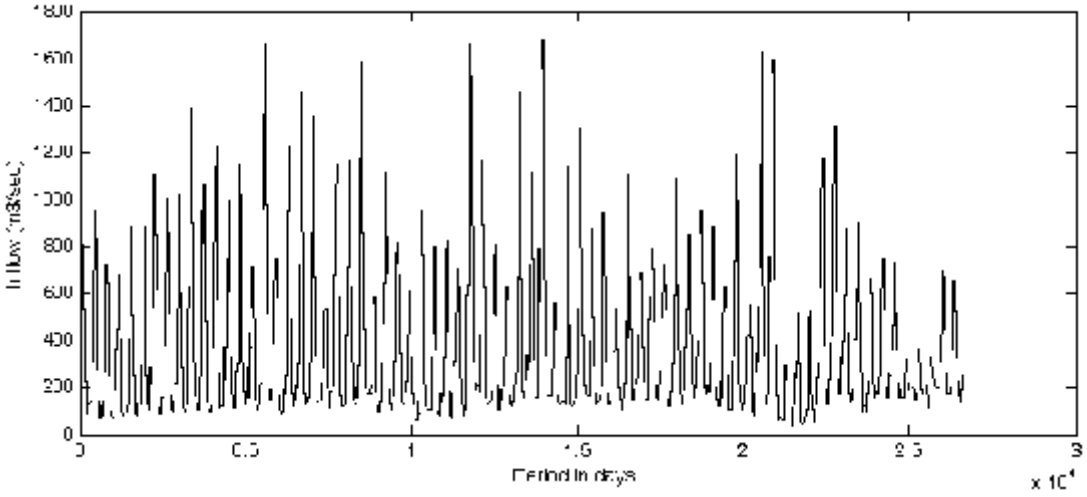

Fig. (2): Daily inflow into BRS over the period 1932-2004 after disaggregation

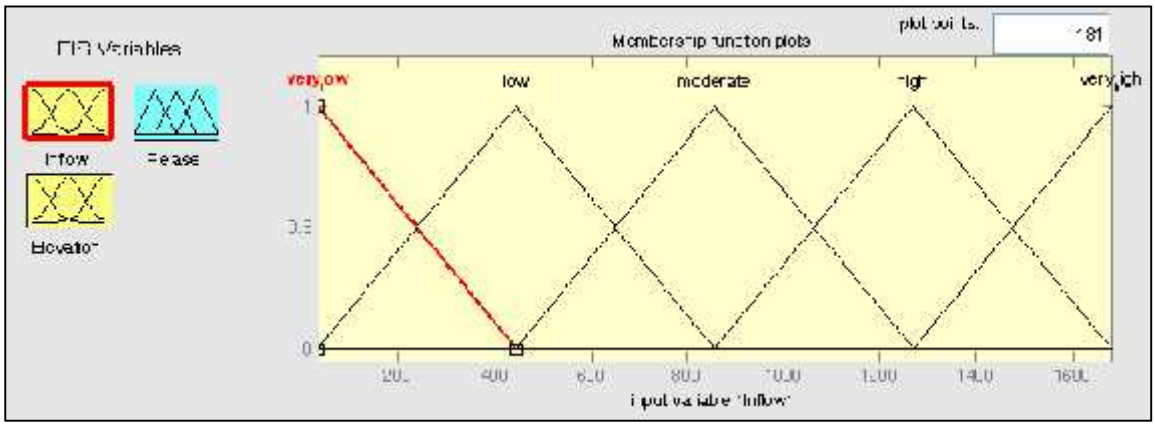

Fig, (3): Membership function of daily inflow into Bekhma Reservoir

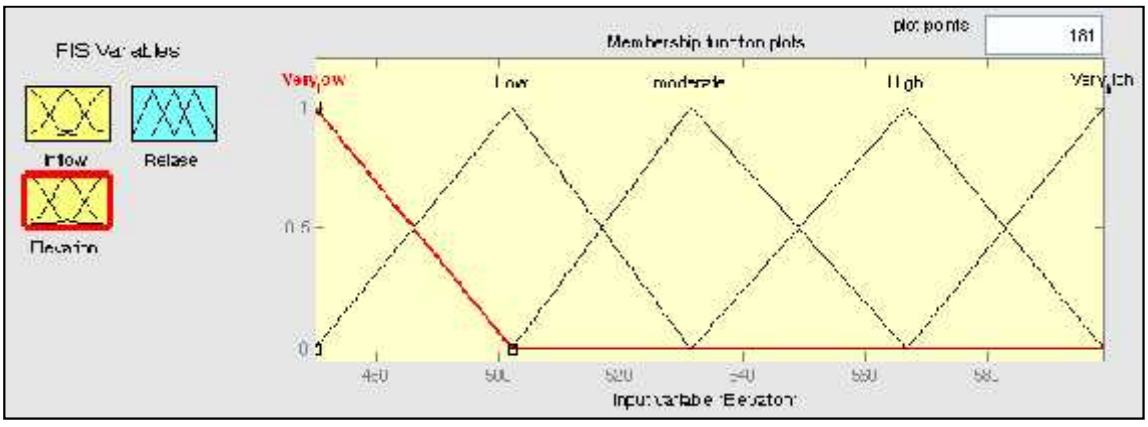

Fig. (4): Membership function of Elevation in Bekhma Reservoir

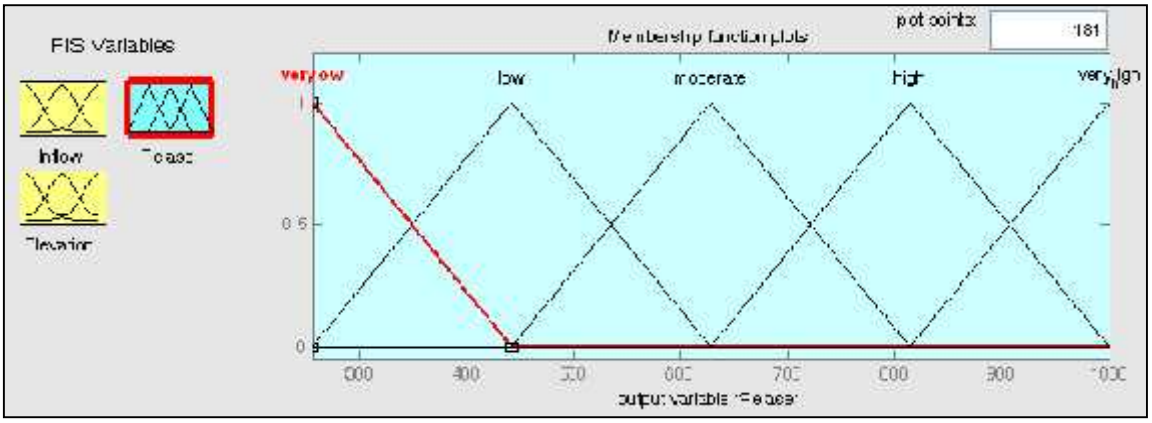

Fig. (5): Membership function of Release (output) in Bekhma Reservoir

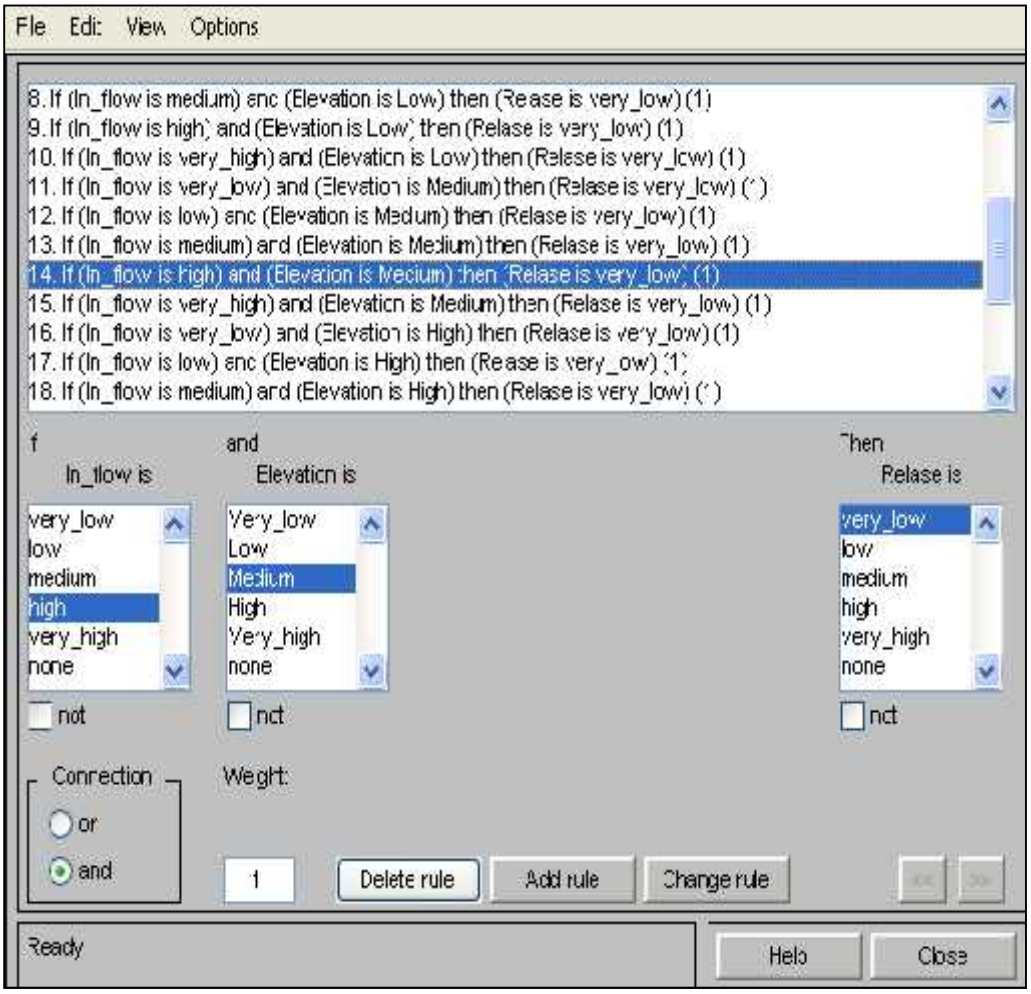

Fig. (6): Rules editor used for fuzzy controller (part of rules)

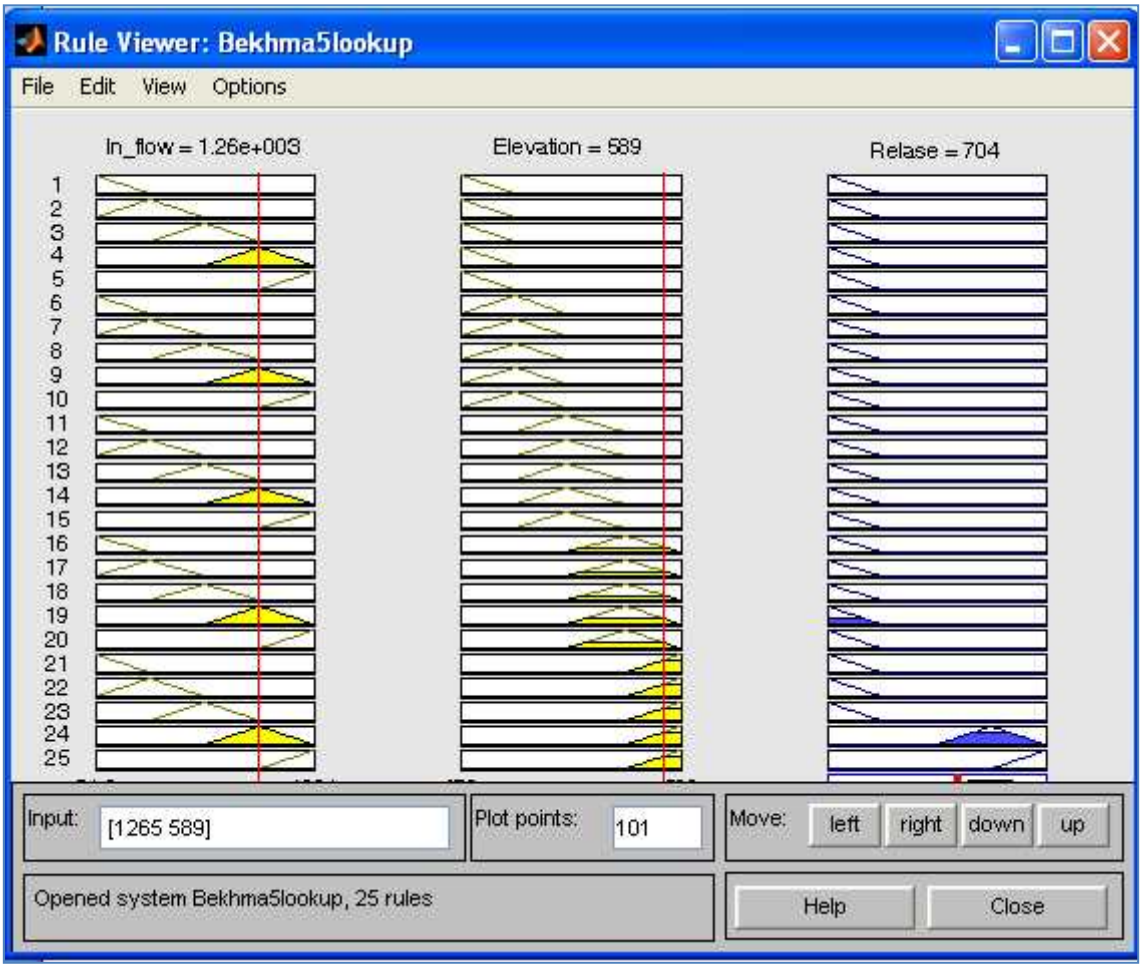

Fig. (7): Rules viewer used for the fuzzy controller

4. SIMULINK -BASED FUZZY SYSTEMS

Fuzzy logic toolbox, designed to work seamlessly with Simulink in Matlab environment. Therefore, the FLC was attached to the Simulink Model (please see the details of Bekhma Reservoir System modeled in Simulink given by Dawood, 2014). Fig. (8) Shows the compatibility of FLC with Simulink Model used in the current study.

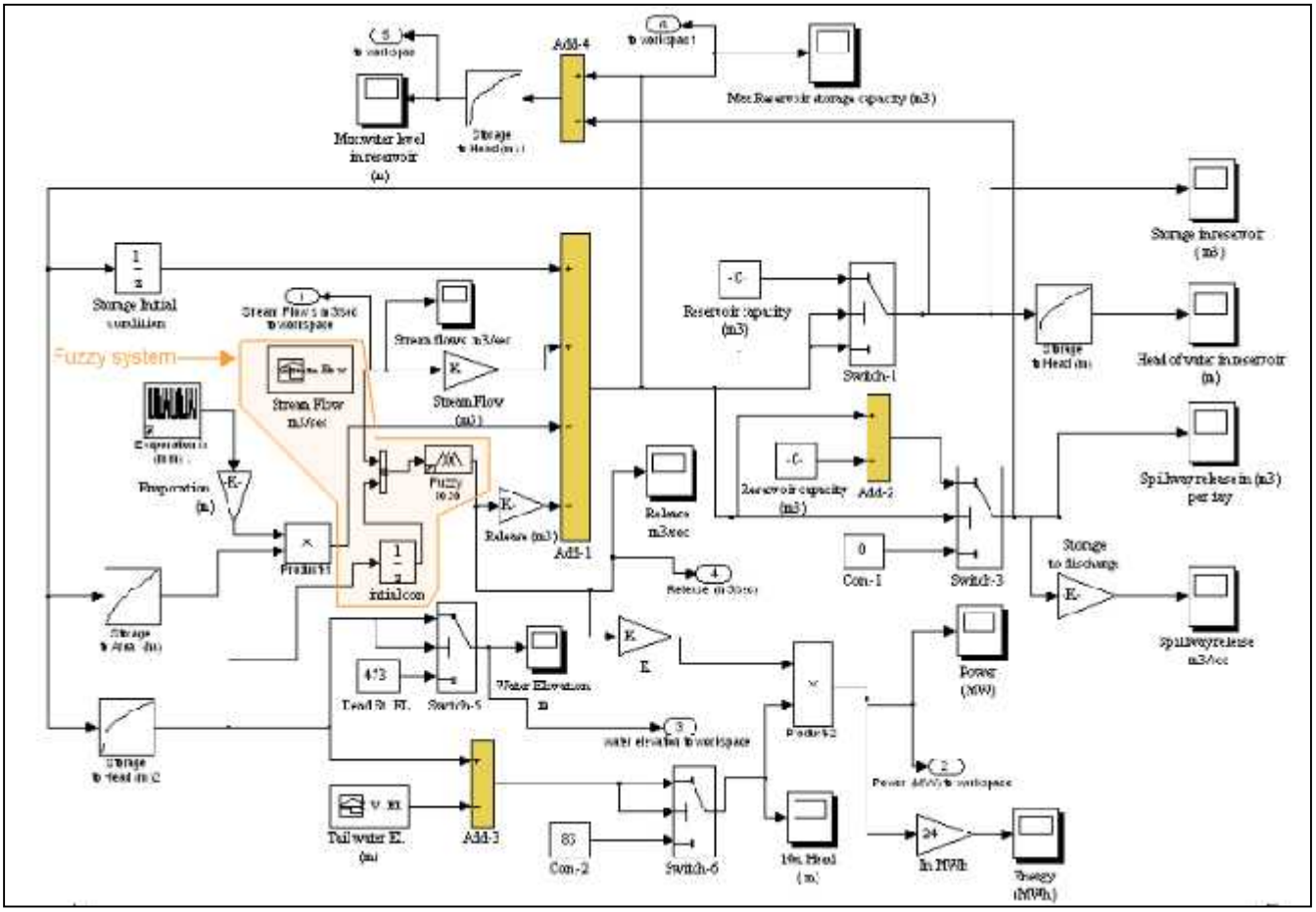

Fig. (8): Simulink based model for BRS with FLC imbedded within the model

5. RESULTS AND DISCUSSIONS

The future possible states of reservoir system can be based on the results of simulation models. Model results can be used in planning and management to analyze and development of policy of reservoir operation. As the policy of operation in Bekhma system is the optimal production of hydropower electricity, fuzzy logic controller rule is employed to the simulation model.

To show the advantage of (FLC) systems, a comparison study with Simulink model for (BRS) that uses constant (uniform) release was carried and the results can be presented as follow:

1-The variation of the water level in the reservoir through (73) years of operation by employing two models are presented in (Fig.9) and table (2), It clear that the minimum water elevations are nearly the same in the two models. The average value of water level is less (1) m in FLC model due the variable release from the reservoir.

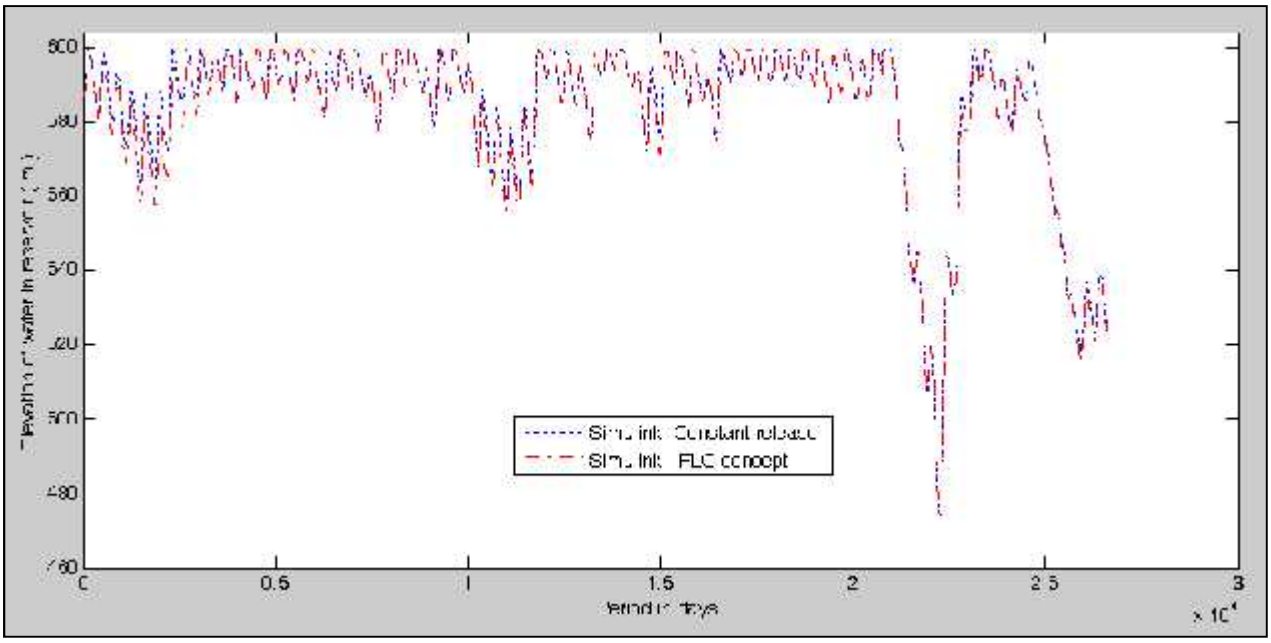

Fig. (9): Daily operating policy for (BRS) - both models

Table (2): Optimal controlled water release and operation characteristics for (BRS) - both models

Models	Optimal release in (m3/sec)	Average water Elevation in reservoir (m)	Max. water Elevation in reservoir (m)	Min. water Elevation in reservoir (m)
Simulink base technique (Constant release)	Constant = 321.45 m3/sec	583.607	599 .00	473.033
Simulink base fuzzy logic system	Variable	582.615	599 .00	473.153

2- For the same period of operation (73 years), the hydropower generated from two models are shown in table (3) and (Fig.10). It can be noted that the average value of the generated power is increased with 8.45% due to variable discharge release which is based on FLC model , in this method maximum turbines discharge capacity allowed to pass during highest inflow discharges entering to the reservoir so that a maximum power can be generated at that times , while the constant release method depends on the head during power generation. Also the maximum value of the generated power is nearly three times than the maximum in the constant release model.

Table (3): hydropower generation characteristics results from both simulation models

Models	Average Power Generated in (Mw)	Max. Power Generated in (Mw)	Min. Power Capacity in (Mw)
Simulink base technique (Constant release)	488.4	527.3	209.5
Simulink base fuzzy logic system	529.7	1543	207 .0

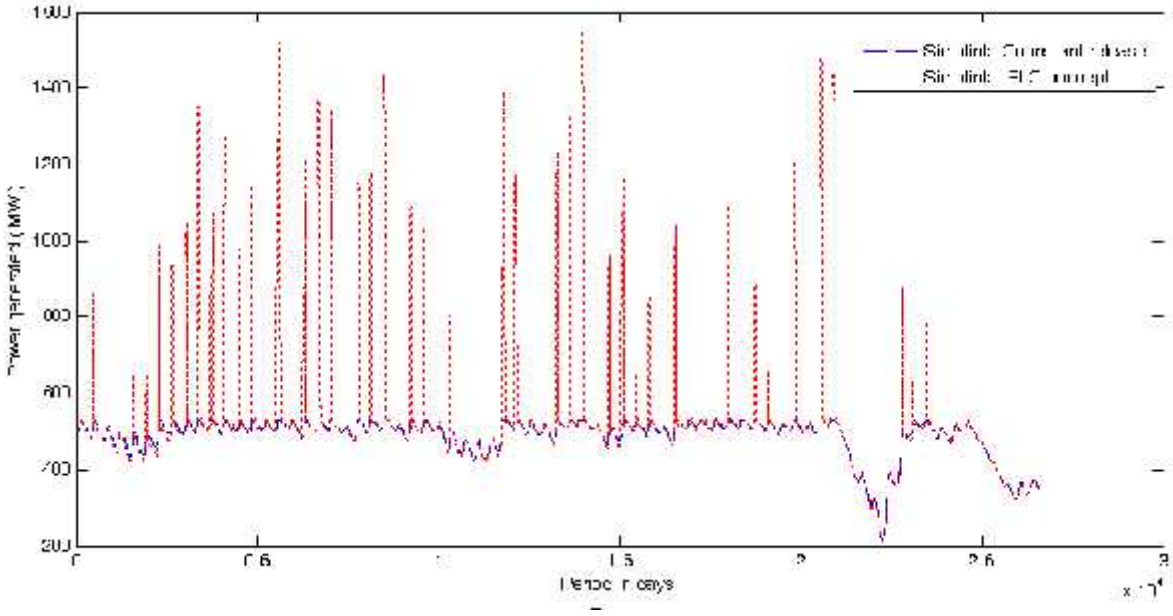

Fig. (10): Generated power produced by both simulation models from Bekhma reservoir (During the period 1932 to 2004)

3-in Fuzzy logic model simulation, maximum and average flow release through turbines more than that in the constant release model. Table (4) and (Fig.11) show the release value through turbines. It can note that ratio of the average release to mean in flow lays in the range which was suggested by Hardson (1972). Hardson show that constant release for mainland United States potential regulation varies from 57 % in lower Colorado to 95 % in Tasmania. The mean value of in flow to Bekhma reservoir is 381.6 m3/sec, so the yield (release) for (BR) as percentage to mean flow is equal to = 84.23% and equal to 91.37% in fuzzy logic model, also it can be notes that the average release satisfies all requirements of (Irrigations, fisher developments, forests, domestic, industrials, and environmental) which is equal to (311m3/sec) at July according to (Al-Gazzal, AW. M. Y, 2002).

Table (4): Controlled water releases characteristics through turbines for hydropower generation in both models simulations

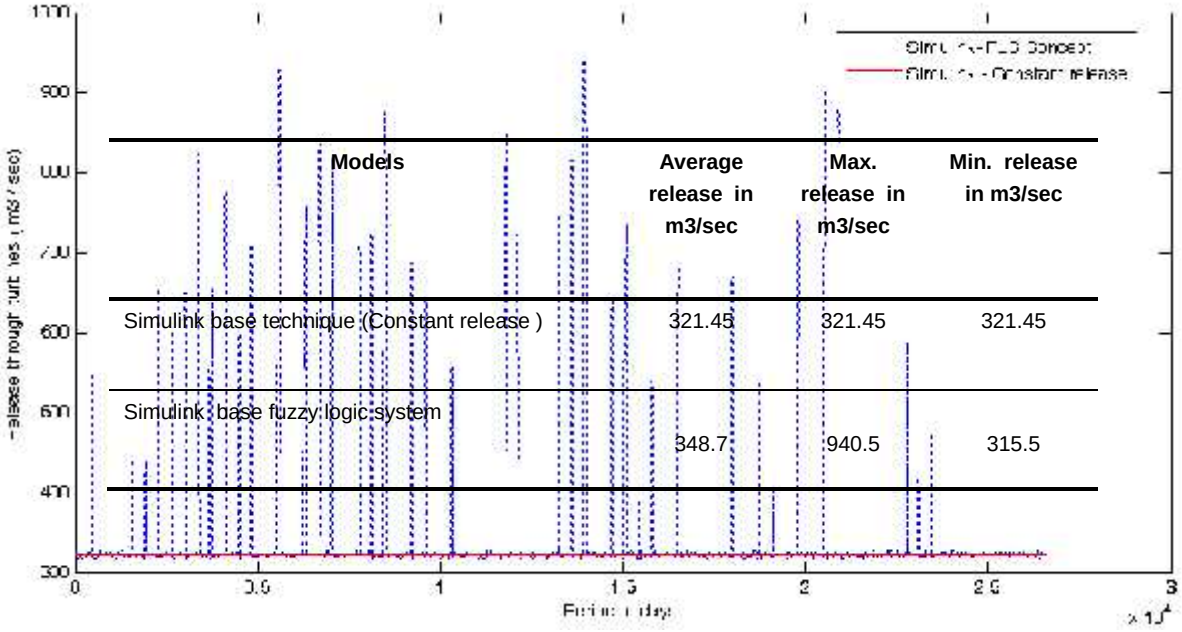

Fig. (11): Controlled water releases through turbines for hydropower generation in both models simulations

4-Spillway controlled releases as a daily operation from models simulations are shown in (Fig. 12)and table (5) , the maximum release through spillway in fuzzy model is 740.5m3/sec , from input data (Fig. 2), the maximum stream flow for greater zab during period (1932 to 2004) was 1681 m3/sec ,this verify that when stream flow discharge at its peak value and water elevation in reservoir is in top of flood control zone , hydropower plant will receive maximum discharge equal to = 940.5 m3/sec not 1000 m3/sec which it is maximum capacity of the Bekhma power plant due to approximately of fuzzy logic concepts , again the maximum release through spillway in constant release model = 1359.55 m3/sec, this mean that (1681-1359.55= 321.45 m3/ sec) will be continue constant release through turbines for power generation during simulation period.

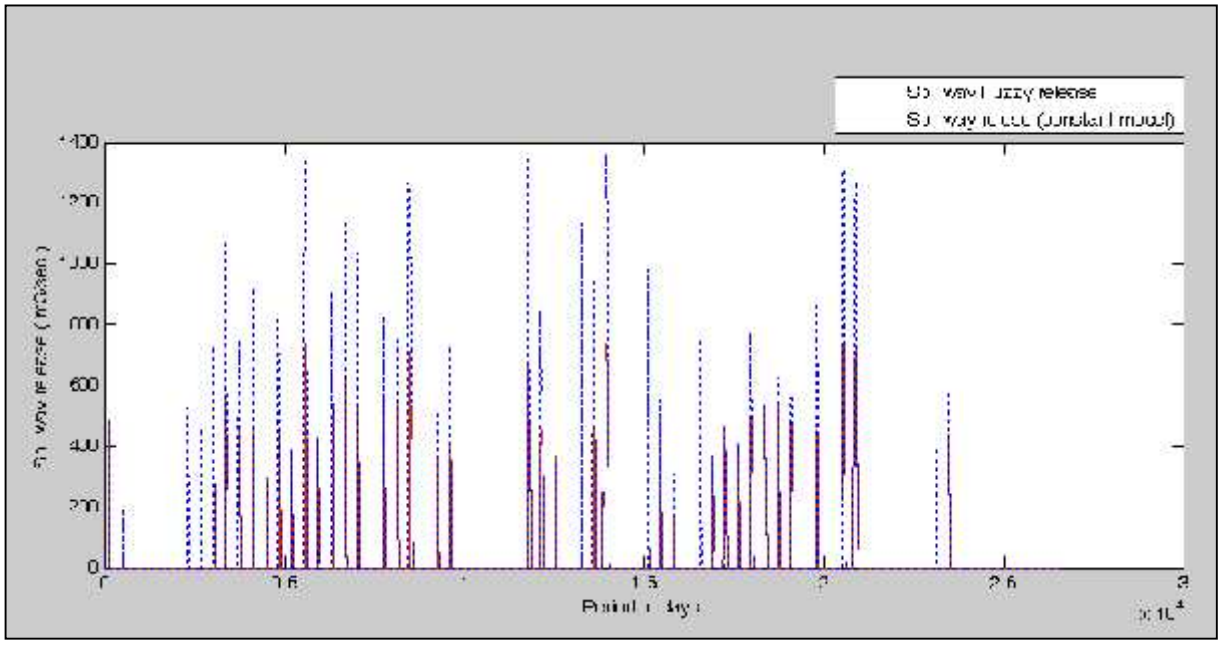

Fig. (12): Controlled release through spillway during simulation of the models from period (1932 to 2004)

Table 5: releases characteristics through spillway from period (1932 to 2004)

Models	Average spillway release in m3/sec	Max. spillway release in m3/sec	Min. spillway release in m3/sec
Simulink base technique (Constant release)	64.03	1359.55	0.0
Simulink base fuzzy logic system	36.88	740.51	0.0

5-The daily operation rule curve(policy operation) resulted from the two models are presented in (Fig.9) above, these data is relatively large and difficult to be analyzed, consequently, hard work has been devoted to extract the average monthly operation policy from 26,633 days for each simulation model. The monthly operation rule curves (Operating polices) in term of elevation of water in reservoir obtained from simulation of models are calculated and presented in table (6) and (Fig. 13) based on water elevation in the reservoir. It can note that the operation policies of average water levels are close to each other's in the two models simulation

Table (6): Monthly operating policies of Bekhma reservoir from simulation of models (In term of elevation of water in the reservoir)

Months	Jan.	Feb.	Mar.	Apr.	May.	Jun.	Jul.	Aug.	Sep.	Oct.	Nov.	Dec.
Simulink base technique (Constant release)	577.74	579.54	584.00	588.31	589.93	589.74	588.18	585.66	582.96	580.51	578.58	577.87
Simulink base fuzzy logic system	576.77	578.51	582.65	586.92	588.93	588.92	587.33	584.80	582.10	579.63	577.65	576.92

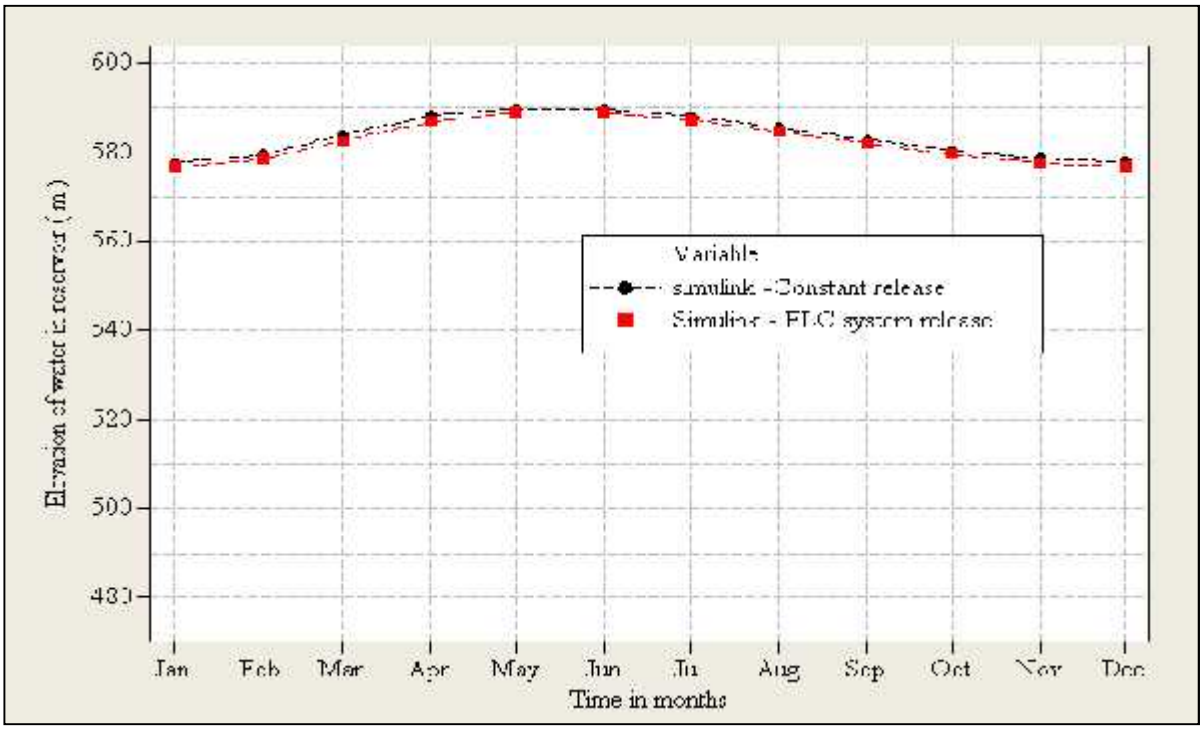

Fig. (13): Monthly operating policies of Bekhma reservoir from simulation of models (In term of elevation of water in the reservoir)

6. CONCLUSIONS

The effect of advanced fuzzy logic computational intelligence techniques on the operation policy of reservoir is studied. The implantation of Fuzzy logic to the Simulink of Bekhma reservoir for generating hydropower, showed that it is a promising tool for operation reservoir systems , the result obtained compared with results of model simulated when a simple rule (constant release) has been used, average monthly flow for period of (1932 to 2004) of the river disaggregated to daily time step (26633 day) with the help of tools available in HEC-ResSim software, the result of this disaggregation has been used in model simulation , the current research work is considered an opportunity to check the ability of Simulink based on fuzzy logic system approach in modeling water resource system in general and reservoir system in particular. It can be conclude that that this new technique would open the door widely for those who work in this area to be able to model more complex systems by making use of the high capabilities of Matlab software which is very rich in terms of built in functions , tools and can be used easily through Simulink technique. The study reveals that model based on (FLC) for operating (BR) have given daily power generation increased 8.45 % more than power generated in the same model used constant release , an average daily power generation of 529.7 MW/day obtained from simulation of models used fuzzy system concepts based on (FLC) for reservoir operation and 488.4 MW/day from model used constant release for generation of hydropower , in the same time very good agreement in target elevation of water in reservoir was noticed in both models in the operation rules for reservoir, this verify that the model with constant release can be adopt in stage of planning and designing of the storage reservoir to calculate the maximum capacity and yield of the reservoir.

REFERENCES

- Dawood, M. G. AlMohseen, K. A. & A. Jalil, Sh (2014) “Simulation Models for Bekhma Reservoir System (Comparison Study) ”, Journal of University of Duhok, Vol. (17), No. (1): 2014.
- AlMohseen, K. A (2003) “Optimal Operation of multi- purpose multi-reservoir water resources system”, PhD Thesis, Department of Civil Engineering, IIT,Delhi, India.
- Vedula & Majumdar, S Vedula P P Mujumdar (2005). Water Resources Systems, .V, New Delhi, Tata McGraw-Hill Education.
- Hydrologic Engineering Center (1991). Optimization of Multiple-Purpose Reservoir System Operations: A Review of Modeling and Analysis Approaches, U.S. Army Corps of Engineers ,609 Second Street, Davis, CA 95616,(916) 756-1104 .
- Loucks D.and Eelco van Beek (2005). Water Resources Systems Planning and Management, an Introduction to Methods, Models and Applications, Netherland, UESCO 2005 and WL /Delft Hydraulics.
- Klipsch, D. J (2009). Reservoir operations modeling with HEC-ResSim , Hydrologic Engineering Center, U.S. Army Corps of Engineers Davis, CA. 530-756-1104 .
- Joan D.Klipsch.Mariln B. Hurst (2007). HEC-ReSim,Reservoir System Simulation User Manual ,version 3.0 U.S. Army Corps of Engineers ,609 Second Street, Davis, CA 95616-4687.
- S.K. JAIN and V.P. SINGH.(2003). Water Resources Systems Planning and Management, Elsevier Science B.V. Amsterdam, the Netherlands.
- AlMohseen, K. A (2008). "Operation of Alaziziya Evaporation Pond Using Simulink Trechnique", Alrafiden Engineering Journal, College of Engineering, Mosul University, Vol.16, No.3, Iraq.
- Steven T. Karris (2008). Introduction to Simulink with Engineering Applications Second Edition Orchard Publications.
- The Math Works, Simulink® Control Design™ (2011). User’s Guide, the Math Works, Inc.3 Apple Hill Drive Natick, MA 01760-2098.
- The Math Works. (1999). Simulink ,Dynamic System Simulation for Matlab, Using Simulink Version 3, The MathWorks, Inc. 24 Prime Park Way Natick, MA 01760-1500.
- Mohammad Karamouz, Ferenc darovszky, Banafsheh Zahraie (2003) Water Resources Systems Analysis ,United States of America, TC409.K37 2003 333.91—dc21, A CRC Press Company, Lewis publishers.
- Ladislav Votruba, Vojtech broza(1989). water management in reservoirs, Elsevier Science Publishers B.V. Sara Burgerhartstraat 25, P.O. Box 211, 1000 AE Aamsterdam, the Netherlands.
- Slobodan P. Simonovic (2008). Managing Water Resources ,Methods and Tools for a Systems Approach, UNESCO Publishing 7, place de Fontenoy, 75352 Paris 07 SP, France.
- Thomas A, McMahon& Russel G.Mein (1978). Reservoir capacity And Yield, Elsevier Science

B.V. 335 Jan van Galenstraat, Amsterdam, the Netherlands.

- B. Roffel· B. H. Betlem (2004). Advanced Practical Process Control, Springer-Veriag Berlin Heidelberg.
- Yang Y. and Soh C.K (2000). Fuzzy logic integrated genetic programming for optimization and design . Journal of Computing in Civil Engineering . ASCE, vol .14(40) .pp.244-254.
- Al-Gazzal, AW. M. Y (2002). Optimal Water Utilization from Tigris Basin Reservoirs North of Fatha for Hydroelectric Power Generation. Ph.D. Thesis Ph.D. Thesis, College of Engineering, Water Resources Department, University of Mosul, 2002.
- Roffel· B. H. Betlem (2004). Advanced Practical Process Control, Springer-Veriag Berlin Heidelberg.
- Qibo Mao • Stanislaw Pietrzko(2013). Control of Noise and Structural Vibration, A ATLAB®-Based Approach, Springer-Verlag London .
- S. Sumathi .Surekha p (2010 .Computational Intelligence Paradigms Theory and Applications using MATLAB, Taylor and Francis Group, LLC. 6000 Broken Sound Parkway NW, Suite 300.
- Ross,T.J.,1995. Fuzzy Logic with Engineering Applications. McGraw-Hill, New York .
- Tze-Fun Chan. Keli Shi (2011).Applied intelligent control of induction motor drives. John Wiley & Sons (Asia) Pte Ltd, 2Clementi Loop, #02-01, Singapore 129809.

THE IMPACT OF THE TYPE 3 IONIC LIQUID VISCOSITY ON THE ELECTROPLATING PROCESS OF SN, ZN AND ZN/SN ALLOYS

HAVAL **A**.H.**B**ARWARI
Dept. of Chemistry, Faculty of Science, University of Duhok, Kurdistan region-Iraq

(Received: September 1, 2014 ; Accepted for publication: March 1, 2015)

ABSTRACT

In this study the impact of type 3 ionic liquid viscosity investigated on the electroplating process of Sn, Zn and Zn/Sn alloys. Three different composition of type 3 ionic liquid were used by altering the molar ratios and type of hydrogen bond donor applied with 1mol of quaternary ammonium salt choline chloride in the preparation process as follow:1 mol ChCl:2 mol urea(Reline),1mol ChCl:1mol urea:1mol ethylene glycol(Hybride) and 1mol ChCl: 2 mol ethylene glycol(Ethaline). It had been shown that the electrodeposition process differ widely by the change in the ionic liquid's viscosity. Also it was found that the oxidation and reduction potentials peaks of Sn − Zn and Zn/Sn alloys were shifting to high negative values when the ionic liquid was changed from ethaline to reline and hybride. Hybride and reline had higher viscosity than ethaline so there was a shift in the oxidation and reduction potential peaks of metal species. The difference in the electrodeposition process of Sn, Zn and Zn/Sn alloys has been shown in this research. Surface morphology has been studied by SEM (scanning electron microscopy) for each of the above metals both individually and as alloys. In addition, elemental analysis was carried out along with SEM by using energy dispersive analysis by X-rays (EDAX) for coated zinc and tin both as individual and as a mixture after their surface morphologies were determined. Finally, cyclic voltammetry for zinc and tin was conducted in each individual ionic liquid by Ivion potential instrument and their voltammograms have been determined. The effect of altering the viscosity of the ionic liquid on the reduction and oxidation potentials' peaks of zinc and tin were also examined both separately and as alloys.

***KEY* WORDS**: metals, electroplating, ionic liquid, viscosity, alloy, ***cyclic voltammetry*.**

INTRODUCTION

Electroplating is a process by which one metal is deposited onto another which can then be applied for such purposes as decorative and metal protection from corrosion (Kanani, 2004). In this process, an electrolytic cell is applied which is composed of metal, metal salts and electrolyte. Metal is placed as the negative charge (cathode) and dipped into the electrolyte solution which contains metal salt ions; due to the opposite charges the metal salt ions which have positive charge are attracted toward the metal (cathode).Furthermore, electrodeposition is widely used in such industries as automobile, airplanes, electronics, jewellery and toys (Lowenheim, 1974).

Ionic liquids are ionic materials with a melting point below 100 ℃ ,in other words, are classified as salts that are liquid below 100 ℃ (Welton, 1999). They have been primarily studied for synthetic and electrochemical applications,but most of the research has focused on imidazolium cations with discrete anions such as BF^{-4},BF^{-6} and $(F_3CSO_2)_2N^-$ because they possess large potential windows,high conductivity and low viscosity (Wasserscheid and Welton, 2003). All aspects of electroplating from these liquids were covered by Endres(Endres 2002 and Endres 2004), but the fundamental aspects of electrochemistry in these ionic liquids were reviewed by Compton and coworkers(Buzzeo et al.,2004),and other electrochemical aspects are described in a book by Ohno(Ohno, 2005). Although the ionic liquids with discrete anions have significant potential for the electrodeposition of electronegative metals such as aluminium. Issues such as toxicity and availability limit their large scale practical use (Endres, 2002).

Ionic liquids have shown an enormous increase in their interest in the last decades. They are used in a wide range of applications including: solvent for organic synthesis and biological reactions due to their low volatility, material separation

processes and electrochemistry (Seddon and Holbrey, 1999; Buzzeo et al.,2004).

Electrodeposition is one of the well-known applications of electrochemistry which is widely used in industry in the last decade (Endres, 2002). Traditionally, modern industries were applying aqueous solution in the electroplating process due to the high solubility of metal salts and electrolytes which produces a highly conducting solution.

However, since water has a relatively narrow potential window, the deposition of metals with large negative reduction potential such as Cr and Zn is hindered by poor current efficiencies and hydrogen embrittlement of the substrate and that is why water or other aqueous electrolytes are no longer used for carrying out the electroplating experiments (Haerens et al., 2009). The reason behind choosing non-aqueous electrolytes was mainly to get rid from drawbacks of water as well as to carry out the electroplating process for the refractory metals such as Ti, Al and W (Abbott et al., 2006). Since ionic liquids possess such practical benefits as: wide potential window, high solubility of metal salts, absence water and high conductivity, they are normally preferable to be used in the area of electroplating comparably to the other non-aqueous solvents (Endres & Zein El Abedin, 2003; Endres, 2004; Endres et al., 2006; Steward et al., 2004; Abbott and McKenzie, 2006; Galinski et al., 2006).

Ionic liquids are normally prepared by starting with a simple quaternary ammonium halide and lowering the freezing point by complexing the anion to effectively delocalise charge (Abbott et al., 2007). The general formula of these eutectic based ionic liquids is written as follow: R1R2R3R4NX: z Y and these ionic liquids are divided into three types depending on the complexing agent Y;

Type 1 Y = MClx, M = Zn, Sn, Fe, Al, Ge

Type 2 Y = MClx *Æ* yH2O

Type 3 Y = RZ, Z = CONH2, COOH, OH4

The physical properties and electrochemistry of Type 1 and 2 ionic liquids with variety of metals have been reported (Abbott et al., 2001-a, Abbott et al., 2001-b, Abbott et al., 2004-a, and Abbott et al., 2004-b).

In this study Type 3 ionic liquid was used which is formed by combining choline chloride(ChCl) as the quaternary ammonium salt with urea and ethylene glycol(EG) as the hydrogen bond donors. In most of the studies, choline chloride was chosen as the quaternary ammonium salt since it is cheap, non-toxic and biodegradable; therefore, it can be applied economically for large-scale processes (Abbott et al., 2006).

The physic-chemical characteristics of ionic liquids are highly affected by changing the component ion structure and design of ionic liquid. Viscosity is an important parameter for any ionic liquid used as electrolyte solution; since Type 3 ionic liquids are in the solid state at room temperature, there are only few studies dealing with their physical properties. Ionic liquids possess different viscosity; the reason for that is the difference in the composition of the starting materials used in their preparations.

The aim of this study is to find the effect of viscosity on the electrochemical properties of Type 3 ionic liquid by altering the molar ratio of starting materials in the preparation of Type 3 ionic liquid as in the following orders: 1mol ChCl: 2 mol urea, 1mol ChCl: 1 mol urea: 1 mol EG, 1mol ChCl: 2 mol EG.

MATERIAL AND METHODS

Cholinechloride $(HOC_2H_5N(CH)_3^+Cl^-)(ChCl)$ (Aldrich 99%), ethylene glycol (EG) (Aldrich 99+ %), urea (Aldrich >99%), $SnCl_2$ and $ZnCl_2$ were used as received. The eutectic mixtures were formed by stirring different molar ratios of ethylene glycol (Aldrich 99+ %) and urea (Aldrich >99%) with 1 mol of choline chloride (ChCl) (Aldrich 99%), and then the mixtures were heated at $50-60℃$ until homogeneous, colorless liquids formed. The molar ratios of materials mixed were 1 mol of choline chloride (ChCl) (Aldrich 99%) with 2 mol of ethylene glycol (Aldrich 99+ %). The ionic liquid formed is commonly named as ethaline which is composed of 1mol ChCl: 2 mol EG. In the second eutectic,1 mol of choline chloride (ChCl) (Aldrich 99%) is mixed with 1 mol urea (Aldrich >99%) ,and 1 mol of ethylene glycol (Aldrich 99+ %) to form hybride, and the third ionic liquid (reline) is formed by mixing1 mol of choline chloride (ChCl) (Aldrich 99%) with 2 mol of urea (Aldrich >99%) .

The electrodeposition process was carried out by bulk deposition. 0.5M of $ZnCl_2$, 0.1M of $SnCl_2$, and a mixture of 0.5M $ZnCl_2$: 0.1M $SnCl_2$ were individually added to each ionic liquid and heated with continuous stirring at a temperature range of

50-60 ℃ until homogeneous, colorless solutions formed.

The electroplating was then carried out by immersing mild steel and Ti mesh electrodes into 100 ml beaker. The mild steel was cathode and Ti mesh was anode. The electric field was then applied, the voltages applied were 3, 4, 5Volts, for 2.5,3,20,30,35,45,60 min, and the current densities used were 0.050, 0.060, 0.12, 0.204, 0.23 and 0.368 $A\,cm^{-2}$.

The cathode (mild steel) was degreased in detergents for 5 min, rinsed thoroughly in deionized water and then dried, and after that, it is degreased in dichloromethane for 5 min, rinsed in deionized and then dried before and after carrying out the electrodeposition for each plate. The anode (Ti mesh) was immersed in dichloromethane for 5 min, thoroughly rinsed in deionised water and then dried, before and after carrying out the electrodeposition for each plate. The surface morphologies were then determined for three samples both zinc and tin individually and as a mixture of zinc and tin alloys in each ionic liquid by scanning electron microscopy (SEM).The scanning electron microscopy used in this project was Philips XL30 ESEM and it had a resolution of 2.0 nm at 30 kV and 10 mbar H_20 vapour with EDAX EDX-detector with software version 3.3. Energy dispersive analysis by X-rays (EDAX) was used for elemental analysis for each coated plate.

Voltammetry was conducted by applying an Ivion potential. A three-electrode system was used which consists of a platinum microelectrode (0.5 mm diameter), a platinum counter electrode and a silver wire as a reference electrode. The working electrode was polished with 0.3 μm alumina paste, rinsed and dried prior to all measurements. All voltammograms were performed at $50-60℃$, and a scan rate of $20\ mVs^{-1}$.

RESULTS AND DISCUSSION

The results for the surface morphologies obtained from SEM show the bulk deposition of zinc from urea and EG based ionic liquids in Fig. 1, 2, and 3.

The energy dispersive analysis by x-rays (EDAX) showed that the proportion of zinc deposited was 92.07% in ethaline, 84.69% in hybride and 90.21% in reline. The reminders being either iron 9% with only traces of chlorine 5% or both as shown in Fig. 4, 5, and 6. Ethaline is considered as the best ionic liquid according to the EDAX results since the mild steel is well coated by zinc and the proportion of zinc deposited is higher in its morphology.

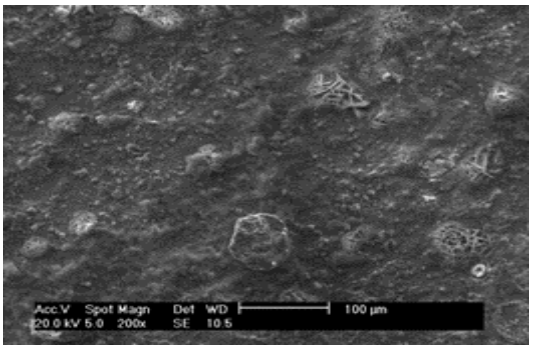

Fig.1: Scanning electron micrograph obtained by the electroplating of 0.5M $ZnCl_2$ in 1ChCl:1Urea:1EG at a current density of 0.12 Amps cm^{-2}, 5V for 35 min.

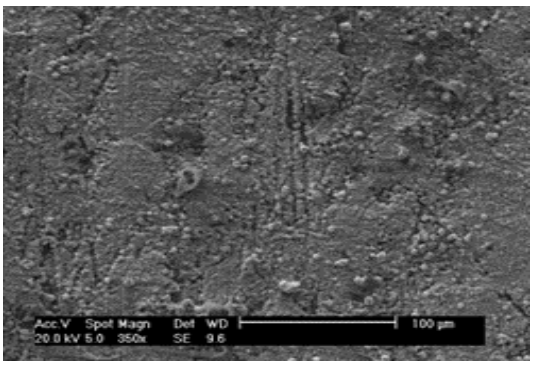

Fig.2: Scanning electron micrograph obtained by the electroplating of 0.5M $ZnCl_2$ in 1ChCl:2Urea at a current density of 0.04212Amps cm^{-2}, 5V for 45 min.

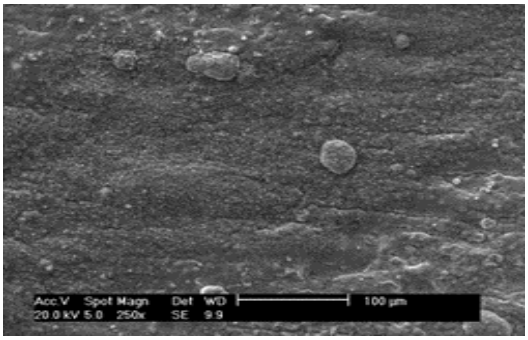

Fig.3: Scanning electron micrograph obtained by the electroplating of 0.5M $ZnCl_2$ in 1ChCl:2EG at a current density of 0.255 Amps cm^{-2}, 3V for 45 min.

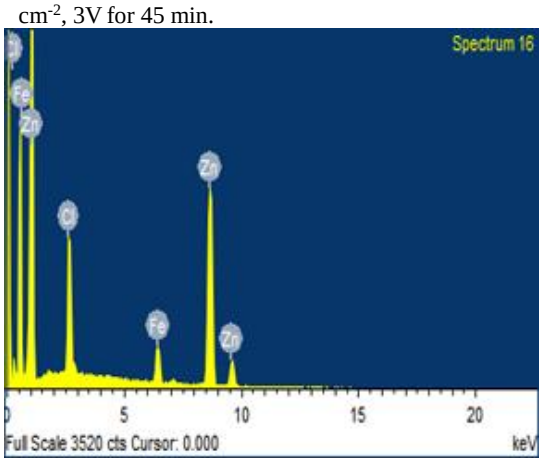

Fig.4**:** EDAX analysis of the sample shown in Fig. 1.

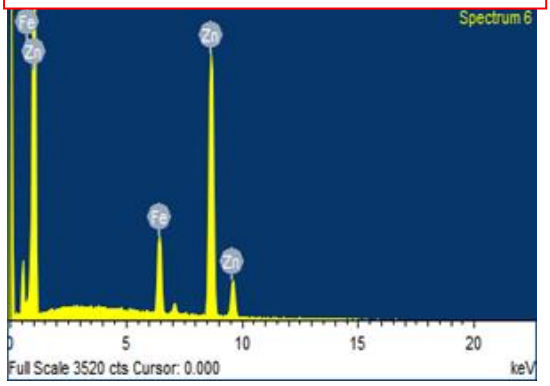

Fig.5: EDAX analysis of the sample shown in Fig. 2.

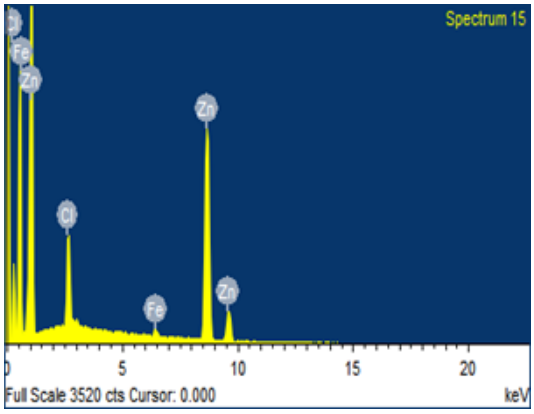

Fig.6: EDAX analysis of the sample shown in Fig. 3.

Depending on the hydrogen bond donor, deposits with different morphologies produced by electrodeposition of a mixture of 0.1M $SnCl_2$:0.5M$ZnCl_2$. In the case of the hybride ionic liquid, the deposit was made up of cubic crystallites which are similar to those found in Fig. 7. In reline and ethaline, clusters of sands were formed as a result of deposition of both tin and zinc on the mild steel as shown in Fig.8 and Fig.9.

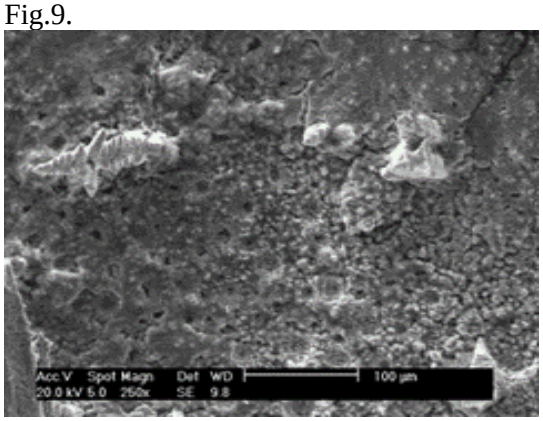

Fig.7: Scanning electron micrograph obtained by the electroplating of 0.5M $ZnCl_2$:0.1M $SnCl_2$ in hybride at a current density of 0.23 Amps cm^{-2}, 5 V for 35 min.

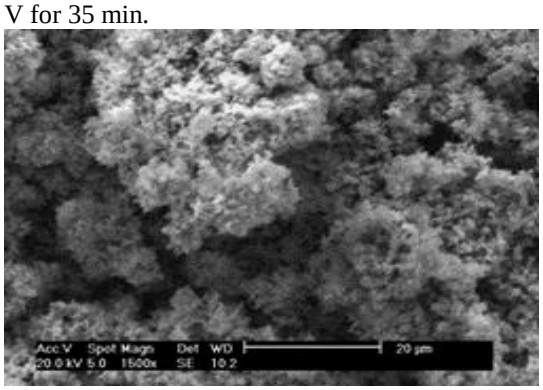

Fig.8: Scanning electron micrograph obtained by the electroplating of 0.5M $ZnCl_2$:0.1M $SnCl_2$ in reline at a current density of 0.050Ampscm^{-2}, 5 V for 60 min.

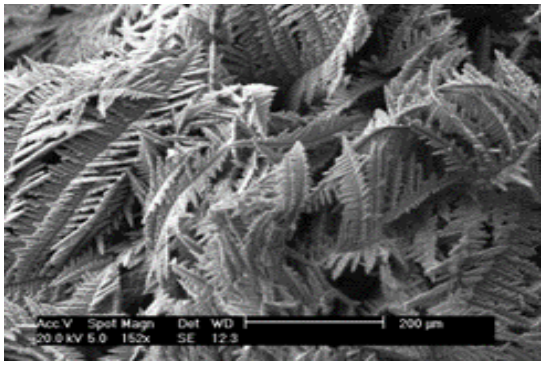

Fig.9: Scanning electron micrograph obtained by the electroplating of 0.5M ZnCl2:0.1M $SnCl_2$ in ethaline at a current density of 0.368 Amps cm^{-2}, 5 V for 20 min.

The EDAX showed that the quantity of zinc deposited was 89.53% in hybride with 5.96%Sn and 4.1%Cl as shown in Fig. 10. The EDAX showed that the majority of the deposited species was zinc 88.7% in reline with the 9.46% being Sn and 1.90% iron as shown in Fig. 11. There is no chlorine in reline compared to hybride. However, EDAX showed much lower proportion of zinc deposited around 49.18% in ethaline (Fig. 12) compared to 89.53% in hybride (Fig. 10) and 88.7% in reline (Fig. 11), while the amount of Sn is 47% in ethaline (Fig. 12), and it is much higher than 5.96% in hybride (Fig. 10), and 9.46% in reline (Fig. 11). EDAX also showed the presence of 3.8% Cl in ethaline. The EDAX results show that zinc and tin metals were not deposited according to their molar ratios, although different proportions of these metals were dissolved in all three ionic liquids. It is evident that reline and hybride are the best ionic liquids for electroplating a mixture of zinc and tin since zinc and tin deposited as a mixture in these ionic liquids.

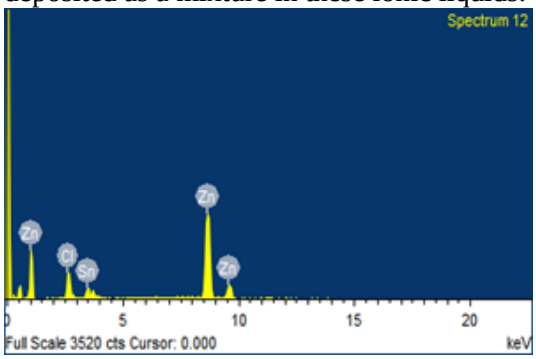

Fig.10: EDAX analysis of the sample shown in Fig. 7**.**

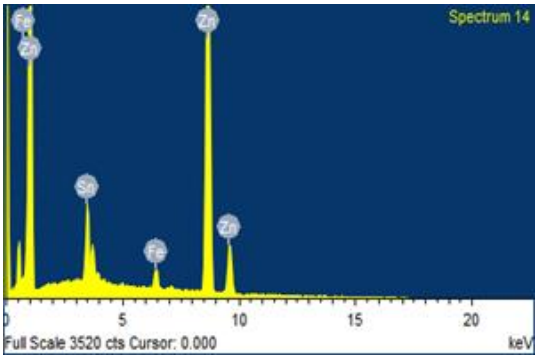

Fig.11: EDAX analysis of the sample shown in Fig. 8.

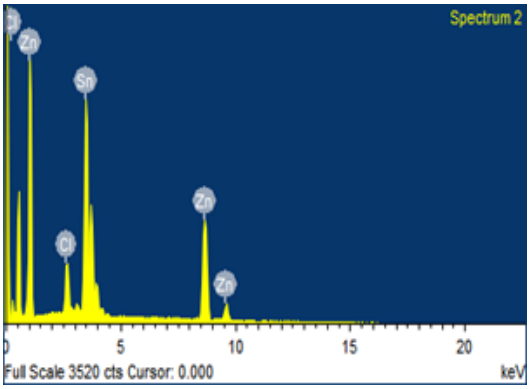

Fig.12: EDAX analysis of the sample shown in Fig. 9.

The electrodeposition of tin has also produced different surface morphologies based on the ionic liquids were used. For instance, in the case of hybride (Fig.13), more dendritic clusters formed. In reline (Fig. 14) the crystals are apparently smaller than ethaline (Fig. 15).

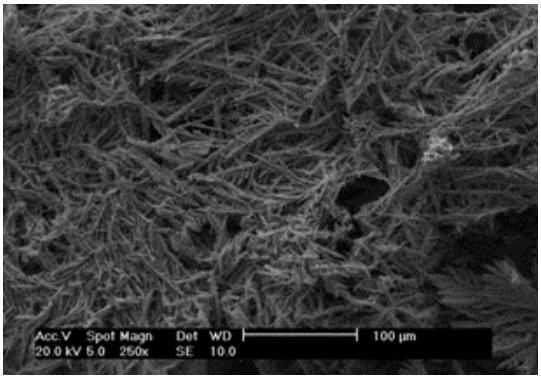

Fig.13: scanning electron micrograph obtained by the electroplating of 0.1M $SnCl_2$ in hybride at a current density of 0.5 Amps cm^{-2}, 5 V for 35 min.

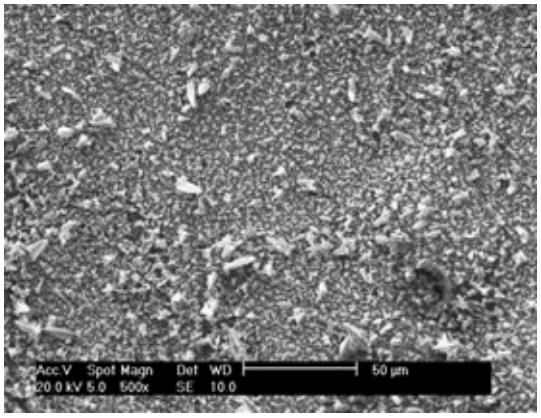

Fig.14: Scanning electron micrograph obtained by the electroplating of 0.1M $SnCl_2$ in reline at a current density of 0.060Amps cm^{-2},5V for 30 min.

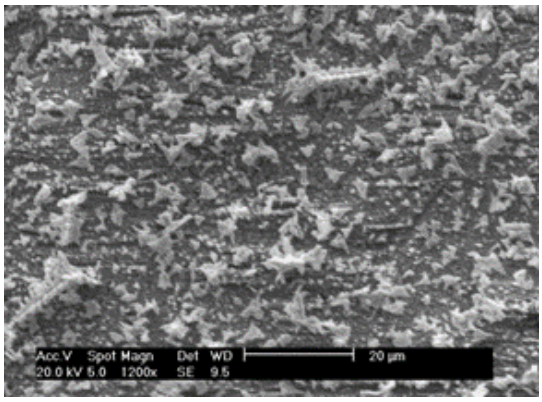

Fig.15: Scanning electron micrograph obtained by the electroplating of 0.1M $SnCl_2$ in ethaline at a current density of 0.204 Amps cm^{-2}, 3 V for 3 min.

In hybride, the proportion of tin is 96.92%, Cl 1.21% and Fe 1.87% (Fig. 16). In reline, iron comprises 42.89% of the deposition occurred and tin 57.11% according to EDAX (Fig. 17). EDAX (Fig. 18) showed that 51.63% of tin (Sn) was deposited on the mild steel and 48.37% was Iron (Fe) in ethaline. Hybride is considered as the best ionic liquid for the tin electroplating since the large proportion of tin is deposited.

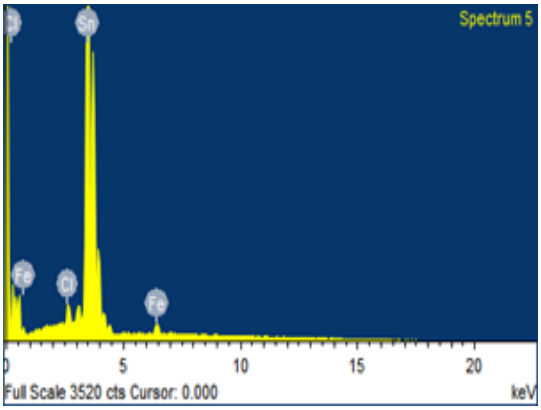

Fig.16: EDAX analysis of the sample shown in Fig. 13**.**

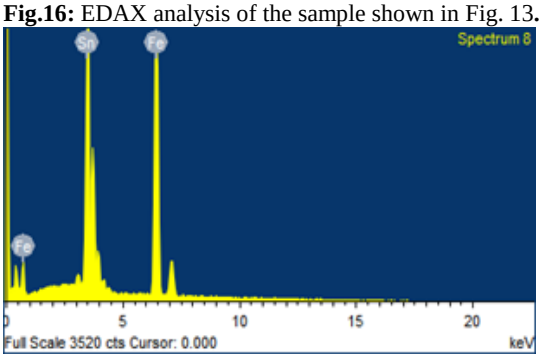

Fig.17: EDAX analysis of the sample shown in Fig. 14**.**

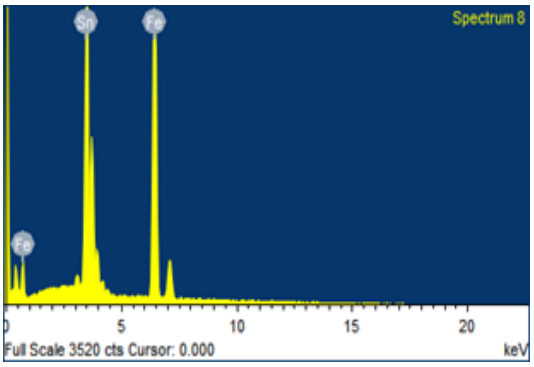

Fig.18: EDAX analysis of the sample shown in Fig. 15.

Cyclic voltammetry is the most effective electroanalytical technique for the mechanistic study of redox systems (oxidation-reduction systems) (Kissinger and Heineman, 1983; Shippy and Lu, 2007). The rapid scan of the electrode potential of redox couples can be made by cyclic voltammetry. A couple can then be characterized once their potential peaks appear on the cyclic voltammogram (Abbott et al., 2001). In this technique, the current developed is measured when the voltage is in excess of that, and it is performed by cycling the potential of the working electrode, and measuring the current results (Seddon and Holbrey, 1999). A cyclic voltammogram is obtained by measuring the

current at the working electrode during the potential scans (Abbott et al., 2001). In cyclic voltammetry, the oxidation and reduction process occur on the working electrode (platinum) and the current is measured as a function of the constant applied potential. In reduction process of both tin and zinc, the deposition of electrons occur onto the surface of working electrode, and the charge of metals (tin and zinc) changes from +2 to 0 as shown below.

$Zn^{+2} + 2e \longrightarrow Zn$ (Reduction)

$Sn^{+2} + 2e \longrightarrow Sn$ (Reduction)

However, in oxidation process stripping of electrons occurs from the electrode and the charge of metals change.

$Zn \longrightarrow Zn^{+2} + 2e$ (Oxidation)

$Sn \longrightarrow Sn^{+2} + 2e$ (Oxidation)

The scanning process for reduction normally runs from negative potential to positive one as shown in arrows labelled in Fig. 19-21 whereas for oxidation process it runs from the positive potential towards the negative. The effect of viscosity can clearly be seen on the oxidation and reduction potentials of tin and zinc. For instance, the peak oxidation potential for tin in ethaline is approximately -1.2V (Fig. 19) while it is roughly -0.1V in hybride (Fig. 19) and -0.15V in reline (Fig. 19). The shift in the peak reduction potentials in both hybride and reline is due to the viscosity effect .The viscosity of ethaline is lower than that of hybride and reline

Ethaline>hybride>reline

Increasing the viscosity(η)

According to walden's rule $\Lambda_m \propto 1/\eta$, the ionic liquid viscosity is indirectly proportional with molar ionic conductivity (Λ_m) so the conductivity will decrease as the viscosity increases since the increase in viscosity will decrease the diffusion coefficient which in turn will slow down the rate of mass transport in solution(Buzzeo et al.,2004). Thus this will then inhibit charge carriers and their mobility in solution at room temperature. As a result, the net diffusion of ions into the metal surface will be reduced (Buzzeo et al., 2004). This means that the diffusion of ions in the case of ethaline is higher than that of hybride and reline. Since the ion transport in reline is quite slow so that it would be difficult for ions to move onto the surface of the electrode. That is why the peak reduction potential for the tin is -0.45V in ethaline while it is – 0.46V in hybride and -0.52V in reline(Fig. 19).This is because the diffusion of ions onto the surface of electrode is slow in the case of reline comparably to ethaline and hybride due to the viscosity effect. Thus not many ions will be oxidized or reduced so the peak for the reduction potential has shifted into a highly negative value (-0.52V) in reline (Fig. 19).

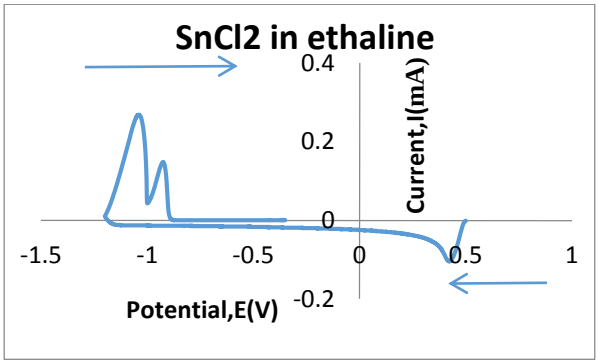

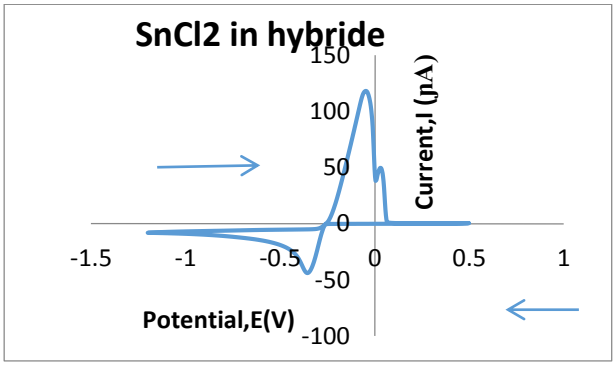

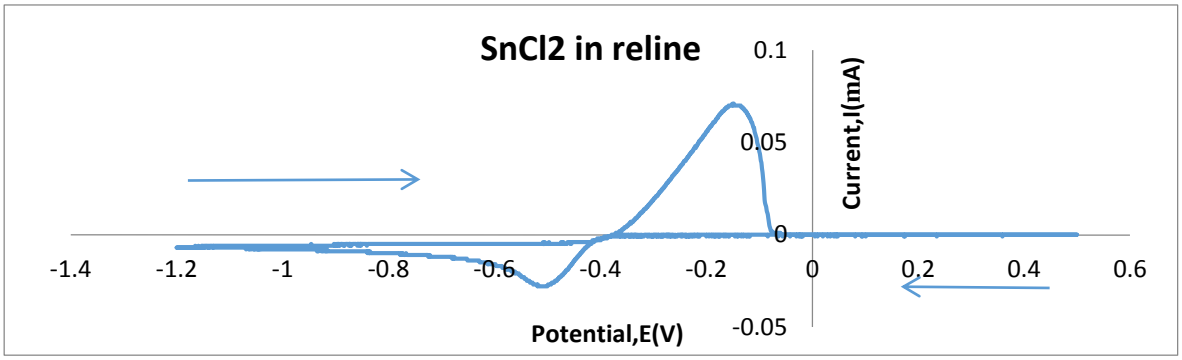

Fig.19:Voltammograms (scan rate 20 mVs^{-1}) for a Pt microdisc electrode (0.5 mm diameter) immersed in ethaline, hybride and reline respectively, each one contains 0.1M $SnCl_2$.

The peak oxidation potentials for tin and zinc in a mixture of 0.5M $ZnCl_2$: 0.1M $SnCl_2$ in ethaline are (-0.2V and -0.83V) respectively (Fig. 20) whereas in hybride are (-0.1V and -0.75V) and (-0.18V and -0.8V) in reline (Fig. 20).There is a shift in the oxidation potential peak in both reline and hybride again due to the viscosity effect. The peak reduction potentials for tin and zinc in a mixture of 0.5M $ZnCl_2$: 0.1M $SnCl_2$ in ethaline (Fig. 20) are (-0.5V and -1.02 V) respectively whereas in hybride are (-0.47V and -1.0V) and (-0.49 V and -1.07V) in reline (Fig. 20).There is a noticeable shift again in the peak reduction potentials in both reline and hybride due to the viscosity effect. The peak oxidation potentials for zinc in both urea (reline Fig. 21) and ethylene glycol (ethaline Fig.21) based ionic liquids are (-0.78 V and -0.9 V) respectively, yet in hybride (Fig. 21), it is -0.7V. The value of the peak reduction potential for zinc in ethaline is roughly -1.3 V while it is roughly -1.25 V in hybride and -1.2 V in reline. These results show a clear shift in the peak reduction potential to a highly negative potential from ethaline to hybride to reline due to the viscosity effect.

Ethaline>hybride>reline

Increasing the viscosity(ɳ)

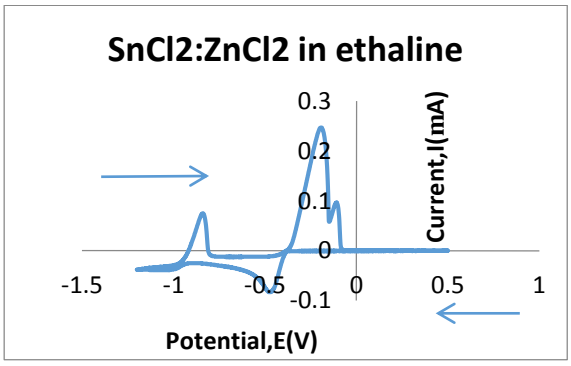

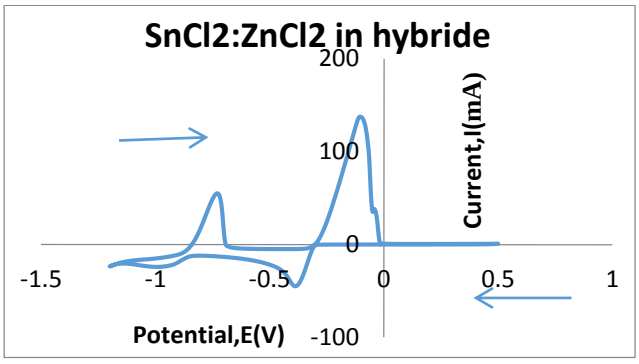

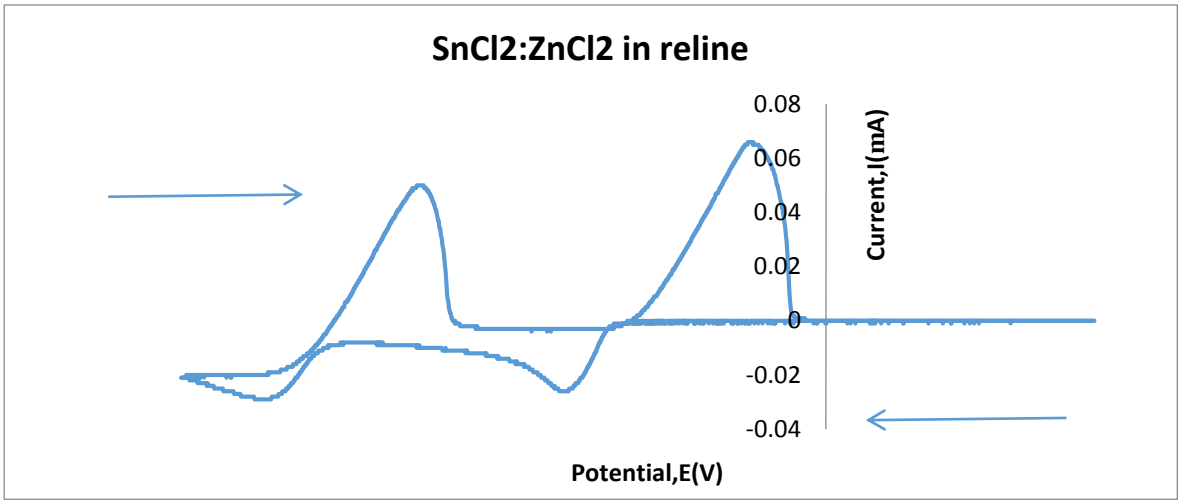

Fig.20: Voltammograms (scan rate 20 mVs^{-1}) for a Pt microdisc electrode (0.5 mm diameter) immersed in ethaline, hybride and reline respectively, each one contains 0.1M $SnCl_2$ and 0.5M $ZnCl_2$.

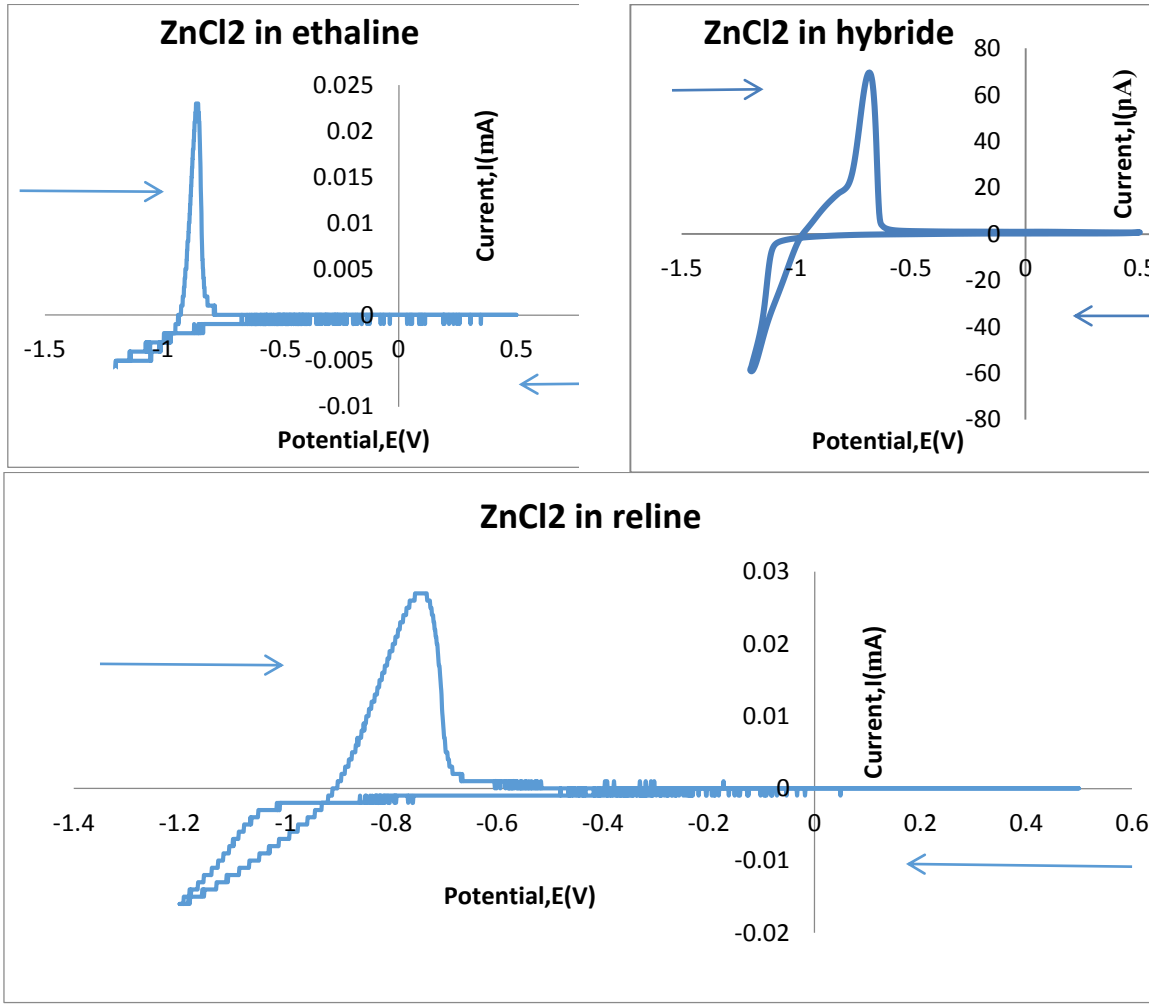

Fig.21: Voltammograms (scan rate 20 mVs^{-1}) for a Pt microdisc electrode (0.5 mm diameter) immersed in ethaline, hybride and reline respectively, each one contains 0.5M $ZnCl_2$.

CONCLUSION

This study showed that ionic liquids based on eutectic mixtures of choline chloride and hydrogen bond donors such as ethylene glycol and urea can be used as electrochemical solvents instead of water to carryout electrochemical applications. It is found that zinc and tin can be electroplated as alloys and also separately in these ionic liquids. It is shown that the alloy morphology and composition alter by changing the DES and also choosing a proper ionic liquid for electrodeposition affects mainly on the alloy's morphology and composition. The difference in the ion transport in term of the difference in the ionic liquid viscosity has also been clarified. It was found that both oxidation and reduction potentials of zinc and tin are changed by altering the ionic liquid viscosity. For instance, in the case of both reline (1 mol ChCl: 2 Urea) and hybride (1 mol ChCl: 1 mol EG: 1 mol urea), the shift in both oxidation and reduction potentials are found to be higher than that of ethaline (1 mol ChCl:2 mol urea) since the viscosity of reline and hybride are higher than that of ethaline.

The electroplating process was also found to be affected by the ionic liquids viscosity, since the viscosity of ethaline was lower than that of hybride and reline, the diffusion rate of both zinc and tin ions onto the electrode surface is quicker that caused more larger quantity of ions deposited onto the electrode surface with time comparably to hybride and reline.

The results showed that ethaline is the best ionic liquid to obtain a large proportion of zinc deposit while hybride and reline to obtain a highly proportion of a mixture of zinc and tin deposit and hybride to achieve a large proportion of tin deposit.

REFERENCES

- **Kanani,** N. (2004). Electroplating: Basic Principles, Processes and Practice; Elsevier Advanced Technology: Oxford, U.K.
- **Lowenheim**, (1974).Frederick Adolph. Modern Electroplating. 3rd ed. New York, N.Y.: J. Wiley and Sons.
- **Welton**, T. (1999). *Chem. Rev.*, 99, pp. 2071.
- **Wasserscheid**, P. and Welton, T. (2003). *Ionic Liquids in Synthesis*, Wiley-VCH Verlag, Weinheim, Germany.
- **Endres, F**. (2002).Ionic liquids: solvents for electrodeposition of metals and semiconductors. ChemPhysChem 3, pp.144-154.
- **Endres, F**. (2004). *Phys. Chem.* 218, pp.255.
- **Buzzeo** M**.C.,** Evans, R.G., and Compton, R.G. (2004) ChemPhysChem 5 .pp.1106.
- **Ohno,** H. (2005). *Electrochemical Aspects of Ionic Liquids*, John Wiley& Sons, New York.
- **Seddon**, K.R. and Holbrey, J.D. (1999).Ionic liquids. Clean Products and Processes 1, pp.223-236.
- **Haerens**,K., Matthijs,E., Chmielarz,A., and B. V. Bruggen, B. V. (2009).The use of ionic liquids based on choline chloride for metal deposition: A green alternative?.*Journal of Environmental Management*.90:pp.3245-3252.
- **Abbott**, A.P., Capper, G., Davies, D.L., and Shikotra, P.(2006).Processing metal oxides using ionic liquids. Mineral Processing and ExtractiveMetallurgy(Trans.Inst.Min.Metall.C)115(1),pp.15-18.
- **Endres, F**. and Zein El Abedin,S. (2003). Nanoscale electrodeposition of metals and *s*emiconductors from ionic liquids. Electrochimica Acta 48:pp. 3053–3061.
- **Endres**, F. (2004).Ionic liquids:promising solvents for electrochemistry.Zeitschrift fuer Physikalische Chemie 218:pp.255-283.
- **Endres, F.**, Liu, Q.X., and Zein El Abedin, S., (2006).Electroplating of mild steel by aluminium in a first generation ionic liquid:a green alternative to commercial Al-plating in organic solvents. Surface and Coatings Technology.201:pp.1352-1356.
- **Steward, A.F**., Pringle, J.M., and MacFarlane, D.R., (2004).Ionic liquids dan overview. *Australian Journal of Chemistry*.57:pp.113-119.
- **Abbott, A.P.**, and McKenzie, K.J. (2006). Application of ionic liquids to the electrodeposition of metals. *Physical Chemistry Chemical Physics*.8:pp.4265-2479.
- **Galinski, M.**, Lewandowski, A., and Stepniak, I. (2006).Ionic liquids as electrolytes Electrochimica Acta.51:pp.5567-5580.
- **Abbott,** A. ,Capper, G. , McKenzie, K.and K. Ryder, (2007).Electrodeposition of zinc-tin alloys from deep eutectic solvents based on choline chloride.*Journal of Electroanalytical Chemistry*,599,pp.288-294.
- **Abbott,** A.P., Capper, G., Davies, D.L., Munro, H.L., Rasheed, R.K., and Tambyrajah, V. (2001-a). *Chem. Commun.*PP.2010.
- **Abbott,** A.P., Capper, G., Davies, D.L., Rasheed, R.K. and Tambyrajah, V. (2001-b).T. Inst. Met. Fin. (79):pp. 204.
- **Abbott,** A.P., Capper, G., Davies, D.L., and Rasheed, R.K. (2004-a). *Inorg. Chem.* 43:pp. 3447.
- **Abbott,** A.P., Capper, G., Davies, D.L., and Rasheed, R.K. (2004-b). *Chem. Eur. J*. (10):pp. 3769.
- **Kissinger**, P. T., and Heineman, W. R. (1983). "Cyclic Voltammetry," *Journal of Chemical Education*, 60, pp.702.
- **Shippy**,S., and Lu, M.(2007). *Cyclic Voltammetry*, pp.1-2.Available online at:www.chem.uic.edu/chem421/cv.PDF.

MEASUREMENT OF DEFLECTION OF A QUARTZ TUNING FORK

DIYAR **A**. **S**. **S**ADIQ
Dept. of Physics, College of Science, University of Zakho, Kurdistan region-Iraq

(Received: September 4, 2014; Accepted for publication: April 6, 2015)

ABSTRACT

The purpose of this article is to measure the deflection of a quartz tuning fork based on using Michelson interferometer. A comparison with simulated model has been done and explained. The measured deflection of a tuning fork is $1.7\ \frac{nA}{nm}$. **This work has been done at the university of Carl von Ossietzky Universität Oldenburg/Germany.**

KEYWORDS: Shear-force feedback, Quartz tuning fork and Michelson interferometer.

1. INTRODUCTION

Studying near-field properties of nanostructures allows the investigation of a number of interesting physical phenomena within sub-wavelength size.Depending on the shape, size and environment of the nanostructures, the near-field essentially decays exponentially when moving far from the surface and it is almost at sub-wavelength scale, typically less than 100 nm. To probe the near field of the nanostructures, it is necessary to bring a sub-wavelength size tip into close proximity to a sample surface at a fixed distance, certainly smaller than the near field strength, and raster scan across the nanostructure and consequently render the non-propagating near field. In order to keep the distance of the tip-sample, an active feedback loop control is required [1]. For example, scanning tunnel microscope uses tunneling electron feedback to control the distance between the tip and the sample [2]. Karrai and Grober [3] introduced the quartz tuning fork (TF) as a noncontact technique for keeping the tip-sample distance. This is based on measuring the damping of the resonant oscillation of the tip that vibrates parallel to the surface of the sample. Shear-force feedback represents the effect of the sample surface on the damping of the oscillation (amplitude, and phase) of the tip and provides a spatial resolution. Combining such spatial resolution of an atomic-force microscopy (AFM) with a local near-field at the tip apex (typically metallic tip) allows us to present a microscope technique called scanning near-field optical microscope (SNOM). Due to the fact that SNOM is based on confining the optical energy into a sub-wavelength region (tip radius), certainly a significant heat will be generated. This is one of the critical aspects of using metallic tip for SNOM application and the life time of the tip is limited by the AFM quality [1]. Therefore, it is important to quantify and understand the mechanism of the shear-force feedback by using the TF, in order to avoid any undesired effects that may destroy the tip.

In principle, TF generates current when driving the arms of a TF by applying an external voltage. The resonant frequency of a TF is typically 32768 Hz. The main advantages of a TF are their high mechanical quality factor Q, high amplitude-phase sensitive and large spring constant [4, 5], which allow the TF to sense force in a piconewton (pN) regime [1]. In practice, the tip is glued to one arm of the TF. The fork is then forced to oscillate at its resonance frequency either mechanically by using dither piezoelectric quartz or directly by exciting the TF with voltage at its resonance frequency [6–8]. By using amplitude, phase and frequency, the feedback loop can be controlled. Throughout this work, a combination of the amplitude and the phase of the TF have been used as s feed-back loop control. Depending on the type of the tip probe, the interaction range between the tip and the sample is between 1-100 nm [1]. The closer the tip is to the sample, the higher the spatial resolution and consequently tip-sample forces. The trade-off between the tip-sample distance, the spatial resolution and the friction force acting on the tip is important.

Intensive researches have been reported on the characterization of piezo electromechanical

properties of tuning fork [9-11]. Fiber optical interferometer has been used to measure surface interaction forces and electrical-mechanical piezo properties [11]. A higher harmonic mode of a tuning fork has been characterized based on the using Michelson interferometer [9, 10].

The present work measures optically the deflection (amplitude) of the arm of a tuning fork based on the use of a conventional Michelson interferometer scheme and using the lock-in amplifier. The result has been compared with a simulated model of the experimental setup.

2. Experimental result and discussion

The principle of the TF amplitude measurement is based on the use of a conventional Michelson interferometry scheme [8, 12-13] shown in Fig.1. A coherent linearly polarized beam from a HeNe laser (JDS Uniphase, 4mW, 543.5 nm) is split into two beams with intensities I_1 and I_2 by a non-polarizing beamsplitter. The beam I_1 is focused to one of the TF arms (active arm) by means of an objective to spot size of 1.4 μm. The TF is mounted on a $\boldsymbol{3D}$ translation stage in order to position the active arm of the TF in the focus plane of the objective. The beam I_2 is directed to the mirror $\boldsymbol{M}$ and consequently reflected back. The two reflected beams I_1 and I_2 interfere and the intensity of the interference is recorded by a photo detector (PD).

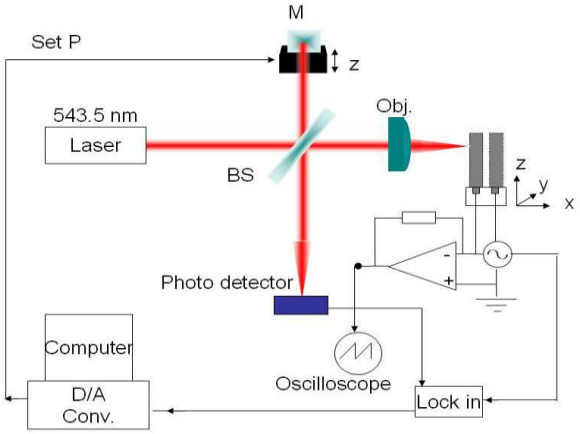

Fig.(1): Schematic diagram of a Michelson interferometer setup for measuring the amplitude of a quartz tuning fork including a laser source of 543.5nm, beam splitter BS, focusing objective and a tuning fork (TF). The setup includes also the schematic diagram of electronics and the controlled data acquisition.

In the case where the two beams have similar intensities $I_1 = I_2$, the output signal detected by the photo detector is proportional to [8]

$$I_{out}(x) = 2 \cdot I_0 \left[1 + cos\left(\frac{4 \cdot \pi \cdot x}{\lambda}\right)\right] \qquad (1)$$

where I_0 is the intensity of the incident light, λ is the wavelength of He-Ne laser, x is the mirror displacement relative to the fixed TF arm and the beamsplitter is considered lossless. The mirror $\boldsymbol{M}$ is mounted on a linear stage in order to control the phase difference between the two beams. First, the active arm of the TF is fixed while the mirror $\boldsymbol{M}$ is moved to vary the phase difference between them and consequently one get a periodic intensity at the detector plane as shown in Fig.2.

In order to increase the sensitivity of the smallest amplitude measurement of the TF arms, the interferometer is positioned at the point $\boldsymbol{P}$ with the corresponding displacement of x_0 , the point where the slope is steepest [11]. Now, we keep the mirror $\boldsymbol{M}$ fixed at the fixed point x_0 (red arrow in Fig.2) and drive the TF at its resonance frequency ($\omega_0 = 2\pi f$) by a variable sinusoidal external voltage ($V(t) = v\sin(\omega_0 t)$). Notice that, the TF excitation has been done electrically. The recorded intensity depends on the TF displacement x_1 , and oscillates at frequency ω_0 according to :

$$I_p(x_1,t) = I(x_0) + I(x_1)\sin(\omega_0 t) \qquad (2)$$

and in terms of displacement :

$$X_p(x_1,t) = x_0 + x_1\sin(\omega_0 t) \qquad (3)$$

where $I(x_0)$ is the optical intensity at position ***P*** and $I(x_1)$ is the varying amplitudes of the optical intensity due to the TF displacement x_1 . From Eq.2 and Eq.3 one can write down the interference intensity form for a TF oscillation and amplitude x_1;

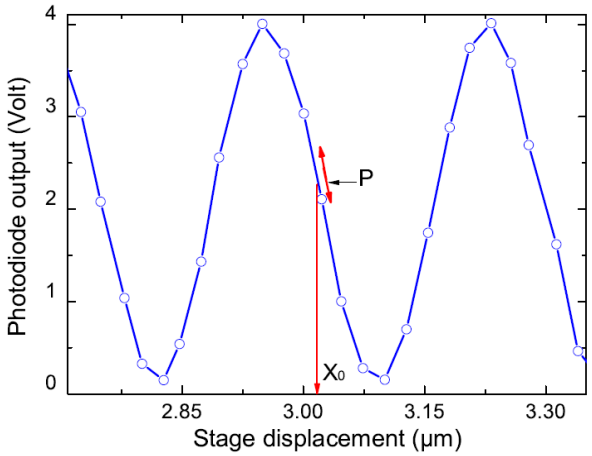

Fig. (1): Intensity of the optical signal oscillates as a function of the mirror displacement. The point P is the active point at position x at which the slope is at maximum.

$$I_p(x_1,t) = I(x_0)(2 + 2\cos\varphi(x_1,t)) \qquad (4)$$

where the phase $\varphi(x_1,t)$ can be written as

$$\varphi(x_1,t) = \frac{4\pi}{\lambda}\cdot X_p(x_1,t)$$

Using Eq.4, one can measure the amplitude x_1 of the TF. In fact, a lock-in amplifier has been used in order to detect the smallest amplitude of the TF (see Fig.2). Then one gets

$$I_{dc}(x_1) = \int_0^{\frac{2\pi}{\omega_0}} A\cos(\omega_0 t)\cdot I_{out}(x_1,t)\,dt \qquad (5)$$

$A\cos(\omega_0 t)$ is the reference signal from the external oscillating voltage. Now the signal to be monitored is a ***dc*** voltage corresponding to the generated ***ac*** current induced by the TF amplitude x_1. At the same time, the TF output voltage (peak-to-peak) has been measured and this corresponds to the current generated by the TF and converted to the voltage by using the current-to-voltage conversion with a gain factor of $10^7\frac{V}{A}$.

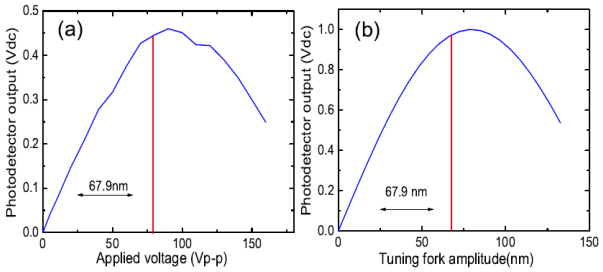

Fig. (2): (a) Measured (b) and calculated (by using Eq.0.17) photodetector signal as a function of the amplitude of the active arm of TF driven by external oscillating voltage. The red line represents the point at which the TF amplitude is deflected by λ/8.

Figure 3(a) and 4(b) show recorded and calculated interferometer readout for large TF amplitude, respectively. The recorded signal of the TF is in terms of voltage. In order to determine the amplitude of TF in terms of displacement, the recorded curve was compare with the calculated one at the point where the TF amplitude is deflected by $\frac{\lambda}{8}$. At this point, the readout of the TF in terms of current (peak-to-peak) is also known. Then, one can measure the TF calibration of current-to-displacement conversion and this gives a root mean

square of 1.7 $\frac{nA}{nm}$. This value is comparable to the value measured by Ref. [8].

ACKNOWLEDGEMENTS

The author would like to thank Professor Dr. Christoph Lienau for the scientific support and devices.

REFERENCE

- Novotny. L and Hecht . B. Principles of Nano-Optics. *CAMBRIDGE*, .2006
- G. Binnig and H. Rohrer. Scanning tunneling microscopy. *Helvetica Physica Acta*, 55:726–735, 1982.
- Khaled Karrai and Robert D. Grober. Piezoelectric tip-sample distance control for near field optical microscopes. *Applied Physics Letters*, .1995 ,44–184:(14)66
- Khaled Karrai and Ingo Tiemann. Interfacial shear force microscopy. *Physical Review B*, 62(19):13174–13181, 2000.
- S. A. Chizhik Vo Thanh and Tran Xuan Hoai. Parameters of tip-sample interactions in shear-mode using a quartz tuning fork afm with controllable q-factor. *Journal of Engineering Physics and Thermophysics*, 82(1):140-148, 2009.
- M. J. Yang W. J. Moore C. H. Yang, T. H. Chang. A low noise transimpedence amplifier for cryogenically cooled quartz tuning fork force sensors. *Review of Scientific Instruments*, 73(7):2713–2716, 2002.
- Khaled Karrai and Robert D. Grober. Piezoelectric tuning fork tip-sample distance control for near field optical microscopes. *Ultramicroscopy*, 61:197, .1995
- Jim Schuck Dan Hessman Peter J. Kindlemann Joao Hespanha A. Stephan Morse Khaled Karrai Ingo Tiemann Robert D. Grober, Jackson Acimovic and Stephan Manus. Fundamental limits to force detection using quartz tuning forks. *Review of Scientific Instruments*, 71(7):2776–2780, 2000.
- Y. Chen R. Toledo Crow, P. C. Yang and M. Vaez Iravani. Near-field differential scanning optical microscope with atomic force regulation. *Applied Physics Letters*, 60(24):2957–2959, 1992.
- Adnen Mlayah Maria Allegrini Pietro Guiseppe Gucciardi, Guillaume Bachelier. Interferometric measurement of the tip oscillation amplitude in apertureless near-field optical microscopy. *Review of Scientific Instruments*, 76(036105):1–3, 2005.
- R. Reifenberger Yexian Qin. Calibration a tuning fork for use as a scanning probe microscope force sensor. *Review of Scientific Instruments*, .2007 ,7–1:(063704)78
- O. Kolosov. P. V. E. McClintock V. B. Efimov, Deepak Garg. Direct measurement of the critical velocity above which a tuning fork generates turbulence in superfluid helium. *Journal of Low Temperature Physics*, .2009 ,461–158:456
- A. K. Gupta R. Bashir S.H. Song G. Zeltzer, J. C. Randel and H. C. Manoharan. Scanning optical homodyne detection of high-frequency picoscale resonances in cantilever and tuning fork sensors. *Applied Physics Letters*, 91:173124, 2007.

پوختە

ئارمانج ژ ڤێ ڤەکولینێ بو پیڤانا لادانا دوولکێ سازدەر یێ کوارتز ب رێکا بەیەکداچوون پیڤێ مایکلسون. بەراوردکرن دگەل مودێلەکێ نواندی یا هاتیە کرن و شروڤەکرن. ئەو لادانا دوولکێ سازدەر ئەوا ان 1.7 nA/nm ب بوو. ئەڤ ڤەکولینە هاتە کرن ل زانکویا کارل ڤون یونیڤێرستات ئولدنبرگ ل وەلاتێ ئەلمانیا.

الخلاصة

ان الغرض من هذا البحث هو قياس انحراف الشوكة الرنانة باستخدام مقياس التداخل لمايكلسون. تمت المقارنة مع موديل تمثيلي. كان مقدار انحراف الشوكة الرنانة مساويا ل $\frac{nA}{nm}$ 1.7 . تم اجراء هذا البحث في جامعة كارل فون اوسيتزكى الالمانية.

SURFACE ROUGHNESS OF SUPER DUPLEX STAINLESS STEEL SAF 2507 DURING TURNING

RAMADHAN **H. G**ARDI , **K**AREEM **A. A**BDULLAH and **H**AWRO **K. S**HAKR
Dept. of Mechanical, College of Engineering, Salahaddin University, Kurdistan Region, Iraq

(Received: September 17, 2014; Accepted for publication: January 7, 2015)

ABSTRACT

This paper presents surface roughness variation with cutting speed and feed rate of 20mm diameter heat treated super duplex stainless steel SAF 2507. The material heat treated at 800ºC for 1 hour ,and dry turning test were conducted at two different cutting speed 12.5m/min and 22.5m/min and five different feed rates (0.06,0.08,0.1,0.12 and 0.14 mm/rev) with constant depth of cut 0.25 mm. The surface roughness of machined surface of heat treated material was found and the results were compared with that of as received condition. Compared to as received material, heat treatment at 800ºC for one hour reduces the surface roughness at lower cutting speed and lower feed rate but this approach inverted at higher cutting speed and lower feed rate. Surface roughness of heat treated SDSS SAF 2507 is higher than that of as received condition for all feed rates during turning with higher cutting speed 22.5m/min. Lower surface roughness can be obtained in as received condition during machining with higher cutting speed and lower feed rate.

KEYWORDS: Duplex, Stainless steel, Surface roughness.

INTRODUCTION

The super duplex stainless steels combine the attractive properties of the ferritic and austenitic stainless steels in just one material, and in this form it possesses better mechanical properties and corrosion resistance than the conventional austenitic stainless steels and ferritic stainless steels. In general Super duplex stainless steels exhibit twice strength compared to austenitic stainless steels with just half of the amount of nickel content in the austenitic stainless steels and this reduces the costs of duplex stainless steels due to reduction of high prices of nickel content [1,2].Super duplex stainless steel SAF 2507 is used in oil and gas industry ,tubing for heat exchanger in refineries ,pipe for sea water transports ,propeller shaft and other product subject to high mechanical loads in sea water and other chloride containing environment[3].

The machining of stainless steels is different in comparison with other types of steels ,its mainly characterized for high strain rate that induce mechanical modification and heterogeneous behavior in generated surface and that take unstable chip formation and vibration.[4].As super duplex stainless steel microstructure consist of random distribution of austenitic and ferritic phase with different properties and each of these phase exhibit in different manner related to cutting and chip formation during machining of it. The surface finish of the component is an important index to evaluate cutting performance in turning operation depend on grain orientation, presence of different phases and cutting condition used during the process. Surface roughness plays a vital role in functioning fatigue life and corrosion resistance of the components since the roughness of the surfaces may form nucleation sites for crack initiation and different types of corrosion.

Ibrahim Ciftci [5] investigated the influence of work piece grade ,cutting tool coating top layer and cutting speed on the cutting force and surface roughness of two different types of austenitic stainless steels AISI 304 and AISI 316.He found that with increasing cutting speed the surface finish value decrease until a minimum value and beyond which they increased .Ihsan Korkot[6] carried turning test to determine optimum machining parameters for machining austenitic stainless steel. They found that the surface roughness value decreased with increasing cutting speed.

Also, W.S. Lin [7] investigated the effect of feed rate and cutting speed on the surface roughness of austenitic stainless steel and reported that increasing feed rate and cutting speed the surface finish of the work piece will deteriorate. K.Philip Selvarage et al[8]studded the effect of cutting condition on the surface roughness of nitrogen alloyed duplex stainless steel. They found

that cutting speed is the most important factors that affect the surface roughness. Literature available on the effect of cutting condition on the surface roughness of super duplex stainless steels is very scare. In the present study the effect of thermal treatment ,cutting speed ,and feed rate on the surface roughness of super duplex stainless steel SAF 2507 have been investigated.

EXPERIMENTAL PROCEDURE :

The work piece material which is used in this study is super duplex stainless steel SAF 2507 rode with the chemical composition given in Table (1). Figure (1) showed the microstructure of super duplex stainless steel in as received condition. The dimensions of the specimens were 120 mm length and 20mm diameters. Figure (2) shows the dimensions of the specimens.

Table (1): Chemical composition of super duplex stainless steel SAF 2507

Element	C	Cr	Ni	Mo	Mn	P	N	Si	S	Fe
Weight %	0.03	25	7.8	4	1.1	0.03	0.25	0.8	0.015	Ball.

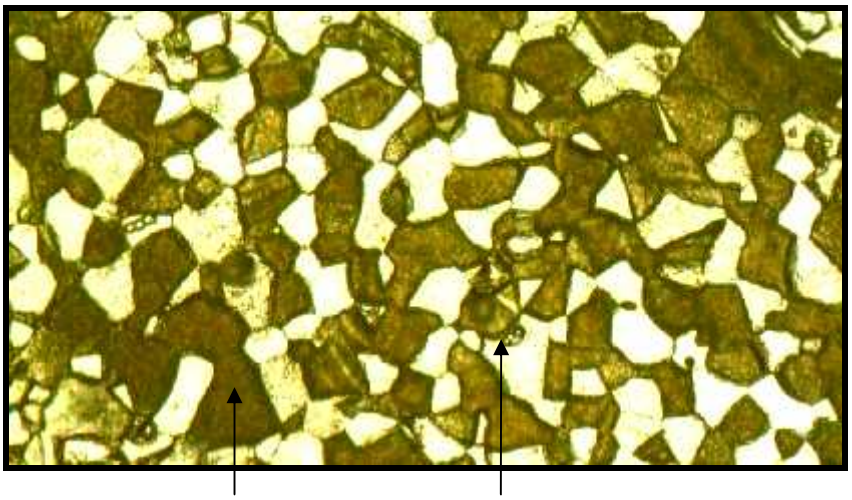

Fig. (1) Microstructure of as received super duplex stainless steel SAF 2507 (x600)

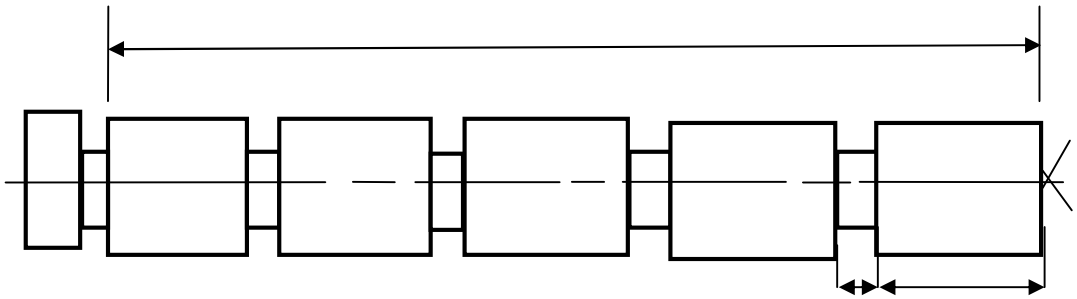

The machining test was performed on the CNC lathe [Machin.type: PROTON 580 CNC, Ser.Nr:134785, Year of constr.:2005, Total power: 15KW, Volt: 400 V, KNUTH Werkzeugmaschinen, Gmbh]. Turning test were conducted without the application of cutting fluid (dry turning)the cutting tool used were TiC insert .Two cutting speed used 12.5m/min and 22.5m/min and five feed rates were selected 0.06,0.08,0.1,0.1.0.12 and 0.14 mm/rev the depth of cut kept constant 0.25 mm. After machining the surface roughness measurement was performed on a Tyler-Hobson surface roughness tester [Taly sur10] figure (3).The measurement were made on the machined surface at three different location and the average value was taken. Moreover for metallographic analyses the specimen were first mechanically polished with the emery paper and then etched chemically according to ASTM standards [9] by ferric chloride and nitric acid reagent in which consist of saturated solution of Fecl3 in HCl to which a little HNO3 is added and etching time equals five minute.

Fig. (3):- Tyler-Hobson Surface roughness measuring device.

RESULTS AND DISSCUSSION:

Experimental results for the surface roughness are given in Table (2). The influence of cutting speed on surface roughness during dry turning of super duplex stainless steel SAF 2507 in as received condition and aged at 800 ºC for 1 hour for five different feed rates (0.06,0.08,0.1,0.12 and 0.14 mm/rev)are shown in figures (4) and (5)

Table (2):- Experimental results for surface roughness

Exp. no	Cutting speed m/min	Feed rate mm/rev.	Surface roughness of as received SAF2507 µm	Surface roughness of heat treated SAF 2507 µm
1	12.5	0.06	2.2	0.52
2	12.5	0.08	1.25	0.55
3	12.5	0.1	0.62	0.81
4	12.5	0.12	0.64	1.06
5	12.5	0.14	0.83	1.5
6	22.5	0.06	0.178	0.4
7	22.5	0.08	0.2	0.5
8	22.5	0.1	0.27	0.57
9	22.5	0.12	0.53	0.62
10	22.5	0.14	0.78	1.25

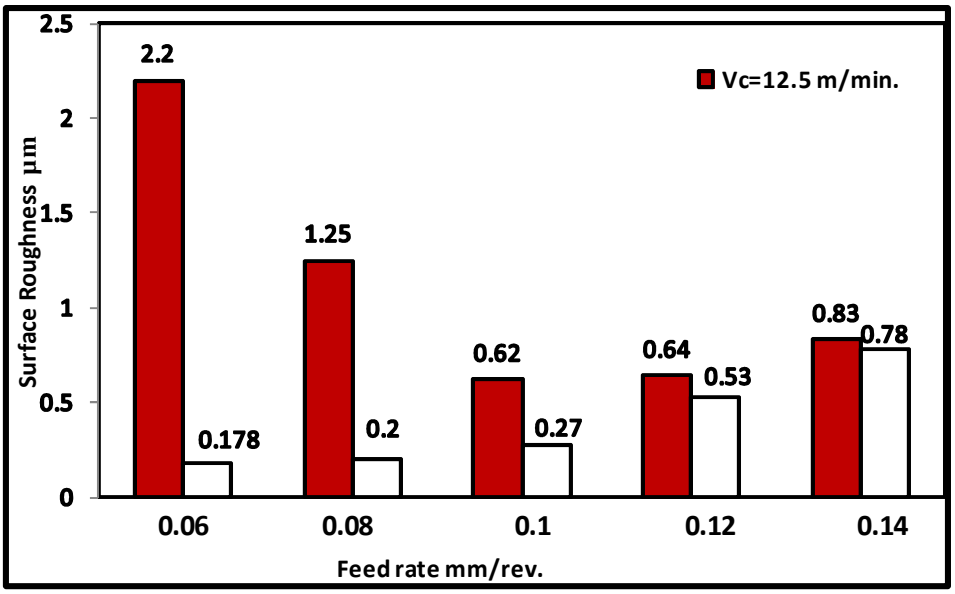

Fig. (4):- Effect of cutting speed on surface roughness of as received SAF 2507

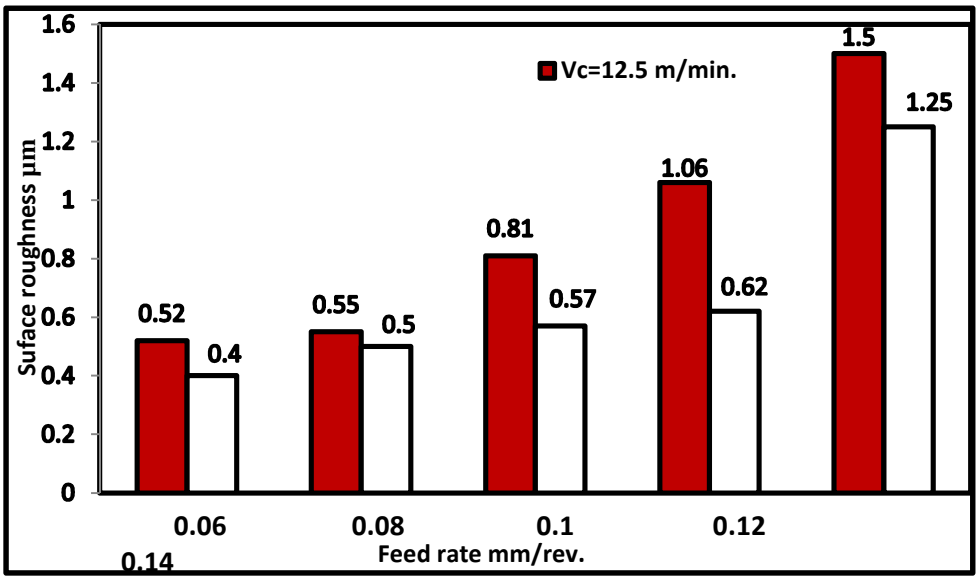

Fig. (5): -Effect of cutting speed on surface roughness of SAF 2507aged at 800 c°for 1 hour

It is observed in figure (4) the surface roughness of SDSS SAF 2507 in as received condition is very high when the feed rate f=0.06mm/rev this is due to chatter phenomenon during turning operation .Chatter phenomenon may cause the deterioration of the surface roughness and chip is discontinuous type as shown in figure (6) but by Increasing the feed rate the surface roughness will decreased and reached to its minimum value 0.62µm. When feed rate equals to 0.1mm/rev, the chip shape converted to continues type as shown in figure (7).

Fig. (7):- Continues chip during turning as receive SAF 2507, Vc=12.5 m/min and F=0.1mm/rev

After that the surface roughness will increase with increasing the feed rate this is due to widening the area of contact between cutting tool and work material. This leads to change of cutting force and produce distortion of chip as shown in figure (8)

Whereas with increasing the cutting speed from 12.5m/min to 22.5m/min the surface roughness will increase for the same feed rate this is probably due to decreasing the built up edge formation tendency with increasing cutting speed.

Fig. (8): Chip morphology during turning as received SAF 2507, Vc =12.5m/min and f=1.4mm/rev

Figure (5) showed that the surface roughness variation of heat treated super duplex stainless steel SAF 2507 at 800 **ºC** for one hour. The heat treated SAF 2507 exhibit in different manner compared to as received material, this refers to micro structural changes that occur during heat treatment .Figure (9) showed the microstructure of aged SAF 2507 at 800 **ºC** for one hour. The figure demonstrates decomposition of ferrite phase to secondary austenite and sigma phases which provide better surface finish particularly at lower cutting speed and lower feed rate after that with increasing the feed rate the surface roughness will increase linearly and reached to its maximum value when the cutting speed Vc=22.5m/min and feed rate F=0.14 mm/rev. This can be explained that increasing the feed rate and cutting speed increases the tool-wok piece contact area, this generate great amount of heat and as super duplex stainless steel SAF 2507 has low thermal conductivity leads to less heat transfer in work material and chip. It concentrated on the tool edge which causes tool wear and difficult chip break and finally leads to high surface roughness. Figure (10) showed the chip morphology of heat treated SAF 2507 during turning with cutting speed Vc=22.5m/min and feed rate=0.14 mm/rev.

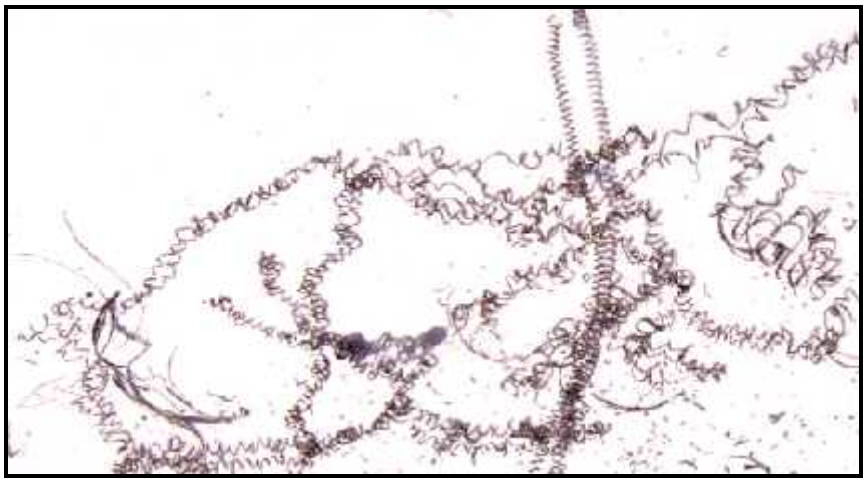

Fig. (9):- Microstructure of SAF 2507 aged at 800 c° for one hour(X600)

Fig. (10):-Chip morphology during turning heat treated SAF 2507, Vc =22.5m/min and F=0.14mm/rev

CONCLUSIONS

1. Smaller cutting speed and smaller feed rate provide high surface roughness in as received condition.

2.Maximum surface finish can be obtained in as received super duplex stainless steel SAF 2507 during turning with high cutting speed Vc =22.5m/min and lower feed rate F=0.06mm/rev.

3. Increasing the austenite phase in duplex stainless steel SAF 2507 deteriorates the surface roughness particularly at low cutting speed and high feed rate.

REFERENCES

- Echnrod J.J. and Opinnow K.E. "Effect of chemical composition and thermal history on the properties of alloy 2205 DSS " Proc Conf. "New development in stainless steel technique ,Detriot,Paper No. 8410-029 pp. 77 (1985).

-Davidson R.M.,Redmont J.D.,A guide to use duplex stainless steel ,Material and Design ,Vol.12 .No 4, P.187-192 (1991).

- Duplex stainless steel ,Sandvic SAF 2507 material data sheet -1875-ENG May (2008).

-Saoubi R.M. ,Outeriro J.C. ,Changeux B.,Lebrun J. L. ,Dias A. M. ,Residual stress analysis in orthogonal machining of standard and resulfurized AISI 316L steel. Journal of material processing technology,Vol 96,P.225-233,(1999).

-Ciftci I., Machining of austenitic stainless steel using CVD multilayer coated cemented carbide tool.Tribology International,Vol 39,No.6,p.565-569,(2006).

-Korkut I.,Kasap M.,Ciftci I., and Sekan U.,Determination of optimum cutting parameters during machining of AISI304

surface finish of nitrogen alloyed duplex stainless steel during dry turning ,Engineering,Vol. 2,P.453-460,(2010).
- ASTM standard test method for metallographic of metals Annual book of ASTM standards Vol.0.3-0.02, Philadelphia, PA: ASTM (1978).

austenitic stainless steel, Journal of Material and design,Vol.25,No4,p.303-305,(2004).
- Lin W.S., The study of high speed fine turning of austenitic stainless steel, Journal of Achievement in Materials and Manufacturing Engineering ,Vol.27,No2,P.191-194,(2008).
- Philip S.D. and Chandramahan P., Influence of cutting speed ,feed rate and bulk texture on the

زەبری ڕووی پۆلای ژەنگ نەگری بالای لێکدراو SAF2507 لە کاتی تۆرنەکردن

پوختە

لەم لێکۆلینەوە پەیوەندی نێوان زەبری ڕووی پۆلای ژەنگ نەگری لێکدراو SAF2507 کە لە شێوەی ئەستون بوو بە تیرەی 20 ملم و چارەسەری گەرمی بۆ کرابوو لە 800 °C بۆ ماوەی کاتژمێرێك لە کاتی تۆرنەکردی وشك. دوو خێرایی برین هەلبژێردران 12,5 م/ خولەك و 22,5 م/خولەك بە بری 0,06 , 0,08 , 0,1 , 0,12 و 0,14 ملم/لە هەر خولێکدا بۆ هەردوو خێرایی برینەکان وە قولایی برین لە هەموو بارەکاندا 0,25 ملم بوو. بەراوردی نێوان زبری ڕووەکان کرا لە نێوان باری وەك بە دەستمان گەیشتبوو لەگەل ئەوەی کە چارەسەری گەرمی بۆ کرابوو. چارەسەری گەرمی لە 800 °C دەبیتە هۆی کەم بوونەوەی زەبری ڕووەکە لە خێرایی کەمدا وە بری نزم پێچەوانەی ئەوە ڕوودەدات لە خێراییە بەرزەکان و بری کەمدا. زەبری ڕووی پۆلای ژەنگ نەگری چارەسەر کراو بە گەرمی زیاترە بە بەراورد لەوەی کە هەروەك بە دەستمان گەیشتبیت لە خێراییە بەرزەکاندا. دەتوانرێت ڕووی زەبری کەم لە پۆلای ژەنگ نەگرلە باری هەر وەك بە دەستمان گەیشتووە کاتێك بە خێرایی بەرز و بری کەم تۆرنە بکرێت.وشەی نەخشە /لێکدراو , پۆلای ژەنگ نەگر , زەبری ڕووەکان

الخشونة السطحية للصلب المقاوم للصدأ المزدوج المتناهى**SAF2507** خلال عملية الخراطة.

الخلاصة

هذا البحث يرسم تغير الخشونة السطحية لعمود من الصلب المقاوم للصدأ المزدوج المتناهى **SAF 2507** المعامل حراريا وذات قطر **20**ملم. المعاملة الحرارية تكونت من التعتيق لمدة ساعة واحدة فى درجة حرارة **800**مî تم عملية الخراطة الجافة .عوامل الخراطة الجافة تتضمن سرعات القطع**12,5** م\دقيقة و**22,5** م\دقيقة وخمسة معدل التغذية (**0,06, 0,08 ، 0,1، 0,12 ، 0,14**)ملم\دورة فى كل سرعة من سرعات القطع وعمق القطع كانت ثابتا **0,25** ملم.تم مقارنة الخشونة السطحية للصلب المقاوم للصدأ المزدوج المعامل حراريا بالخشونة السطحية للصلب كما في الحالة المستلمة.مقارنة بحالة كما المستلمة,العاملة الحرارية فى **800**مî تقلل الخشونة السطحية فى سرعة قطع المنخفضةومعدل التغذية منخفض وتحدث عكس ذلك فى سرعة القطع العالية ومعدل التغذية منخفض.الخشونة السطحية للصلب المزدوج المعامل حراريا أعلى من الصلب المزدوج كما فى الحالة المستلمة فى كل معدلات التغذية عندما تتم عملية الخراطة فى السرعات العالية **22,5** م\دقيقة .يمكن الحصول على سطح أقل الخشونة للصلب المزدوج كما فى الحالة المستلمة عندما يتم التشغيل فى السرعات العالية ومعدل تغذية منخفض.

EVALUATION OF NOISE POLLUTION IN RESTAURANTS OF DUHOK CITY, KURDISTAN REGION OF IRAQ

MANAF A. MAHAMMED1 SINAN KHORSHEED SALEEM 2
1- Dept. of Physics, Faculty of Science, University of Duhok, Kurdistan region-Iraq
2- School of Planing, Faculty of Engineering, University of Duhok, Kurdistan region-Iraq

(Received: September 17, 2014 ; Accepted for publication: December 30, 2014)

ABSTRACT

The indoor and outdoor noise levels were measured in six of Duhok city restaurants using two digital sound level meters. The indoor noise level is higher than the outdoor noise level for Azaim, Safin, Shindokha and Malta restaurants, while for Dunya and Sarki restaurants there was alternation between them. The correlation coefficient between the indoor and outdoor noise levels indicated that there were strong relationships between them. Majority of indoor noise level was due to conversation between customers, music noise, air conditioning and ventilation noises, and kitchen noise, besides the bad design of the restaurants and the lack of sound absorption materials covering walls and ceils of restaurants. It was concluded that the average noise levels for the selected restaurants are high. They ranged between 68 dBA and 78 dBA that are higher than the permissible noise level of residential areas (55 dBA) which is the standard of World Health Organization (WHO).

1. INTRODUCTION

Duhok city has been subjected to persistent fast development, urbanization and expansion of economy, travel and tourism. Thus it became one of the most important cultural, commercial and tourist centers of Duhok governorate within Kurdistan region of Iraq. This leads to the requirement of expansion in different fields. The presence of Duhok university and many other educational, cultural and technical institutes, besides a lot of commercial and tourist companies in Duhok city has made many people like teachers who teach or attend different conferences in educational fields, business men, tourists who visit Duhok city or people who work in business offices depend mainly on restaurants for their eating meals. This makes the many restaurants of the city to be crowded as well as noisy. The noise from various sources interrupt conversation and create stress and annoyance in the general population, and it reduces the efficiency and output workers (Nagi et al., 1999, Sinan, 2013). The measurement of noise levels in restaurants at Morogoro municipality in Tanzaniahas been carried out by Samagwa (Samagwa et al. 2009). Their results show that customers who visit restaurants to have a meal are at risk of developing effects of noise pollution such as hearing loss in a long term. Also they concluded that the observed sources of noise pollution in most restauants at Morogoro municipality resulted from lack of proper planning for restaurants areas and other use zones. In a recent work, Lao (Lao et. al., 2013) measured the noise exposure and hearing impairment among Chinese restaurant workers and entertainment employees in Hong Kong and concluded that excessive noise exposure is common in the Chinese restaurant and entertainment industries and a substantial proportion of restaurant workers and entertainment employees suffer from noise-induced hearing loss. Noise can cause hearing impairment, hypertension, annoyance, sleep disturbance, and decreased school performance. Although some hearing loss occurs naturally with age (Rosenhall et al., 1990), (Schmid, 2007), also elevated noise levels can create stress, increase workplace accident rates, and stimulate aggression and other antisocial behaviors (Kryter, 1994).

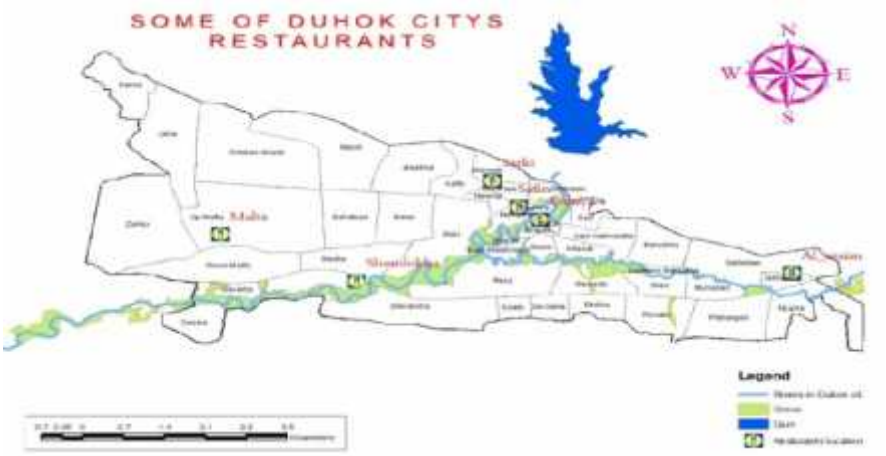

Fig. (1): The map of Duhok city showing the six selected restaurants

In this research, the results of noise level measurements of the six of selected Duhok city restaurants will be introduced and the role of different noise sources affecting both indoor and outdoor noise levels will be discussed. The selected restaurants are Azaim, Safin, Dunya, Sarki, Shndokha and Malta restaurants. Those restaurants have been chosen according to their location in residential, commercial, industrial and touristic areas. Figure (1) shows the map of Duhok city on which selected restaurants are shown. The correlation coefficient between the indoor and outdoor restaurant noise levels will be calculated for each restaurant. The average noise level for all selected restaurants will be compared with the standard permissible noise levels for residential, commercial and industrial areas that are dependent by WHO. Finally suggestions will be presented to help in decreasing noise level in Duhok city restaurants.

3. Methodology:

The noise level for each restaurant was measured twice a day for one day in a week along a period of five weeks by using a digital noise level meter. The device was placed on stand at distance of at least 1.5 m from each of walls and floor. For each measurement day, the noise level was measured afternoon from 1:00 PM to 3:00 PM each 15 minutes and in evening from 7:00 PM to 9:00 PM.these time intervals were chose because commonly noon and evening launch times start at those time intervals respectively. For each restaurant the indoor and outdoor noise levels where measured. Details of this work is mentioned (Saleem, S. K. 2013). In the following subsections, those measured noise levels will be introduced. Average noise levels will be calculated and the relationship between inside and outside average noise levels will be plotted as a function of time. The effects of different sources of noise on the noise level will be discussed.T

4. RESULTS AND DISCUSSION

1. Azaim Restaurant:

Azaim restaurant is ranked as one of the popular restaurants situated in an industrial area as shown in figure (1). The comparision between the indoor and outdoor average noise levels for this restaurant is plotted in figure (2).

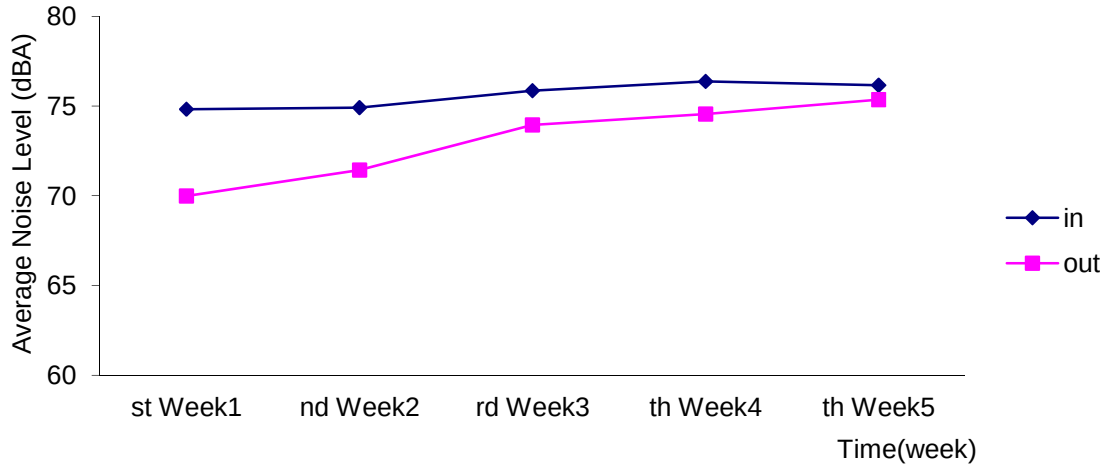

Fig. (2): The comparison between the indoor and outdoor average noise levels forAzaim restaurant

It can be shown from figure (2), that the indoor average noise level of this restaurant increases slowly after the second week, while the outdoor noise level increases gradually almost faster. The main reason for the high outdoor noise levels at this restaurant is because it is located near busy roads that cause high traffic noise, loud sound of audio systems from nearby shops specially vehicles maintenance shops and all disturbances and noises caused by the industrial area. On the other hand, the reasons for higher indoor noise levels are due to the small size of the restaurant with more customers than they can accommodate at any time, conversations of the customers, Kitchen noise, the loud sound levels provided by the music systems inside the restaurant, the air conditioning systems, and the meal tables are too close to each other, besides of the lack of sound absorbers that must be attached to the walls ceiling and floor of the restaurant. Also there are no efficient sound barriers to prevent the transmission of outdoor sound from entering inside. Therefore the noise created outside the restaurants (street) enters easily into the restaurant and causes the increasing of the indoor noise level as shown in figure (2). This is assisted by the value of the correlation coefficient between the indoor and outdoor noise level for this restaurant which is calculated to be 0.95 as shown in table (1).

Table (1): Calculated correlation coefficients between the indoor and outdoor noise levels for the selected restaurants

Restaurant	Rank	Correlation Coefficient
Azaim	P(*)	0.95
Safin	T(*)	0.45
Dunya	P	0.88
Sarki	T	0.57
Shendokha	T	0.53
Malta	T	0.95
(*) P= Public, T= Tourist		

2. Safin Restaurant:

Safin restaurant is ranked as a touristic restaurant and is located in a commercial area which is very crowded with vehicles and people. This restaurant's building consists of two floors. The outdoor noise sources of this restaurant include the noise of busy traffic because it situates on a main street, besides the noise caused by the shopping centers surrounding the restaurant. Most of the indoor noise is due to the its small size, including

large number of consumers, high radio and TV sounds, air conditioning system sounds, poor design (there are no sound insulating shielding materials within the construction of walls) and lack of sound absorbers.

The comparison between the indoor and outdoor noise levels is shown in figure (3). It seems that there is a contrary relationship between the average indoor noise level and the average outdoor noise level for this restaurant. Between first and second weeks, the average indoor noise level decreased, and the average outdoor noise level increased and between the second and third weeks the reverse case occurred. After the third week it seems that there is a correspondence between them, almost increasing together and decreasing together.

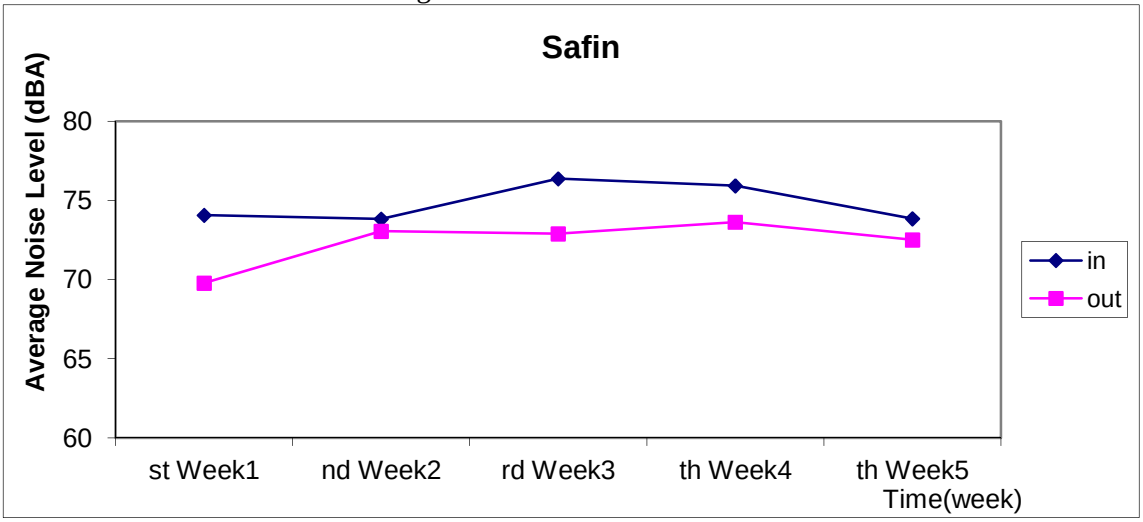

Fig. (3): The comparison between the indoor and outdoor average noise levels for Safin restaurant

The value of the correlation coefficient is equal to 0.45 which means that there is a medium directly proportional relationship among indoor and outdoor average noise levels. The low value of the correlation coefficient can be interpreted that the outdoor noise level has less impact on the indoor noise, because of the noise shielding of the restaurant walls that act to prevent the transmission of noise across them.

3. Dunya Restaurant:

Dunya restaurant is ranked as a popular restaurant which is located in the city center that is considered to be a commercial area. It is located on main road which is very crowded with vehicles and people. There are many noise sources surrounding the restaurant that cause discomfort and disturbance for the customers and workers. Among these sources, vehicles noise, crowded people noise, the shopping centers noise. The indoor sources of noise for this restaurant comprise customer's conversation noise, air conditioning noise, kitchen noise, music noise, besides the poor sound isolation. The comparison between the indoor and outdoor average noise levels is plotted in Figure (4). It can be observed from this figure that both indoor and outdoor average noise levels are almost identical for the first and second weeks. After the second week, both of them start increasing and the values of the average outdoor noise level seems to be higher than the average indoor noise level.

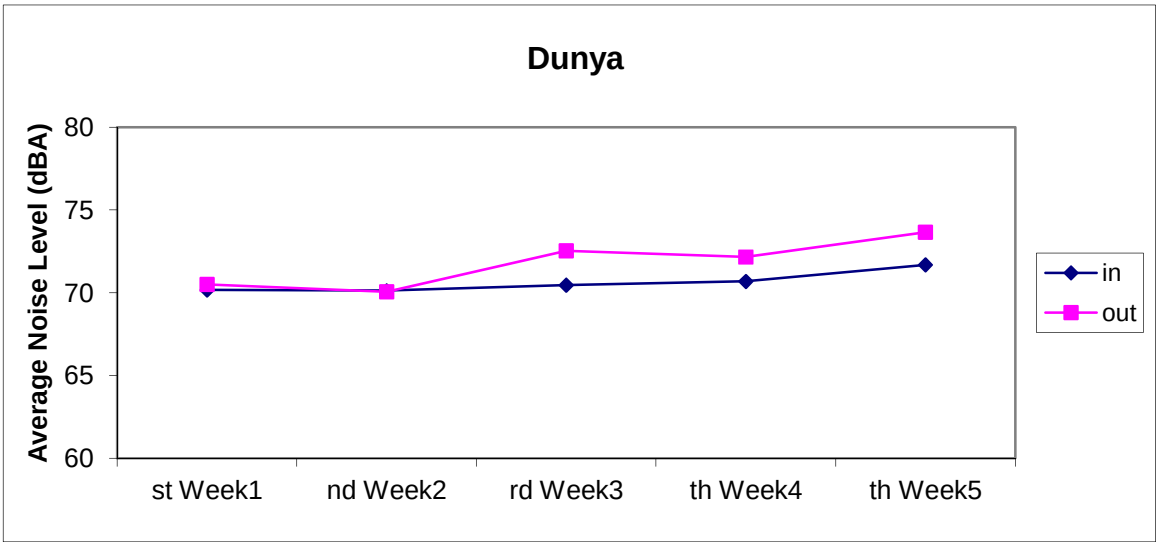

Fig. (4): The comparison between the indoor and outdoor average noise levels for Dunya restaurant

The value of the correlation coefficient is equal to 0.88 which means that there is a strong directly proportional relationship among indoor and average outdoor noise levels. This proves that there is a strong effect on the indoor noise caused by the outdoor noise.

4. Sarki Restaurant:

Sarki restaurant is considered as a touristic restaurant. It situates on the main road near Duhok preparatory school and the area exactly behind the restaurant is a residential area. The outdoor sources of noise comprise traffic noises, crowded of people noise, shopping centers noise. While the indoor sources of noise comprise almost the same sources as for previous mentioned restaurants like kitchen noise, dishes noise, music noise, conversation noise and air conditioning system noise. The comparison between the indoor and outdoor noise levels is plotted in figure (5). This figure shows that the average outdoor noise level in general is greater than the average indoor noise level except for the third week measurement in which the situation was reversed.

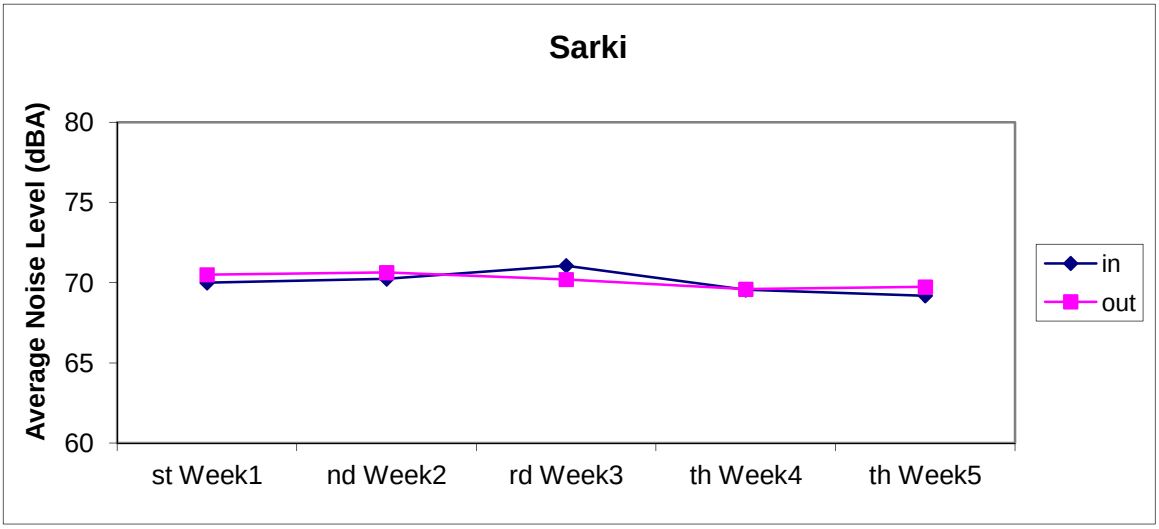

Fig. (5): The comparison between the indoor and outdoor average noise levels for Sarki restaurant

The value of the correlation coefficient is equal to 0.57 which means that there is a strong directly proportional relationship among indoor and outdoor average noise levels. Thus there is a contribution of the outdoor average noise level in the increasing of the indoor average noise level.

5. Shendokha Restaurant:

Shendokha restaurant is a touristic restaurant which is located in a touristic area. It is located on the main road and has a large area and gardens with a multi-story hotel. There are a considerable distance between the restaurant and the main road. The sources of indoor noise are few, while the outdoor noises are the sound of driving cars speedily on the main road. The relationship between the indoor and outdoor nose level is plotted in figure (6). It is clear that the noise inside the restaurant is more than the noise outside of the restaurant.

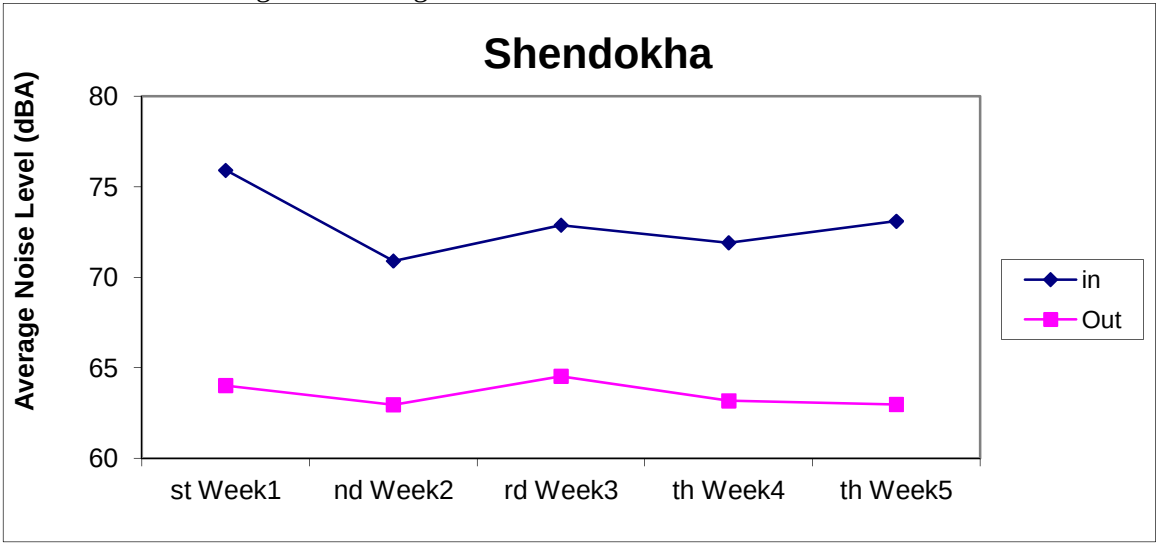

Fig. (6): The comparison between the indoor and outdoor average noise levels for Shendokha restaurant

The value of the correlation coefficient is equal to 0.53 which means that there is a strong directly proportional relationship among indoor and outdoor noise which indicates that the outdoor noise contributes in increasing the indoor noise level. This is clear from the two curves of the indoor and outdoor average noise levels of figure (6) for the first, second third, and fourth week.

6. Malta Restaurant:

Malta restaurant is ranked as a touristic restaurant which is located on the main road with enough distance between the restaurant itself and the main road. It is located in a touristic area. This restaurant to some extent has followed the standards about comfort and customers care. They have used some sound isolation materials and the tables are not close to each other. The sources of outdoor and indoor noise are too little. The existence of trees around the restaurant is considered as a barrier for sound isolation for preventing the transmission of noise from outside to inside the restaurant. The comparison between the indoor and outdoor noise levels is plotted in figure (7).

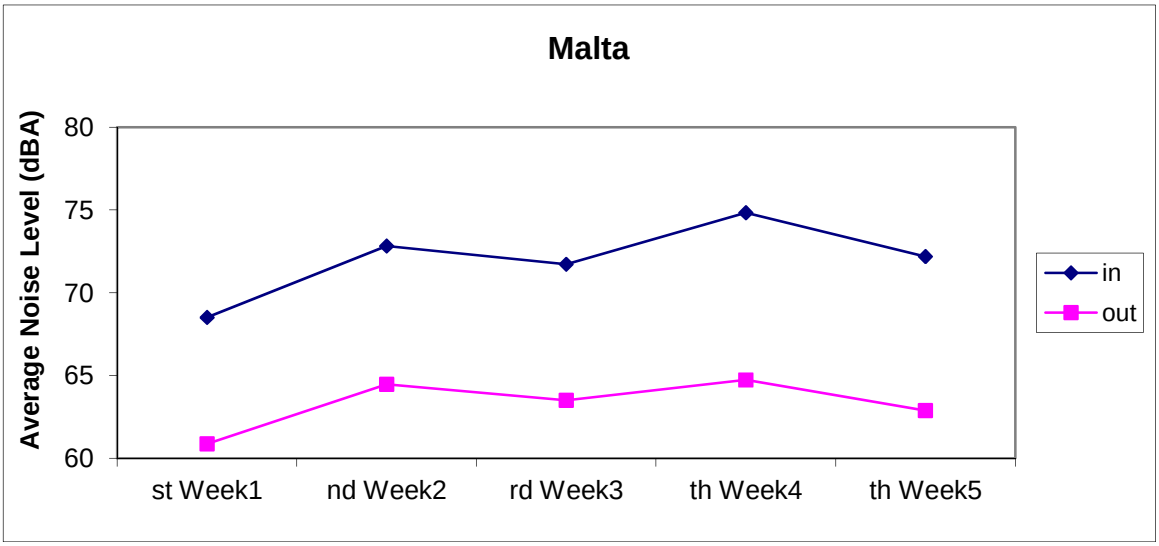

Fig. (7): The comparison between the indoor and outdoor average noise levels for Malta restaurant

The value of the correlation coefficient is equal to 0.94 which indicates that there is a strong directly proportional relationship among indoor and outdoor noise.

10. **Comparing the Results with Literature:**

People visit restaurants to have their breakfast, their lunch and their dinner. The acoustics of such restaurants play a great role in the design of any modern restaurant. The diners must not be bothered by the effects of reverberation produced by visitor's conversations and the noise and echoes emitted from the kitchen besides the noise of the nearby traffic outside the restaurant (Rohrmann, B.2003).

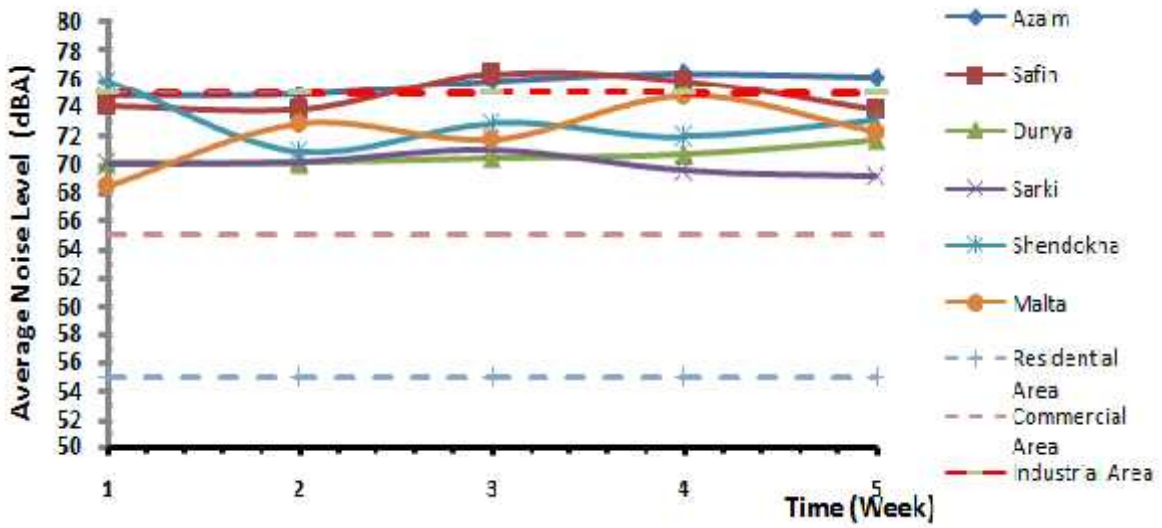

Fig (8): Comparison between the average indoor noise level of the selected restaurants with the permissible noise levels for resedential, commercial and industrial areas

There is no standard value (according to the knowledge of the researcher) for the maximum accepted value of the noise level in restaurants, however, according to some researchers (Rohrmann, B.2003) acceptable noise level in restaurants must be below 55 dBA, while some other researches used 55 dBA as the permissible noise level for the residential areas and 60 dBA as the permissible noise level for commercial areas and 75 dBA for industrial areas (Vijayalakshmi, K.S., 2003). In order to compare the average noise level values that were measured for the selected restaurants (i.e. indoor noise level) with the permissible noise levels for the areas mentioned in table (1). The measured values during five weeks were plotted as shown in figure (8), The permissible noise levels for the residential, commercial, industrial, and silence zone were also plotted on the same figure. It seems that the majority of the measured values situate at the upper part of the industrial region and some few measured vales even exceed the permissible noise level of the industrial area.

CONCLUSION

It is concluded that the outdoor noise sources like traffic noise, music shops, people noise, etc., contribute in increasing of the indoor noise level. This is clear because there is a strong relationship and proportionality between the outdoor and indoor noise levels. In comparison with the permissible noise level in residential areas (55 dBA), it is concluded that the average noise levels in the selected restaurants are high (i. e. some measurements were close to 80 dBA.) The results indicate that the workers doing eight hours or more in restaurants and the customers are more probably at risk of the harmful effects of noise pollution of the restaurants like hearing. It can be concluded that the bad design of the restaurants that do not cover their walls and ceilings with sound absorber materials, (that if used may absorb the majority of the sounds inside the restaurants), is the main reason behind the high values of noise levels.

REFERENCES

- Nagi, GK; Dhillon, MK; Dhaliwal, GS (1999). Noise Pollution. Coomonwealth Publishers, New Delhi. pp. 5 – 22.
- Samagwa, D, Mkoma, S, Tungaraza, C, 2009, Investigation of Noise Pollution in Restaurants in Morogoro Municipality, Tanzania, East Africa, J. Appl. Sci. Environ. Manage. December, 2009, Vol. 13(4) 29 – 33).
- Saleem, S. K., 2013, "Investigation of Noise Pollution in Duhok City Restaurants", MSc thesis, School of Planning, University of Duhok .
- Lao, X. Q.,, Sun Yu, I. t.,, Au, D. k. Yuk Lan Chiu, Claudie Chiu Yi Wong, Tze Wai Won 2013, "Noise Exposure and Hearing Impairment among Chinese Restaurant Workers and Entertainment Employees in Hong Kong ", Published online 2013 August 15. doi: 10.1371/journal.pone.0070674.
- (Kryter, K. D. (1994). *The handbook of hearing and the effects of Noise: physiology*,psychology, and public health. Boston: Academic Press. ISBN 0-12-427455-2)
- Rosenhall, U.; Pedersen K.; Svanborg A, (1990). *Presbycusis and noise-induced hearingloss*. Ear Hear 11 (4): pp. 257–263.
- Schmid, 2007 (Schmid, Randolph E. "Aging Nation Faces Growing Hearing Loss" 18 February 2007. 28 January 2009. <**http://www.cbsnews.com/stories/2007/02/18/ap/health/mainD8NC00AO0.shtml**>.)
- Rohrmann, B. Soundscapes in restaurants , http://www.rohrmannresearch.net/pdfs/spp-brsir.pdf, In: World Forum Acoustic Ecology (Eds.) Proceedings of the International Symposium of Acoustic Ecolog Melbourne - March 2003
- Vijayalakshmi, K.S., (2003). Noise Pollution, Proceeding of the third conference on environment and health, p. 597-603, Chenna, India.

PRINTED MULTIBAND MONOPOLE ANTENNA WITH INDEPENDENT TUNING SUITABLE FOR COMPACT WIRELESS DEVICES

FAYYADH **H. A**HMED
Dept. of Electrical and Computer, Collage of Engineering, University of Duhok, Kurdistan Region-Iraq

(Received: November 27, 2014; Accepted for publication: March 1, 2015)

ABSTRACT

A new configuration of planar multi-band antenna is demonstrated in this paper. The proposed antenna is generally based on a printed rectangular monopole antenna (PRMA) that covers a wideband of 3.3 GHz WiMAX frequency range. To generate a multi-band property, an asymmetric triangular shaped slot (ATSS) is inserted into the center part of PRMA in order to construct two right angles triangle strips, which possess several quarter wavelength parts. The Quad band resonant modes of 1.8GHz, 2.4GHz, 3.7GHz, and 5.3GHz were realized due to the different lengths and widths of the triangular planar monopole strips. The distinctive aspect of the antenna is that it can serve several different communication systems simultaneously. These systems include various combinations of GSM1800, DCS, PCS, WLAN, and WiMAX applications. Moreover, the four individual frequency bands can be adjusted and set independently over wide ranges of 12.86%, 9.72%, 17%, and 6.54%, respectively, using simple parameters of the antenna. This basically means that a variety of other communication systems can be conveniently served by only one antenna.

The designed antenna has a simple planar structure and a compact size of 30×45 mm. Simulation results showed that the peak realized gain of the antenna at different operating bands of 1.8GHz, 2.4GHz, 3.7GHz, and 5.3GHz were 1.5dBi, 2.75dBi, 4.7dBi, and 4dBi, corresponding to 75.8%, 83.6%, 81.6%, and 82.5% radiation efficiency, respectively.

Simulation results were obtained from the commercial CST Microwave Studio.

KEY WORDS: Multiband, GSM1800 and WiMAX, printed antenna, slot, and independent tunig

INTRODUCTION

Wireless communications have undergone great development in the last few years. Many wireless systems have emerged, including cellular-radio systems, mobile satellite systems, wireless local area networks, and worldwide interoperability for microwave access (WiMAX). The development of the wireless systems greatly influences the field of antennas. Moreover, modern communication systems require a single antenna to cover several allocated wireless frequency bands.

Planar printed monopole antennas, due to their attractive features such as low cost, simple structure, ease of fabrication, wide bandwidth, and omni-directional radiation pattern, have received great attention for hand- held wireless systems [1]–[3]. In recent years, there have been several reports regarding the development of low-profile multiband antennas. The traditional approach is to use multi-branched strips to realize multiband operations [4], which generally leads to a large volume or requires a large ground plane. However, most of them are single-band or dual-band (i.e., do not provide the desired bandwidths) [5]–[13]. There are other designs that are capable of operating over all WiFi and WiMAX wireless frequency bands [14]–[21]. In most cases, the antenna size is large, and the geometry of the antenna is complicated and high profile. Also, it could not cover the Global System for Mobile communications (GSM900) and Personal Communications System (PCS) bands, which, at such low frequencies, requires a relatively large antenna size for this purpose, which will render it incapable of simultaneously covering GSM900/PCS and WLAN/WiMAX. One simple way to cover all frequency bands is via the usage of wideband antennas [1] and [22]. However, in order to avoid interfering with nearby communication systems, we need to design an antenna that can operate only at the desired narrow frequency bands.

In this paper, a compact and low profile planar monopole antenna is proposed and designed for

quad-band operations. It satisfies the following operational bands: DCS (1744-1880MHz), PCS (1850-1990MHz), GSM1800 (1805-1880), LET 2300 (2305-2400MHz), two operation bands in the IEEE 802.11WLAN standards, 2.4GHz (2400-2484MHz), 5.2GHz (5150-5350 MHz), and one WiMAX operating band 3.5 (3400–3690MHz). Quad-band operation of the proposed antenna is achieved by several quarter wavelength dimensions of two right-angled triangles with a step-by-step design procedure. The antenna bandwidth can also be independently adjusted at different resonant frequencies simply by tuning just one key parameter of the antenna; therefore, the proposed antenna can serve other wireless standards.

ANTENNA CONFIGURATION AND DESIGN PROCEDURES

1. Design of Single Wide-Band Antenna:

The structure of a suitable planar monopole radiator that can be used as a reference for the eventual multi-band antenna, operating over the single wide-band frequency range, is shown in Fig. 1.This reference wide-band antenna can be referred to as the printed rectangular monopole antenna (PRMA).The antenna uses an FR4 substrate with dimensions of 45×30×1.6mm^3, $\varepsilon_r = 4.3$, and a loss tangent of 0.025. A simple rectangular conducting ground plane of width W_g and length L_g is placed on the other side of the substrate.

To estimate the lower band-edge frequency of printed monopole antennas, a formula is suggested by [23], equating its area with a cylindrical monopole antenna with a large effective diameter. The standard formulation given for a cylindrical monopole antenna can be used with suitable modifications [24]. The lower band-edge frequency is given in [23]:

$$f_L = \frac{c}{\lambda} = \frac{7.2}{\{(L+r+P)\times k\}} GHz \qquad \ldots(1)$$

where p is the length of the 50Ω feedline in cm, and L and r are the height and radius of the equivalent cylindrical monopole antenna in cm, respectively, while $k = \sqrt{\varepsilon_{reff}}$, and the approximated value of ε_{reff} is given by [25]:

$$\varepsilon_{reff} \approx \frac{\varepsilon_r+1}{2} \qquad \ldots. (2)$$

With reference to the PRMA configuration in Fig.1 b, L and r are calculated in the following manner [23]:

For PRMA, if length=L and width= W, hence

$$L=L, \text{ and } r = \frac{W}{2\pi} \text{ for PRMA} \qquad \ldots.. (3)$$

For FR4 substrate, its thickness is 1.6mm and $\varepsilon_{reff} = 2.65$, and consequently, k is equal to 1.627. But for commonly used substrate with $\varepsilon_r = 4.4$ and $h = 1.59mm$, the empirical value of $k = 1.15$ estimates lower band-edge frequency within 10% [26]. Therefore, if the lower frequency f_L is chosen to be 2GHz, then the estimated lower edge side Lp, using equation(1), is equal to 22.1.However, for generating 2GHz resonant frequency, larger physical length of L_p is required. However, L_p =32mm is selected to be multiples of $\lambda_{eff}/4$ according to the following equation [25]:

$$L_p = \frac{\lambda_{eff}}{4} = \frac{\lambda}{4k} = \frac{c}{4kf_L} \qquad \ldots. (4)$$

where λ and c are free space wavelength and speed of the light, respectively , λ_{eff} is effective wavelength and is given by [27]:

$$\lambda_{eff} = \frac{\lambda}{\sqrt{\varepsilon_{reff}}} \qquad \ldots. (5)$$

The PRMA is fed with a microstrip-feed line with a width of W_f, and length of L_f. To achieve 50Ω characteristic impedance, the microstrip line width has been calculated using the following equation [28]:

$$Z_0 = \frac{87}{\sqrt{\varepsilon_r+1.41}} \ln\left(\frac{5.98\,h}{0.8\,W_{strl}+t}\right) \qquad \ldots. (6)$$

where Z_0 is the characteristic impedance of the microstrip line, h is the substrate's thickness taken at 1.6 mm, t is the metallization thickness of 0.035mm, W_{strl} is the microstrip line width, and ε_r for the FR4 substrate is 4.3. Therefore, according to (6), for a characteristic impedance of 50Ω, W_{strl} must be set equal to 3mm.

To obtain a wide band antenna that covers the WLAN/WiMAX range, the antenna parameters are optimized using a CST package. The optimum dimensions of the antenna shown in Fig.1 (a) are given in Table1, and the result of the Return Loss is shown in Fig.2.

The corresponding -10 dB bandwidth is 1.79GHz (3.813-2.023GHz), covering LET 2300/2500 (2305-2400MHz/ 2500-2690MHz), the IEEE 802.11WLAN standard, 2.4GHz (2400-2484MHz), and WiMAX operating band3.5 (3400–3690) [29].

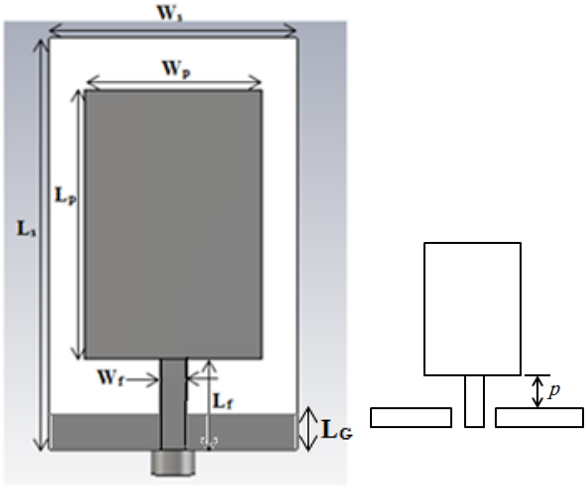

(a) (b)

Fig (1): (a) Geometry of the proposed WLAN/WIMAX PRMA antenna (b) a regular shape printed rectangular monopole antenna (PRMA).

Table (1): Optimum dimensions of the antenna shown in Fig.1 (a).

Antenna's parameter	L_s	W_s	L_p	W_p	L_f	W_f
Dimension in (mm)	45	30	32.5	21.5	11.1	3
Antenna's parameter	Lg	Total Volume				
Dimension in (mm)	3.8	$45\times30\times1.6$ mm^3				

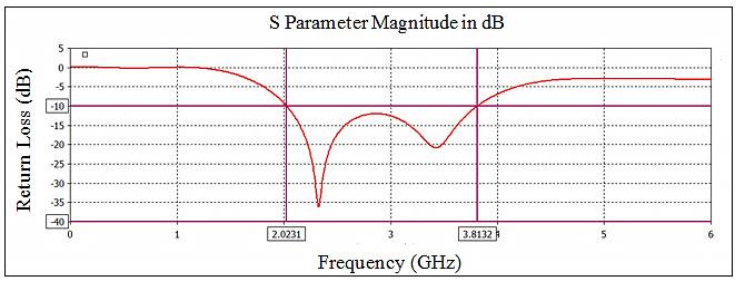

Fig (2): Return Loss of the proposed antenna depicted in Fig (1)a with dimensions given in Table 1.

2. Design of Fixed Multi Band Antenna:

The geometry of the proposed quad-band antenna, having four frequency bands, numbered 1, 2, 3, and 4, at 1.8, 2.4, 3.7, and 5.5GHz, respectively, are shown in Fig. (3). Table 2 lists the key parameters. The antenna consists of two right-angled triangles strips, a 50Ω- feed line, feed strip, arm strip, ground plane, and ground strip. The design steps can be described with the aid of Fig 4, as follows:

Step 1: It can be shown that the current distribution over the printed monopole antenna is mostly concentrated over the outside edges of the patch, with negligible current at the center region [30]. Thus, if a section along the axis of the PRMA antenna is removed, this will not affect the overall antenna impedance bandwidth and radiation characteristics leading to the wideband antenna [31]. In our design, an asymmetrical triangular – shaped slot (ATSS) is inserted into the center part of the PRMA in such a way that its apex arrives at the feed line without affecting PRMA's behavior, as shown in Fig. 4(a). PRMA is changed into two different base right-angled triangles strips, one on the right of feed line, while the other on the left, named triangular #1 and #2,

respectively. However, the antenna still introduces wideband impedance bandwidth at 2.4 GHz for the wireless local area network WLAN and WiMAX bands, and its dimensions are optimized to broaden the reflection coefficient across the band via computer simulation using CST software package.

Step2: Asymmetry of ATSS is further increased in the direction of right-angle triangular #1, leading to completely separate triangular #1 from the feed line, while triangular #2 remains in contact with the feed line. Separating one part of the antenna is detrimental to the PRMA wideband behavior. Deterioration antenna behavior generates unwanted frequencies at 2.23 to 3.9 GHz, and this changes the single wideband antenna (as described in step 1) to two narrow bands, band1 (2.1GHz), which will be seen later in step 3, by inserting the rectangular slot into the right-angled triangular #2, will tune the resonant frequency to 2.4GHz, and band 2 (3.65 GHz). Moreover, the separation of right-angled triangular #1, which fed through proximity coupling from the feed line, will construct another resonator, where its dimension L_5 is optimized to be almost equal to half-wave length of 5.5GHz resonance frequency, thereby

generating band3 (5.5GHz WiMAX band). With this configuration, three prominent resonant frequencies are obtained, as shown in Fig (4) b.

Step 3: Cutting slots on the radiator of an antenna will alter the current's path, and can be used to generate dual-band or even multiple-bands operations [32]. In our proposed design, if the slots are absent in the right-angled triangular, the antenna will have only one major current path on each. However, in the presence of the slot on the elements, the current path on each is disturbed, creating dual-band operations. In order to generate band 4 (1.8GHz), a rectangular slot is inserted into triangular #2 to change the current patch and transform triangular #2 to a pair of quarter wave length resonators L_2 and L_7 for generating band 4 (1.8GHz) and tuning band 1 at 2.4 GHz, as shown in Fig 4(c). However, L_2, on its own, does not give exact 1.8GHz resonance, so arm strips with a length of 3mm and width of 1mm is added to the end of L_2 to tune it to 1.8GHz.

A ground strip with a length L_{GS} and a width of W_{GS} is placed on the bottom side of the substrate under the microstrip feed line, as shown in Fig 3(b), to cancel unwanted far field radiation from the current on the feed line. Feed strips, with dimensions L_{fs} and W_{fs} equal to 2.5mm and 5mm, are also added to end of the feed line to improve antenna impedance matching. Dimensional details of the antenna shown in Fig.3 (a) are given in Table2.

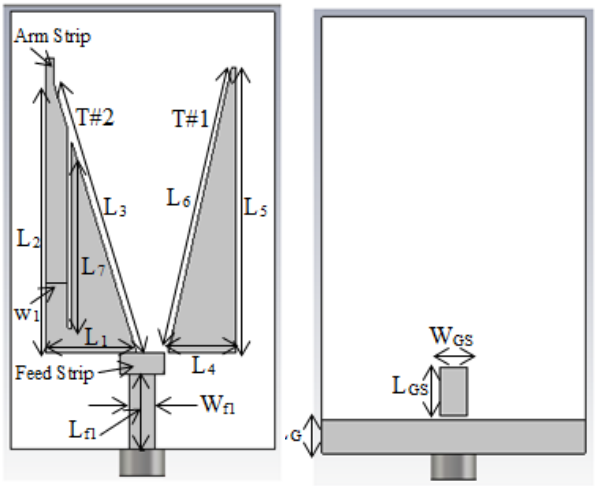

(a) (b)

Fig.(3): The geometry of the proposed fixed multiband antenna (a) Top View; (b) Bottom View.

Table 2: Optimum dimensions of the antenna shown in Fig. 3.

Antenna Parameter	L_1	L_2	L_3	L_4	L_5	L_6
Dimension in (mm)	11.34	32.5	31.9	7.67	32.5	33.2
Antenna Parameter	L_7	L_{f1}	W_{f1}	L_G	L_{GS}	W_{GS}
Dimension in (mm)	21.2	8.6	3	3.5	5.6	3
Antenna Parameter	W_1	Total Volume				
Dimension in (mm)	2.5	$45\times30\times1.6$ mm^3				

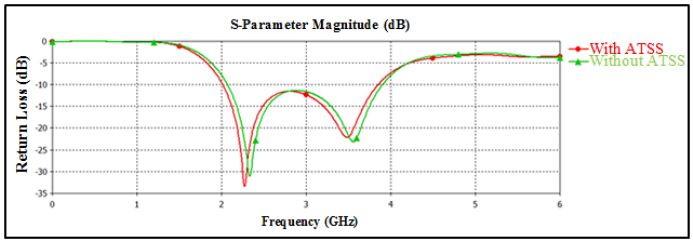

(a)

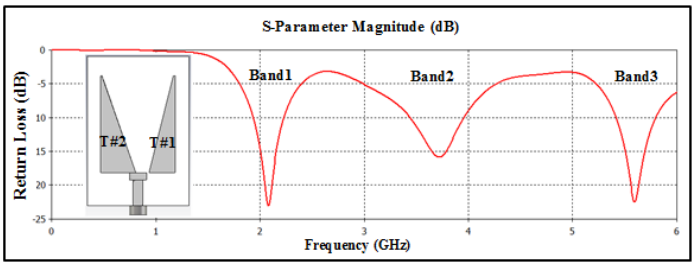

(b)

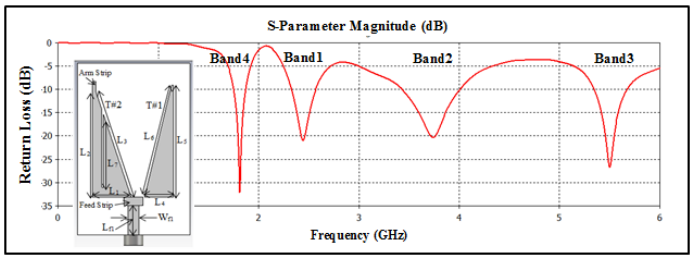

(c)

Fig (4): Design steps of proposed antenna in Fig. (3).

RESULT AND DISCUSSION

1. Return Loss:

The dimensions of the antenna shown in Fig.3 are optimized in terms of minimizing the reflection coefficient at the desired frequencies and broadening impedance bandwidth. The optimized dimensions are given in Table 2; and the result of the Return Loss is presented in Fig.5. For band 4 (1.8GHz), the corresponding -5 dB bandwidth is 239MHz (1.697GHz-1.936GHz), which is suitable for DCS (1744-1880MHz), PCS (1850-1990MHz), GSM1800 (1805-1880), while for band1 (2.4GHz), band2 (3.65GHz), and band 3 (5.3GHz), the corresponding -10dB impedance bandwidths are 235MHz (2.330GHz-2.565GHz), 620MHz (3.299GHz-3.919GHz), and 351MHz

(5.226GHz-5.577GHz) respectively, which can cover LET 2300/2500 (2305-2400MHz/ 2500-2690MHz), the IEEE 802.11WLAN standard, 2.4GHz (2400-2484MHz), and WiMAX operating band 3.5 (3400–3690), IEEE 802.11 WLAN standard 5.2GHz (5150-5350MHz), and 5.5 GHz (5250–5850 MHz) WiMAX band.

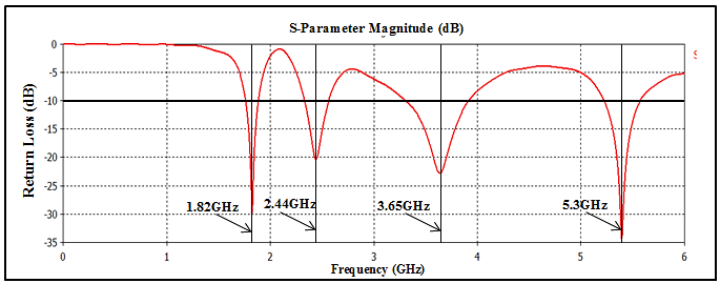

Fig (5): Return Loss of the proposed antenna depicted in Fig (3) a with dimensions given in Table 2.

2. Current Density Distribution:

In order to explain the excited resonant mode being proposed, the simulated surface current density distribution on the radiating elements at resonant frequencies (1.8GHz, 2.4GHz, 3.65GHz, and 5.3GHz) of the first fourth excited mode, are shown in Fig.(6). For band 4 at 1.8 GHz, Fig. 6(a) shows that the current density mainly flows along dimension L_2 of the right-angled triangle 2 (T#2) (y-direction), which indicates that the arm L_2 is the major radiating element for the antenna at the 1.8 GHz band. For band 1 at 2.45 GHz, Fig. 6(b) shows that the current density is mainly concentrated along the arm L_7 on the T#2 (y-direction), and this arm contributes the most to radiation at 2.45GHz. Dense surface current density distribution around the bottom (base L_1) of T#2 (x-direction) at 3.7 GHz is seen, which demonstrate that the third resonant mode of T#2 element is excited. Finally, for the 5.3GHz operation, it is observed that the surface current density distribution on the right-angled triangular 1 (T#1) (y-direction) along L_5 element gradually increases, indicating that this dimension is responsible for generating the resonance frequency for this band.

Figs. 6(a) to (d) show the major current density paths at the resonant frequencies, corresponding to approximately total resonant strip length (dimensions in our design), which is a multiple of quarter-wavelength, and can be calculated approximately by [33].

$$L_{total} \approx n\frac{\lambda_g}{4} \qquad \ldots\ldots (7)$$

where $\lambda_g = \frac{\lambda_0}{\sqrt{(\varepsilon_r+1)/2}}$, and λ_0 is the free space wave-length.

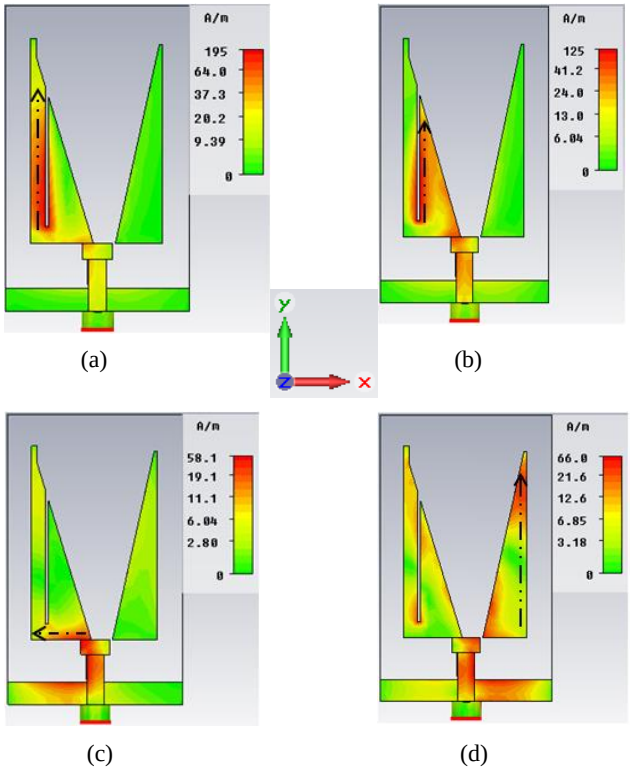

(a) (b) (c) (d)

Fig (6): Simulated surface current density distributions for the proposed quad-antenna at (a) 1.8GHz, (b) 2.4GHz, (c) 3.65GHz, (d) and 5.3GHz.

3. Independent Control Concept:

When designing multiband antennas, it is desirable to have the ability to set the frequency bands independently from each other, but this remains quite the challenge [34]. Very often, when some parameters are adjusted to set a band to a particular frequency, the frequencies of all other bands are affected [35]–[37], and the antenna has to be re-designed. However, in our proposed multiband antenna, we can independently set the individual frequency bands, one by one, without affecting other bands. In previous sections, we have identified the current paths responsible for radiation and related antenna parameters at different resonant frequencies, as shown in Fig. 6. These parameters are the key parameters determining the resonant frequencies. Thus, we can change those antenna's parameters, which in turn alter the lengths of the current paths and set the resonant frequencies independently.

Fig. 7 shows the simulation results of the effects of varying the w_1, L_7, L_1, and L_5 parameters on the frequency bands. Fig 6 (a) shows that the current density is mainly distributed along the arm L_2, which is responsible for exciting the resonant frequency of 1.8GHz, so altering the width (w_1) of dimension L_2 will alter the 1.8GHz resonant frequency over a wide range (15.4%) without affecting other bands, as shown in Fig 7(a). Applying this same principle to Fig. 6(b) to (d), the lengths L_7, L_1, and L_5, respectively, can be used to independently set the corresponding frequencies of 2.4, 3.65, and 5.3 GHz to other values. Fig. 7 (b) to (d) shows the simulation results on the effects of varying the L_7, L_1, and L_5 parameters on the frequency bands. It can be seen from Figs. 7(b) to (d) that the parameters L_7, L_1, and L_5 can be used to independently adjust the frequency bands at 2.4, 3.65, and 5.3 GHz over a wide range of 22.4%, 11%, and 10.3%, respectively. Table 3 summarizes these results.

Table (3): Effects of changing w_1, L_7, L_1 and L_5, on antenna impedance bandwidth.

Parameter	1.8GHz	2.4GHz	3.65 GHz	5.3GHz
W_1	1.54GHz-1.82GHz. (15.4%)	Almost constant	Almost constant	Almost constant
L_7	Almost constant	2.22GHz-2.78GHz (22.4%)	Almost constant	Almost constant
L_1	Almost constant	Almost constant	3.47GHz-3.88GHz (11%)	Almost constant
L_5	Almost constant	Almost constant	Almost constant	5.11GHz-5.67GHz (10.3%)
Variation range	8.34-14.34mm	18.2-24.2mm	2.5-0.5mm	22.5-38.5mm

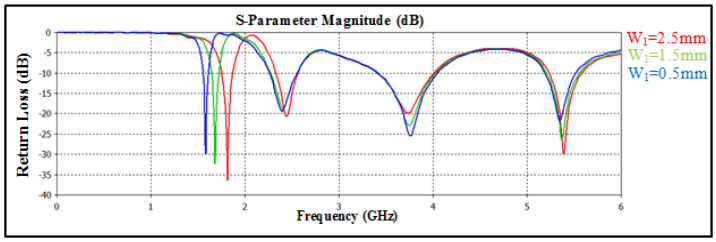

(a)

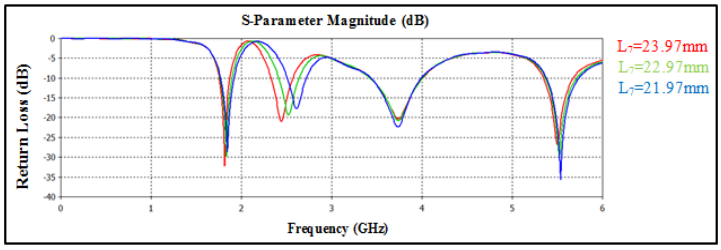

(b)

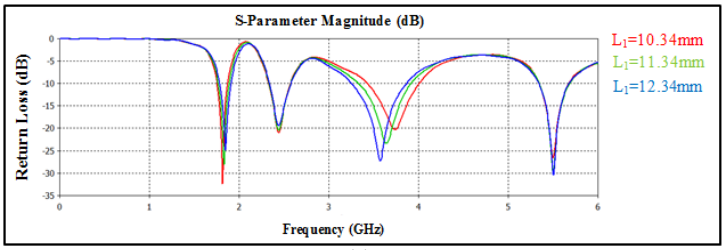

(c)

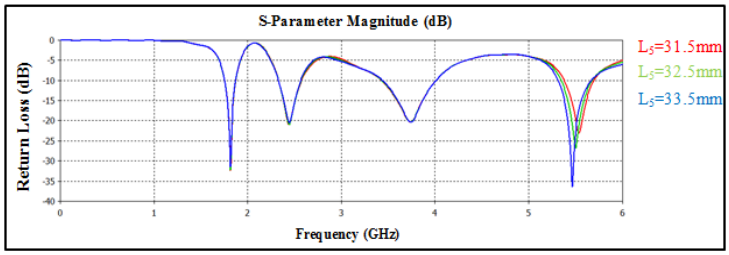

(d)

Fig7: Simulated effects of varying (a) $w_1$on 1.8GHz, (b) L_7 on 2.4 GHz, (c) L_1 on 3.65 GHz and (d) L_5 on 5.3 GHz.

4. Antenna Gain and Radiation Efficiency:

The realized gain of the proposed multi-band antenna at all available frequency bands is shown in Fig.8. The peak realized gains of the antenna at different operating bands of 1.8GHz, 2.4GHz, 3.65GHz, and 5.3GHz are 1.5dBi, 2.75dBi, 4.7dBi, and 4dBi, respectively. The radiation efficiency corresponding to those values of realized gain at resonant frequencies are 75.8%, 83.6%, 81.6%, and 82.5% respectively, as shown in Fig. 9.

According to the obtained gain and radiation efficiency values, the proposed antenna can be used for indoor and outdoor wireless communications.

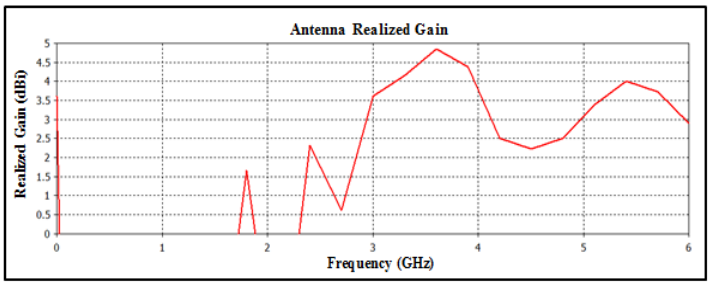

Fig (8): Realized gain of proposed quad-band antenna.

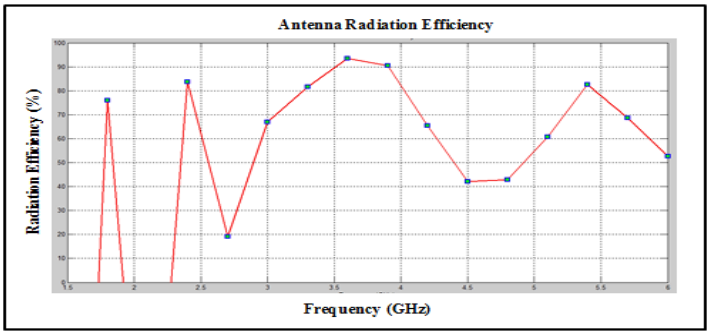

Fig (9): Radiation efficiency of proposed quad-band antenna.

5. Radiation Pattern:

The simulated 3D far-field radiation patterns of the proposed antenna at the center of operating frequency bands at 1.8 GHz, 2.4GHz, 3.7GHz and 5.3GHz are shown in Fig. 10. From Fig. 10 (a) and (b), it can be seen that the antenna at the first two resonant frequencies of 1.8GHz and 2.4GHz exhibited nearly an omnidirectional radiation on the H-plane (XZ-Plane), while the E-plane (X-Y-plane) pattern is found to be eight (8) shaped, which shows a bidirectional pattern. However, from Figs. 10 (c) and (d), unidirectional patterns in both E and H-plane are observed, which may be due to its radiation behavior being reasonably affected partly from antenna's ground plane.As noticed from the current density distribution in Figs. (6) c, d, the ground plane contributes to radiation to a certain extent.

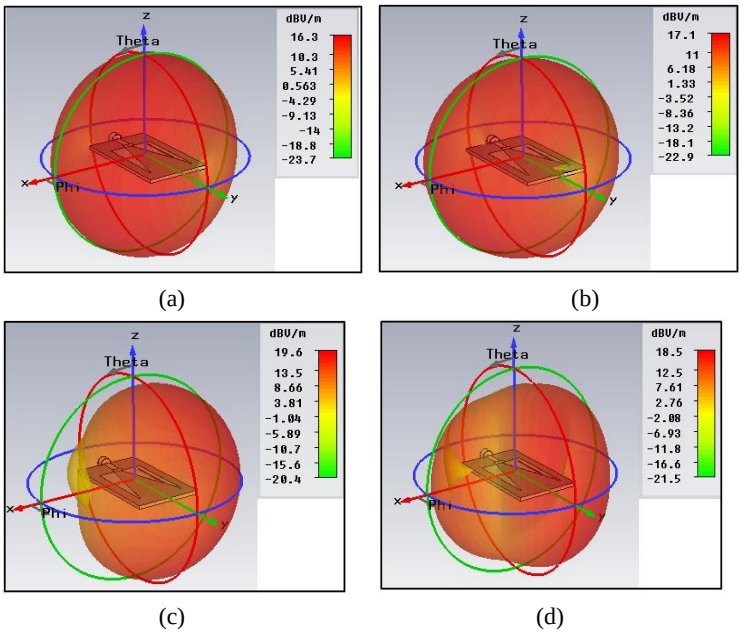

Fig (10): 3D radiation pattern of proposed quad-band antenna.at (a) 1.8GHz, (b) 2.4GHz, (c) 3.65GHz, and (d) 5.3GHz.

CONCLUSION

This paper presented the designs of a compact quad-band printed rectangular monopole antenna (PRMA) for fixed communications systems. By inserting an asymmetrical triangular – shaped slot (ATSS) and rectangular slots in the ordinary PRMA antenna, the wide impedance bandwidth of PRMA were converted to several quarter wavelength resonators, resulting in to multiresonance characteristics. The frequencies in the quad-band modes can independently control frequencies over a wide range using these quarter wavelength resonators without affecting the performance of other bands. The four bands encompass GSM1800, GSM900, PCS, GSM1800,GSM1900, UMTS, WLAN/Bluetooth, WiMAX, and 5 GHz WLAN bands. Radiation patterns and gain showed that the four bands are capable of serving the aforementioned services, with good performances. The main advantage of the proposed antenna are its low profile, light weight, and ease of fabrication, simple structure targeting, and the possibility of integrated it as a smaller wireless communication devices in the future.

REFERENCES

– H. Abutarboush, H. Nasif, R. Nilavalan, and S. W. Cheung,"Multiband and Wideband Monopole Antenna for GSM900 and other Wireless Applications", *IEEE Antennas wireless propag. Lett.*, vol. 11, pp. 539-542. 2012.

– J. Zhu, M. A. Antoniades, and G. V. Eleftheriades, "A Compact Tri-Band Monopole Antenna with Single-Cell Metamaterial Loading", *IEEE Trans. Antennas Propag.*, vol. 58, no. 4, pp. 1031-1038, April 2010.

– C. Pan, T. Horng , W. Chen, and C. Huang, "Dual Wideband Printed Monopole Antenna for WLAN/WiMAX Applications", *IEEE Antennas wireless propag. Lett.*, vol. 6, pp. 149-151, 2007.

– Y. Ge, K. Esselle, and T. Bird, "Compact Triple-Arm Multiband Monopole Antenna", *IEEE International Workshop on Antenna Technology, Small Antennas and Novel Metamaterials*, pp. 172-175, Mar. 2006.

– C. Su, W. Chen, and K. Wong, "Compact Dual-Band Metal-Plate Antenna for 2.4/5.2-GHz WLAN Operation," *Microw. Opt. Technol. Lett.*, vol. 38, pp. 113–115, 2003.

– X. Gao, H. Zhong, Z. Zhang, Z. Feng, and M. F. Iskander, "Low-Profile Planar Tripolarization Antenna for WLAN Communications," *IEEE Antennas Wireless Propag. Lett.*, vol. 9, pp. 83–86, 2010.

– K. Wong, L. Chou, and C. Su, "Dual-Band Flat-Plate Antenna with a Shorted Parasitic Element for Laptop Applications," *IEEE Trans. Antennas Propag.*, vol. 53, no. 1, pp. 539–544, Jan. 2005.

– T. Chang and J. Jiang, "Meandered T-Shaped Monopole Antenna*," IEEE Trans. Antennas Propag.,* vol. 57, no. 12, pp. 3976–3978, Dec. 2009.

– H. Nakano, Y. Sato, H. Mimaki, and J. Yamauchi, "An Inverted FL Antenna for Dual-Frequency Operation," *IEEE Trans. Antennas Propag.*, vol. 53, no. 8, pp. 2417–2421, Aug. 2005.

– N. Ghouddane and M. Essaaidi, "A Novel Compact Multiband Planar Antenna for Wireless and Mobile Handsets," *Mediterrannean Microwave Symposium (MMS)*, pp. 1 – 4, 15-17 Nov. 2009.

– S. Hwang, G. Park, J. Byun, and A. S. Kim, "A PCB Embedded Antenna for 2.4 / 5.2 GHz WLAN and 2.6 GHz SDMB / WIMAX Applications," *Antennas and Propagation Society International Symposium*, pp. 1 – 4, 5-11 July 2008.

– Y. Tawk, K. Y. Kabalan, A. El-Hajj, C. G. Christodoulou, and J. Costantine, "A Simple Multiband Printed Bowtie Antenna", *IEEE Antennas And Wireless Propag. Lett.*, vol. 7, pp. 557-560, 2008.

– H. Halheit, A.Vorst, "A Simple Wideband Antenna for Mobile Handset," *3rd European Conference on Antennas and Propagation EuCAP*, pp. 553 – 555, 23-27 March 2009.

– Y. Ch. and Ch. Chiu, "An Internal Multiband Inverted-F Antenna for Mobile Devices", *IEEE International Workshop on Antenna Technology (iWAT)*, pp.1 – 4, 2-4 March 2009.

– M. Maindarkar and V. Kasabegoudar, "CPW Fed Slot Coupled Wideband and Multiband Antennas for Wireless Applications," *International Journal of Advances in Engineering & Technology*, vol. 5, Issue 1, pp. 456-461, Nov. 2012.

– A. Mehdipour, A. Sebak, "Compact Multiband Planar Antenna for 2.4/3.5/5.2/5.8-GHz Wireless Applications", *IEEE Antennas and Wireless Propag. Lett.*, Vol. 11, 2012.

– Y. Tawk, K. Kabalan, A. El-Hajj, S. Sadek, and M. Al-Husseini," A Modified Bowtie Antenna Design for Wi-Fi and WIMAX Applications," *Wireless Communications and Mobile Computing Conference. IWCMC '08. International*, pp: 729 – 732, 6-8 Aug. 2008.

– H. Lavakhamseh, Ch. Ghobadi, J. Nourinia, and M. Ojaroudi, "Multiresonance Printed Monopole Antenna for DCS/WLAN/ WIMAX Applications," *Microwave and Optical Technology Lett.*, vol. 54, No. 2, Feb. 2012.

– D. Elsheakh and A. Safwat, "Meander Lineloaded Planar Monopole Antennas," *Microwave and Optical Technology Lett.*, vol. 54, No. 8, August 2012.

– J. Li, D. Wu, and Y. Wu, "A Compact Multi-Band Inverted-F Antenna for Laptop Operations", *IEEE 5th International Symposium on////Microwave, Antenna, Propagation and EMC Technologies for Wireless Communications (MAPE)*, pp: 432 – 437, 29-31 Oct. 2013.

– M. Moosazadeh and S. Kharkovsky, "Compact and Small Planar Monopole Antenna with Symmetrical L-And U-Shaped Slots for WLAN/WIMAX Applications," *IEEE Antennas and Wireless Propaga. Lett.* ,vol. 13, pp. 388-391, 2014.

– N. Abbasi, R. Langley, "A Wideband Printed Monopole Antenna over Dual-Band AMC," *Loughborough Antennas & Propagation Conference, Loughborough, UK*, pp: 221 – 224, 8-9 Nov. 2010.

– K. Ray, "Design Aspects of Printed Monopole Antennas for Ultra- Wide Band Applications," *International Journal of Antennas and Propagation*, vol. 2008, Article ID 713858, 8 pages, 2008. doi:10.1155/2008/713858.

– N. Agrawall, G. Kumar, and K. Ray, "Wide-Band Planar Monopole Antennas," *IEEE Trans. on Antennas and Propag.*, vol. 46, no. 2, pp. 294–295, 1998.

– C. Balanis, Antenna Theory Analysis and Design, John Wiley & Sons, Inc., Hoboken, New Jersey, USA, 2005.

– M. John and M. J. Ammann, "Optimization of Impedance Bandwidth for The Printed Rectangular Monopole Antenna," *Microwave and Optical Technology Lett.*, vol. 47, no. 2, pp. 153–154, 2005.

– A. Foudazi, H. Hassani, and S. Nezhad, "Small UWB Planar Monopole Antenna with Added GPS/GSM/WLAN Bands," *IEEE Trans. on Antennas and Propag.*, vol. 60, no. 6, jun. 2012.

– H. Wheeler, "Transmission-Line Properties of a Strip on a Dielectric Sheet on a Plane," *IEEE Trans. Microwave Theory and Techniques*, vol.:25 , pp: 631-647 , Aug., 1977.

– M. Khan, and M. Morsy, "Dual Band Antenna for Wireless Network (WLAN) Applications," *IEEE International Symposium on Antennas and Propagation (APSURSI)*, pp: 1397 – 14003, 8 July 2011.

– R. K. Gupta, "Printed Tri-Band Monopole Antenna Structures for Wireless Applications*," Microw. Opt. Technol. Lett.*, vol. 51, no. 7, pp. 1781–1785, Jul. 2009.

– W. Li, L. Cai, B. You, and C. Huang, "Design of Printed Notched-Monopole UWB Antenna," *IEEE International Conference. Intelligent Computing and*

Intelligent Systems, vol. 3, pp. 271–274, 20-22 Nov. 2009.

– H. Abutarboush, R. Nilavalan, S. Cheung, and K. Nasr, "A Reconfigurable Wideband and Multiband Antenna Using Dual-Patch Elements for Compact Wireless Devices", *IEEE Trans. on Antennas and Propagation*, vol. 60, no. 1, Jan. 2012.

– S. Mohammad A .Nezhad and H. Hassani, "A Novel Tri-Band E-Shaped Printed Monopole Antenna for MIMO Application," *IEEE Antennas Wireless Propag. Lett.*, vol. 9, pp. 576–579, 2010.

– H. AbuTarboush, R. Nilavalan, T. Peter, and S. Cheung, "Multiband Inverted-F Antenna with Independent Bands for Small and Slim Mobile Handsets," *IEEE Trans. Antennas Propag.*, vol. 59, no. 7, July 2011.

– [35] N. Bayatmaku, P. Lotfi, M. Azarmanesh, and S. Soltani, "Design of Simple Multi-Band Patch Antenna for Mobile Communication Applications Using New E-Shape Fractal," *IEEE Antennas Wireless Propag. Lett.*, vol. 10. pp: 873 – 875, 18 Aug. 2011

– R. Sujith, V. Deepu, D. Laila, C. Aanandan, K. Vasudevan, and P. Mohanan, "A Compact Dual-Band Modified T-Shaped CPW-Fed Monopole Antenna," *Microw. Opt. Technol. Lett.*, vol. 51, no. 4, pp. 937–939, 2009.

– B. Lee, W. Chen, W. Chang, F. Yen, and Y. Lin, "Five-Band Printed Antenna for Mobile Phone and WLAN Applications," *IEEE Antennas and Propagation Society International Symposium (APSURSI)*, pp: 1–4, 11-17 July 2010.

هوائي أحادي القطب المطبوع ذات التوليف المستقل الملائم لأجهزة الاتصالات اللاسلكية المصغرة

الخلاصة

تم تقديم شكل جديد من هوائي المستوي متعدد الحزمة في هذا البحث, ويستند الهوائي المقترح عموماً على هوائي احادي القطب المطبوع مستطيل الشكل (PRMA) الذي يغطي عرض حزمة واسعة من النطاق الترددي لحزمة 3.3GHz WiMAX . لتوليد خاصية الحزم المتعددة تم ادخال شقب مثلثي الشكل غير متماثل (ATSS) في مركز (PRMA) من اجل تكوين شريحتين مثلثيتين قائمتي الزاوية اللتان تمتلكان عدة مسارات ذات ارباع اطوال موجية. وتم تحقيق انماط عمل رنينية رباعية الحزمة 1.8GHz و 2.4GHz و 3.7GHz و 5.3GHz نتيجة لعدة اطوال واعراض مختلفة في هذه الشرائح المثلثية. الجانب المميز للهوائي انه يخدم عدة انظمة اتصالات مختلفة انياً وتشمل هذه النظم توليفات مختلفة من GSM1800 و DCS و PCS و WLAN و تطبيقات WiMAX . علاوة على ذلك فان الحزم الترددية الاربعة المنفردة يمكن توليفها بشكل مستقل على نطاقات ترددية واسعة بـ 12.88% و9.72% و 17% و 6.54% على التوالي وذلك بأستخدام معاملات بسيطة للهوائي وهذا يعني اساساً ان مجموعة متنوعة من انظمة الاتصالات الاخرى يمكن ان تخدم بسهولة بأستخدام هوائي واحد فقط.

الهوائي المصمم يمتلك بنية مستوية بسيطة وحجم صغير 45×30 ملم^2 واظهرت نتائج المحاكاة بأن ذروة الكسب المحقق للهوائي عند ترددات العمل المختلفة 1.8GHz و 2.4GHz و 3.7GHz و 5.3GHz هي 1.5dBi و 2.75dBi و 4.7dBi و 4dBi والتي تقابل كفاءة اشعاع 75.8% و 83.6% و 81.6% و82.5% على التوالي. تم الحصول على نتائج المحاكاة بأستخدام برنامج CST مايكروويف ستوديو.

AN ENHANCED STEGANOGRAPHY TECHNIQUE FOR CRYPTING &HIDING ARABIC TEXT IN TO DIGITAL IMAGE

NADA **E**LYA**T**AWFIQ AND **B**ARA'A **W**ASFI **S**ALIM
Dept. of Computer Science, College of Computer and information Technology, Nawroz University

(Received: December 14, 2014; Accepted for publication: June 1, 2015)

ABSTRACT

Steganography techniques are concerned with hiding the existence of sensitive data in other cover media which may be image file, sound or video. Today, text steganography has become particularly popular. This paper presents a modified steganographic technique for using Arabic text in steganography. The Arabic characters have many shapes depends on its position in the word, the idea is to superimpose multiple shapes in visible instances of Arabic diacritic marks over each other. This is possible because of the way in which diacritic marks are displayed onscreen and printed to paper. In this paper, an algorithm to crypt and hide Arabic texts within adigital image was proposed as steganography technique. This algorithm consists of four stages; the first stage deals with a procedure to crypt the Arabic text, each character in each form(including special characters) has a special 16 bit code which called Unicode instead of 8 bits to increase the complexity of retrieving data. The second stage is a procedure to hide a crypt text within digital image using LSB techniques. The third stage is a procedure to extract a hidden text from that image. Finally, the fourth stage is a procedure to decrypt the crypted text by returning the original code of each character. The program of the proposed algorithm has been built using Delphi 2010, and the results were obtained with high and security which proved the efficiency of the algorithm, where the hidden Arabic text didn't make any distortion or change over the cover image.

KEYWORDS :Data Hiding, LSB submission, Arabic text, Delphi 2010

INTRODUCTION

The ever increasing number of network users, such as Internet, mobile communications and drives the process of enhancing security into more serious measures as more victims and attackers are brought into these networks. Thus, how to protect the transmitted data effectively on the internet has become more important (Adnan and Yousef Salem Elarian, 2008).

Data communication is a field where the security issues have their own priority. While exchanging data electronically depends on privacy and secrecy of data primarily. Encryption, transforming data (plain text) into cipher text and decryption, a reverse process, plays a vital role in concealing the confidentiality of the data. The data (message) before exchange or transmission has to be encrypted with a secret key which provides another level of secure communication between the sender and receiver. The proposed approach is recommended since it combines the benefits of hiding the existence of a secret message with security of encryption. The secret message is embedded into the cover data using available steganographic techniques (Ramzi Haraty and Catherine Ghaddar, 2004). Once received, the encrypted secret message will be extracted, and then the message can be decrypted with the appropriate key. Figure1 represents the general steganographic mechanism:

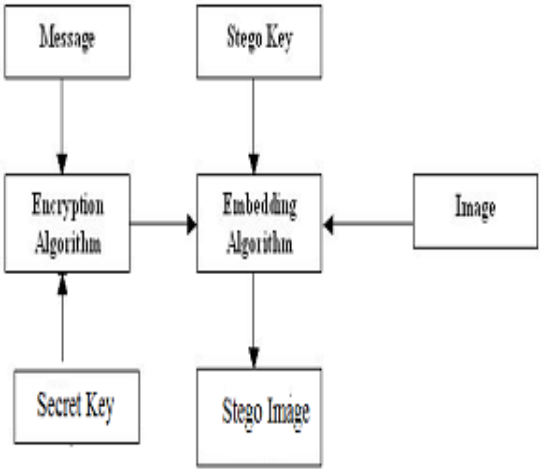

Fig.(1): General steganographic mechanism.

Steganographyis defined as the ability of hiding information in redundant bits of any unremarkable cover media. The cover media used to hide the message can be a text, aimage, video or audio files. The main idea of steganography is sending messages between two parties without any suspicions from intruders.

When the message is transmitted over an untrusted channel, it is necessary to protect our messages. Mainly there are two scenarios for this purpose:

1- Cryptography: Hidden data meaning.

2-Steganography: Hidden data existence.

Usually the first scenario (cryptography) was used where data transferred from readable form (plain text) into scribbled data (cipher text), and then rely on transmitting cipher text message by using a secrete key. While with the second scenario, steganography will hide data existence by using another file as carrier and a strategy to insert secret data inside it. Then will passes the data through the communication channel. In this case everyone can read the carrier file but no one can notice the hidden message(Ramzi Haraty, Catherine Ghaddar et al 2004). Steganography Imaging system is a system that capable of hiding the data inside the image. The system is using 2 layers of security in order to maintain data privacy. Data security is the practice of keeping data protected from corruption and unauthorized access (Sofiene Haboubi, Samia Maddouri, Hamid Amiri, 2003)

Clearly the purpose of steganography is to avoid drawing suspicion to the transmission of hidden information.

A message is a hidden information in the form of plain text, cipher text, images or anything that can be encoded into a bit stream. This message is embedded in a cover-carrier to create a stego-carrier. A possible formula of the process may be represented as follows:

Stegomedium=Covermedium+Embedded message+StegokeyTurn MathJaxon Choosing carrier file is very sensitive as it plays a key role to protect the embedded message.

Basic techniques of steganography

The steganography system has two inputs as shown in Figure 1:

-A Cover Object" and a "Secret Object", which is confidential. Steganography algorithm comes into picture to do the embedding part for the two inputs, i.e. these two objects output the "Stego Object".

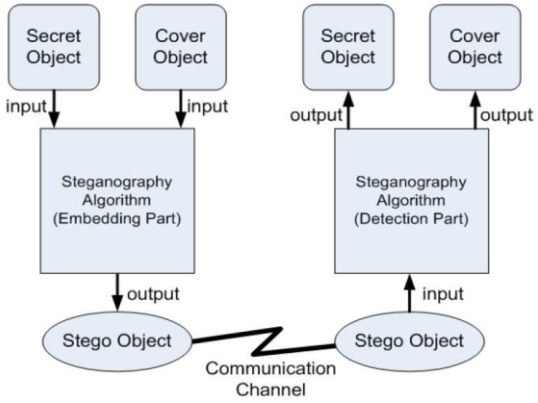

Fig. (2): Steganography System.

There are many techniques for hiding information or messages in images. Common approaches are including.

(I) Least significant bit insertion (LSB).

(II) Masking and filtering.

(III) Transform techniques.

Data Hiding by LSB substitution

Least Significant Bits (LSB) insertion is a simple approach to embed data in image file. The easiest steganographic methods embed the bits of the message directly into least significant bit plane of the cover-image in a sequence. Modulating the LSB does not camp up with in human-perceptible difference because the amplitude of the change is small. (Anwar H. Ibrahim, Waleed M. Ibrahim, 2009).

Masking and Filtering

These techniques, usually restricted to 24 bits and gray scale images, hide information by making an imaimage, in the same way as to paper watermarks.

These techniques embed the information in the more significant areas than just hidden message is more integral to the cover image, watermarking techniques may be applied without the fear of image destruction due to lossy compression as they are more integrated into the image.(Anwar H. Ibrahim, Waleed M. Ibrahim,2009).

Transformation

A more complex way of hiding a secret inside an image comes with the use and modifications of discrete cosine transformations (DST), are used by JPEG compression algorithm to transform successive 8 x 8 pixel blocks of the image, into 64 DCT coefficient each (Pye P. Aung, Tun M. Naing,2014).

Structural Features of Arabic and Latin Scripts

The Arabic alphabet has 28 letters which have different shapes. These forms vary according to their positions in the word, their widths, number and position of the diacritical points. The Latin alphabet contains 26 letters which have different shapes. These forms vary according to their statements lowercase or uppercase and the presence of accents in the character, items, and other forms that vary by language. These factors increase the total number of different types of characters into more than 100for each of the scripts (Arabic and Latin). Figure 3 shows an example of different forms for Arabic letters and Latin letters .The first step is to see the structural aspect of each script of Arabic and Latin. We note that the general shape of the Arabic script is totally different from the Latin script (Nasser Hamid, 2010).

Arabic Text Specific Difficulties

The following difficulties are specific to Arabic text segmentation and recognition. Arabic characters can have more than one shape according to their position in a word whether it is in the beginning, middle, final, or stanalon (Firas A. Jassim et al 2013).

Figure (3)is an example of different forms for Arabic letter. There are (22) Arabic letters which have (4) shapes(D. Seetha1, Dr.P.Eswaran2,et al 2013,Vipul Sharma, Sunny Kumar,et al 2013 ,Rosziati Ibrahim and Teoh Suk Kuan,et al 2011)

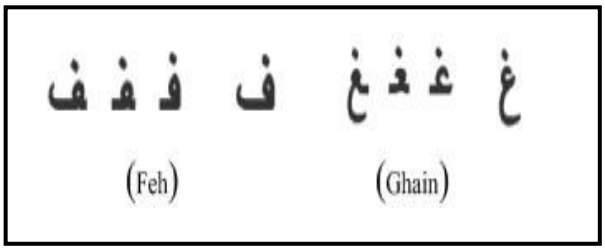

Fig. (3): Different shapes of letters.

Arabic language is the largest living member of the Semitic language family in terms of speakers(There are 270 million speakers). This language contains 28 alphabet characters; 15 of which have points (one point, two points or three points) as shown in figure(4)(Nasser Hamad, 2010)

Character with three points	**Character with two points**	**Character withone point**	**Character with no points**
ث ش	ت ق ي	ب ج خ ذ ز ض ظ غ ف ن	أ ح د ر س ص ط ع ك ل م هـ و

Fig. (4): Arabic Letters with Points.

The Arabic alphabet has Semitic origins derived from the Aramaic writing system. Arabic diacritic marks decorate consonant letters to specify (short) vowels. Those marks, shown in Figure 5, normally come over/beneath Arabic consonant characters. Arabic readers are trained to deduce these marks (Ali J. Mohammed, Ali A. Dawood AL-Zuky and Fatin E.Muhy,et al 2007).

Vowels generally exist frequently in many languages. Particularly in Arabic, the nucleus of every syllable is a vowel. Inside the computer, these are represented as characters. The use of diacritics is an option not very common, which is practiced in modern standard Arabic, except for holy scripts (D.Seetha1, Dr.P.Eswaran2, 2013).

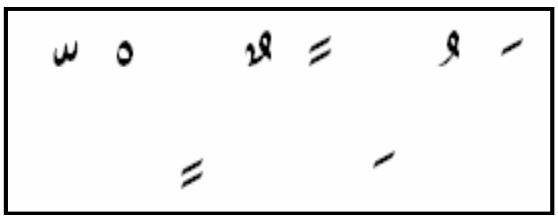

Fig. (5): Arabic diacritic marks

Figure (6) presents the codes of each structural feature used with their many appearances in letters, taking into account the different forms of each letter.

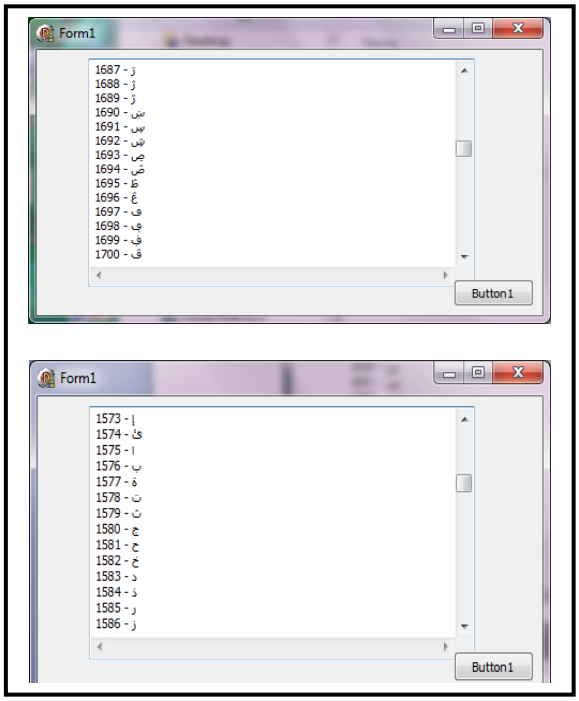

Fig. (6): Code of Characters

PROPOSED TECHNIQUE

In our proposed algorithm, aprogram of crypting and embedding data was proposed, which embed the cipher text in a cover medium. This system combines the effect of these two methods to enhance the security of the data. The proposed system encrypts the data with a crypt algorithm and then embeds the encrypted data in a cover file. The block diagram of the proposed system is shown in figure (7).

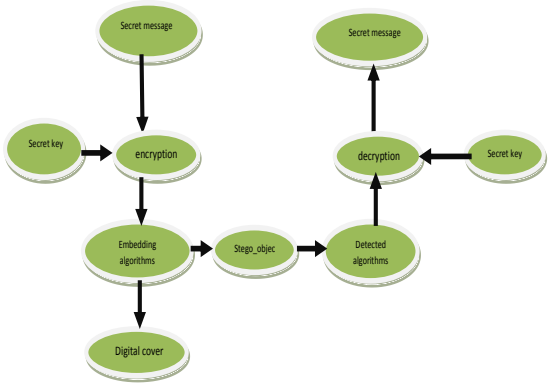

Fig. (7): Block diagram of proposed system

For the embedding stage, LSB (most commonly used) technique is used due to its simplicity and easy implementation. The change in the LSB of the pixel in image renders the visual quality of image on hiding the message does not much affect the image and make it unnoticeable to unintended person.

In this paper, in order to hide the message produced after encryption a method was proposed to embed the message within the image as the cover media. The result would produce a step_ image which then be transmitted over the channel. In this section, the colored bmp images are used as cover medium and the procedure is addressed.

The code of Arabic characters is begin from 1556 to 1775 Unicode which include all characters in different forms as shown in figures (3,4 and 5).

Following are the major steps involved in data hiding and extraction:

Inputs: - Text file, cover image 1, cover image 2 and secret key.

Output: - Stego image.

Begin

A. Hiding Algorithm

The suggested algorithm is to hide an Arabic text into BMP- image based on taking LSB from each image pixel values. This performs as follows:

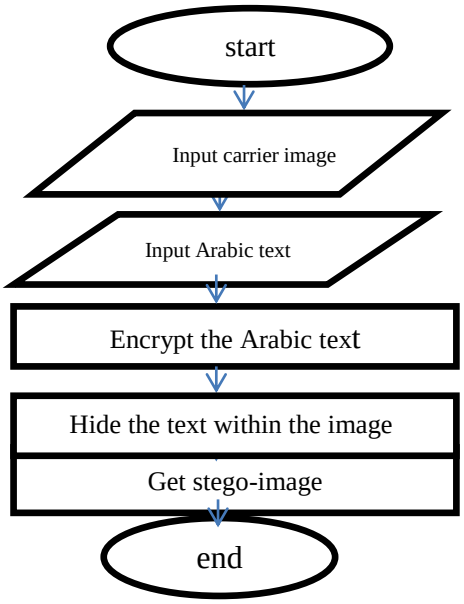

1. Input BMP-image.

2. Convert each image pixel value from decimal system into binary digital system.

3. Input the text message, then convert each character into binary number, each character represented by 16-bits.

4. Encrypted the text message using secret key then, the bits of each character will be embed in the bits LSB part of image pixel.

5. Output stego-image.

6. End

B. Extract hiding information Algorithm

Start decoding algorithm as follows:

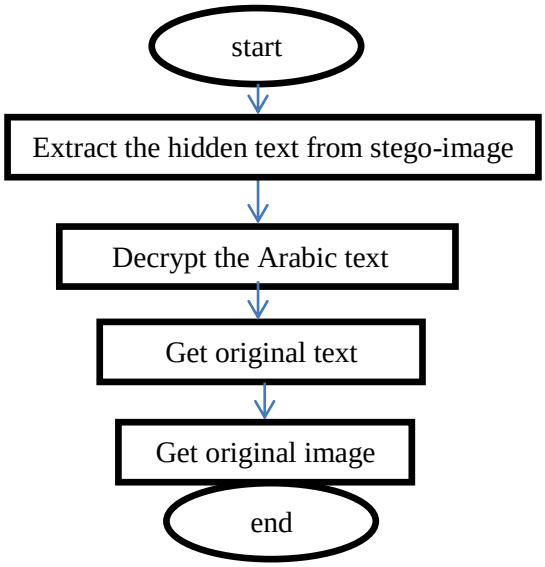

1. Input stego-image.
2. Convert each image element into binary system.
3. Extract from each image element first 2 bits (LSB). Then arrange these data into a stream of bits.
4. Divide the stream of bits into blocks each block contains 16 bits.
5. Then each 16 bits is decrypted using the secret Key and converted into represented symbols, to reconstruct the text-message again.
6. The output is the text message.
7. End algorithm

The first step in the proposed algorithm is to convert the data into the bytes in which each character in message is converted to its equivalent Unicode.

For example 1:

The Unicode of character (ن) is 1606 and equivalent binary is (0000011001000110) plus the code of the key(101)= (000011001001110).

Example 2:

Suppose we have the message (ندى), then each character of the message is converted to its binary as shown: (0000011001001011000001100011000 0000011001001110).

Then the message is embeds 2-bits into the LSB position of each pixel position, as shown below:

RGB: 00100111-11101001-11001000

ن :0000110010011 10

Figure (8) represents the image before embedding the text.

Fig. (8): The original Bitmap image (image1)

We can save any number of characters into 24 bit BMP image, Figure (9) represents the image and the Arabic text which embedded within that image:

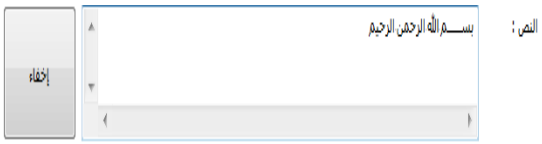

Fig. (9): Image1 within Embedded Arabic Text

Fig, (10): Image2 within Embedded Arabic Text

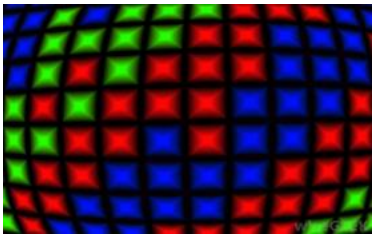

Fig. (11): Image3 within Embedded Arabic Text

Next step is to save the new image with hidden text.

Finally extract the text from the image as shown in figure (12):

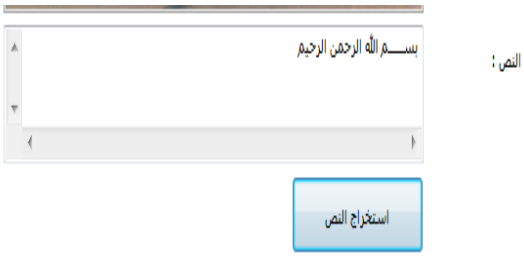

Fig. (12): Extract the text

The PSNR for the proposed algorithm is tabulates as shown in Table (1):

Table (1): PSNR for test images

Stego-image	PSNR	MSE
Image1	67.6164	3.7559
Image2	72.4925	0.0037
Image3	64.8610	0.0212

Mean Square Error:

$$MSE=\frac{1}{m*n} * \sum_{i=1}^{m} \sum_{j=1}^{n} (CI(i,j) - SI(i,j))^2$$

Where: *CI* is cover-image of size (M x N) and *SI* is stego-image (M x N), $1 \leq i \leq M$, $1 \leq j \leq N$.

The equation to calculate Peak Signal to Noise Ratio (PSNR):

$$PSNR= 10*\log_{10}(\frac{R^2}{MSE})$$

If cover-image is grayscale image of integer values [0-255], then R =255

The results obtained by this paper indicate that the embedding process introduces high Peak Signal to Noise Ratio (PSNR) with less perceptual distortion. The PSNR value was observed for some images, which is constantly above 51 dB as illustrated in Table (1). This is mean that the quality degradations could hardly be perceived by a human eye.

CONCLUSION AND FUTURE WORK

- The practical results have proved that the suggested algorithm is sufficient in terms of no much changes nor noticeable distortion appeared at the hidden information on the used cover file.
- With regard to the results of PSNR for different file sizes which demonstrated in table (1), the values of the PSNR are sophisticated and really very good compared with other algorithms.
- The system has been built to provide high security in a style to be very difficult to infer and detect the existence of any hidden information.
- It is possible to hide huge amount of data in the existed image.
- The hiding system can be used with high flexibility and simplicity.
- with PSNR measure a large number implies a better stego-imag
- As a future work it is suggested to design an algorithm to hide Kurdish texts.

REFERENCES

- Adnan Abdul-Aziz Gutub, Yousef Salem Elarian," ARABIC TEXT STEGANOGRAPHY USING MULTIPLE DIACRITICS", Computer Engineering Department, King Fahd University of Petroleum & Minerals, Saudi Arabia,2008.
- Ramzi Haraty and Catherine Ghaddar," Arabic Text Recognition", The International Arab Journal of Information Technology, Vol. 1, No. 2, July 2004, Lebanese American University, Lebanon.
- Sofiene Haboubi, Samia Maddouri, Hamid Amiri," Identification of arabic word from bilingual text using character features, National Engineering School of Tunis BP 37, Belvedere 1002, Tunis, 2003
- Anwar H. Ibrahim, Waleed M. Ibrahim," Text Hidden in Picture Using Steganography: Algorithms and Implications for Phase Embedding and Extraction Time", Department of Electrical and Electronics Engineering, Infrastructure University Kuala Lumpur, February, International Journal of Information Technology & Computer Science (IJITCS) (ISSN No : 2091-1610) Volume 7 : No : 3 : Issue on January / February, 2013.
- Nasser Hamad," Hiding Text Information in a Digital Image Based on Entropy Function", Faculty of Information Technology, Arab American University, Palestine, The International Arab Journal of Information Technology, Vol. 7, No. 2, April 2010.
- Firas A. Jassim, " A Novel Steganography Algorithm for Hiding Text in Image using Five Modulus Method", International Journal of Computer Applications (0975 – 8887 Volume 72– No.17, June 2013, Irbid National University.
- D. Seetha1, Dr.P.Eswaran2, "A Study on Steganography to Hide Secret Message inside an Image", International Journal of P2P Network Trends and Technology (IJPTT) - Volume3Issue5- June 2013, india.
- Suresh Kumar, Ganesh Singh, Tarun Kumar, Maninder Singh Nehra," Hiding the Text Messages of Variable Size using Encryption and Decryption Algorithms in Image Steganography", International Journal of Computer Applications, Volume 61– No.6, January 2013.
- Vipul Sharma, Sunny Kumar," A New Approach to Hide Text in Images Using Steganography", Volume 3, Issue 4, April 2013 ,Bahra University, Shimla Hills, India

- Ali J. Mohammed, Ali A. Dawood AL-Zuky and FatinEzzatMuhy, "Text Hiding Technique in Digital Image", Al-Mustansiriyah University, College of Science, Department of Physics, Baghdad, Iraq. Al- Mustansiriya Journal. Sci Vol. 18, No 4, 2007.
- Rosziati Ibrahim and Teoh Suk Kuan ," Steganography Algorithm to Hide Secret Message inside an Image ", Faculty of Computer Science and Information Technology" , University Tun Hussein Onn Malaysia(UTHM),Malaysia,Computer Technology and Application 2 (2011) 102-108February 2011, David publishing.
- Pye Pye Aung and Tun Min Naing," A Novel Secure Combination Technique of Steganography and Cryptography", International Journal of Information Technology, Modeling and Computing (IJITMC) Vol. 2, No. 1, February , 2014.

پوختە

تەکنیکێت فەشارتنا بێزانینا دهێتە بکارئینان بو فەشارتنا بێزانینێت گرنگ دناف فایلەکێ ئەو فایلە ج وێنە بیت یان دەنگ یان فیدیو. و ئەف تەکنیکە لفان دوماهیکا وەك تەکنیکێت بەربلاف دهێنە بکارئینان. دفی لاپەرەیدا سیستەمێ فەشارتنا تێکستا ب پیتێت ئەرەبی کو پیتێت ئەرەبی دهێتە نیاسین کو بشێوێت جوراوجورن لدیف جە و ووشان. و هەروەسا دگەل وان پیتێت بشێوێ (حرکە) ئەوێت دهێنە بکارئینان لسەر پیتێن ئەرەبی لدیف جەوانیا دیارکرنا وێ لسەر شاشەی یان کوبیکرنێ. وەك زێدەهی دهێتە زانین کو هندەك پیتێت ئەرەبی ژ خالەکێ یان دوو یا نسێ خالا بێك دهێت. دفی لاپەرەیدا خوارزمیەك هاتیە دیزاین کرن ژبو فەشارتنا پیتێت ئەرەبی ب هەمی جور و شێوێت وێفە وەك وێنەیەکێ دیجیتالی. ئەف خوارزمیە بێك دهێت ژجەند پارجا: پارجا ئێکێ کارێ وێ فەشارتنا بێزانینا تێکستا ئەرەبی کو هەمی پیت دهێنە گهورین (ئەو ژی کو هێمایێ وێ (bit16 یە بو هێمایەکێ دی داکو پتر کارێ زفراندنا تێکستا ئوریجینال ب زحمەت بیت, پارجا دووێ بێك دهێت ژ رێکا فەشارتنا بێزانینا ل وێنێ دیجیتالی دا ب بکارئینانا بتێ کێم کار (البت الاقل اهمیه), پارجا دی ژ خوارزمیێ بێك دهێت ژ کارێ زفراندنا تێکستا هاتیە فەشارتن بشێوێ ئەرەبی ژ وێنەی و زفراندنا هەمی هێماییێت دناف پیتێت ئەرەبی دا هەین.

زمانێ پروگرامی یێ هاتیە بکارئینان دفی لاپەرەیدا زمانێ Delphi 2010 بو جێکرنا فی سیستەمی, هەروەسا ئەنجامێت وێ بشێوەکێ زور باش و سیکیور دیاردبیت, کو تێکستا ئەرەبی بێ گهورین هاتیە زفراندن بشتی فەشارتنا وێ دناف وێنەیدا.

الخلاصة

ان تقنيات الاخفاء تختص بأخفاء البيانات والمعلومات المهمة والحساسة داخل الملفات الحاملة التي قد تكون صورا او ملفات صوت او فيديو. وهذة التقنيات اصبحت اليوم شائعة الاستعمال. تم في هذا البحث بناء نظام لاخفاء النص العربي حيث ان الحروف العربية تتميز بان لها اشكالا مختلفة حسب موقعها في الكلمة , وايضا هناك الحركات التي توضع على الحروف والتي تعتبر هي ايضا كأي حرف اخر نظرا لامكانية عرضها على الشاشة او طباعتها, اضافة الى ان بعض الحروف العربية لها نقطة واحدة او نقطتان اوثلاثة نقاط. في هذا العمل تم تصميم خوارزمية لتشفير واخفاء الحروف العربية بكافة اشكالها واخفائها ضمن صورة رقمية , هذه الخوارزمية تتألف من عدة اجزاء : الجزء الاول عبارة عن طريقة لتشفير النص العربي حيث يتم تغيير كل حرف (والذي له رمز خاص يتألف من 16 bit بدلا من 8 bit) الى رمز اخر وذلك لزيادة تعقيد عملية استرجاع المعلومات. الجزء الثاني من الخوارزمية يتضمن طريقة لأخفاء النص العربي ضمن الصورة الرقمية باستخدام اسلوب البت الاقل اهمية. الاجزاء الاخرى من الخوارزمية المقترحة تتضمن عملية استرجاع النص من الصورة الرقمية , وثم اعادة الرموز والحروف الاصلية العربية للنص.

تم استخدام لغة البرمجة Delphi 2010في الجانب العملي لتصميم النظام, وقد اثبتت النتائج العملية كفاءة وامنية الخوارزمية المقترحة, حيث ان النص العربي المخفي لم يحدث اي تشوه او تغيير في الصورة الرقمية الحاملة

STUDY THE EFFECT OF AGING TEMPERATURE AND SLIDING DISTANCE ON WEAR PROPERTY OF SDSS SAF 2507

RAMADHAN **H**. **G**ARDI and **A**HMED **S**AMIR **A**
Dept. of Mechanical, College of Engineering, University of Salahaddin, Kurdistan Region-Iraq

Received: January 25, 2015; Accepted for publication: June 1, 2015)

ABSTRACT

The purpose of this paper is to study the effect of heat treatment on sliding wear property of super duplex stainless steel SAF 2507.Sliding wear volume determined as a function of aging temperature. Four different aging temperatures were selected 700îC, 800îC, 900îC, and 1000îC .The specimens remained at these temperatures for 60 minutes and then quenched in water. During aging super duplex stainless steel SAF 2507 various transformations at microstructure will induced involving precipitation of chromium carbides and nitrides, sigma (σ) phase and other intermetalic phases which influence the wear property. The specimens aged at (800îC) exhibit highest wear resistance.

KEYWORD: Wear, Super duplex stainless steel SAF 2507, Sigma phase.

INTRODUCTION

Duplex Stainless Steels DSSs are Iron (Fe) –Chromium (Cr)-Nickel (Ni) alloys with approximately 50%austenitic-ferritic microstructure at room temperature.The dual phase microstructure of DSSs lead to combination of attractive properties like mechanical strength and corrosion resistance that cannot be attainable readily using single phase austenitic or ferritic stainless steel individually [1]. Super Duplex Stainless Steel SAF 2507 is used in oil and gas industry, tubing for heat exchangers ,gauges, fasteners, ships, valves, refineries, pipe for sea water transport, propeller shafts, and other products subjected to high mechanical loads in sea water and other chloride containing environment [2].

During welding and high temperature exposure the alloying elements disturbed by the formation of precipitates. The most common precipitates are chromium carbides and nitrides and intermetalic precipitates such as sigma phase and chi phase. These microstructure changes have great influence on mechanical and corrosion properties of stainless steels.

D.J.Whitefield and A. Van Bennekon [3] investigated the influence of aging at 1050°C for one hour on wear resistance of duplex stainless steel SAF 2205 and reported that wear resistance of heat treated specimens slightly more than that of as received material.

A. M. Do Nascimento et al [4] reported that injection of WC particle by Laser Melt Injection (LMI) to the surface of cast duplex stainless steel substantially improved sliding wear resistance. G. Bregliozzi et al [5] studied the effect of grain size and relative humidity on friction and wear behavior of AISI 304 austenitic stainless steel and they found that AISI 304 austenitic stainless steels with finer grain are more wear resistance and lower coefficient of friction compared to coarse grain for all load range also they reported that with increasing relative humidity the wear rate decrease. Ram Subbiah and R.Rajavel [6] studied the effect of gas nitriding for different times on wear behavior of AISI 316L N austenitic stainless steel and they concluded that gas nitriding effectively improves wear resistance and as the nitriding time increased the wear rate decrease. N.L.Parthasarathi and Muthukannan Duraiselvam [7] studied the effect of Ni CrB SiCFe plasma sprayed AISI 316 austenitic stainless steel substrates at various operating temperature and reported that the plasma sprayed Ni CrB SiCFe coating increases wear resistance up to 4.5 times compared to the uncoated AISI 316 austenitic stainless steel substrate. The present research was performed to identify the effect of heat treatment on wear resistance and micro structural changes of SDSS SAF 2507.

EXPERIMENTAL PROCEDURE

Materials: The work piece materials used in this study is super duplex stainless steel (SDSS) SAF 2507. The dimensions of materials are 4mm diameter round bars. The chemical compositions of work piece materials are given in Table (1). Elementary chemical composition detected using spectrometer metal analyzer model spectromaxx, spectro company, Germany 2010.

Table (1): Elementary chemical composition of super duplex stainless SAF2507

Material	Cr%	Ni%	C%	Mo%	Mn%	P%	N%	Si%	S%	Fe
SAF2507	25	7.8	0.03	4	1.1	0.03	0.25	0.8	0.015	Bal.

The samples as shown in figure (1) were cut from the bar. To investigate the effect of heat treatment on wear resistance of super duplex stainless steel SAF 2507, four temperature of heat treatment were carried out in this study .The temperatures 700°C, 800°C, 900°C, and 1000°C, were selected and the holding time is 60 minutes were selected for each of these temperature after that the specimens water quenched. Previous to wear test the specimens mechanical finished with the aid 600 grit emery papers. Sliding wear test were performed using wear tester [Model: TE91/1, Pin on Disc Model, Serial No.: U 9259/3, TQ]. Test were done at a constant load of 25 N and linear velocity 12.5 m/min. Different distance were considered 125m, 250 m, 375 m, and 500 m and wear volume was determined.

For metallographic examination the specimens were mechanically finished with the aid of 120, 320, 600, and 1000 grid emery papers subsequently with using water to avoid overheating, polishing has been done using diamond paste. The specimens etched chemically according to ASTM standard. The solution consists of saturated solution of $FeCl_3$ in HCl to which a little HNO_3 is added and etching times equals to five minutes. The microstructures were examined in an optical microscope .The austenite has a bright contrast, ferrite yellow and carbide containing chromium appears as a darker phase [8].

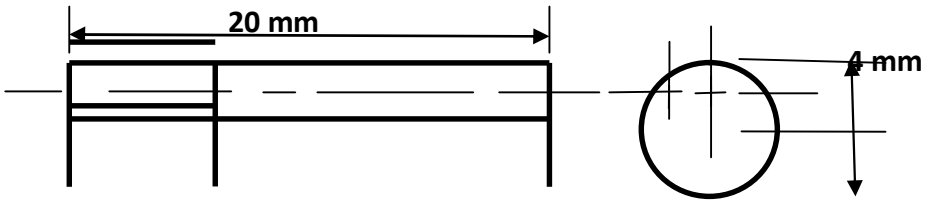

Fig. (1): Dimensions of wear specimens

RESULTS AND DISCUSSION

The microstructure of as received super duplex stainless steel SAF 2507 is shown in figure (2) .The austenite phase is white and ferrite phase reveled colored.

During heating of the super duplex stainless steels microstructural transformation mainly take place in ferrite phase this can be explained that the diffusion rate of alloying element in ferrite phase is nearly 100 times faster than that in austenite phase this attributed to bcc crystal structure of ferrite. In addition to this the ferrite phase is reach in Cr and Mo compared to austenitic phase, which are known to promote the formation of intermetalic phases [9].

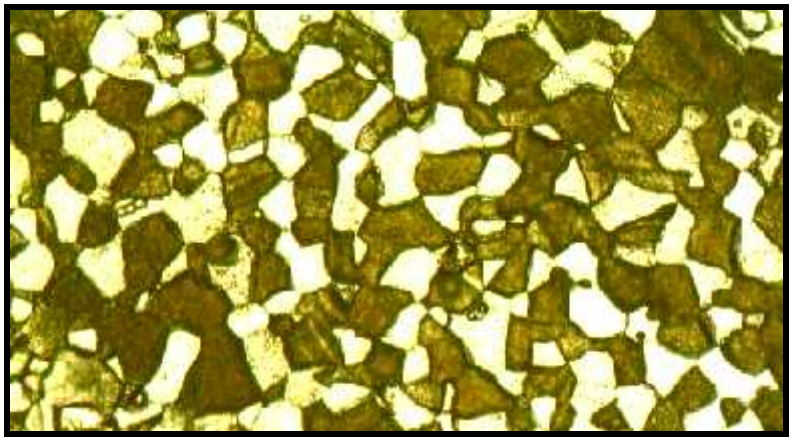

Fig. (2): Microstructure of as received super duplex stainless steel SAF 2507 (x600)

Figure (3) shows the results of the wear volume as a function of sliding distance for as received super duplex stainless steel SAF 2507 which is 6 mm^3 at 125m and increased gradually to 18.6 mm^3 at 500m sliding distance.

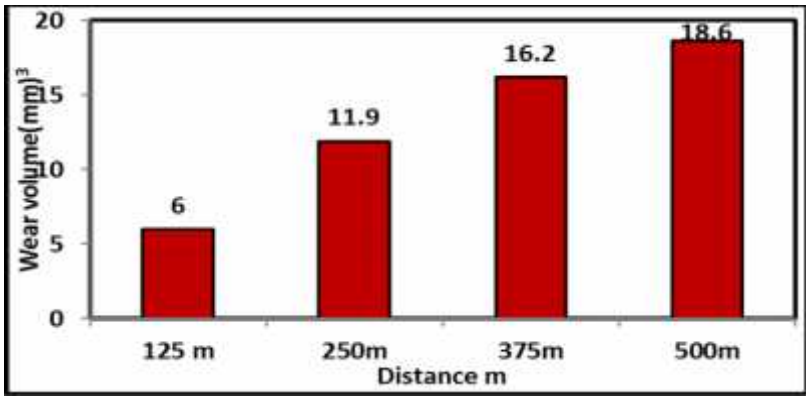

Fig. (3): Wear volume of SDSS SAF 2507 at as received condition vs. sliding distance

Figure (4) shows the wear volume as a function of sliding distance for the specimen heat treated at 700^{o}C for one hour. It was observed that the wear volume at 125m is (13.5) mm^3 increased gradually with increasing the sliding distance reached to (46.98) mm^3 at 500m sliding distance. The wear volume of specimens aged at 700°C for one hour increased compared to that of as receive specimens which is (18.8) mm^3 at 500m sliding distance ,this attributed to the micro structural changes that occurs

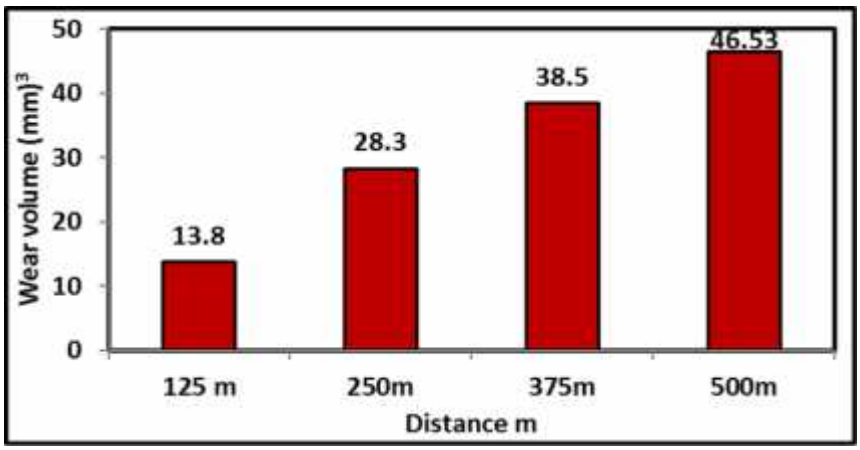

Fig. (4): Wear volume of SDSS SAF 2507 heat treated at700°C for one hour vs sliding distance

in which aging super duplex stainless steel SAF 2507 at 700°C results small amount of sigma phase. Figure (5) shows the microstructure of specimens aged at 700°C for one hour.

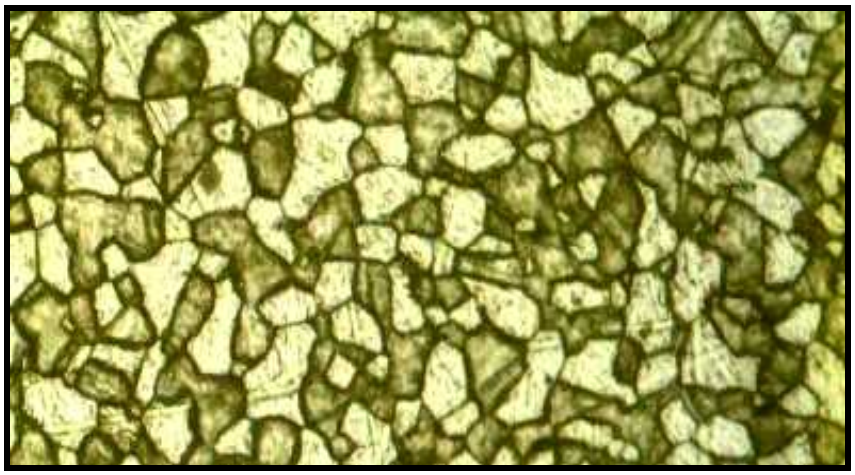

Fig. (5): Microstructure of SDSS SAF 2507 aged at 700°C for one hour(X600)

Increasing the aging temperature from 700°C to 800°C the wear behavior of super duplex stainless steel SAF 2507 will altered in which minimum wear rate can be seen for the specimens aged at 800°C as shown in figure (6), among all the temperature selected in this study which is (5.1) mm^3 at first 125m sliding distance and reached to (16) mm^3 wear volume through 500 m sliding distance, this may attribute to decomposition of ferrite phase at this temperature to hard, brittle, hexagonal closed packed sigma phase in addition to this phase some precipitation which expected to be chromium nitride along the grain boundaries can be seen and effectively contribute to wear resistance. Figure (7) shows the microstructure of specimens aged at 800°C for one hour.

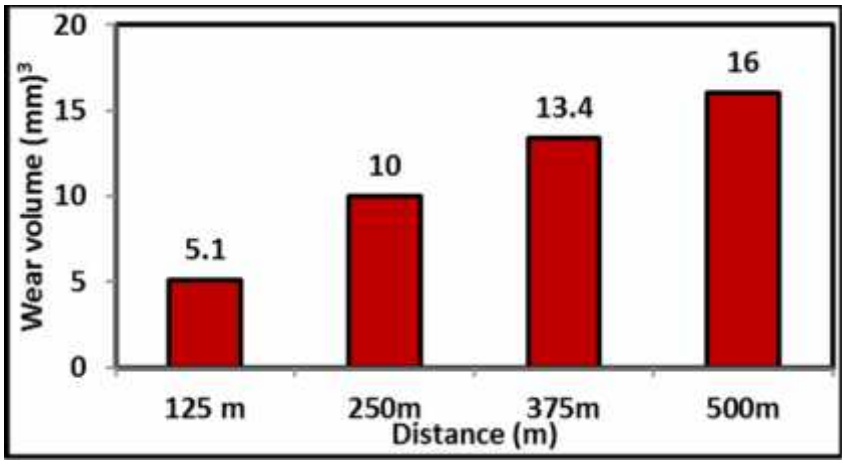

Fig. (6): Wear volume of SDSS SAF 2507 heat treated at800°C for one hour vs sliding distance

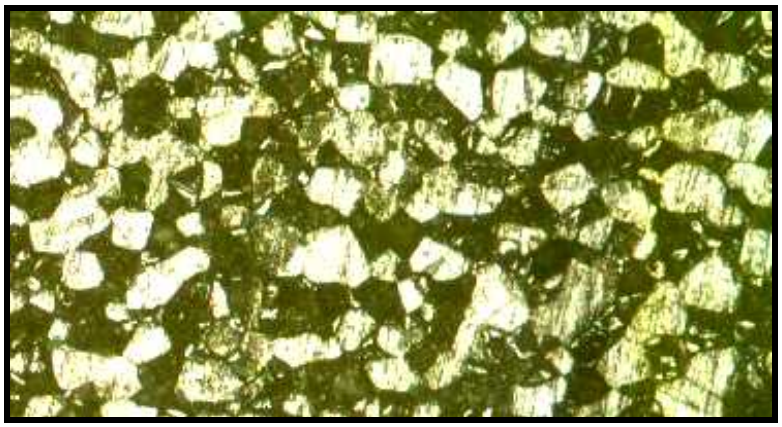

Fig. (7): Microstructure of SDSS SAF 2507 aged at 800°C for one hour(X600)

Figure (8) shows that the increasing the aging temperature to 900°C the wear rate showed small increases compared to the specimens aged at 800 °C but less than that exhibited by specimens aged at 700°C. The wear volume at 125m is (11.7) mm^3 and increased to (43.59) mm^3 at 500m sliding distance this may be attributed to the amount of sigma phase which appear less than at the specimens aged at 900°C compared to that aged at 800°C but at the same time in addition to sigma phase some precipitations which is expected to be chromium nitride can be seen along the grain boundaries which contribute to wear resistance. Fig. (9) Shows the microstructure of the specimens aged at 900°C for one hour.

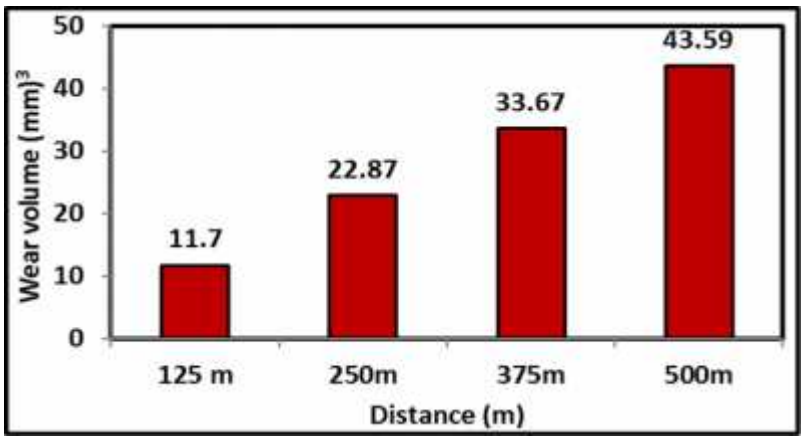

Fig. (8): Wear volume of SDSS SAF 2507 heat treated at 900°C for one hour vs. sliding distance

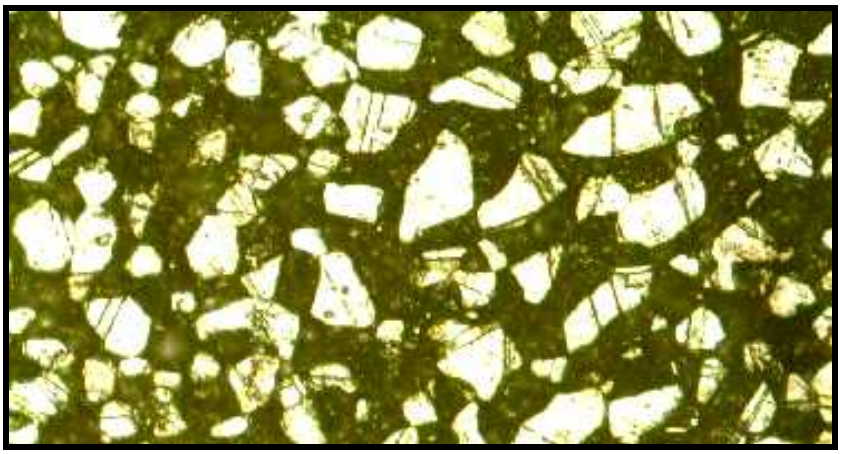

Fig. (9): Microstructure of SDSS SAF 2507 aged at 900°C for one hour(X600)

Figure (10) shows that the further increasing the aging temperature to 1000°C the wear resistance of super duplex stainless steel SAF 2507 decreased compared to the specimens aged at 800°C and 900°C in which the wear volume at 125m sliding is (16.45) mm^3 and reached to (52.23) mm^3 through 500 m sliding the results can be explained that the precipitates in which main contributor to wear resistance of super duplex stainless steel reduced to its minimum amount .Fig. (11) Shows the microstructure of specimens aged at 1000°C

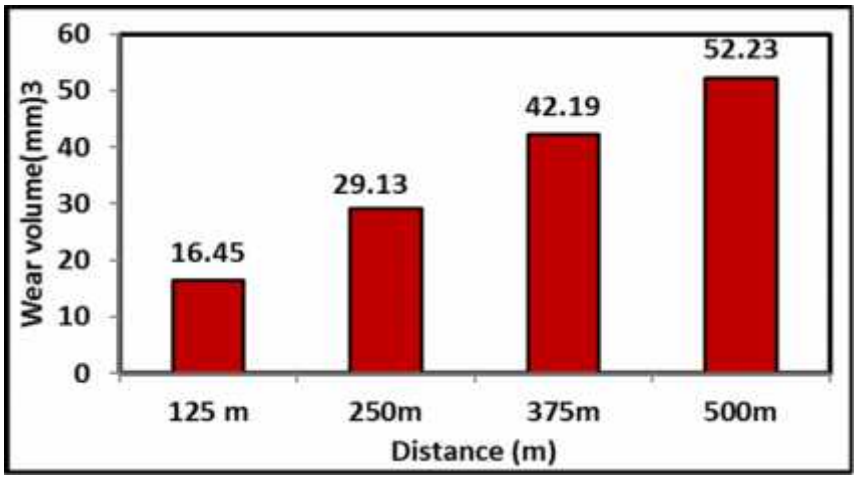

Fig. (10): Wear volume of SDSS SAF 2507 heat treated at1000°C for one hour vs sliding distance

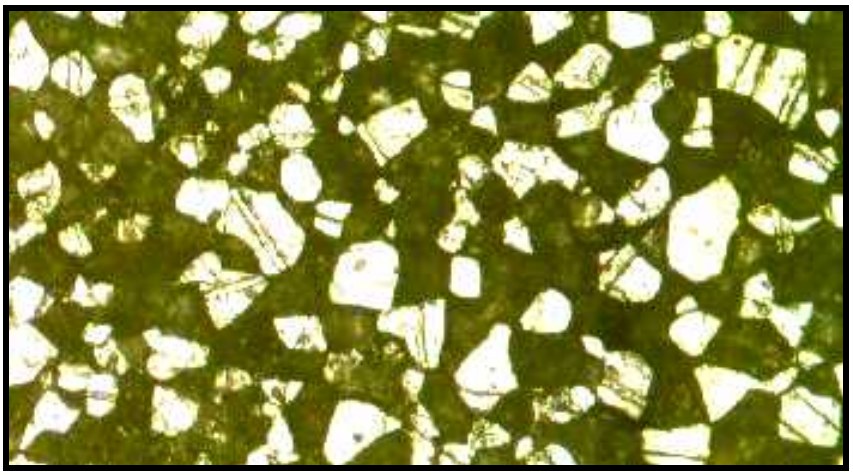

Fig. (11): Microstructure of SDSS SAF 2507 aged at 1000℃ for one hour(X600)

CONCLUSIONS

The effect of aging temperature on wear resistance of super duplex stainless steel SAF 2507 was investigated. The following conclusions were drawn:

1. Maximum wear resistance of SDSS SAF 2507 can be obtained at specimens aged at 800°C for one hour.

2. With the same aging time (1 hour) the aging temperature range of wear resistance from high to low is (800°C, 900°C, 700°C, and 1000°C).

3. Increasing the intermetalic compound in SDSS SAF 2507 increases the wear resistance.

REFERENCES

- Davidson R.M., Redmont J.D.,A guide to use duplex stainless steel ,Material and Design ,Vol.12 .No 4,P. 187-192 (1991).
- Duplex stainless steel, Sandvic SAF 2507 material data sheet -1875-ENG May (2008).
- D.J.Whitefield and A.Van Bennekom Abrasive wear properties of experimental detestable duplex stainless steels. Wear, Vol. 196, pp.92-99, (1996).
- A.M.DoNascimento, V.Ocelik, M.C.F.Ierardi, and J.Th.M.De Hosson, Wear resistance of WCp/Duplex stainless steel metal matrix composite layer prepared by laser melt injection, Journal of Surface and Coating Technology, Vol.202, pp.4758-4765, (2008).
- G.Bregliozzi, S.I-U. G. Ahmed,A.Di Schino,J.M.Kenny and H.Haefke, Friction and wear behavior of austenitic stainless steel; influence of atmospheric humidity, load range and grain size, Tribology Letters,Vol.17,No.4, pp.697-704. (2004),
- Ram Subbaiah and Dr R.Rajavel, Dry sliding wear behavior analysis of nitride 316L grade austenitic stainless steel using gas nitriding process, Journal of theoretical and applied information technology ,2005-2010,JATIT,pp.98-101.
- N.L.Parthasarathi and Muthukannan Duraiselvam, Improvement of high temperature wear resistance of AISI 316 ASS through NiCrBSiCFe plasma spray coating, Journal of Materials and Materials Characterization and Engineering, Vol, 9, No.7, PP.655-670,(2010).
- ASTM standard test method for metallographic of metals Annual book of ASTM standards Vol.0.3-0.02, Philadelphia, PA: ASTM (1978).
- STopolska and J.Labanowski,Effect of microstructure on impact toughness of duplex and super duplex stainless steels, Journal of achievements in materials and manufacturing engineering", Vol.36, No.2, pp.142-149,(2009).

لێکۆلینەوە لە کاریگەری پلەی گەرمی بەکۆن کردن و دووری خلیسکان لەسەر داخورانی پۆلای ژەنگ نەگری لێکدراو SAF 2507

پوختە

ئامانج لەم توێژینەوە لێکولینەوەیە لەکاریگەری چارەسەرە گەرمیەکان لەسەر رەوشتی داخورانی پۆلای ژەنگ نە گری لێکدراو SAF 2507 . قەبارەی داخورانی ئەم پۆلایە دۆزرایەوە وەک نەخشەیەک بۆ پلەی گەرمی. بۆ ئەم مەبەستەش چوار پلەی گەرمی oC, 800oC, 900oC, 1000oC700 هەلبژێردرا. ئەویش بەمانەوەی نمونەکان لەم پلە گەرمیانە بۆ ماوەی کاتژمێرێک دوای ساردکردنەوەیان لە ئاودا. ئەم چارەسەرە گەرمیانە دەبێتە هۆی گۆران لەپیکهاتەی مایکروسکۆبی وەک نیشتنی نیترات و کاربیداتی کرۆم و رەوگەی سیگما، چەند لیکدراوێکی دارشتەیی تر. بەرزترین بەرگری داخورانی لەم نمونەیە دەستدەکەوێت کە چارەسەری گەرمی بەکونکردنی بۆ کراوە لە (oC800).

دراسة تأثير درجة حرارة التعتيق و مسافة الانزلاق على خاصية البلى ل SAF2507.

الخلاصة

تم دراسة تأثير المعالجة الحرارية على خاصية البلى لصلب المقاوم للصدأ المزدوج المتناهي SAF2507. وتم ايجاد البلى كدالة لدرجة الحرارة. وتم اختيار اربعة درجة الحرارة $700^{o}C$, $800^{o}C$, $900^{o}C$, $1000^{o}C$ كانت عمليت التعتيق تتضمن البقاء في هذه الدرجات لمدة ساعة واحدة بعد ذلك التبريد السريع بالماء. تؤدي عملية التعتيق الصلب المقاوم للصدأ المزدوج المتناهي في هذه الدرجات الحرارية الى عدة تغيرات في البنية المجهرية مثل ترسيب نيتريدات وكاربيدات الكروم، و طور سكما ومركب سبيكي و اطوار اخرى على خاصية البلى. تم الحصول على أعلى مقاومة للبلى عندما تمت عملية التعتيق في درجة $800^{o}C$ ولمده ساعه واحده.

ON γVNL-RINGS

SHAIMAA S. ESA
Dept. of Mathematics, College of Basic Education, University of Duhok, Kurdistan region-Iraq

(Received: January 25, 2015; Accepted for publication: June 1, 2015)

ABSTRACT

In this paper we define a new type of regular rings called γVNL-ring, that is, a ring R is γVNL-ring if for every $a \in R$, at least a or $1-a$ is γ-regular element. So we will study some basic properties of elements of this ring. Also we discuss the relation between γVNL-ring with other rings such VNL-ring and VN-regular ring.

***KEYWORDS*: γVNL-ring, VNL-ring, γ-regular ring, VN-regular ring.**

1. INTRODUCTION:

Throughout this paper, every ring is an associative with unity. A ring R is called VN-regular ring if for every $a \in R$, there exists $x \in R$ such that $a = axa$ [5].
Muhammad and Salih [2], called a ring R is γ-regular ring if for every $a \in R$, there exists $x \in R$ and $\gamma \neq 1$ positive integer such that $a = ax^{\gamma}a$, Consequently, R is called strongly γ-regular ring if for every $a \in R$, there exists $x \in R$ and $\gamma \neq 1$ positive integer such that $a = a^2x^{\gamma}$.
Esa [1], called an element a a γ-semi unit if there exists $x \in R$ and $\gamma \neq 1$ such that $a = a^2x^{\gamma}, x^{\gamma} = x^{2\gamma}a$ and $x^{\gamma}a = ax^{\gamma}$.
Clearly every γ-regular rings is regular rings, since if $\gamma = 1$ then for every $a \in R$ there exists $x \in R$ such that $a = ax^1a$.
Osba, Herriksen and Alkam [3], called a ring R is a VNL-ring if for every $a \in R$, at least a or $1-a$ is VN-regular element.

2. SOME BASIC DEFINITIONS:

In this section we view some basic definitions and relations on γ-regular rings.
Theorem 2.1. Every strongly γ-regular ring is γ-regular ring.
Theorem 2.2. Every strongly γ-regular element is γ-semi unit.
Lemma 2.1. If y is an element of a ring R such that $a - ay^{\gamma}a$ is γ-regular element then a is regular element, where $\gamma \neq 1$ is a positive integer.
For the proof Theorems 2.1, 2.2 and Lemma 2.1 see [1] and [2].
Definition 2.1.[2], A ring R is said to be a quasi-commutative if for every $a, b \in R$ when $1 \neq a$ there exists m positive integer such that $ab = b^m a$.
Remark 2.1.
(i): For every $a, b \in R$ when $1 \neq a$ there exists $m > 1$ positive integer such that $ab = b^m a$, For $a = 1$ the above condition does not satisfy.
(ii): For $1 \cdot b = b^m \cdot 1$ then $b = b^m$ and this is a trivial case where $m = 1$.

3. γ-VON NEUMANN LOCAL RING:

In this section we introduce the definition of γ-Von Neumann Local ring with some basic properties.
Definition 3.2. A ring R is called γ-Von Neumann Local ring, denoted by γVNL-ring if for every $a \in R$, at least a or $1-a$ is γ-regular element.
Some examples:
1. Every field is a γVNL-ring as well as Z_{pq} for any two distinct prime numbers p and q, because in each case a or $1-a$ is γ-regular element.
2. $M_{2\times 2}(Z_2)$ is γVNL-ring, because in each case either A or $E-A$ is γ-regular element, for all $A \in M_{2\times 2}(Z_2)$ where $E = \begin{pmatrix} 1 & 1 \\ 1 & 1 \end{pmatrix}$.
3. Boolean rings are γVNL-rings.
Remark 3.2. Clearly every γ-regular ring is γVNL-ring, since by definition of γVNL-ring at least a or $1-a$ is a γ-regular element. But the converse is not true, for example the ring $M_{2\times 2}(Z_2)$ is not γ-regular ring, because at least $\begin{pmatrix} 1 & 1 \\ 0 & 1 \end{pmatrix} \in M_{2\times 2}(Z_2)$, where $\gamma = 2$ is not γ-regular element
Theorem 3.4. Let R be a γVNL-ring, then the centre of R is γVNL-ring.
Proof: let R be a γ-regular ring and let $cent\, R$ is a centre of a γ-regular ring
Let $a \in centR$ then for every $r \in R$, $ar = ra$
Since a is γ-regular element then there exists $x \in R$ and $1 \neq \gamma$ positive integer such that $a = a^2x^{\gamma}$.
So a is strongly γ-regular element, but every strongly γ-regular element is γ-semi unit then $a = a^2x^{\gamma}$, $x^{\gamma} = x^{2\gamma}a$ and $x^{\gamma}a = ax^{\gamma}$.

So for every $r \in R$, $rx^{\gamma} = x^{\gamma}r$ and $ar = ra$

This shows that $x^{\gamma} \in cent\ R$.

Hence a is γ-regular element in $cent\ R$. So $cent\ R$ is γVNL-ring. ■

Theorem 3.5. Let R be a γVNL-ring, then eRe is also γVNL-ring, for every idempotent element e in R.

Proof: let R be a γVNL-ring then at least a or $1-a$ is γ-regular element in R and let $a \in eRe$. If a is γ-regular then there exists $x \in R$ and $1 \neq \gamma$ positive integer such that $a = ax^{\gamma}a$

Since $a \in eRe$ then there exists $b \in R$ such that $a = ebe$

So $a = (ebe)x^{\gamma}(ebe)$ that is $a = e(bex^{\gamma}eb)e$

Since $bex^{\gamma}eb \in R$ then $e(bex^{\gamma}eb)e \in eRe$.

If $1-a$ is γ-regular then there exists $y \in R$ and $1 \neq \gamma$ positive integer such that $(1-a) = (1-a)y^{\gamma}(1-a)$

Since $a \in eRe$ then there exists $b \in R$ such that $a = ebe$

So $e(1-a)e = e((1-a)y^{\gamma}(1-a))e$

Implies $(e-ea)e = (e-ea)y^{\gamma}(e-ea)e$

$(e^2-eae) = (e^2-eae)y^{\gamma}(e^2-eae)$

And so $(e-a) = (e-a)y^{\gamma}(e-a)$

Thus $e-a$ is γ-regular in eRe

Therefore eRe is a γVNL-ring. ■

Theorem 3.6. The homomorphic image of a γVNL-ring is a γVNL-ring.

Proof: let R and $\acute{R}$ be γVNL-rings and let f be a homomorphism from R onto $\acute{R}$

Let $b \in \acute{R}$ then there exists $a \in R$ such that $f(a) = b$

Since R is γVNL-ring then at least a or $1-a$ is γ-regular element.

If a is γ-regular then there exists $x \in R$ and $1 \neq \gamma$ positive integer such that $a = ax^{\gamma}a$

$b = f(a) = f(ax^{\gamma}a) = f(a)f(x^{\gamma})f(a) =$

But $b(f(x^{\gamma}))b$

So $b = b(f(x))^{\gamma}b$ therefore b is γ-regular element.

And if $1-a$ is γ-regular then there exists $y \in R$ and $1 \neq \gamma$ positive integer such that

$(1-a) = (1-a)y^{\gamma}(1-a)$

But $f(1-a) = f\big((1-a)y^{\gamma}(1-a)\big) = f(1-a)f(x^{\gamma})f(1-a)$

$= \big(f(1)-f(a)\big)(f(x))^{\gamma}\big(f(1)-f(a)\big)$

$= \big(\acute{1}-b\big)(f(x))^{\gamma}\big(\acute{1}-b\big)$

So $\big(\acute{1}-b\big) = \big(\acute{1}-b\big)(f(x))^{\gamma}\big(\acute{1}-b\big)$ therefore $\big(\acute{1}-b\big)$ is γ-regular element.

Hence $\acute{R}$ is a γVNL-ring. ■

Theorem 3.7. Let R is a γVNL-ring, then for every idempotent e of R either eRe or $(1-e)R(1-e)$ is a γ-regular ring.

Proof: let R be a γVNL-ring and let $e \in R$ be an idempotent

Let $\begin{pmatrix} eRe & eR(1-e) \\ (1-e)Re & (1-e)R(1-e) \end{pmatrix} = \acute{R}$

If we will prove that $R \cong \acute{R}$ then R is γVNL-ring.

Under the homomorphism from R onto $\acute{R}$ with 1-1 function and by theorems 3.4 and 3.5 R must be γVNL-ring.

Now, suppose $x \in eRe$ and $y \in (1-e)R(1-e)$ are two non γ-regular element then both matrices $a = \begin{pmatrix} x & 0 \\ 0 & 1-y \end{pmatrix}$ and $(1-a) = \begin{pmatrix} 1-x & 0 \\ 0 & y \end{pmatrix}$ are also non γ-regular

So its contradiction.

Therefore, either eRe or $(1-e)R(1-e)$ must be γ-regular ring. ■

Theorem 3.8. Let R be a ring and let I be a γVNL-ideal of R. Then R is a VNL-ring if R/I is a γVNL-ring.

Proof: let R be a ring and let I be a γVNL-ideal of R.

Since R/I is γVNL-ring, that is $a+I \in R/I$ for every $a \in R$.

So at least $a+I$ or $(1-a)+I$ is γ-regular.

If $a+I$ is a γ-regular then there exists a coset $x+I$ and $1 \neq \gamma$ positive integer such that $(a+I) = (a+I)(x+I)^{\gamma}(a+I)$

So that $(a+I) = (ax^{\gamma}a)+I$, so $a - ax^{\gamma}a \in I$

By lemma 2.1, a is regular element.

And if $(1-a)+I$ is γ-regular then there exists a coset $y+I \in R/I$ and $1 \neq \gamma$ positive integer such that $(1-a)+I = \big((1-a)+I\big)(y^{\gamma}+I)((1-a)+I)$

So $(1-a)-(1-a)y^{\gamma}(1-a) \in I$

Also by lemma 2.1, $(1-a)$ is a regular element

Therefore R is a VNL-ring. ■

Corollary 3.1. Let R is a γVNL-ring and let I be an ideal of R. Then R/I is a γVNL-ring.

Proof: let R be a γVNL-ring then at least a or $1-a$ is γ-regular element.

Since $a+I \in R/I$ for every $a \in R$.

So at least $a+I$ or $(1-a)+I$ is γ-regular

If $a+I$ is γ-regular then there exists $x \in R$ and $1 \neq \gamma$ positive integer such that

$a = ax^{\gamma}a$

So $a + I = (ax^{\gamma}a) + I = (a + I)(x^{\gamma} + I)(a + I) = (a + I)(x + I)^{\gamma}(a + I)$

Therefore $a + I$ is γ-regular.

Also, if $(1 - a) + I$ is γ-regular then there exists $y \in R$ and $1 \neq \gamma$ positive integer such that $(1 - a) = (1 - a)y^{\gamma}(1 - a)$

So that $(1 - a) + I = \big((1 - a)y^{\gamma}(1 - a)\big) + I$

$= \big((1 - a) + I\big)(y^{\gamma} + I)\big((1 - a) + I\big)$

$= \big((1 - a) + I\big)(y + I)^{\gamma}\big((1 - a) + I\big)$

Therefore $(1 - a) + I$ is a γ-regular. Hence R/I is a γVNL-ring. ■

4. γVNL-RING WITH SOME RINGS:

In this section we discuss the relation between γVNL-rings, VNL-rings and VN-regular rings. We will explain this relation by using the Definition 2.1, with Remark 2.1.(i).

Theorem 4.9. Every γVNL-ring is VNL-ring.

Proof: let R be a γVNL-ring then at least a or $1 - a$ is γ-regular.

So, if a is γ-regular element then there exists $x \in R$ and $1 \neq \gamma$ positive integer such that $a = ax^{\gamma}a$.

But every γ-regular element is regular element, we conclude that a is regular element

And, if $(1 - a)$ is γ-regular element then there exists $y \in R$ and $1 \neq \gamma$ positive integer such that $(1 - a) = (1 - a)y^{\gamma}(1 - a)$.

Since every γ-regular element is regular element, also we conclude that $(1 - a)$ is regular element, therefore, R is a VNL-ring. ■

Remark 4.3. The converse of the Theorem 4.1 is not true.

For example,

let $R = \{(q_1, q_2, \dots, q_n, z, z, z, \dots) : n \geq 1, q_i \in \mathbb{Q} \text{ and } z \in Z_2\}$

where $Z_2 = \{0,1\}$. Then R is a VNL-ring but it is not γVNL-ring, because the element such $a = (q_1, q_2, \dots, q_n, z, z, z, \dots)$ is not γ-regular element, also $(1 - a)$ is not γ-regular.

Theorem 4.10. Let R be a quasi-commutative ring as defined in Remark 2.1.(i). Then R is γVNL-ring if R is a VNL-ring.

Proof: let R be a VNL-ring then at least a or $1 - a$ is regular element.

So, if a is regular element then there exists $x \in R$ such that $a = axa$.

Since R is a quasi-commutative ring with Remark 2.1.(i), then

$a = axa = (x^n a)a = x^n a^2$ also

$a = axa = a(ax^n) = a^2 x^n$ where $n > 1$ positive integer. Then $a = x^n a^2 = a^2 x^n$

If $a = x^n a^2$, let $ax^n = (x^n a^2)x^n = x^n(a^2 x^n) = x^n a$

Implies that $ax^n = x^n a$

So, multiplying both sides from the right by a, we get $ax^n a = x^n a^2 = a$

Therefore a is γ-regular element.

And, if $1 - a$ is γ-regular element then there exists $y \in R$ and $1 \neq \gamma$ positive integer such that $(1 - a) = (1 - a)y^{\gamma}(1 - a)$.

Since R is a quasi-commutative ring with remark 2.1.(i)

Then $(1 - a) = (1 - a)y(1 - a) = \big(y^n(1 - a)\big)(1 - a) = y^n(1 - a)^2$ also

$(1 - a) = (1 - a)y(1 - a) = (1 - a)\big((1 - a)y^n\big) = (1 - a)^2 y^n$, where $n > 1$ positive integer. Then

$(1 - a) = y^n(1 - a)^2 = (1 - a)^2 y^n$

If $(1 - a) = y^n(1 - a)^2$, let $(1 - a)y^n = (y^n(1 - a)^2)y^n = y^n((1 - a)^2 y^n)$

Implies that $(1 - a)y^n = y^n(1 - a)$//////So, multiplying both sides from the right by $1 - a$, we get

$(1 - a)y^n(1 - a) = x^n(1 - a)^2 = (1 - a)$//////Therefore $1 - a$ is γ-regular element/////Hence R is γVNL-ring. ■//////**Remark 4.4.** There is no relation between γVNL-rings and VN-regular rings, since there is no relation between VNL-rings and VN-regular rings.//////For example, Z_{12} is a VNL-ring that is neither VN-regular ring nor a local ring.

Theorem 4.11. Let R be a quasi-commutative ring with Remark 2.1.(i). Then R *is* γVNL-ring *if* R is a VN-regular ring.

Proof: let R be a VN-regular ring then for every $a \in R$ there exists $x \in R$ such that $a = axa$.

Since R is a quasi-commutative ring with Remark 2.1.(i), then

$a = axa = (x^n a)a = x^n a^2$ also

$a = axa = a(ax^n) = a^2 x^n$ where $n > 1$ positive integer, so $a = x^n a^2 = a^2 x^n$

If $a = x^n a^2$, let $ax^n = (x^n a^2)x^n = x^n(a^2 x^n) = x^n a$

Implies that $ax^n = x^n a$

So, multiplying both sides from the right by a, we get $ax^n a = x^n a^2 = a$

Therefore a is γ-regular element

If $b \in R$ and $b = (1 - a)$ such that $a + b = 1$, by similar way b is γ-regular element

So, $(1 - \square)$ is a $\square$-regular element.

Hence R is γVNL-ring. ■

5.CONCLUSION: we have this diagram

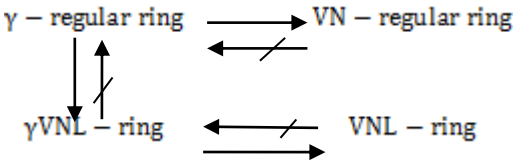

REFERENCES

– Esa, Sh. S.,"***A Study of some types of Strongly regular rings***", M. Sc. Thesis, Mosul University,(2010).

– Mohammad, A. J. and Salih, S. M.,"*On γ -regular rings*", J. Edu. Sci., Vol.18, No.4, (2006), pp.118-139.

– Osba, E. A., Henriksen, M. and Alkam O., *"The Combining Local and Von Neumann Regular Rings*", Communication in Algebra, Vol.32, No.7, (2004), pp.1-10.

– Lam, T. Y., "***Exercises in Classical Ring Theory***", Springer-Verlag, New York Berlin Heidelberg, (2000).

– Lam, T. Y., "***A First Course in Non Commutative Rings***", Springer-Verlag, New York, (1990).

– Grover, H. K. , and Khurana, D., " *Some Characterizations of VNL-rings*", Department of Mathematics, Panjab University,Chandigarh-160014, India , (2008), pp.1-21 arXiv:0801.2470v1 [math.RA] 16 Jan 2008.

پوختە

ئارمانج ژ ڤێ ڤەکولینێ ناساندنا جورەکێ نوی ژ بازنێن ڕێکخستیە بناڤێ (γVNL-ring). بازنێن ڕێکخستی دبنە (γVNL-ring) ئەگەر بو هەر a∈R , ب کێماتی a یان a-1ببیتە γ-regular element. لەورا ئەم دێ هندەك ژ سالوخەتێن بنەرەتی ییّن ڤان بازنان خوینین. هەروەسا ئەم دێ دیراسەتا پەیوەندیا دناڤبەرا γVNL-ring و VNL-ring و VN-regular ring دا کەین.

الخلاصة

الهدف من هذا البحث هو تقديم نوع جديد من الحلقات المنتظمة سميناها حلقات فون نيومان المحلية المنتظمة من النمط-γ. تسمى الحلقة R بانها حلقة فون نيومان المحلية المنتظمة من النمط-γ اذا كانت a او $1 - a$ منتظمة من النمط- γ, حيث قمنا بدراسة الخصائص الاساسية لها. كذلك ناقشنا علاقة هذه الحلقة مع حلقات اخرى وعلى وجه الخصوص حلقات فون نيومان المنتظمة وحلقات فون نيومان المحلية المنتظمة على التوالي.

EFFECT OF CRUDE OIL ON PERFORMANCE OF RC COLUMNS WRAPPED WITH CFRP IN KURDISTAN ENVIRONMENT

GULAN **H**ASSAN, **Y**ASSAMIN **A**LOGAIDI and **A**LAA **A**LSAAD
Dept. of Civil Engineering, College of Engineering, University of Duhok, Kurdistan Region-Iraq

(Received: January 27, 2015; Accepted for publication: July 13, 2015)

ABSTRACT

This paper reports the results of an experimental investigation of the application of carbon fiber reinforced polymer (CFRP) to concrete petroleum construction in Kurdistan environment. The study involved testing reinforced concrete (RC) columns. A set of 20 specimens were grouped and investigated to evaluate the performance of CFRP wrapped RC circular columns. The specimens were immersed for different periods (for up to 720 days) in crude oil, which are common conditions for petroleum construction. The specimens were identical and had a diameter of 150 mm and an overall height of 550 mm. Period of immersion was the main test parameter and the investigation focused on the performance of the columns wrapped with CFRP in terms of load capacity, deformation and ductility. The test results showed that the ultimate load capacity of the RC columns wrapped with CFRP was not noticeably affected by immersion in crude oil. However, there was a significant reduction in ultimate axial displacement and radial strain. Hence, there was a significant effect of immersion in crude oil on the ductility of RC columns confined with CFRP.

***KEY WORDS**:* Kurdistan environment, CFRP, reinforced concrete, crude oil, petroleum construction

INTRODUCTION

Past few decades have witnessed a development of many different types of materials for the purpose of repairing and strengthening of reinforced concrete (RC) structures, as the demands of the construction industry have risen for some concrete problems exists, such as deterioration, and structure post-strengthening to ensure its serviceability and safety (Toutanji and Deng 2002). Among these materials, fiber reinforced polymer (FRP) has been widely used in construction engineering because of its tensile strength, corrosion resistance, and easier handling, in addition to the economic advantages (Almusallam 2006, El-Hacha, Green et al. 2010, Saadatmanesh, Tavakkolizadeh et al. 2010).

Many studies have investigated RC strengthened using FRP. These studies have covered many aspects of FRP-wrapped RC columns, including mechanical properties like strength capacity and ductility (Wu, Lü et al. 2006, Chastre and Silva 2010, Marques and Chastre 2012, Seffo and Hamcho 2012), durability (Toutanji 1999, Belarbi and Bae 2007, Maaddawy 2008, Bae and Belarbi 2010, El-Hacha, Green et al. 2010) and others (Doran, Koksal et al. 2009, Varma, Barros et al. 2009). Chastre and Silva (2010) investigated the mechanical behavior of RC circular columns confined with CFRP to evaluate the effects of some parameters, including the diameter of the columns and the number of CFRP layers. They proposed an equation to predict the compressive strength capacity and deformation of circular RC columns wrapped with CFRP, based on their experimental data and the results of other researchers (Matthys 2000, Paula and Silva 2002, Braga 2005, Matthys, Toutanji et al. 2006). Toutanji (1999) has reported improvements in strength and ductility due to the confinement of RC columns with CFRP.

Some researchers have studied the influence of crude oil on the performance of plain and reinforced concrete (Abdul-Ahad and Mohammad 2000, BŁSaszczyŃAski 2011, Ajagbe, Omokehinde et al. 2012, Alban Chidiebere Ogbonna 2013). Abdul-Ahad and Mohammad (2000) reported the effect of crude oil on compressive strength and flexural tensile strength of concrete under short term and long term loading. A significant reduction in compressive strength and splitting-tensile strength were noticed due to the absorption of large amount of the oil, while the modulus of rupture was increased by 4%.

BŁSaszczyŃAski (2011) reported that a significant reduction of compressive strength and the bond to rebar can occur when RC structures expose to a crude oil environment. Effect of an aggregate contaminated with crude oil was reported by Ajagbe et. al. (2012) to investigate the effect of different ratio of crude oil on compressive strength of concrete. It was concluded that an aggregate containing more than 5% of crude oil contamination reduces the compressive strength of concrete by more than 50%.

However, yet there is no research concerning the influence of crude oil on RC elements enhanced with CFRP.

RESEARCH SIGNIFICANCE

Due to the rapid development of Kurdistan Region especially in the field of construction and petroleum industries, the use of new materials and technology is needed. Hence, the main goal of this paper is to investigate, in long term, the behavior of reinforced concrete strengthened with CFRP sheets in Kurdistan environment. The purpose is to evaluate the aggressiveness of crude oil in this environment on the performance of RC columns wrapped with CFRP and unwrapped ones for the same period of exposure. However, the main focus is on the effect of immersion in crude oil on CFRP-wrapped columns.

EXPERIMENTAL PROGRAM

Materials

*Concrete:*Portland cement concrete was produced in the laboratory according to the ratios of the adopted mix design and used for casting all specimens. Moist curing was used for at least 28 days. Standard concrete cylinders 152mm x 304mm were cast, cured in water for 28 days and tested as per the ASTM test method (ASTM 2005) in order to obtain the compressive strength of concrete. The average value of concrete compressive strengths at 28 days was 45MPa.

The concrete mix proportions were 1:1.5:2 (cement: sand: gravel) by weight, with a water-cement ratio of 0.45. Crushed natural gravel with a maximum size of 10 mm and natural sand were used as coarse and fine aggregate, respectively.

Composite materials: A unidirectional carbon fiber reinforced polymer (CFRP) from the SIKA Company was used for the wrapping of column specimens, and ASIKAdu-330 adhesive was used in the wrapping process. Table (1) shows the properties of the composite materials with accordance to the manufacturer.

Table (1): Typical mechanical properties of CFRP and epoxy resin

Material	CFRP	Epoxy Resin
Tensile E-modulus (MPa)	238000	4500
Tensile strength (MPa)	4300	30
Ultimate elongation (%)	1.8	0.90
Density (gm/cm^3)	1.76	-

Specimen layout and test set-up

A set of 20 specimens were grouped and investigated in order to evaluate the performance of CFRP-wrapped RC circular columns explained in table (2). All specimens were identical. The diameter of the cross-section was 150 mm and the height of each column was 550 mm. Deformed steel bars with a yield strength of 420 MPa were used for longitudinal and transverse reinforcing with nominal diameters of 10mm and 5mm, respectively. A scheme of an RC column specimen is shown in figure (1). The concrete cover to the longitudinal steel bars was 25mm. Columns were wrapped in accordance with manufacturer (SIKA) instructions. The two components of the adhesive material were mixed with a ratio of 1:4 by weight, and applied to the clean dry surface of the concrete using a paintbrush and roller. Then CFRP sheet was wrapped manually around the RC column with the fiber orientation around the circumferential direction with 100 mm overlap. An extra layer of adhesive material was applied on the installed sheet. Additional 50mm strips of CFRP sheet were installed at the ends of each specimen in order to prevent premature failure. Two weeks later, the specimens were immersed into crude oil for different periods, as per the experimental program. Prior to testing, specimens were capped at both ends to ensure their ends were straight and smooth. A universal testing machine with a capacity of 3000 kN was used to load column specimens axially in compression until failure.

All tests were carried out based on monotonic loading at a constant rate of 0.3 MPa/sec. Longitudinal displacements were measured by using two linear variable differential transducers (LVDTs) with a range of 10 mm and accuracy of 0.01mm over a length of approximately 420mm. In addition, strain gauges 50 mm in length were placed at the mid-height of the specimens with the fiber direction of the CFRP sheet to measure the radial strain. The test set-up is shown in figure (2).

Table (2): Details of tested specimens

Group	Specimen	Strengthening	Immersion condition	Number of specimens
A1	O-CN-WO	Without	Control (no immersion)	2
	O-30d-WO	Without	30 days in crude oil	2
	O-60d-WO	Without	60 days in crude oil	2
	O-90d-WO	Without	90 days in crude oil	2
	O-720d-WO	Without	720 days in crude oil	2
A2	O-CN-CFRP	With CFRP	Control (no immersion)	2
	O-30d-CFRP	With CFRP	30 days in crude oil	2
	O-60d-CFRP	With CFRP	60 days in crude oil	2
	O-90d-CFRP	With CFRP	90 days in crude oil	2
	O-720d-CFRP	With CFRP	720 days in crude oil	2

All tests were carried out based on monotonic loading at a constant rate of 0.3 MPa/sec. Longitudinal displacements were measured by using two linear variable differential transducers (LVDTs) with a range of 10 mm and accuracy of 0.01mm over a length of approximately 420mm. In addition, strain gauges 50 mm in length were placed at the mid-height of the specimens with the fiber direction of the CFRP sheet to measure the radial strain. The test set-up is shown in figure (2).

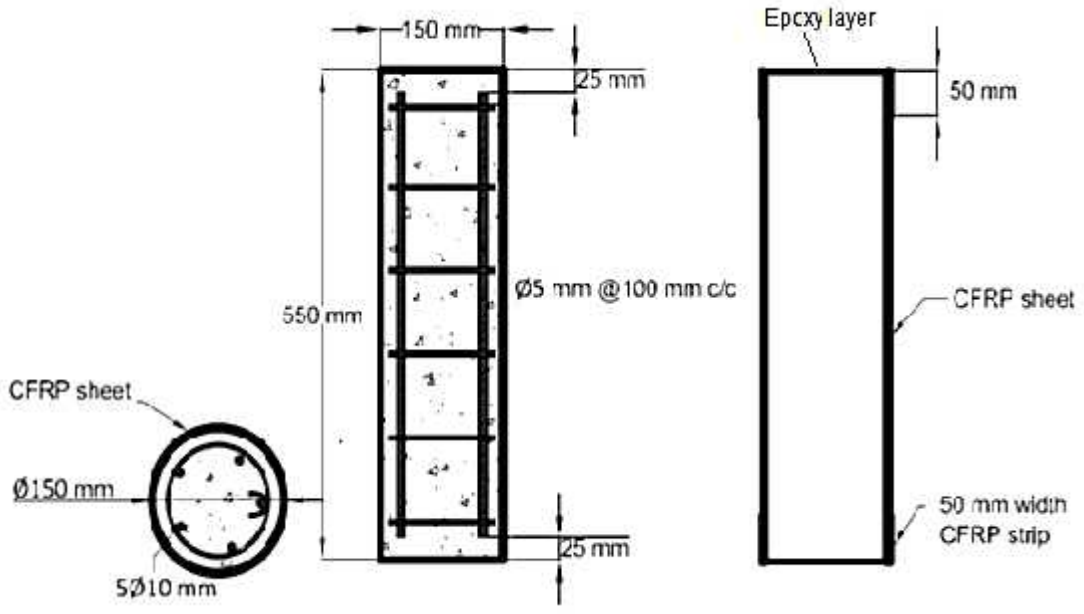

Fig. (1): Steel reinforcement and CFRP wrapping details of RC specimens

Fig. (2). Test set-up

Environmental Conditions

Throughout the duration this study, the specimens were exposed and kept at natural weather condition of Kurdistan Region (instead of standard condition of laboratory). The range of temperature was approximately from -5^{o}C (winter) to 50^{o}C (summer) and freezing period was not more than one week.

Also, in order to apply CFRP with petroleum constructions, the specimens were investigated after exposing the columns to crude oil periodically (for up to 720 days). The crude oil used in this investigation was Iraqi heavy type collected from the *Tawka Station*, Kurdistan Region.

RESULTS AND DISCUSSION

Ultimate strength capacity

Test results of the compressive load tests for all RC columns, with and without CFRP wrapping, that were immersed in crude oil for different periods are presented in figure (3). The ultimate load capacities and the comparisons between specimens with CFRP wrapping and control specimens are shown in this figure.

The ultimate load capacity of each column in Group A2 (CFRP-wrapped RC columns) was compared with the control specimen (without immersion in crude oil) and also with the ultimate load capacity of Group A1 (without CFRP), which were immersed for the same period in crude oil. Figure 4 explains these comparisons in terms of strength capacity percentages due to immersion in crude oil. It can be seen that the capacity of CFRP- wrapped columns was not affected and there was a slight increase in capacity, which may be attributed to the ageing of the concrete. In contrast, the capacity of unwrapped columns was significantly affected by immersion in crude oil for 30, 60, 90 and 720 days, and the negative changes in load capacity were 11%, 16%, 18% and 25%, respectively.

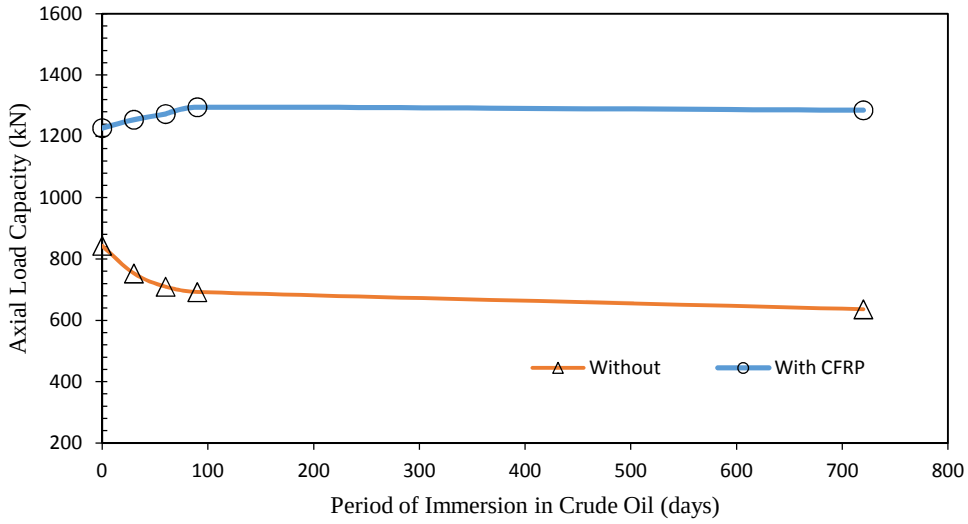

Fig. (3): Ultimate axial load capacity of test specimens immersed in crude oil

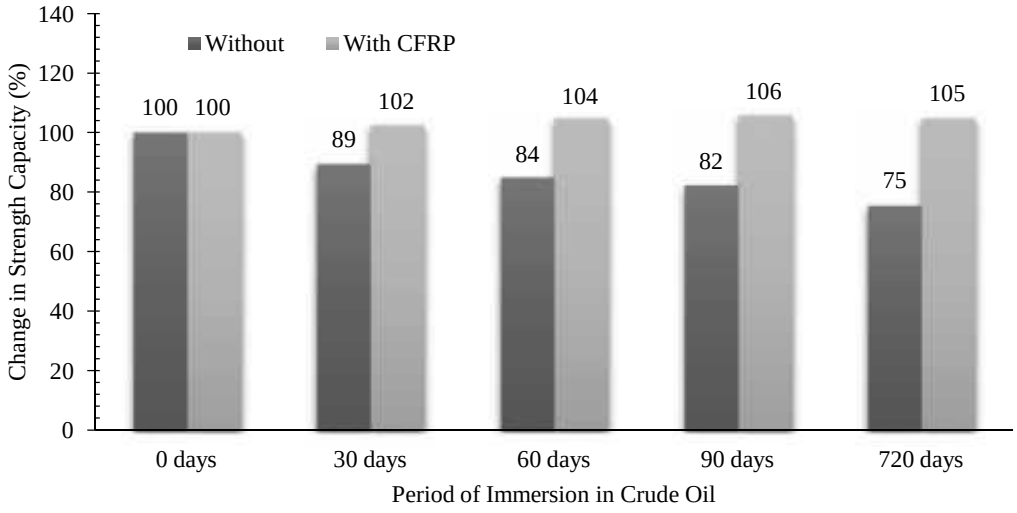

Fig. (4): Change in ultimate load capacity of test specimens immersed in crude oil

Load-deformation relationships

The ultimate deformations obtained for columns wrapped with CFRP are summarized in table (3). The axial displacement against axial load for specimens wrapped with CFRP is plotted in figure (5). It is evident that the ultimate axial displacements decreased due to immersion in crude oil. The maximum reduction in ultimate axial displacement was about 49% after 720 days of immersion in crude oil. The trends of the curves for different periods of immersion in crude oil also changed. These curves give an indication of the ductility of CFRP-wrapped RC columns after immersion in crude oil, and the ductility was clearly reduced with the period of immersion.

Table (3): Summary of results of tested specimens immersed in crude oil

Specimen	Ultimate load Pu (kN)	Ultimate axial displacement δ_a (mm)	Ultimate axial strain* ϵ_a (x10^{-6})	Ultimate radial strain ϵ_r (x10^{-6})	Ultimate stress σ_u (MPa)	Dilation ratio**
O-CN-CFRP	1227	1.580	3807	8421	69.4	2.21
O-30d-CFRP	1254	1.083	2610	5821	71.0	2.23
O-60d-CFRP	1273	1.006	2424	5109	72.0	2.11
O-90d-CFRP	1295	0.997	2402	4742	73.3	1.97
O-720d-CFRP	1285	0.801	1907	3625	72.7	1.90

***** Based on average vertical distance of 420mm

****** Dilation ratio = radial strain / axial strain

The radial stress-strain curves of the columns wrapped with CFRP are presented in Figure 6. The ultimate radial strain decreased with the period of immersion in crude oil. The maximum reduction in ultimate radial strain was about 57% after 720 days of immersion. The trends of the radial stress-strain curves also enhanced the effect of crude oil immersion on the ductility of RC columns wrapped with CFRP.

Table (3) also indicates the variation in dilation ratio due to immersion in crude oil. This ratio represents the ultimate radial to axial strain and gives an indication of the damage that can be caused to column geometry due to excess loading.

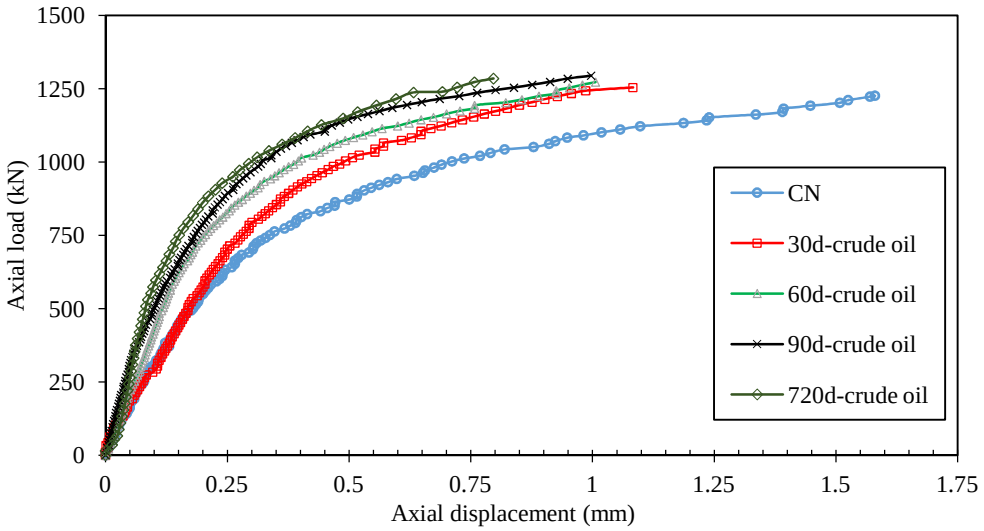

Fig. (5): Axial load-displacement curves of CFRP-wrapped specimens immersed in crude oil

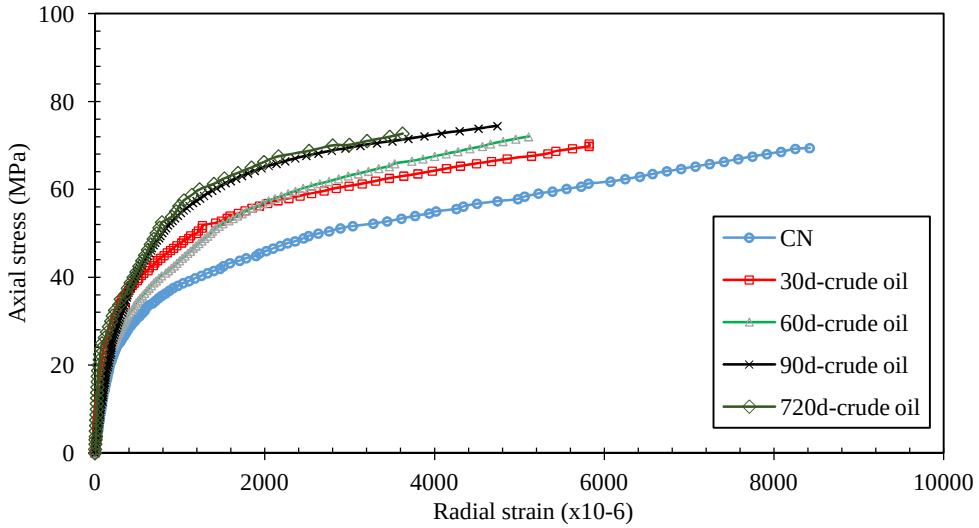

Fig. (6): Radial stress-strain curves of CFRP-wrapped specimens immersed in crude oil

Mode of Failure

The failure pattern of all tested specimens wrapped with CFRP and immersed in crude oil for different periods was governed by an explosive and sudden type of failure. It is evident that failure occurred as the CFRP sheet reached its maximum tensile strength. The damage locations were at the upper third of the height for specimens O-CN-CFRP, O-30d-CFRP, O-90d-CFRP and O-720d-CFRP, while they were at the lower third for specimen O-60d-CFRP, as shown in figure (7).

Fig. (7): Failure mode of CFRP-wrapped specimens after immersion in crude oil

CONCLUSIONS

Based on the results obtained from experiments on RC columns wrapped with CFRP and immersed in crude oil for different periods up to 720days in normal local environment, which are common conditions for petroleum constructions, the following conclusions can be drawn:

1. The ultimate load capacity of the RC columns wrapped with CFRP was not affected due to immersion in crude oil. There was a significant reduction in the load capacity of the control columns (without CFRP) due to immersion in crude oil.

2. Noticeable decreases in the ultimate axial displacement of the CFRP-wrapped columns were observed after immersion in crude oil. The maximum decreases in axial displacement were 49% after 720 days of immersion.

3. Noticeable decreases in the radial strain of CFRP-wrapped columns were observed after immersion in crude oil. The maximum decreases in axial displacement were 57% after 720 days of immersion.

4. A significant effect was observed on the ductility of RC columns confined with CFRP due to immersion in crude oil.

5. All tested specimens wrapped with CFRP and immersed in crude oil for different periods were governed by an explosive and sudden failure type after reaching the maximum tensile strength of the CFRP sheet.

ACKNOWLEDGMENTS

We sincerely thank the Scientific Research Center at the Faculty of Engineering, University of Duhok for supporting the research. Our special thanks also go to Mr. Sherzad T. Tahir for his assistance.

REFERENCES

– Abdul Ahad Ramzi B. and Mohammed, Azad A. (2000). "Compressive And Tensile Strength Of Concrete Loaded And Soaked In Crude Oil." Engineering Journal of Qatar University 13: 123-140.

– Ajagbe, W. O., O. S. Omokehinde, G. A. Alade and O. A. Agbede (2012). "Effect of Crude Oil Impacted Sand on compressive strength of

concrete." Construction and Building Materials 26(1): 9-12.
– Alban Chidiebere Ogbonna, E. E. O., Tanko Daraha (2013). "Laboratory Investigation of the Effect of Crude Oil Spill on Engineering Properties of " IOSR Journal of Mechanical and Civil Engineering 10(2): 11-17.
– Almusallam, T. H. (2006). "Load–deflection behavior of RC beams strengthened with GFRP sheets subjected to different environmental conditions." Cement and Concrete Composites 28(10): 879-889.
– ASTM (2005). Standard test method for compressive strength of cylindrical concrete specimens. C39/C39M. West Conshohocken, PA, USA, ASTM International. .
– Bae, S. W. and A. Belarbi (2010). "Effects of Various Environmental Conditions on RC Columns Wrapped with FRP Sheets." Journal of Reinforced Plastics and Composites 29(2): 290-309.
– Belarbi, A. and S.-W. Bae (2007). "An experimental study on the effect of environmental exposures and corrosion on RC columns with FRP composite jackets." Composites Part B: Engineering 38(5–6): 674-684.
– BŁSaszczyŃAski, T. (2011). "Assessment of RC structures influenced by crude oil products." Archives of Civil and Mechanical Engineering 11(1): 5-17.
– Braga, A. (2005). Reforço de pilares de betão simples com mantas de CFRP-influência do diâmetro do pilar. M Sc, Universidade Técnica de Lisboa.
– Chastre, C. and M. A. G. Silva (2010). "Monotonic axial behavior and modelling of RC circular columns confined with CFRP." Engineering Structures 32(8): 2268-2277.
– Doran, B., H. O. Koksal and T. Turgay (2009). "Nonlinear finite element modeling of rectangular/square concrete columns confined with FRP." Materials & Design 30(8): 3066-3075.
– El-Hacha, R., M. Green and G. Wight (2010). "Effect of Severe Environmental Exposures on CFRP Wrapped Concrete Columns." Journal of Composites for Construction 14(1): 83-93.
– Maaddawy, T. E. (2008). "Behavior of corrosion-damaged RC columns wrapped with FRP under combined flexural and axial loading." Cement and Concrete Composites 30(6): 524-534.
– Marques, P. F. and C. Chastre (2012). "Performance analysis of load–strain models for circular columns confined with FRP composites." Composite Structures 94(11): 3115-3131.
– Matthys, S. (2000). Structural behavior and design of concrete members strengthened with externally bonded FRP, Ghent University.
– Matthys, S., H. Toutanji and L. Taerwe (2006). "Stress–Strain Behavior of Large-Scale Circular Columns Confined with FRP Composites." Journal of Structural Engineering 132(1): 123-133.
– Paula, R. and M. Silva (2002). Sharp edge effects on FRP confinement of RC square columns. third international conference on composites in infrastructure, ICCI 02.
– Saadatmanesh, H., M. Tavakkolizadeh and D. Mostofinejad (2010). "Environmental Effects on Mechanical Properties of Wet Lay-Up Fiber-Reinforced Polymer." ACI Materials Journal 107(3): 267-274.
– Seffo, M. and M. Hamcho (2012). "Strength of Concrete Cylinder Confined by Composite Materials (CFRP)." Energy Procedia 19(0): 276-285.
– Toutanji, H. and Y. Deng (2002). "Strength and durability performance of concrete axially loaded members confined with AFRP composite sheets." Composites Part B: Engineering 33(4): 255-261.
– Toutanji, H. A. (1999). "Durability characteristics of concrete columns confined with advanced composite materials." Composite Structures 44(2–3): 155-161.
– Varma, R. K., J. A. O. Barros and J. M. Sena-Cruz (2009). "Numerical model for CFRP confined concrete elements subject to monotonic and cyclic loadings." Composites Part B: Engineering 40(8): 766-775.
– Wu, G., Z. T. Lü and Z. S. Wu (2006). "Strength and ductility of concrete cylinders confined with FRP composites." Construction and Building Materials 20(3): 134-148.

كارتصكرنا نەڤتا خاو ل سەر بجهئینانا ستوینصن كونكریتی یص بهیزكری ب رشالین كاربونی ل ژینگەها كوردستانص

پوختە

دڤص ڤەكولینص دا ڤەگولین ل سەر بكارئینانا رشالصن كاربونی لعمبارصن نەڤتص د ژینگەها هەرصما كوردستانص دا هاتە كرن. ل ناف ڤەكولینص دا بشكنین ل سەر ستینن كونكریتی یصن شیشدار ب ئاسنی هاتە ئەنجام دان. ژمارا ستینا (20) بوون هاتە دابەشكرن ل سەر چەند بەشەكا و بشكنین ل سەر هەلسەنكاندنا ستوونصن بازنە یصن دورپصچ كری ب رشالصن كاربونی.

ستین هاتنە نقور كرن ل ناڤ نەڤتا خاو دا دماوەیصن جودا دا تا (720) روژا دا بهصنە گونجین ل گەل عمبارصن نەڤتص دا.

تیرەیا هەمی ستینا وەك ئصك بوو (150) ملم وهەر وەسا بلنداهیا وان ژی (550) ملم بوو.

ماوص مانا ستینا ل ناڤ نەڤتا خاو دا كارتصكەرص سەرەكی بوو ل بشكنینن ڤص ڤەكولینص دا ل بەر كارتصكرنا وص ل سەر بەرگریا بلند و تصك چوونا وان.

د ئەنجامصن بشكنینص دا هاتە روون كرن چی كارتیكرن نەبوو ل سەر بەرگریا بلند یا ستینن دورپصچ كری ب رشالصن كاربونی دناڤ نەڤتا خاو دا ب بەراوەردی د گەل ستینن نە دورپصچ كری.

هەروەسا كصمبوونەكا بەر چاڤ ل لادانا تەوەری و هەلچوونا تیشكی هەبوو ئەوا هزرەكص ددەتە ل كصمبوونا (Ductility) یص دا ژ ئەنجامصن كارتیكرنا نەڤتا خاو ل سەر.

EFFECT OF ROLLER BURNISHING ON SURFACE ROUGHNESS OF AUSTENITIC STAINLESS STEEL AISI 316L

RAMADHAN **H**. **G**ARDI and **A**HMED **S**AMIR **A**
Dept. of Mechanical, College of Engineering, University of Salahaddin, Kurdistan Region-Iraq

(Received: February 7, 2015; Accepted for Publication: November 5, 2015)

ABSTRACT

Burnishing is a cold working process improves surface roughness, wear resistance, corrosion resistance… etc by introducing residual compressive stress into the surface of the work piece. In this study burnishing process was applied to machined AISI 316L austenitic stainless steel at two different spindle speed 560rpm and 1030 rpm, with five different depth of burnishing (0.04, 0.08, 0.12, 0.16 and 0.2mm) for two different burnishing time 30 sec. and 60 sec. Surface roughness of burnishing surface in addition of reduction in spindle diameter were detected. The lower surface roughness of burnished surface can be obtained during burnishing austenitic stainless steel AISI 316L with lower spindle speed 560rpm, depth of burnishing equals 0.2mm and 60 second burnishing time.

KEYWORDS: Burnishing, surface roughness, Austenitic Stainless Steel AISI 316L.

INTRODUCTION

Due to its high corrosion resistance, the austenitic stainless steel AISI 316L used in critical applications like nuclear and chemical industries, biomedical applications like artificial implants in joints, but these artificial joints will subject to wear as a result of contact stresses, surface roughness. One of the most effective and inexpensive methods to improve surface roughness, fatigue strength, stress corrosion cracking, and wear resistance is burnishing. Burnishing is a chip less, cold working process induces plastic deformation to the surface of the work pieces by applying burnishing pressure higher than the yield strength of the material of the surfaces which causes the surface irregularities to be flatten and hardened as shown in figures (1 and 2). [1]

Burnishing Parameters consists of burnishing force, feed, burnishing tool material, work piece material, number of tool pass, and lubrication. In recent years, burnishing becomes one of the most topics of research. The effect of process parameters on surface finish, corrosion resistance, fatigue strength, dimensional accuracy, surface hardness…etc. has been studied by many researchers. K. Palka et al. [2] carried out an experimental study on corrosion resistance of burnished X5CrNi 18-9 stainless steel and they concluded that burnishing causes increasing of yield strength from 230MPa to 450MPa and break down potential and the re-passivation potential were decreased with the burnishing load.

J. Labanowski and A. Ossowska [3] studied the effect of burnishing on stress corrosion cracking susceptibility of UR52N duplex stainless steel in boiling $MgCl_2$ solution at 125^0C. They discovered that increasing the burnishing force increases the crack initiation time. Wojciecn Labuda, et al. [4] undertaken an experimental analysis on influence of burnishing on corrosion resistance of AISI 304L stainless steel applied to sea water pump shafts and concluded that burnishing process caused 44% increase of electro chemical corrosion resistance in sea water when compared with turning.

S. Thamizhmani et al. [5] have presented their work on effect of burnishing on surface hardness and circularity of AISI 420 Martensitic stainless steel and observed that the surface hardness improved at high rotation speed than at low speed, but the circularity of work material is increased at low rotational speed than at high. C.S. Jawalkar and R.S. Walia [6] studied the roller burnishing process on En-8 steel using design of experiment and they found that the average surface roughness value observed is 0.21μm and the finest is 0.13μm in addition number of tool passes and speed contributes maximum for the % improvement in the surface hardness. Qawabeha et al [7] presented a work on influence of burnishing force on corrosion resistance of steel; it was observed

that corrosion potential and corrosion current decrease with increasing burnishing force and reached to its minimum value at about 80 N.

Hryniewicz and Rokosz [8] studied the influence of roller burnishing on corrosion resistance of C45 carbon steel in 3% NaCl water solution and they reported that corrosion rate may be decreased many times after roller burnishing process.

Khalid S. Rababa et al[9] investigated the effect of roller burnishing on mechanical properties and surface quality of O_1 alloy, it was observed that there was 76.6%, 103.3%, 113.3% increasing ductility at 140, 175, 210 ‟’

A work on the effect of lubrication on the surface roughness during burnishing aluminum alloy was presented by J.Naga Malleswara Raw et al [10] and concluded that the lubrication has considerable effect on the reduction in the surface roughness and a light oil such as kerosene oil produce better surface finish values than heavy oil such as SAE 40 engine oil. P. Ravidra Babu et al [11] worked on effect of burnishing speed on surface roughness and surface hardness of mild steel, it is observed that surface hardness and surface roughness increases with increasing speed up to 62m/min. and beyond that they will decrease.

The originality of this paper is, although large numbers of burnishing paper have been reported up to date the information about burnishing of stainless steels is very scarce. The aim of this study is to examine the effect of burnishing parameters on surface roughness and reduction in diameter of AISI 316 L austenitic stainless steel rode.

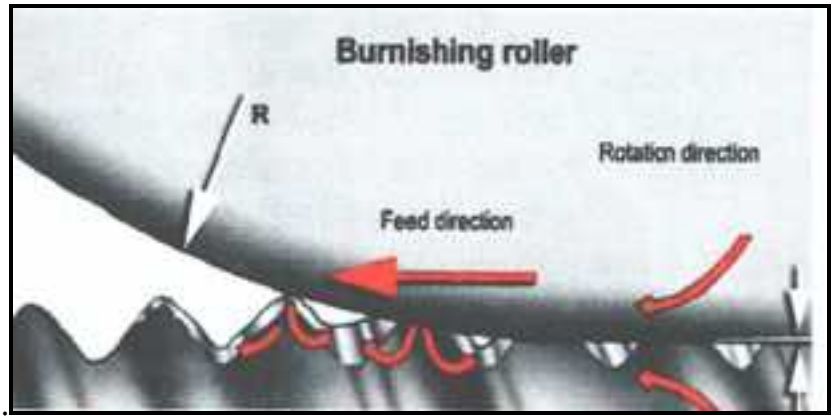

Fig.(1): Roller burnishing process [1]

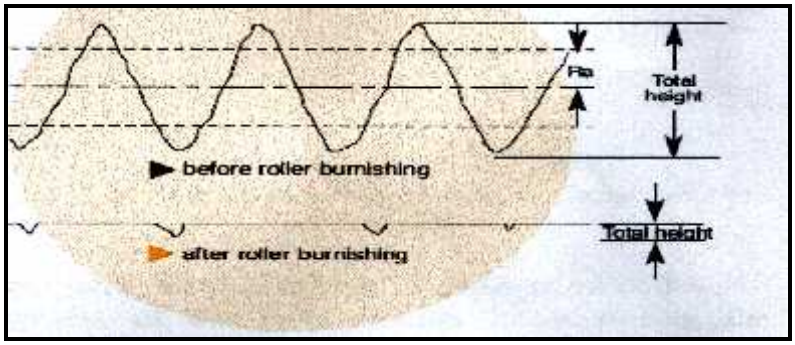

Fig.(2): Surface profile during burnishing [1]

EXPERIMENTAL PROCEDURE

Material: The work piece material used in this study is austenitic stainless steel AISI 316L, round bar with 15mm diameter. The chemical composition of workpiece material is given in table (1). Chemical composition detected using spectrometer metal analyzer model Spectromaxx Spectro Company. Germany 2010. For metallographic examination the specimens were

mechanically finished with the aid of 600, 1000, and 2000grid abrasive paper subsequently with using water to avoid over heating. Polishing has been done using diamond starry. The specimen etched chemically according to ASTM standard. The solution consists of saturated solution of $FeCl_3$ in HCl to which a little HNO_3 is added and etching time equal to three minutes [12]. Figure (3) showed the microstructure of austenitic stainless steel AISI 316L in as received condition.

The 15mm diameter AISI 316L austenitic stainless steel rode is machined using turning without the application of cutting fluid (dry turning) the cutting tool used were Tic inserted, the cutting speed was 1800 rpm, 0.11 mm/rev. feed rate and 0.2mm depth of cut. The AISI 316L specimen is turned to have five steps and grooves in between them for applying five different burnishing depths on steps. The geometry of the specimen showed in figure (4). After turning the surface roughness was performed, the measurements were made on three different locations and the average value was taken which is 1.3 µm.

Burnishing tool:

Roller burnishing tool consist of Roller, bolt, washer as shown in figure (5). Burnishing operation are conducted on turning machine, the workpiece is fixed between the centers of lathe. The burnishing tool is fixed in the tool post of the lathe as shown in figure (6).

Burnishing operation was conducted without the application of lubricant (dry burnishing), two spindle speed 560rpm and 1050rpm were selected and five different burnishing depths (0.04, 0.08, 0.12, 0.16, 0.2mm) and two different burnishing times 30 sec and 60 sec. were selected for each case.

Table (1): Chemical composition of austenitic stainless steel AISI 316L.

Material	Cr%	Ni%	C%	Mo%	P%	Mg%	Si%	Fe%
AISI 316L	17.5	12	0.03	2.25	0.045	2	1	Bal.

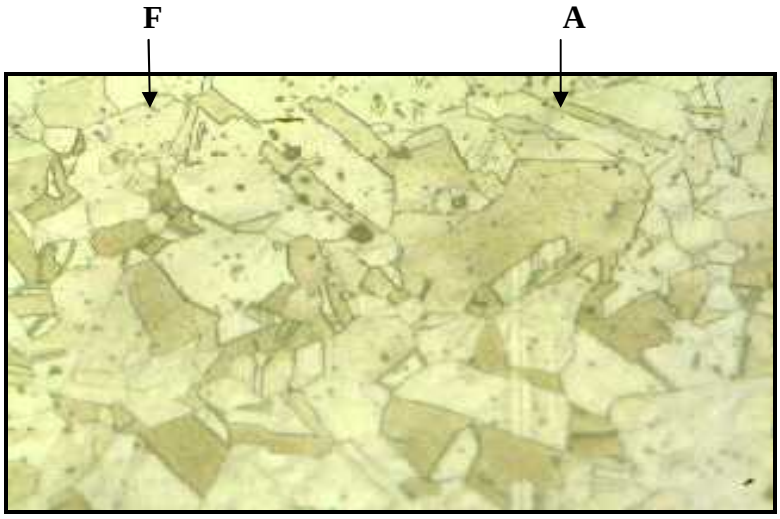

Fig.(3): Microstructure of as received austenitic stainless steel AISI 316L.(x600) F=Ferrite, A=Austenite

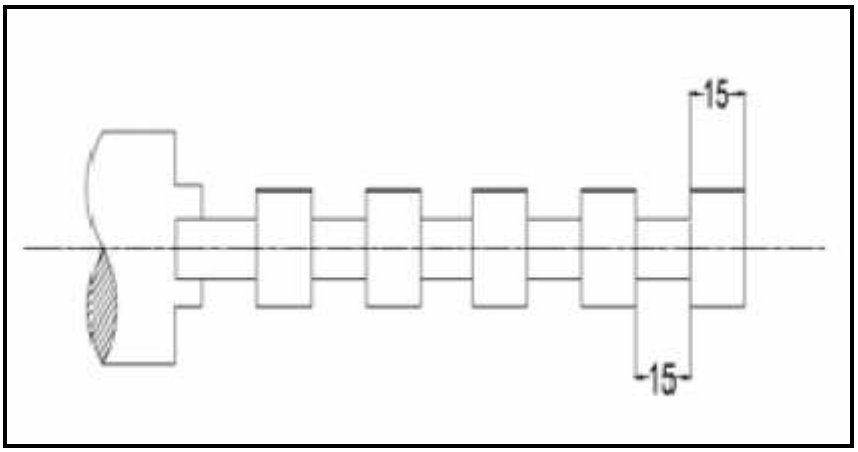

Fig.(4): AISI 316L stainless steel for roller burnishing.

Fig.(5): Roller burnishing tool.

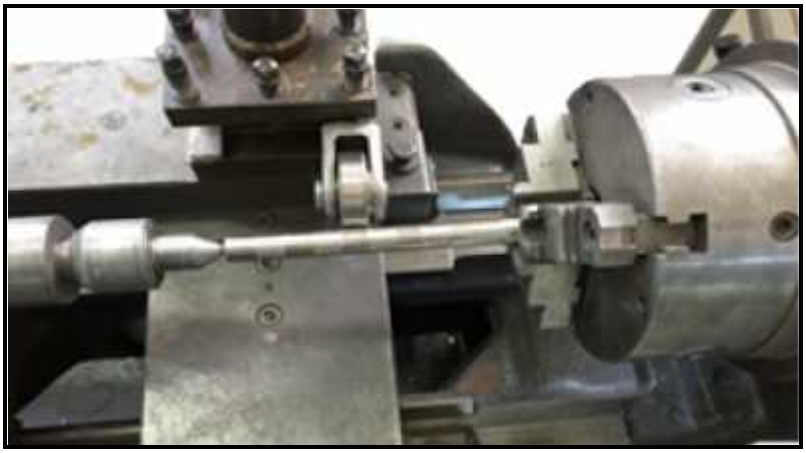

Fig.(6): Roller burnishing operation on lathe.

Surface roughness:

After burnishing surface roughness measurement was performed on Tyler – Hobson surface roughness tester [Talysurlo] figure (7). The measurements were made on the burnished surface at three different locations and the average value was taken as shown in tables (2) and (3).

Table (2): Surface roughness of austenitic stainless steel AISI 316L.

Depth of burnishing (mm)		0.04	0.08	0.12	0.16	0.2
Speed (rpm)	Time (sec)	Surface roughness (μm)				
560 rpm	30	1	0.9	0.76	0.75	0.8
	60	0.48	0.47	0.4	0.35	0.3
1050 rpm	30	0.8	1	0.99	0.97	0.8
	60	0.5	0.48	0.47	0.45	0.42

Table (3): Reduction in diameter of austenitic stainless steel AISI 316L.

Depth of burnishing (mm)		0.04	0.08	0.12	0.16	0.2
Speed (rpm)	Time (sec)	Reduction in diameter (mm)				
560 rpm	30	0.03	0.04	0.05	0.04	0.04
	60	0.1	0.11	0.12	0.11	0.13
1050 rpm	30	0.01	0.01	0.02	0.03	0.06
	60	0.07	0.08	0.1	0.11	0.13

Fig.(7): Surface roughness measuring device.

RESULTS AND DISCUSSIONS

Table (2) shows the surface roughness of average value of three tests for austenitic stainless steel AISI 316L at two different spindle speed 560 rpm and 1050 rpm and two different burnishing time 30sec.and 60 sec. Table (2) and figure (8) shows the variation of surface roughness of burnished AISI 316L austenitic stainless steel with five different depths of burnishing 0.4, 0.08, 0.12, 0.16, and 0.2mm, at 560 rpm spindle speed and 30 second burnishing time. The surface roughness value at low depth of burnishing 0.04 mm is 1μm. By increasing the depth of burnishing the surface roughness decreased gradually and reached to its minimum value 0.75 μm when depth of burnishing is 0.16mm and beyond that which is increased.

Table (2) and figure (9) shows the variation of surface roughness of burnished AISI 316L austenitic stainless steel with five different depths of burnishing 0.04, 0.06, 1.2, 1.6, and 0.2 mm at 560 rpm and 60 second. The surface roughness value at low depth of burnishing 0.04mm is 0.48 μm, increasing the depth of burnishing the surface roughness decreased gradually and reached to its minimum value 0.3 μm at higher depth of burnishing 0.2mm.When the spindle speed is 560 rpm increasing the burnishing time from 30 seconds to 60 second decreases the surface roughness at all burnishing time.

At low spindle speed 560 rpm, high burnishing time 60 second, and high depth of burnishing 0.2 mm, the average roughness will decrease of about 77% compared with turned specimens.

Table (2) and figure (10) shows the relationship between the surface roughness of burnished AISI 316L austenitic stainless steel and five different depths of burnishing 0.04, 0.08, 0.12, 0.16, and 0.2mm at 1050 rpm spindle speed and 30 seconds burnishing time. At low

burnishing depth of burnishing 0.04 the surface roughness is 0.8 µm with increasing the depth of burnishing surface roughness will increase and reached to its maximum value 1µm when AISI 316L stainless steel burnished with 0.08 mm depth of burnishing. Increasing the depth of burnishing further the surface roughness decreased gradually and reached to 0.8 µm when the depth of burnishing is 0.2mm.

Table (2) and figure (11) shows the variation of surface roughness of burnished AISI 316L austenitic stainless steel with five different depth of burnishing 0.04, 0.08, 0.12, 0.16, and 0.2mm at 1050 rpm spindle speed and 60 seconds burnishing time .At low depth of burnishing 0.04mm the surface roughness is 0.5 µm, increasing the depth of burnishing the surface roughness reduced gradually and reached to 0.42µm at higher depth of burnishing 0.2mm,this can be attributed to increasing plastic deformation as a result of increasing burnishing force.

At higher spindle speed 1050 increasing the burnishing time from 30 second to 60 second decreases the surface roughness at all depth of burnishing. At high spindle speed 1050 rpm, high burnishing time 60 second and high depth of burnishing 0.2 mm the average roughness will decrease of about 68% compared to turned specimen. Table (3) and Figures (12, 13, 14, and 15) show the reduction in spindle diameter at various spindle speed and burnishing time. Maximum reduction in diameter can be seen during burnishing AISI 316L stainless steel with higher spindle speed 1050 rpm, higher depth of burnishing 2mm and high burnishing time 60 second which is 0.13 mm and the lowest reduction in diameter can be seen during burnishing AISI 316L stainless steel with low spindle speed 550 rpm and low burnishing time 30 second.

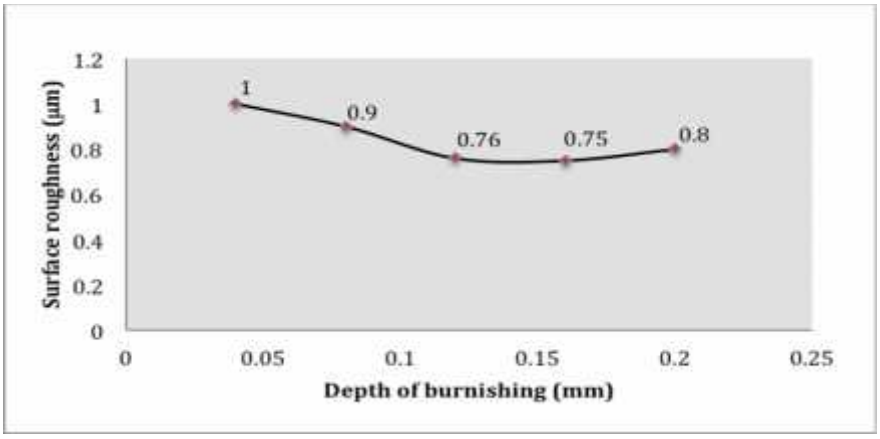

Fig.(8): Surface roughness of burnished AISI 316L stainless steel at 560 rpm and 30 seconds

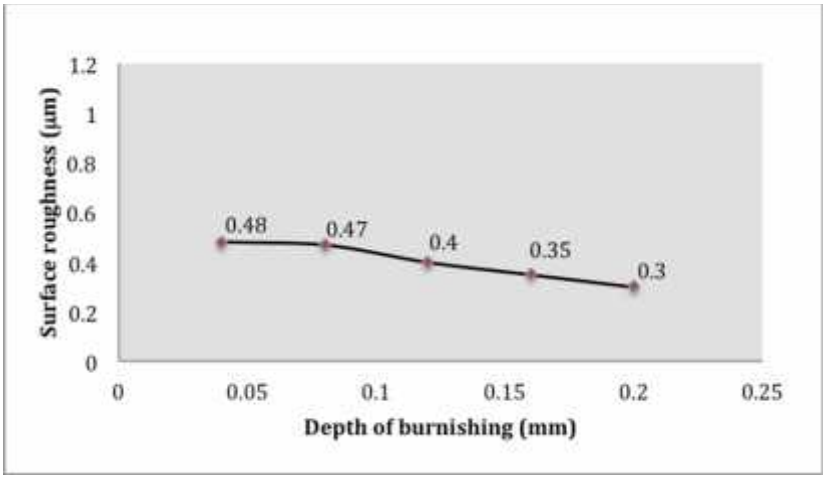

Fig.(9): Surface roughness of burnished AISI 316L stainless steel at 560 rpm and 60 seconds

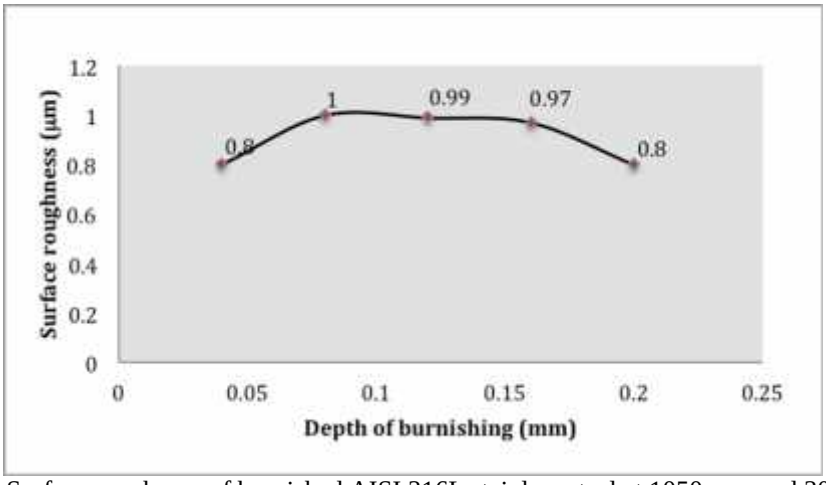

Fig.(10): Surface roughness of burnished AISI 316L stainless steel at 1050 rpm and 30 seconds

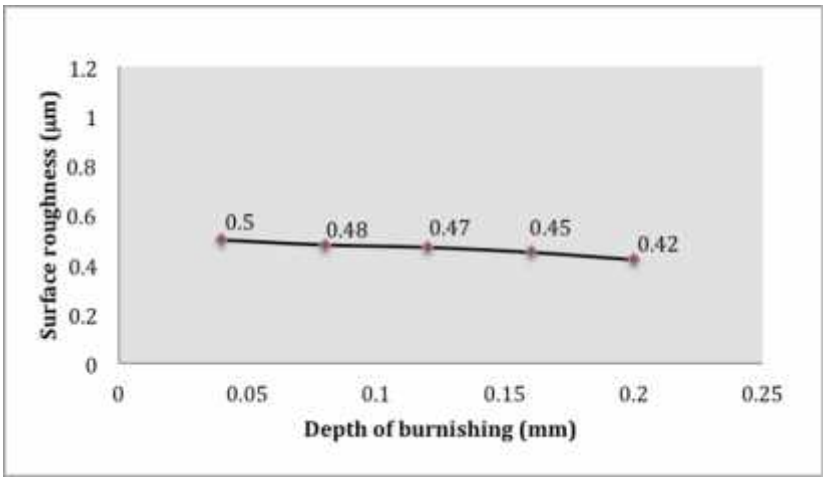

Fig.(11): Surface roughness of burnished AISI 316L stainless steel at 1050 rpm and 60 seconds

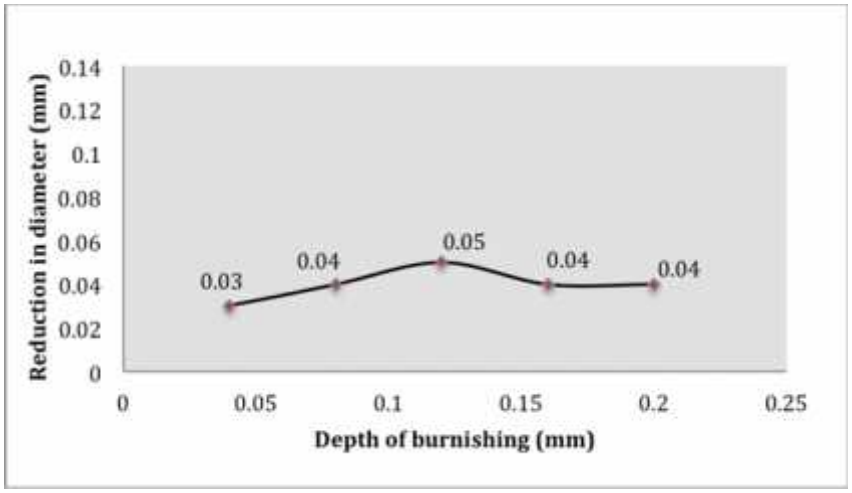

Fig.(12): Reduction in diameter of burnished AISI 316L stainless steel at 560 rpm and 30 seconds

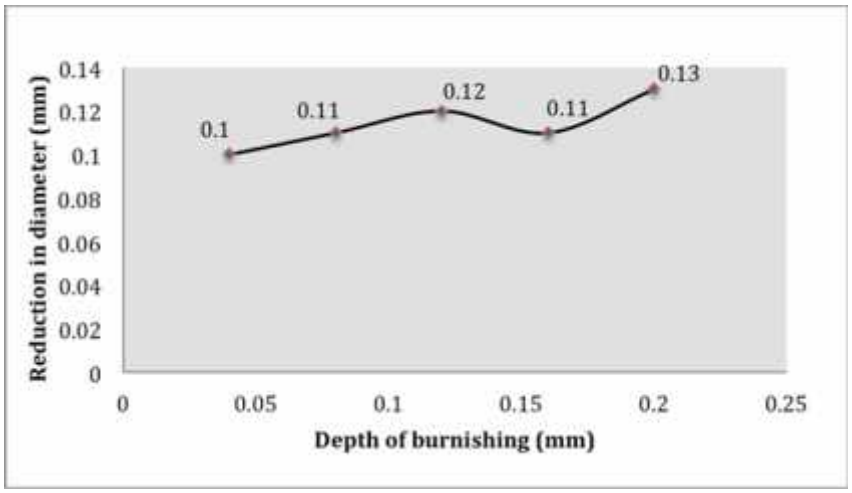

Fig.(13): Reduction in diameter of burnished AISI 316L stainless steel at 560 rpm and 60 seconds

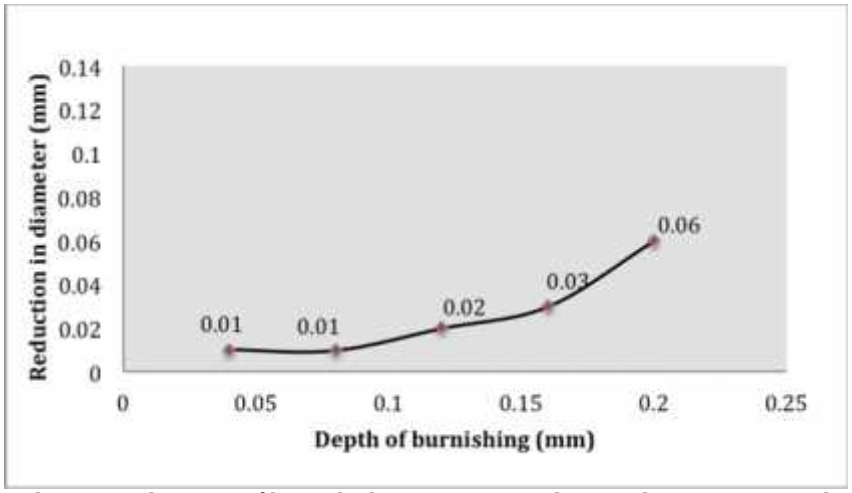

Fig.(14): Reduction in diameter of burnished AISI 316L stainless steel at 1050 rpm and 30 seconds

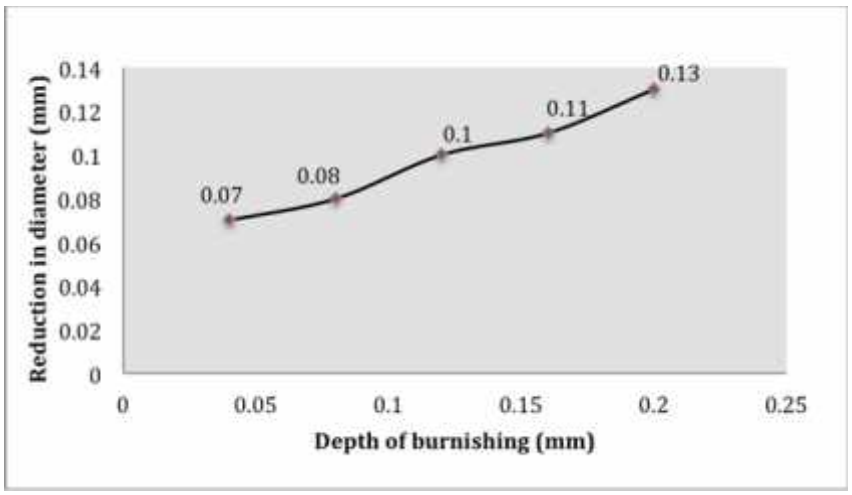

Fig.(15): Reduction in diameter of burnished AISI 316L stainless steel at 1050 rpm and 60 seconds

CONCLUSIONS

This paper presents the effect of roller burnishing process parameters, spindle speed, depth of burnishing, and burnishing time on surface roughness of AISI 316L austenitic stainless steel and the following conclusions can be drawn:

1. Spindle speed, depth of burnishing and burnishing time have a significant role on surface roughness of burnished AISI 316L austenitic stainless steel.
2. Lowest surface roughness in burnished AISI 316L can be obtained during burnishing with 560 rpm spindle speed, 60 second burnishing time, and 0.2mm depth of burnishing.
3. At high spindle speed increasing the spindle speed and depth of burnishing, the reduction in diameter increased gradually.

REFERENCES

- E.Rafati and M. S. Mahadiea ,Investigation of variance of roller burnishing parameters on surface quality by Taguchi approach, Int. journal of advanced design and manufacturing technology,Vol.6 ,No.3,pp.77-pp81 /September –(2013).
- K.Palka, A. Weronski, K. Zaleski, Mechanical properties and corrosion resistance of burnished XCrNi 18-9 stainless steel, Achievements in materials and manufacturing engineering, Vol.16, issue 1-2, June (2006).
- J. Labanowski, A. Ossowska, Influence of burnishing on stress corrosion cracking susceptibility of duplex stainless steel. Achievements in Materials and manufacturing Engineering Vol.19 issue 1, Nov. (2006).
- Wojciech Labnda, Robert Starosta, Adam Charchalis, The analysis of the influence of burnishing process on corrosion properties of steel applied to sea water pump shaft, Journal of Kones power train and transport, Vol.18. No.4, 2011 P 221-228 (2011).
- S. Thamizhmani, Rajendran, Rasool Mohideen and Sulaiman, Investigation on surface integrity on STAVAX ESR AISI 420 martensitic stainless steel by cryogenically treated steel balls with low plastic burnishing tool, Key Engineering Materials Vol.504-506, PP 1347-pp1352. (2012).
- C.S. Jawalkar and R.S.Waila, Study of roller burnishing process on En-8 specimens using design of experiments. Journal of mechanical engineering research Vol.1 (1) PP. 038-045,(2009).
-Ubeidulla Al-Qwabeha,EimanEid Al-Rawajfeh,Ehab Al-Shamaileh, Influence of roller burnishing on surface properties and corrosion resistance in steel, Anti-corrosion methods and materials, Emerald group publishing limited,Vol.56,pp261-265,(2009).
- Tadeusz Hryniewicz,Krzystof Rokosz, Corrosion behavior of c45 carbon steel ball burnishing,Hradec nad Moravici. Metal, Vol.5,pp 24-26,(2005).
- Khalid S. Rababa ,Mayas Mohamad Al Mahasna, Effect of roller burnishing on mechanical behavior and surface quality of O_1 alloy steel ,Research journal of applied science ,Engineering and technology ,Vol.3.,No.3,pp.777-pp. 233,(2011).
- J. Naga Malleswara Raw ,A.Chenna Kesava Reddy and P. V. Rama Raw ,Design and fabrication of new type of dynamometer to measure radial component of cutting force and experimental investigation of optimum burnishing force in roller burnishing process ,Indian journal of science and Technology ,Vol.3 ,No.7,July (2010).
- P. Ravindra Babu,T Siva Prassad,A V S Raju,and A Jawahar Babu, Effect of internal roller burnishing on surface roughness and surface hardness of mild steel, Journal of scientific and industrial research,Vol.68, ,pp29-31. January (2009)
- ASTM standard test method for metallographic of metals Annual book of ASTM standards Vol.0.3-0.02, Philadelphia, PA: ASTM (1978).

تاثير دوار التصقيل على خشونة السطح للصلب المقاوم للصدأ الاوستنايتي AISI 316L

الخلاصة

تعتبر التصقيل عملية التشكيل البارد تؤدي الى تحسين خشونة السطح، مقاومة البلى ومقاومة التأكل...الخ وذلك عن طريق ادخال الجهد الضاغط الى السطح الشغلة. فى هذا البحث تم دراسة تاثير عملية التصقيل على خشونة السطح وتقليل قطر العمود من الصلب المقاوم للصدالاوستنايتى AISI 316L ذات قطر 15mm فى سرعتين مختلفتين لدوران العمود 560 rev/min و1050rev/min. وتم اختيار خمسة اعماق التغلغل (o.04,0.08,0.12,0.16,0.2)mm وذلك لفترتين زمنيتين مختلفتين .30sec و 60sec لكل حالة من الحالات .وتم الحصول على اقل الخشونة عندماتتم عملية التصقيل لصلب المقاوم للصدأ الاوستنايتي AISI 316L بسرعة منخفضة 560 rev/min و عمق التصقيل 0.2 mmوزمن التصقيل .60 sec .

كاريگەری پەستنەوە لە سەر زبری رووی پۆلای ژەنگ نەگری ئۆستەنایتی LAISI316

پوختە

پرۆسەی پەستنەوە بە دروستکردنی سارد دادەنرێت کە دەبێتە هۆی چاککردنی زبری رووەکان، بەرگری سوان، بەرگری داخوران... ئەمەش لە رێگەی دانانی ئەرکی پالنراو بۆ رووی پارچەکان . لەم لێکۆلینەوە پەستنەوە بۆ ئەستوندەی تیرە 15ملم پۆلای ژەنگ نەگری ئۆستەنایتی LAISI 316کرا لە دوو خێرایی جیاواز 560 سوڕانەوە\خولەک و 1050 سوڕانەوە\خولەک وە پێنج قولایی(0.04, 0.08, 0.12, 0.16, 0.2)ملم وە دوو کاتی پەستنەوە 30 چرکە و 60 چرکە. زبری رووەکان و کەمبوونەوە لە تیرەی ئەستوندەکە لێکۆلرایەوە. تاقیکردنەوەکان دەریان خست دەکرێت کەمترین زبری لەکاتی پەستنەوەی پۆلای ژەنگ نەگری ئۆستەنایتی LAISI 316بەدەست بێت لەخیراییەکی نزم560 سوڕانەوە\خولەک و قۆلایی 0.2 ملم وەکاتی پەستنەوە 60 چرکە بێت.

THE WIRELESS CONTROL SYSTEM SIMULATION AND NETWORK ADAPTIVE CONTROL

AHMED **M**. **F**ADHIL, **T**URKAN **A**. **K**HALIL and **R**ANA **K**H. **S**ABRI
Dept. of Computer, College of Engineering, University of Mosul-Iraq

(Received: February 16, 2015; Accepted for publication: June 4, 2015)

ABSTRACT

At present time a trend is centered around the use of applications that work in real time. Challenges in real time network control systems have become the subject attention of researchers in this field. The presence of time delay that affects the stability of the system is the main problems facing these systems. This paper aims to discuss the impact of the network in control systems and the solutions to reduce the problems in the systems, a True time toolbox was chosen as a tool used for co-simulation between network and control system designed in MATLAB program. By comparing the performance of the servo-motor system before and after putting wireless network it was found that the time delay is due to sending and receiving packet between the plant and controller. The Servo-Motor system was also used for studying the effect of the presence of intermediate nodes during transmission. It was observed that an increase in the number of nodes (2, 5, 15 and 20) decreased the stability of the system reaching to instability due to the large interference with other nodes for a specific value of data rate used. Therefore, it is found that the data rate of the wireless network must be changed as the same percentage increase in the number of nodes in order to avoid delays as a result of interference with an intermediate node in the road, also to keep the battery age and making the system works for a longer time.

KEYWORDS: wireless network, IEEE802.11b wireless network ,Network Control System,TRUETIME, Co-Simulation, Realtime.

1. INTRODUCTION

In the last decades the development in network technology made a huge interest of control systems and how to exchange data from one point to another in the control systems by the networks. The primary benefit of wireless control technology is reduced the installation cost [1]. And because of the increasing need to find solutions to the problems of wireless networks This kind of communication technology became more cost effective in distributed control systems[2]. Many computer systems are distributed systems consisting of nodes and a communication networks which link the various systems. Network Control Systems (NCSs) combine between two fields, control and computer networks[3] this system is known as a closed loop system that transfers data between a plant and a controller at regular intervals over a real time communication medium[4]. The plant sends its current state to the controller, which compares the plant state against a reference model and sends any updates back to the Plant [4], the use of network control systems have many advantages such as low cost, reduced weight and power requirements (battery powered), simple installation and maintenance especially when used for the purpose of exploring the environment[5]. Figure (1) represents an example of a network control system.

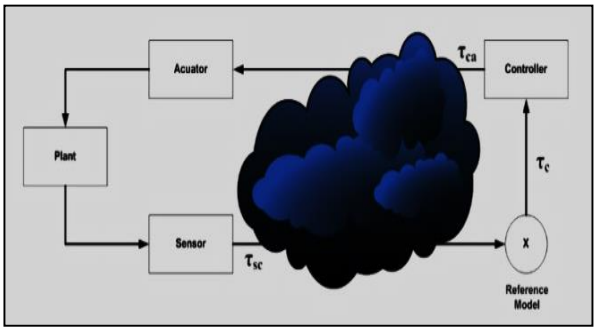

Fig(1): Network Control System [4]

The functionality of a typical NCS is established by the use of four basic elements: (Sensors: to acquire information, Controllers: to provide decision and commands, Actuators: to perform the control commands and Communication network: to enable exchange of information).

To get a good performance of the system work software tools must be used for the purpose of analysis and simulation the effect of time delay on control system performance, the tool that is used in this research is the TRUETIME toolbox which is used in the simulation software environment MATLAB. TRUETIME toolbox is a MATLAB/Simulink-based simulator for real-time control systems[6][7], in addition to the possibility of co-simulation between the network simulation and control system, TRUETIME also provides a collection of MATLAB functions. For an example, A/D and D/A conversion, send and receive network messages, set up timers, and change task attributes. The TRUETIME blocks are connected with ordinary continuous Simulink blocks to form a real-time control system [8]. The IEEE802.11b wireless network has been chosen in this research, as one of the networks that used in networks control systems, this wireless network work in four types of data rate (1, 2, 5.5 and 11 Mbps) when the maximum amount of power to be sent is 50mW [9].

1.1. Previous work

The network control systems have become the subject of researchers interest, where there are many studies dealing with this subject, some of them deals with the development of the simulation tools for NCS, in the year 2003 Henriksson and others [8] worked on the development of a tool called the TRUETIME toolbox in MATLAB software for the purpose of simulating simple models to see the impact on the control system and they found that the presence of a network in the system cause large delay in the response. Other researchers tried to study the effect of the mobile nodes on the system performance, in the year 2005, Andersson and others [10] studied the behavior of a network consisting of mobile nodes and how the movement of these nodes affect the distance between them, which adds a time delay on the network because of the re-transmission and waiting for a reply from the other side. In the year, 2007, Cervin and others [11] made a complete description of TRUETIME toolbox, they presented the advantages of using it in simulation purposes in network control systems, and should that it could be used for the purposes of co-simulation with different types of wired and wireless networks. Some researchers went to compare different types of networks. In the year 2009 Fan and others[12] used two types of wireless networks, a IEEE802.15.4 and IEEE802.11b by using TRUETIME toolbox they made a simulation for the two types, they expected that the first type is the future for industries more than the second type because of being a little power, low cost wireless network, and its use for short distances so it is good in some areas that need to keep the energy for a long time. On the other hand, in the year 2011, Urban and others[5] studied the effect of increasing the sample time in wired and wireless networks, they also studied the effect of increasing the network size and the amount of packets losses in transmission, and they found that the two types of network are affected by these factors (increase in sample time, network size and packet loss). In the year 2011 Faqarn peng and others[13] compared between the simulation of a first order and a second order control system and they noted the difference between the two systems in terms of the performance and how to design a PID controller suitable for these types of systems, they also studied the impact of that change on system performance. In the year 2013 Khamari[14] worked to design a network control system and analyzed the system with the presence of time delay and packets losses, he used a technique for the purposes of compensation for the time delay to get a better performance. In the year 2013 Y. Wanga and L. Heb[15] studied the causes and integral part of delay based on the analysis of structure of networked control system, they used the TRUETIME simulation tool to build the simulation model of network control system delay, and Discussed the effects of network delay on the performance of the control system in three cases. They found that minimize the forward delay, during the design of vehicle NCS, could improve the performance of the NCS. In the year 2013 Srinivasan and others[16] proposed a simple adaptive regulator that uses first order approximation for computing the controller gains based on prior knowledge of channel delays. Simulation results indicate that the adaptive regulator performs well even with an approximation of delay like Gaussian distribution. In the year 2014 Nishanth and Sashank[17]

proposed an application based on the architecture targeting Distributed embedded control systems (DECS) with a single CPU and limited computational sources. The application provides an approach for integration of hard and critically hard control mechanisms with TRUETIME toolbox in MATLAB, the control task consists of target task to be controlled and adaptation task that implement's control algorithms, also they compared the time sharing concurrency and efficiency of real time operating systems like rate monolithic and earliest deadline first process.

2. THEORETICAL

BACKGROUND

2.1. Simulation of network control systems:

The simulation part is very important in network control system researches and the simulation process must carry on through the network when the packets are transferred between the plant and the controller, so a software tool must be used to combine the simulation of the control system and the network simulation. This is called a Co-Simulation[18], in this work the TRUETIME tool box were used as a software tool for Co-simulation and MATLAB program also used as a Simulink because it is a high performance computing technique[19].

2.2. TRUETIME Tool box:

It is a set of tools used for the simulation in real time, This toolbox facilitates co-simulation of controller task execution in real-time kernels, network transmissions and continuous plant dynamics. It is written in C++ MEX language, uses event based simulation and external interrupts, it often used to study effect of network transmission time delay uncertainty to the control performance, and can be used on simulation of multi scheduling algorithm in the NCS. The TRUETIME mainly includes six functional modules as shown in figure(2): TRUETIME Kernel, TRUETIME Network, ttGetMsg, ttSendMsg, TRUETIME Wireless Network and TRUETIME Battery. A control system simulation model can be build by connect the modules in TRUETIME and Simulink. TRUETIME Kernel often work as nodes in the NCS, used to analog sensor, controller, actuator and other control elements, include A/D and D/A converter , etc[15].

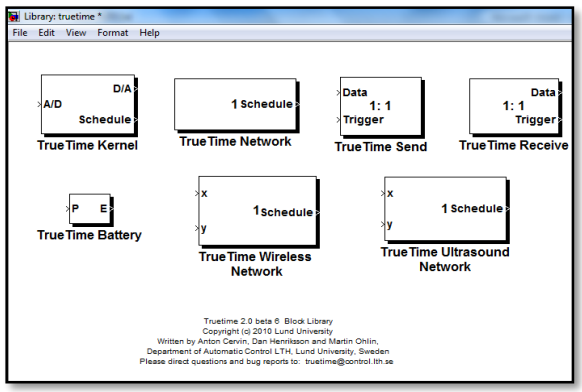

Fig(2): TRUETIME block library

TRUETIME also consists of a kernel block and a network block, both variable-step S-functions written in C++. TRUETIME provides a collection of MATLAB functions used to do A/D and D/A conversion, send and receive network messages, set up timers, and change task attributes. The TRUETIME blocks are connected with ordinary continuous Simulink blocks to form a real-time control system. The TRUETIME kernel block simulates a computer with an event-driven real-time kernel, A/D and D/A converters, a network interface, and external interrupt channels. The kernel executes user-defined tasks and interrupt handlers, representing. Execution is defined by user-written code functions (C++ functions or m-files) or graphically using ordinary discrete Simulink blocks. The simulated execution time of the code may be modeled as constant, random or even data-dependent[8].

2.2.1 The TRUETIME Kernel Block:

The kernel block is a Simulink S-function that simulates a computer with a real-time kernel, A/D and D/A converters, a network interface, and external interrupt channels. The kernel executes user-defined tasks and interrupt handlers. Internally, the kernel maintains several data structures that are commonly found in a real-time kernel: a ready queue, a time queue, and records for tasks, interrupt handlers, monitors and timers that have been created for the simulation.[20]

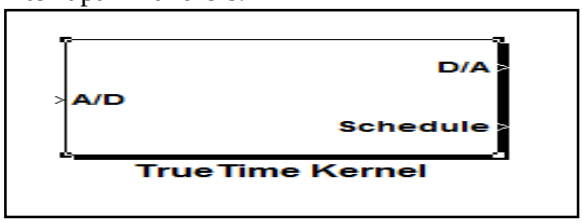

(a)

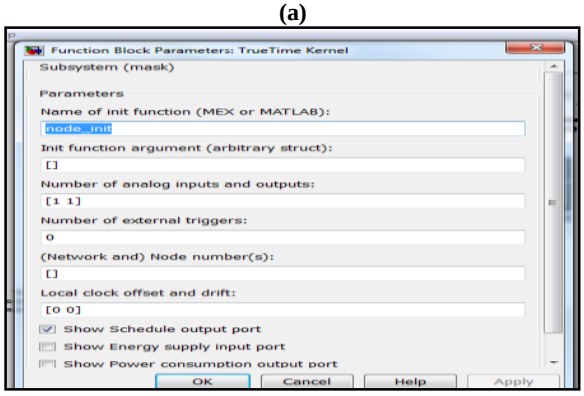

(b)

Fig(3): (a) TRUETIME Kernal (b) TRUETIME block mask dialog

The block mask dialog shown in figure(3) contain the following parameters[21]:

1. Init function: The name of the initialization script.

2. Init function argument: an optional argument to the initialization script.

3. Battery Enable: check box if the kernel should depend on a power source.

4. Clock drift: The time drift (0.01) if the local time should run 1% faster than the nominal time (the actual simulation time).

5. Clock offset: a constant time offset from the nominal time).

2.2.2.The TRUETIME Wireless Network:

It simulates the wireless network in control systems. Two network protocols are supported at this moment: IEEE 802.11b/g（WLAN）and IEEE 802.15.4 （ZigBee）. This tool has several parameters as shown in figure(4), some of following important parameter [21]:

1. Network type: Determines the MAC protocol to be used. Can be either 802.11b/g(WLAN) or 802.15.4 (ZigBee).

2. Network number: The number of the network block.

3. Number of nodes: The number of nodes that are connected to the network, this number will determine the size of the Snd, Rcv.

4. Data rate (bits/s): The speed of the network.

5. Transmit power: determines how strong the radio signal will be and thereby how long it will reach.

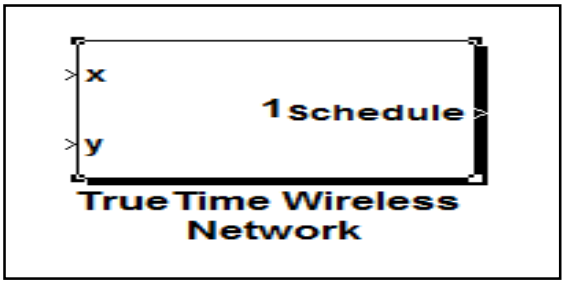

(a)

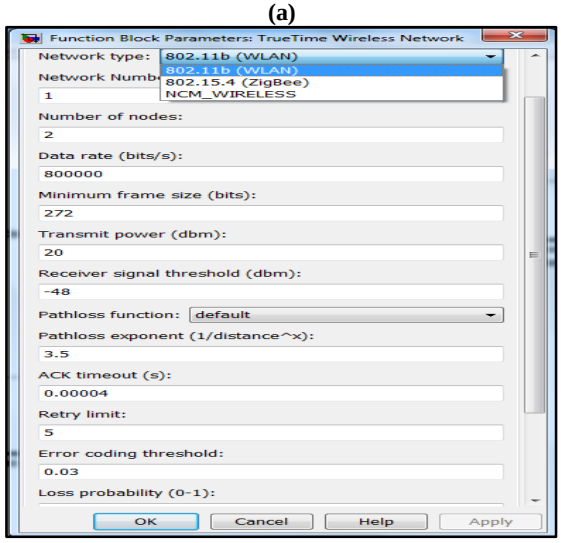

(b)

Fig(4): (a) TRUETIME Wireless network (b) TRUETIME Wireless network dialog

2.2.3 The TrueTime Battery Block

The battery block acts as a power source for the battery enabled kernel blocks. It uses a simple integrator model so it can be both charged and recharged. To use the battery, enable the check box in the kernel configuration mask and connect the output of the battery to the (E) input of the kernel block[21]. Battery block can be shown in figure(5).

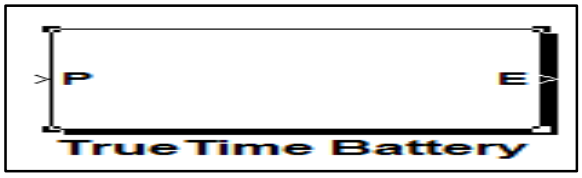

(a)

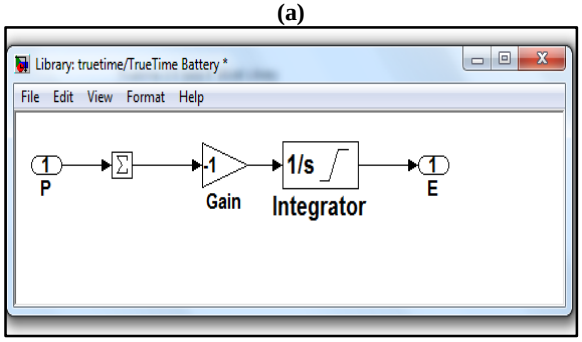

(b)

Fig(5): (a): TRUETIME Battery block (b) TRUETIME Battery block content

3 .THE WORK

The Servo-Motor second order system were chosen to simulate an example of network control system to find the solution of problems that face these type of control systems by comparing between the simulation system responses in different sample times. Also The servo-motor system were used for study the effect of the change in network size in different data rate on the system performance and cost. The wireless technology used in the network can be Zigbee or IEEE 802.11b, and because of Zigbee can not work in more than 250Kb/s data rate[22] and because of needing to testing the affect of different data rate responses system effective so the IEEE802.11b were chosen in work.

3.1.Simulation of Servo-Motor system model:

This model was used to find the effect of the Time delay on the system performance when using it as control system and network control sysem. Equations (3.1) to (3.4) represent a mathematical modeling of the system, where equation (3.1) represent the Servo-Motor (plant) [23] and the equations (3.2), (3.3) and (3.4) represent PD-controller[7][8].

$$\boldsymbol{G(s) = \frac{1000}{s(s+1)}} \qquad (3.1)$$

$$\boldsymbol{P(k) = K\big(r(K_h) - y(K_h)\big)} \qquad (3.2)$$

$$\boldsymbol{D(K_h) = a_d D(K_h - h) + b_d\big(y(K_h - h) - y(K_h)\big)} \qquad (3.3)$$

$$\boldsymbol{u(K_h) = P(K_h) + D(K_h)} \qquad (3.4)$$

Where: $a_d = \frac{Td}{Nh+Td}$ **and** $b_d = \frac{NK_{Td}}{Nh+Td}$

P, I and D : Channels react on the error signal.
$R(K_h)$: Reference square signal.
$y(K_h)$: Output plant analog signal.
$u(K_h)$: Input plant analog signal.
N :Used to limit the gain for higher frequencies=100
K : Proportional gain=1
K_{Td} : Gain of derivative part of the controller
T_d :Derivative time constant of the controller=0.04s
h : Sampling time=0.01s

3.2. Servo-Motor models simulation

The figures (6) and (7) represent the simulation model of the Servo-Motor using MATLAB with wireless network and without it, figures (8) and (9) represent the content of sensor/actuator node and controller node, figures (10-13) represent the simulations model after increasing the network size from (2 to 20) nodes, figure (14) represents the transmitter and receiver for each node and the contents of the Plant_node and the Controller_ node and intermediate node and figure (15) represents the servo motor simulation model with energy battery block.

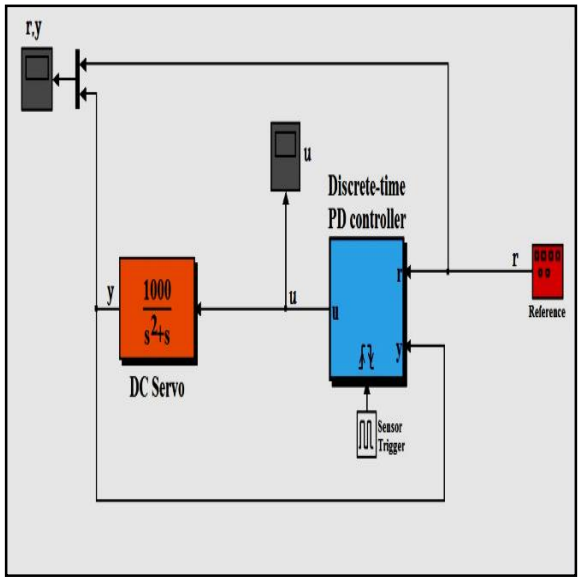

Fig(6): Servo-Motor simulation control model without using network

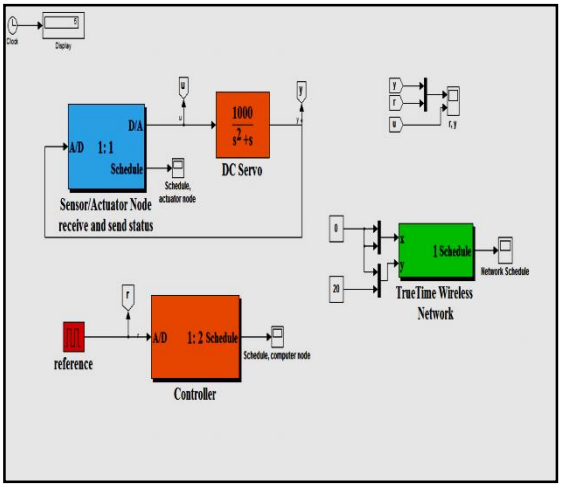

Fig(7): Servo-Motor simulation model with network(an example of network control system)

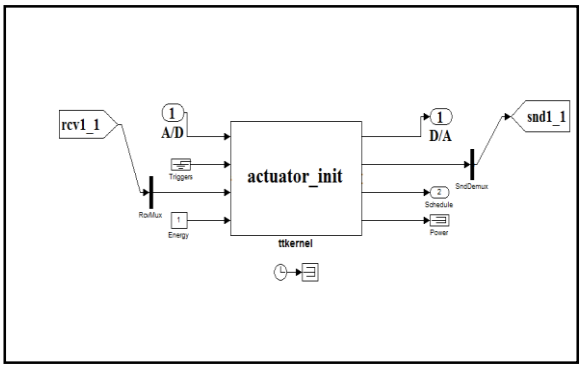

Fig(8): sensor/actuator node conetnt

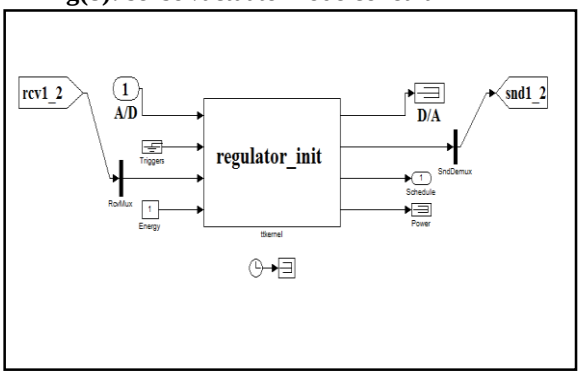

Fig(9): controller node content

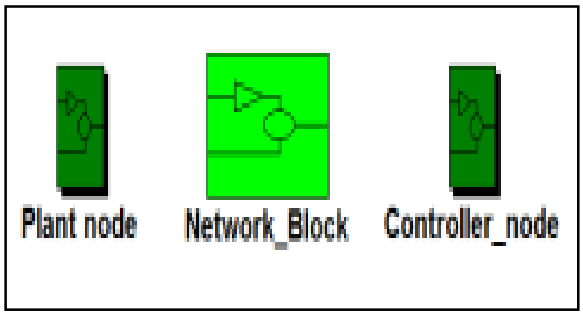

Fig(10): Servo-Motor simulation model when the size of the network is 2 nodes(one node represents the plant and another one represents the controller

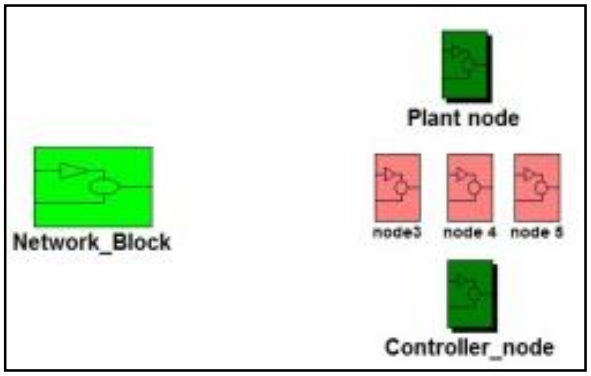

Fig(11): Servo-Motor simulation model when the size of the network is 5 nodes(one node represents the plant and another one represents the controller, the rest of the nodes represent intermediate nodes between them)

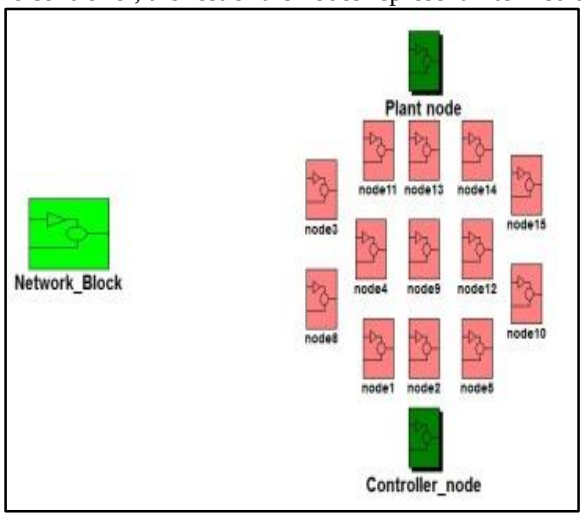

Fig(12): Servo-Motor simulation model when the size of the network is 15 nodes

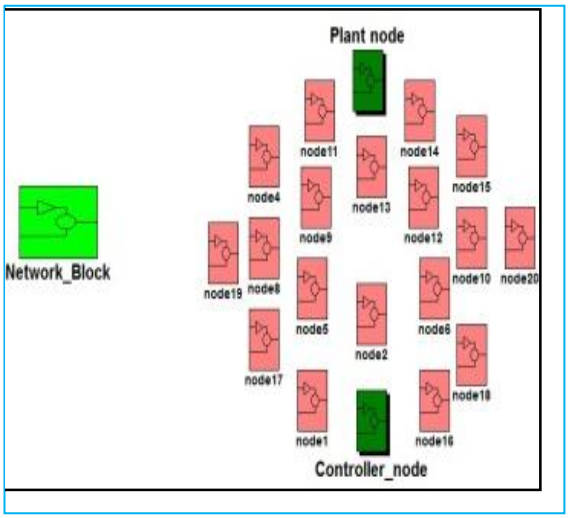

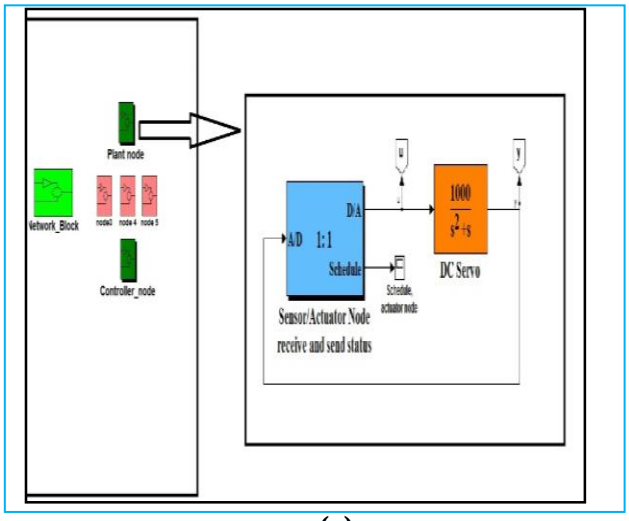

(a)

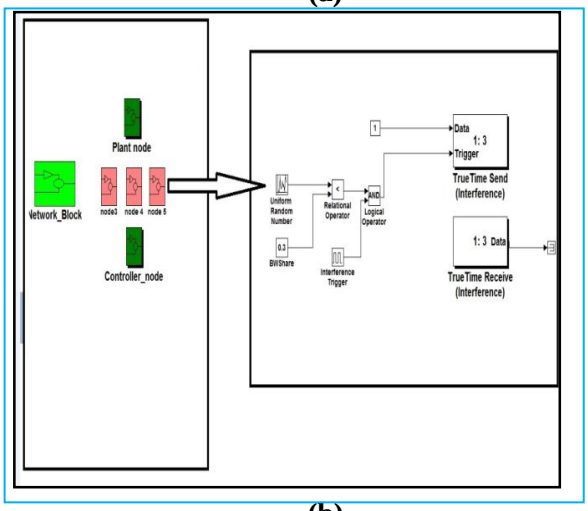

(b)

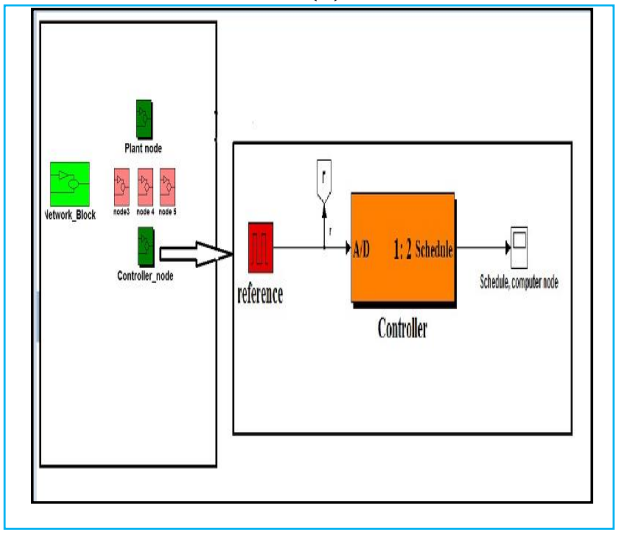

(b)

Fig(14): (a) The Plant_node contents (b) The intermediate nodes with the transmission and receiving process (c) The controller_node contents

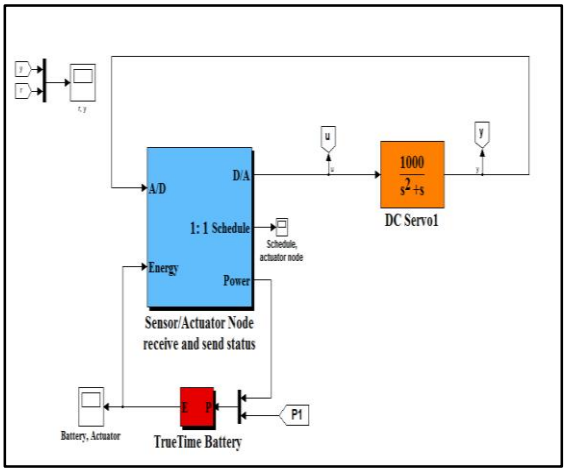

Fig(15): The Plant node with TrueTime Battery

Sensor/Actuator node uses one D/A in the output channel and one (A/D) in the input part and one network output (Send) on the output and one network input (Receive) on the input. Sensor/Actuator node periodically Receives messages from the controller by the network and actuates the plant by converts data from digital to analog then it convert the new analog data to digital and sends it to the network. It uses following initial function which is called once in TrueTime kernel (line by line description is shown in inline comments) when simulation starts:

```
……..
function actuator_init
 % Initialize TrueTime kernel
ttInitKernel('prioFP'); % fixed priority
ttSetKernelParameter('energyconsumption',0.01);
% 10 mW
……..
% Create mailboxes(Create a mailbox for inter-
task communication).
ttCreateMailbox('control_signal', 10)
ttCreateMailbox('power_ping', 10)
ttCreateMailbox('power_response', 10)
……..
% Create sensor task
data.y = 0;
offset = 0.0;
period = 0.010;
prio = 1;
% Create an periodic task
ttCreatePeriodicTask('sens_task', offset, period,
'senscode', data);
ttSetPriority(prio, 'sens_task');
…….
% Create actuator task
deadline = 100;
prio = 2;
% Create an aperiodic task
ttCreateTask('act_task', deadline, 'actcode');
ttSetPriority(prio, 'act_task');
……..
% Create power controller task
offset = 2.07;
period = 0.025;
prio = 3;
power_data.transmitPower = 20;
power_data.name = 1;     % We are node number
1 in the network
power_data.receiver = 2; % We are
communicating with node 2
power_data.haverun = 0;  % We have not run yet
ttCreatePeriodicTask('power_controller_task',
offset, period, 'powctrlcode', power_data);
ttSetPriority(prio, 'power_controller_task');
……..
% Create power response task
deadline = 100;
prio = 4;
ttCreateTask('power_response_task',      deadline,
'powrespcode');
ttSetPriority(prio, 'power_response_task');
…….
% Initialize network
ttCreateHandler('nw_handler',1,'msgRcvActuatr');
ttAttachNetworkHandler('nw_handler');
……..
```

Sensor/Actuator node periodecaly call senscode.m function by using this command ttCreatePeriodicTask('sens_task', offset, period, 'senscode', data) value 1 put firstly in input, next if the seg has value 2 then the output

values send, if it is 3, then finish and exit, the function ttAnalogIn that periodically reads data from input plant and stores its value to the structure, it also contain the Function ttSendMsg which periodically sends 80 bits of converted analog signal to the plant. The senscode.m function commands is:

```
function [exectime, data] = senscode(seg, data)
switch seg,
case 1,
data.msg.msg = ttAnalogIn(1);
exectime = 0.0005;
case 2,
data.msg.type = 'sensor_signal';
ttSendMsg(2, data.msg, 80); % Send message (80 bits) to node 2 (controller)
exectime = 0.0004;
case 3,
exectime = -1; % finished
end
……..
```

Also the Sensor/Actuator node call actcode.m using command ttCreateTask('act_task',deadline, 'actcode') which fetch the control signal then convert the data to analog output to the plant. The actcode.m function commands is:

```
function [exectime, data] = actcode(seg, data)

switch seg,
 case 1,
 % Read all buffered packets
 temp = ttTryFetch('control_signal');
 while ~isempty(temp),
 data.u = temp;
 temp = ttTryFetch('control_signal');
 end

 exectime = 0.0005;
 case 2,
 ttAnalogOut(1, data.u)
 exectime = -1; % finished
end
……..
```

The function of controller node is regulator_init:

```
function regulator_init
% Receives messages from the sensor node, computes control signal
% and sends it back to the sensor/actuator node.
 % Initialize TrueTime kernel
ttInitKernel('prioFP'); % fixed priority
ttSetKernelParameter('energyconsumption', 0.010); % 10 mW
 ……
% Create mailboxes
ttCreateMailbox('sensor_signal', 10)
ttCreateMailbox('power_ping', 10)
ttCreateMailbox('power_response', 10)
 ……
% PD Controller parameters
h = 0.010;
N = 100000;
Td = 0.035;
K = 1.5;

% Create task data (local memory)
data.u = 0.0;
data.K = K;
data.ad = Td/(N*h+Td);
data.bd = N*K*Td/(N*h+Td);
data.Dold = 0.0;
data.yold = 0.0;
……
% Create controller task
deadline = h;
prio = 1;
ttCreateTask('pid_task', deadline, 'ctrlcode', data);
ttSetPriority(prio, 'pid_task');
……
% Create power controller task
offset = 2;
period = 0.025;
prio = 2;
power_data.transmitPower = 20;
power_data.name = 2;      % We are node number 2 in the network
power_data.receiver = 1; % We are communicating with node 1
power_data.haverun = 0;  % We have not run yet
ttCreatePeriodicTask('power_controller_task', offset, period, 'powctrlcode', power_data);
ttSetPriority(prio, 'power_controller_task');
……..
% Create power response task
deadline = 100;
prio = 3;
ttCreateTask('power_response_task', deadline, 'powrespcode');
ttSetPriority(prio, 'power_response_task');
……
% Initialize network
ttCreateHandler('nw_handler', 1, 'msgRcvCtrl');
ttAttachNetworkHandler('nw_handler');
……..
```

Each time the task is invoked, the code function ctrlcode.m should be executed. This function is given below:

```
switch seg,
case 1,
% Read all buffered packets
temp = ttTryFetch('sensor_signal');
while ~isempty(temp),
y = temp;
temp = ttTryFetch('sensor_signal');
end

r = ttAnalogIn(1);    % Read reference value
P = data.K*(r-y);
D = data.ad*data.Dold + data.bd*(data.yold-y);
data.u = P + D;
data.Dold = D;
data.yold = y;
exectime = 0.0005;
case 2,
msg.msg = data.u;
msg.type = 'control_signal';
ttSendMsg(1, msg, 80);    % Send 80 bits to node
1 (actuator)
exectime = -1; % finished
end
```

……..

4. RESULTS

4.1. Servo-Motor responses: Figures (16) and (17) represent the response of Servo-Motor and controller without network, while the figures (18 to 26) represent the response of Servo-Motor and controller with network using different sample time from 0.009 s to 0.02s.

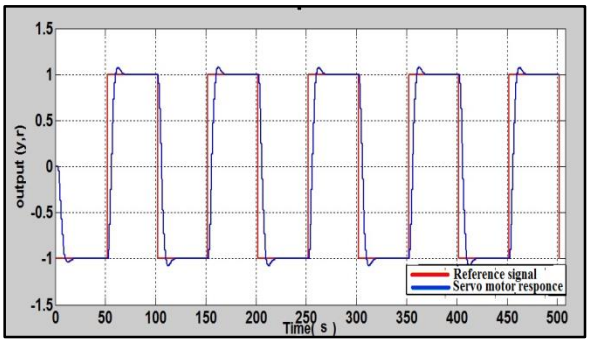

Fig (16): Servo-Motor response without network

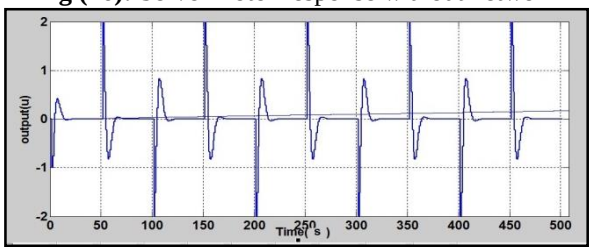

Fig (17): controller response without network

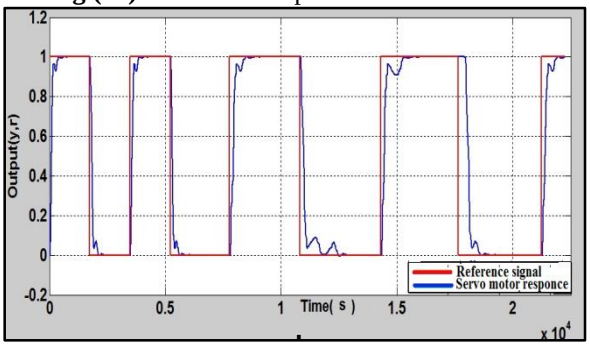

Fig(18): Servo-Motor response with network when h = 0.009s

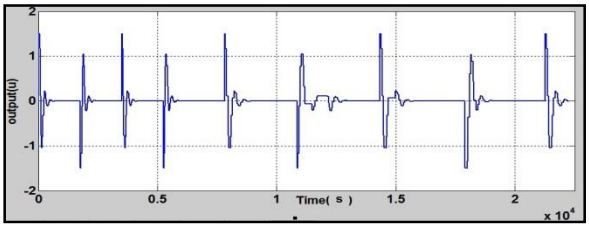

Fig(19): controller response with network when h = 0.009s

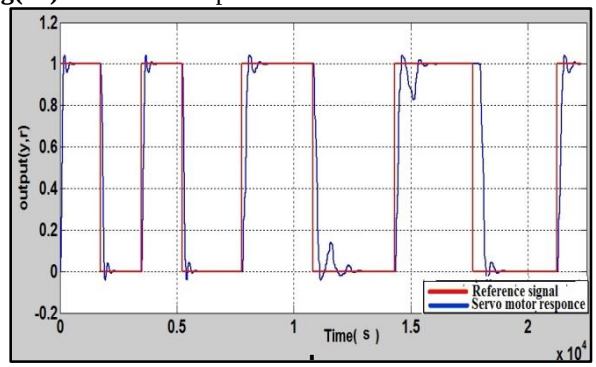

Fig(20): Servo-Motor response with network when h = 0.01s

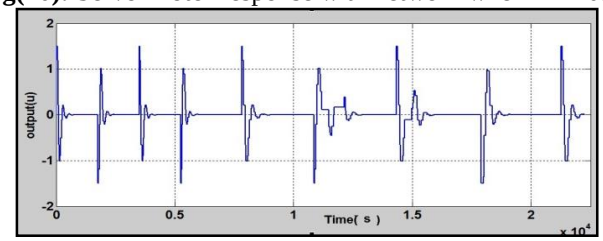

Fig(21): controller response with network when h = 0.01s

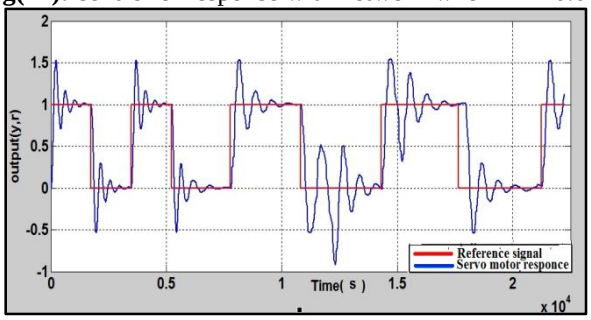

Fig(22): Servo-Motor response with network when h = 0.02s

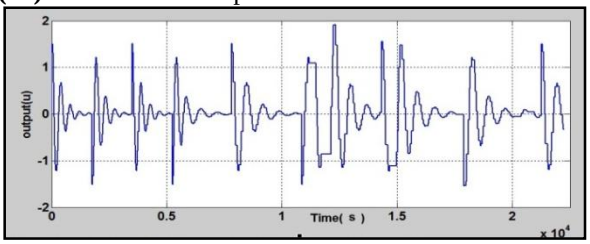

Fig(23): controller response with network when h = 0.02s

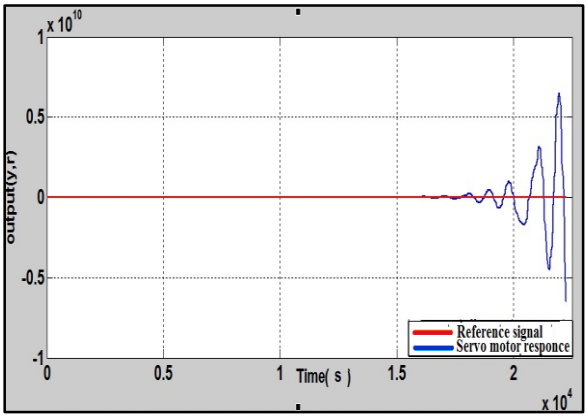

Fig(24): Servo-Motor response with network when h = 1s

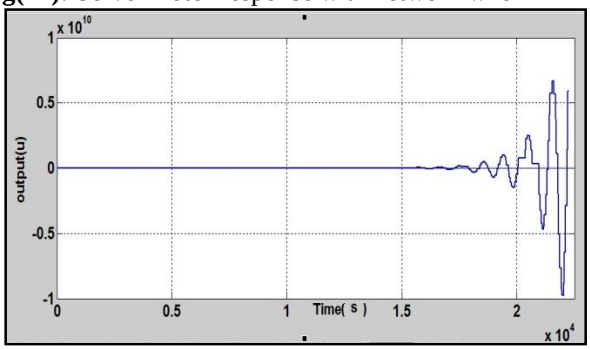

Fig(25): controller response with network when h = 1s

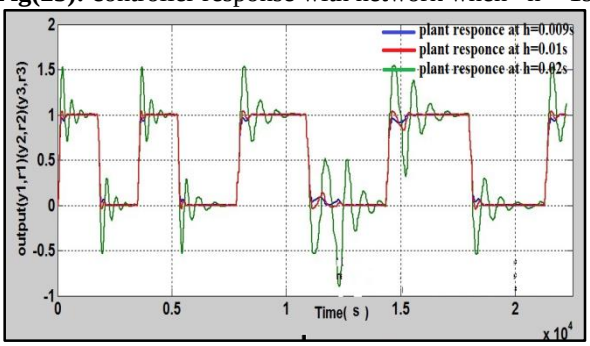

Fig(26): Servo-Motor responses at sample time(h) = 0.009s and 0.01s and 0.02s

From the above results the best performance of the system was when the system works without network, while the system with network adds more time delay and reduce the system performance, when the sample time is reduced to (0.009s) the performance is enhanced compared with the performance of the system working at a sample time equal to (0.01s), but by increasing the sample time to (0.02s) and more, an error in system will appear (overflow) that will reduce the performance of the system to reach an instable system at sample time equal to (1s).

4.2 Effect of network size on Servo-Motor performance: Figures (27-42) represents the Servo-Motor simulation models for different data rate and different network sizes (2-20 node). Figures (27-30) represent the network responses for two nodes and different data rates, figures (31-34) network responses for five nodes and different data rates, figures(35-38) network responses for fifteen nodes and different data rates and figures(39-42) network responses for twenty nodes and different data rates .

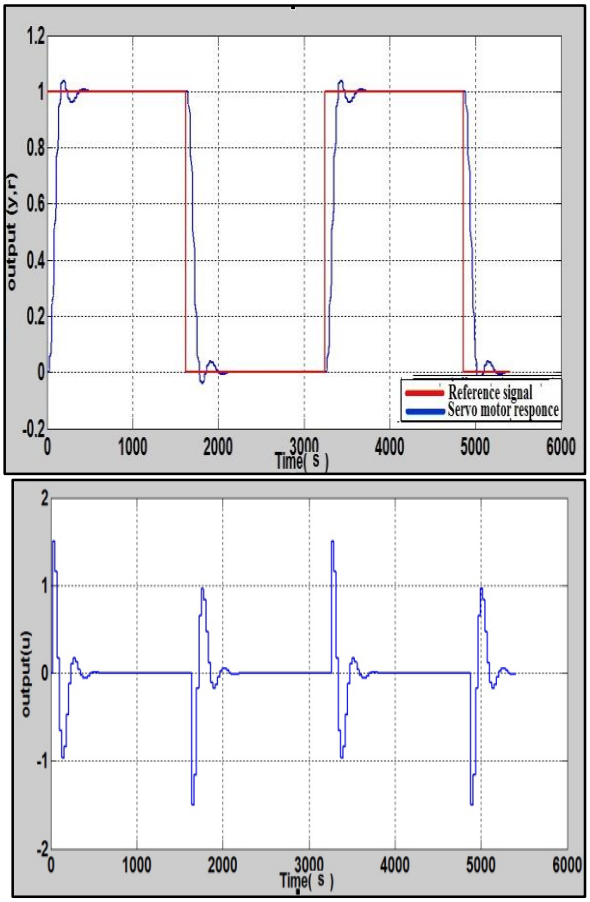

Fig (27): Servo-Motor and controller response when the Data rate = 1Mbps

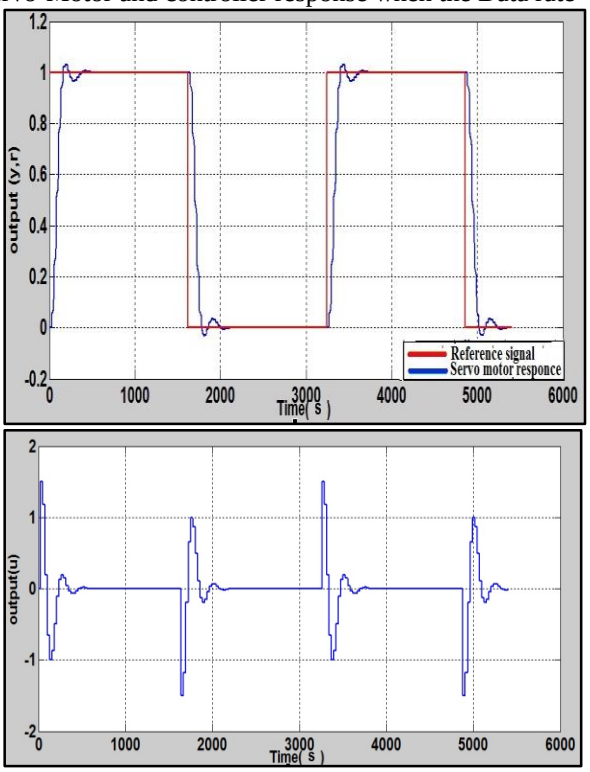

Fig (28): Servo-Motor and controller response when the Data rate = 2Mbps

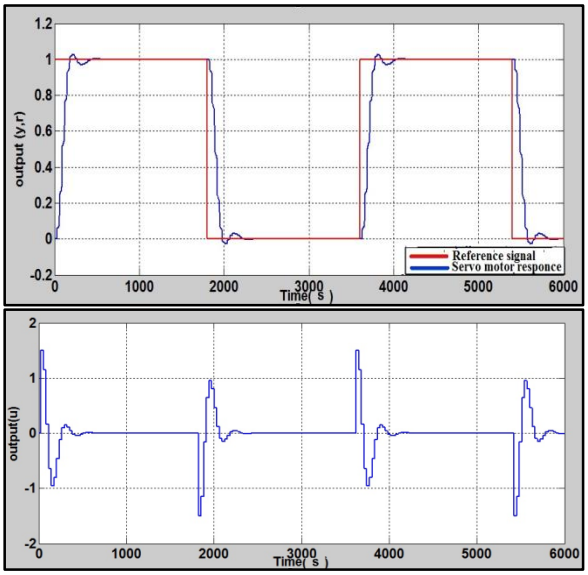

Fig (29): Servo-Motor and controller response when the Data rate = 5.5Mbps

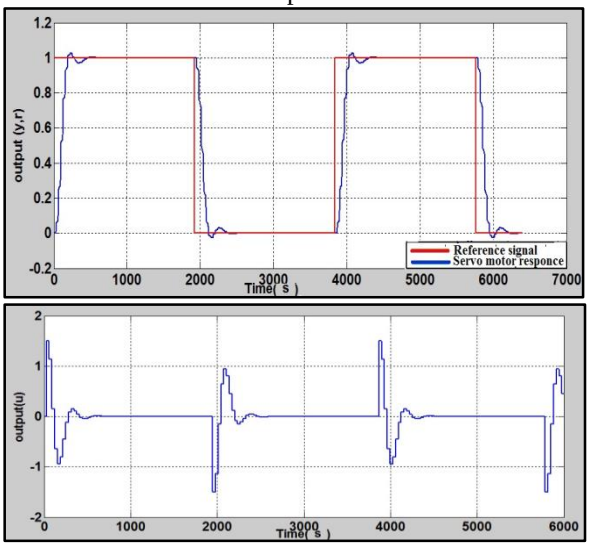

Fig (30): Servo-Motor and controller response when the Data rate =11Mbps

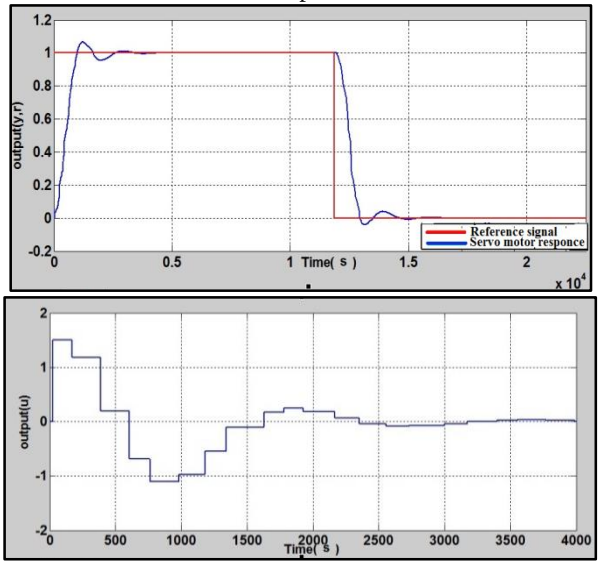

Fig (31): Servo-Motor and controller response when the Data rate = 1Mbps

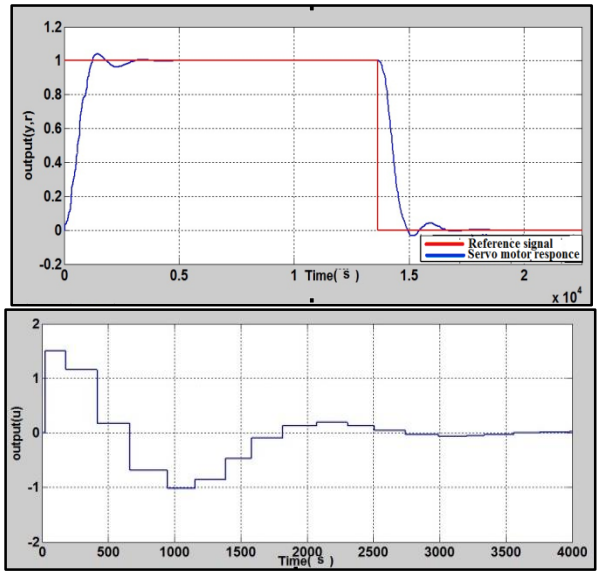

Fig (32): Servo-Motor and controller response when the Data rate = 2Mbps

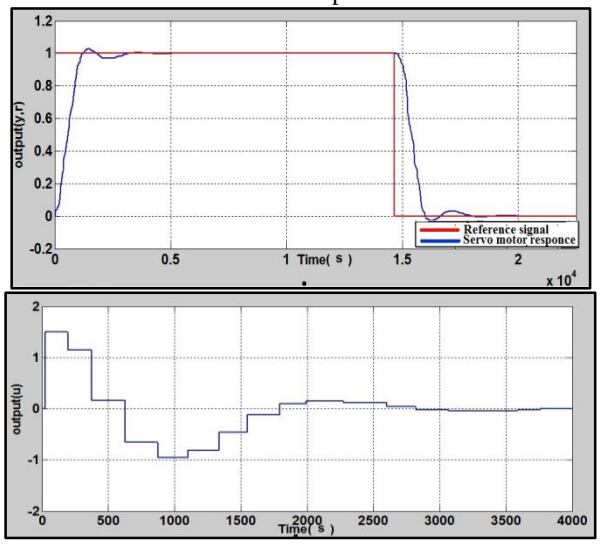

Fig (33): Servo-Motor and controller response when the Data rate = 5.5Mbps

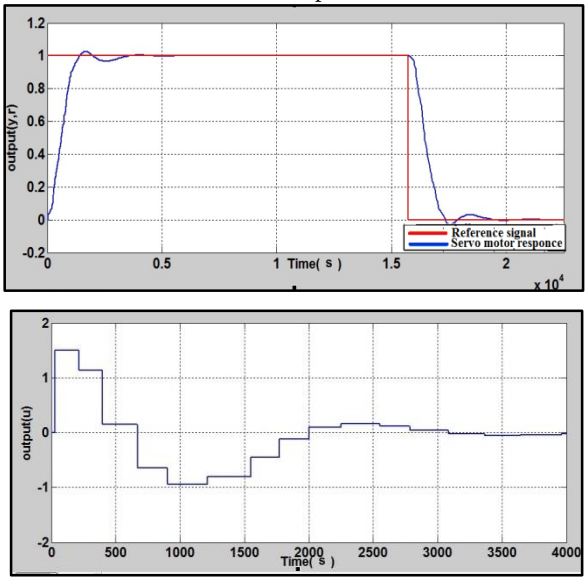

Fig (34): Servo-Motor and controller response when the Data rate = 11Mbps

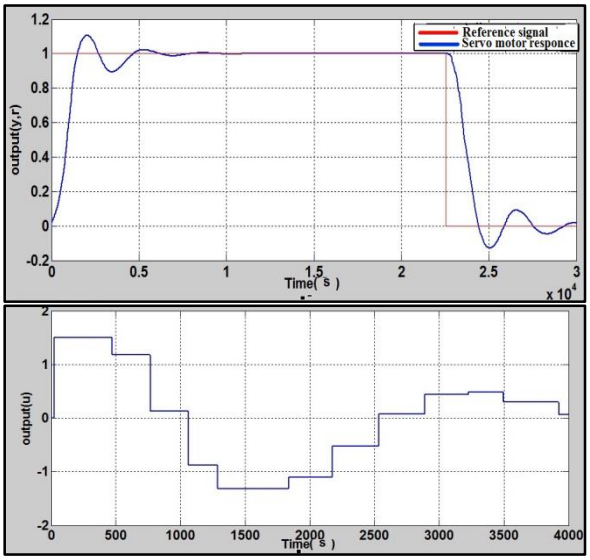

Fig (35): Servo-Motor and controller response when the Data rate = 1Mbps

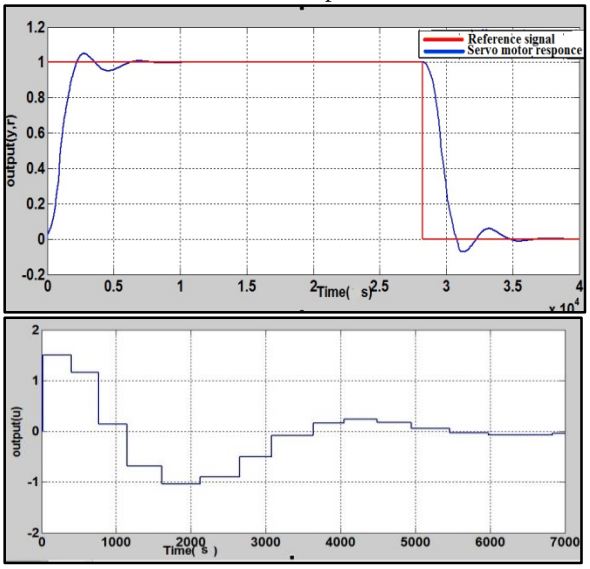

Fig (36): Servo-Motor and controller response when the Data rate = 2Mbps

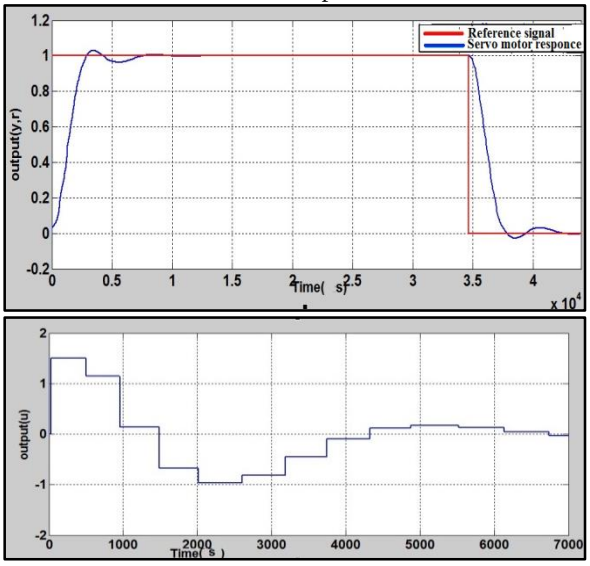

Fig (37): Servo-Motor and controller response when the Data rate = 5.5Mbps

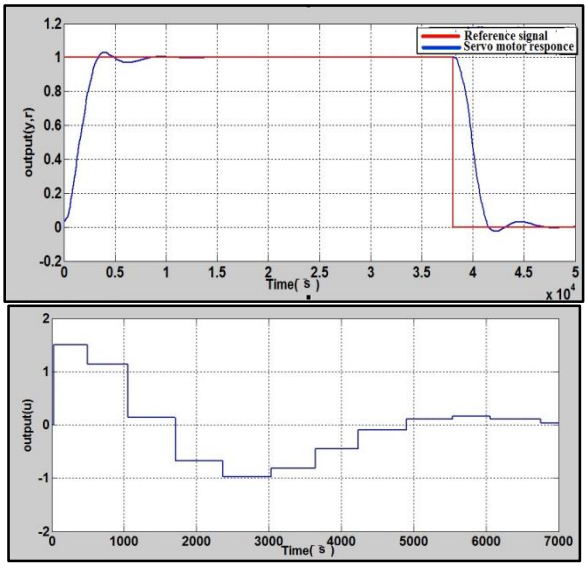

Fig (38): Servo-Motor and controller response when the Data rate = 11Mbps

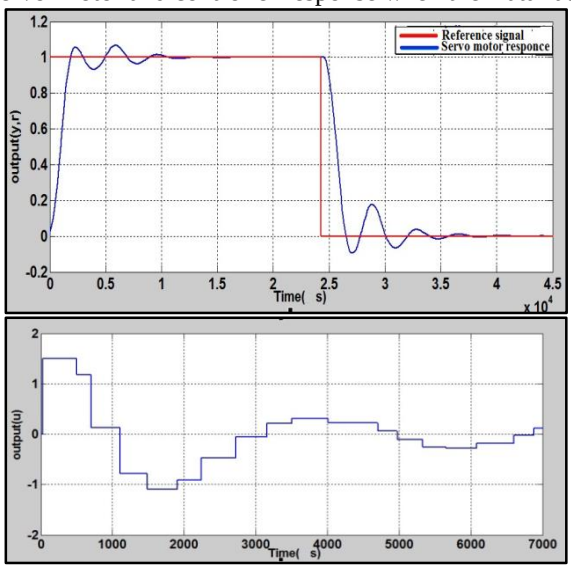

Fig (39): Servo-Motor and controller response when the Data rate= 1Mbps

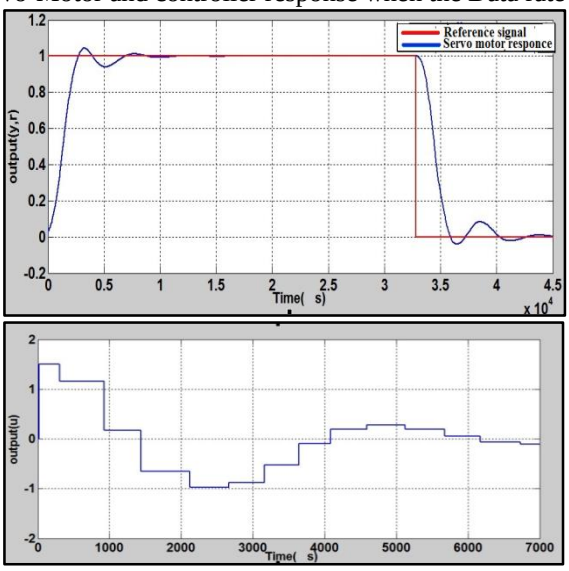

Fig (40): Servo-Motor and controller response when the Data rate= 2Mbps

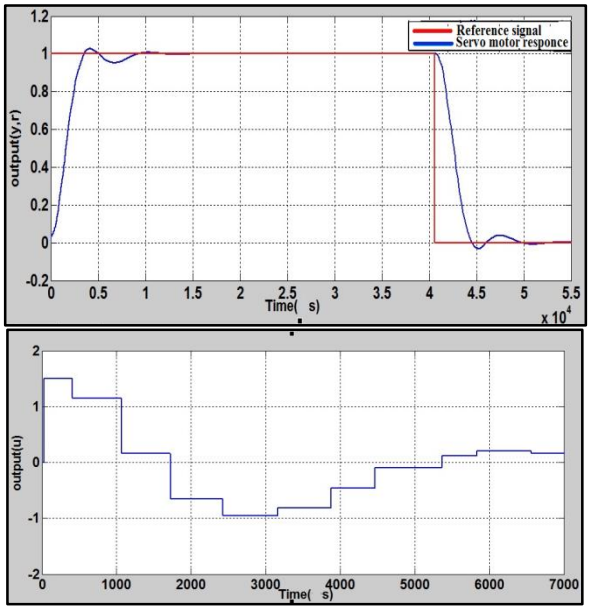

Fig (41): Servo-Motor and controller response when the Data rate= 5.5Mbps

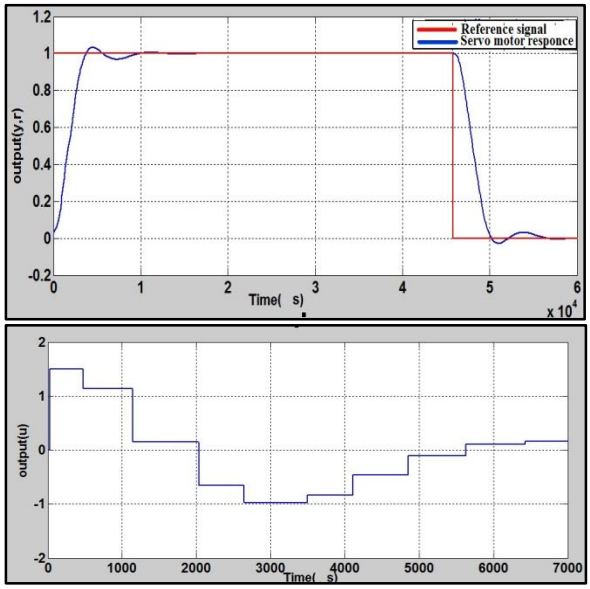

Fig (42): Servo-Motor and controller response when the Data rate= 11Mbps

4.3 Servo-Motor energy cost in different data rate and network size:

Figure (34) represents the Actuator battery energy discharge in working system:

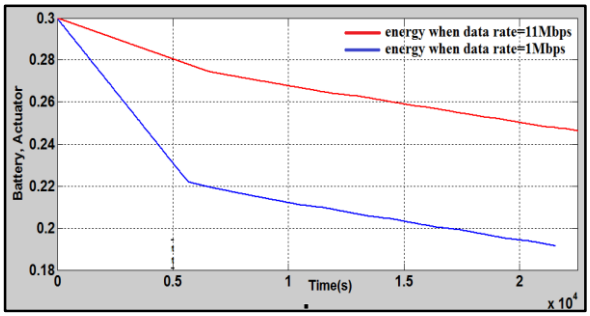

Fig(43): energy battery discharge when the network size of two node with different data rate = 1Mbps and 11Mbps

From the above results the overflow become smaller when using large data rate, and when increasing the network size a large data rate should be used to keep a stability of the system also the large data rate keep the battery work more time than using small data rate this will make this system more cost effective.

5. CONCLUSION

A different sample time from (0.009s to 1s) were chosen to obtain an stable system with small delay, when using a small sample time the system performance become better but the second order system servo-motor is not able to cope with a sample time larger than 0.02s, also the plant can't follow up with the change in the event at a large time delay and it only offers stable Plant with different data rate using a network size of two nodes when using a sample time equal to 0.01s and 0.009s.

As an overall conclusion, an increase in size of the network requires a proportional in the data rate to enhance the system performance because of an increase in the number of nodes decreased the stability of the system reaching to instability due to the large interference with other nodes so specific value of data rate used and compensate time delays as a result of interfering with intermediate nodes.

6.REFRENCES

- **BJÖRKBOM, Mikael**. "Wireless control system simulation and network adaptive control". PhD Thesis. Helsinki University of Technology Control Engineering, 2010.
- **KHUDER, Ena'am F**., **ABD ALRAZAAQ, Sura N., and ABD AL-KAREEM, Omar**. "Performance Analysis of Wireless Network Control Systems Using Different Controllers". Al-Rafadain Engineering Journal, VOL 20, NO 4,2012.pp.47-59.
- **BIMALI, Sandeep**. "Networked control system: Theory and simulations". PhD Thesis. Wichita State University. 2005.
- **HARDING, Christopher A.** "Development of a Delay Algorithm and a Co-Simulation Framework for NCS over MANETs". PhD Thesis. Staffordshire University.2010.
- **URBAN, M-BLAHO, M. MURGAŠ, and J. FOLTIN.** "Simulation of Networked Control Systems via TRUETIME".Technical Computing Prague, 2011.
- **SHAH, Kunjesh, TIBERIU Seceleanu, and MIKAEL Gidlund**. "Design and implementation of a WirelessHART simulator for process control". In: Industrial Embedded Systems (SIES), 2010 International Symposium on. IEEE, 2010. pp. 221-224.
- **FAN, Shurui, LI, Jingbo, LI, Jie, SUN, Hexu.** "Performance Analysis of Wireless Network Measurement Control System using MATLAB/Simulink". International Journal of Intelligent Engineering and Systems, Vol.3, No.2,2010.pp. 42-49.
- **HENRIKSSON, Dan, CERVIN, Anton, ÅRZÉN, Karl-Erik.** "TRUETIME: Real-time control system simulation with MATLAB/Simulink". In: Proceedings of the Nordic MATLAB conference ,Copenhagen, Denmark. 2003.
- http://en.wikipedia.org/wiki/IEEE_802.11
- **ANDERSSON, Martin, HENRIKSSON, Dan, CERVIN, Anton, and ARZEN, Karl-Erik.** "Simulation of wireless networked control systems". Decision and Control, 2005 and 2005 European Control Conference. CDC-ECC'05. Proceedings of the 44th IEEE Conference on Decision and Control, and the European Control Conference 2005. pp. 476-481.
- **CERVIN, Anton, OHLIN, Martin, HENRIKSSON, Dan.** "Simulation of networked control systems using TRUETIME". In: Proc. 3rd International Workshop on Networked Control Systems: Tolerant to Faults. 2007.
- **FAN, Shurui, LI, Fei, SUN, Hexu, LIN, Tao.** "Study and Simulation of Wireless Network Measurement and Control System". In: Intelligent Networks and Intelligent Systems, 2009. ICINIS'09. Second International Conference on. IEEE, 2009. pp. 237-241.
- **PENG Daogang, ZHANG, Hao, HUANG, Conghua , LIN Jiajun, and LI, Hui.** "Study of Immune PID Networked Control System Based on TRUETIME". Journal of Networks , VOL. 6, NO. 6, JUNE 2011.pp.912-915.
- **KHAMARI, Ramesh Chandra.** "Model predictive controllers for a networked DC servo system", PhD Thesis, National Institute of Technology, Rourkela, 2013.

[15]**WANGA, Y., and HEB, L.** "Analysis and Simulation of Networked Control Systems Delay Characteristics Based on TRUETIME" Computer Modelling and New Technologies, Vol.17, No. 4, 2013, pp. 210-216.

- **SRINIVASAN, Seshadhri, VALLABHAN, Mishiga, RAMASWAMY, Srini, and KOTTA, ¨Ulle**. Adaptive regulator for networked control systems: MATLAB and true time implementation. In: Control and Decision Conference (CCDC), 2013 25th Chinese. IEEE, 2013. p. 2551-2555.
- **NISHANTH, Kondabolu, and SASHANK, Pendyala Sai Sundara.** "Real Time Computer Control of Distributed Control Systems Using True Time Toolbox in MATLAB" International Journal of Advanced Science, Engineering and Technology, Vol 3, Issue1, 2014, pp8-13.

- **AL-HAMMOURI, Ahmad, T., BRANICKY, Michael, S., and LIBERATORE, Vincenzo.** "Co simulation tools for networked control systems". In: Hybrid Systems: Computation and Control. Springer Berlin Heidelberg, 2008. pp. 16-29.

- **ALI, Qutaiba, Ibrahem, ABDULMAOWJOD, Akram, and MOHAMMED, Hussein, Mahmood.** "Simulation & performance study of wireless sensor network (WSN) using MATLAB". In: Energy, Power and Control (EPC-IQ), 2010 1st International Conference on. IEEE, 2010. pp. 307-314.

- **Farkas, L., and J. Hnát.** "Simulation of Networked Control Systems using TrueTime." 17th Annual Conference Technical Computing Prague. 2009.

- **CERVIN Anton, HENRIKSSON, Dan, and OHLIN, Martin.** "TRUETIME 2.0 beta 1-reference manual". Department of Automatic Control, Lund University, Sweden, 2009.

- http://en.wikipedia.org/wiki/ZigBee

- **GHOSTINE, Rony, THIRIET, Jean-Marc, AUBRY, Jean-François.** "Influence of transmission faults on the dependability level of networked control systems: application to a control loop". In: 8th IFAC Symposium on Cost Oriented Automation: Affordable Automation Systems. 2007.

الخلاصة

في الوقت الحاضر أصبح الاتجاه يتمحور حول استخدام التطبيقات التي تعمل في الزمن الحقيقي, و أصبحت منظومات السيطرة الشبكية وما تواجهها من تحديات موضع اهتمام الباحثين في هذا المجال, و إن ابرز المشاكل التي تعترض دراسة هذا النوع من المنظومات هو وجود تأخير زمني غير مرغوب به يؤثر على أداء المنظومة و استقراريتها, يهدف هذا البحث إلى دراسة تأثير وضع شبكة في منظومة السيطرة على الأداء و ايجاد الحلول للحد من المشاكل التي تتعرض لها المنظومة, في هذا البحث تم اختيار أداة تسمى بأداة الزمن الحقيقي (TRUETIME toolbox) لأغراض المحاكاة في برنامج MATLAB وعمل المحاكاة الثنائية بين منظومة السيطرة والشبكة اللاسلكية على اساس ان العقد يتم التحكم بها عن بعد. و لغرض دراسة تأثير زيادة سرعة البيانات (data rate) على اداء المنظومة تم اختيار شبكة من نوع (WLAN) 802.11b كونها تعمل بسرعة نقل للبيانات عالية (11Mbps). تم دراسة تأثير وجود شبكة وعدم وجودها لمنظومة سيطرة من نوع محرك سيرفو (Servo-Motor) فتبين ان التأخير الحاصل نتيجة وجود شبكة سببه عمليات الارسال والاستلام التي تتم بين المنظومة والمسيطر, ووجد انه بتقليل زمن العينات (Sampling time) يصبح الاداء افضل لكن المحطة (Plant) لا تستطيع متابعة التغيير الحاصل عند حدوث تأخير زمني اكبر من 0.02s كذلك تم استخدام منظومة محرك السيرفو لأغراض دراسة تأثير وجود عقد وسطية اثناء الارسال, حيث لوحظ انه بزيادة عدد العقد (2 و 5 و 15 و 20) تقل استقراريه المنظومة لتصل الى عدم الاستقرار بسبب التداخل الكبير مع العقد الوسطية عند قيمة محددة لمعدل نقل البيانات, لذا تم تغيير معدل سرعة نقل البيانات(data rate) للشبكة اللاسلكية, فتبين وجوب زيادة سرعة نقل للبيانات بنفس نسبة الزيادة في عدد العقد لتلافي التأخير الحاصل نتيجة حصول تداخل مع عقد وسطية في الطريق, وان الزيادة في معدل سرعة النقل تزيد من عمر البطارية وبالتالي تحافظ على منظومة مستقرة وتعمل لفترة اطول.

IMPACTS OF *NOISE POLLUTION* ON ARTERIAL *SYSTOLIC BLOOD PRESSURE, DIASTOLIC BLOOD PRESSURE, HEART PULSE RATE* AND *BLOOD OXYGEN SATURATION* OF *NURSES* IN DUHOK HOSPITALS – IRAQ

BADAL **H**. **E**LIAS , **W**ALAT **A**. **H. A**LHAMDI and **M**OHAMMED **H. K**HALIL
Collage of science, University of Duhok, , Kurdistan Region-Iraq

(Received: February 26, 2015 ; Accepted for publication: May 11, 2015)

ABSTRACT

This study had been done to estimate the effect of noise pollution on the systolic and diastolic blood pressure (SBP, DBP), heart rate (HR) and oxygen saturation (SpO2) for 41 nurses, aged 18-43 years old, in two selected hospitals of Duhok Governorate. These two hospitals (Azadi and Shelan Hospitals) where chosen randomly in different location of Duhok City and the tests were done for both male and female before exposure to noise and after 4 to 5 hours of work. The minimum and maximum value of sound pressure level measured during working hour in Azadi hospital (19 - 94dB) while in Shelan Hospital (24-86dB) respectively. Whereas, the average of sound pressure level (SPL) measured in both selected Hospitals were (66.5 and 58.5dB) which were perceived below the limited threshold (85 dB). Person's correlation coefficient (r) and P-values for all dependent variable were calculated. r for SBP, DBP, HPR and SpO2 were 0.141, 0.212, 0.511 and 0.412 respectively while P-value for all studied variable P > 0.05, these results indicate that there is no strong association between dependent variable and independent variable, sound pressure level (SPL).

***KEYWORDS*:** Blood pressure, Oxygen saturation, Heart pulse rate, Noise pollution and Duhok Hospitals

INTRODUCTION

Noise is defined as undesirable sound (Alexandros *et al*, 2008). It considered potentially dangerous pollutant and threat to human health. It becomes environmental pollution, when it tempers with the environment noise (Ta-Yuan Chang *et al*, 2003). There are numerous things were created in order to constitute an environment such as, water, land and animals. These things were significant for human life survival. An ecological impact will produce, if any changes occur to these things. According to some researcher air pollution, noise pollution and industrial pollution are the three branches of Environmental pollution (Shahid *et al* 2013). Among these, noise pollution will become the major problem for the human being, which produc stress (Tomei *et al*, 2000). In some research conducted worldwide, more than 130 million people in Europe suffered to noise level above 60 dB (A) (Oyedepo and Saadu, 2009).

According to US Environmental Protection Agency Standard the average level of sound should not be more than 40 dB (A), while according to Occupational Safety Health Administration (OSHA) average level of noise should not reach to 60 dB (A) (Khadija, 2012). Whereas exposure to high level of noise more than described range, it has become very significant factor of stress in the environment of man (Shahid *et al* 2013) and lead to many health problem on human including Hypertension, heart problems, sleep disturbance and hearing loss (Elise *et al*, 2002). Human health problems are different from one person to another depending on level of sound, noise pollution duration and sound frequency (Khadija, 2012). So, noise pollution is the most important element that affects the well-being of the human in many daily work location including hospitals, School and dental office etc.

The level of noise in hospitals goes on increase. Also researcher reported that with the passage of time the stress increase by noise even in new hospital construction. This situation has been worsening steadily. Because there are many source of load sound which present in the hospital likes medical device, air conditioning, crowd of human (human sound with high level). These load sounds produce negative effect and lapses to the hospital staff. It produces many physical and psychological health effects on population that are exposed to high level of sound (Rashid *et al*, 2014). Systolic blood pressure (SBP) and diastolic blood pressure

(DBP) increase during exposure to occupational noise. This situation produce stress which lead to increasing in heart rate and decreasing Oxygen concentration (Maurin and Lambert, 1990 and Green *et al*, 1995).

MATERIALS AND METHODS

The procedure of this study include taking the data from main hospitals in Duhok City. Various parameters were measured like, blood oxygen saturation (SpO2), heart rate (HR), Systolic blood pressure (SBP) and Diastolic blood pressure (DBP) to study the impact of noise on nurses health. The studied samples consist of 21 nurses, 12 male and 9 female in Azadi Hospital and 20 nurses, 10 male and 10 female in Shelan Hospital. The selection of sampling area and the information about sample concerning the study for instant, age, employment duration, sex and having another jobs most significant aspect when noise data were taken. Therefore, this study applied to the nurses located between 18- 43 years old and had at least two year's work duration. The level of noise was measured from 8:30 am to 1:30 pm during June, 2014 to September, 2014 at the different locations of both selected Hospitals. The measurements were taken two times during working hours. Systolic blood pressure, Diastolic blood pressure, Oxygen concentration and heart rate of all selected nurses in two Hospitals were measured two times: firstly in the morning before they expose to noise pollution and secondly at the end of the shift after they exposured to noise. In order to obtain the accurate measurement, data were taken under suitable condition i.e. no wind, no rain in the study area, using the Sound Pressure level meter. While Pulse oximeter was used to measure the level of oxygen saturation in blood. According to Noorhan (2013) (95-100%) oxygen saturation is normal. While, less than this range are dangerous and create a serious of symptom for example, 80-94% oxygen is considered as hypoxemia. Digital blood pressure manomitor model (LBPK1) was utilized to measure blood pressure and heart rate.

RESULTS AND DISCUSSION

Sound pressure level (SPL)

The recorded measurements of SPL of both selected hospitals approximately for four to five working hours in day shift were plotted in Figures 1 and 2. Both figures shows that the minimum and maximum noise recorded in Azadi and Shelan Hospitals during selected hours were [19- 94 dB(A)] and [24 – 86.4 dB(A)] respectively. Whereas, both hospitals had an average values of noise [66.5 and 58.8 dB(A)] respectively. It can be shown from the noise level results that the average noise in Azadi Hospital higher than Shelan hospital. While, this result indicated that the SPL for two samples Hospitals were lower than the limited threshold (85 dB(A)) (Badal, 2013).

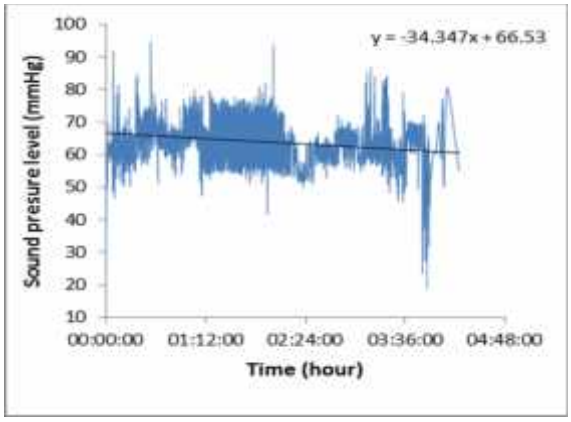

Fig. (1):- *The values of SPL and best linear fit of the means as a function of time in Azadi hospital*

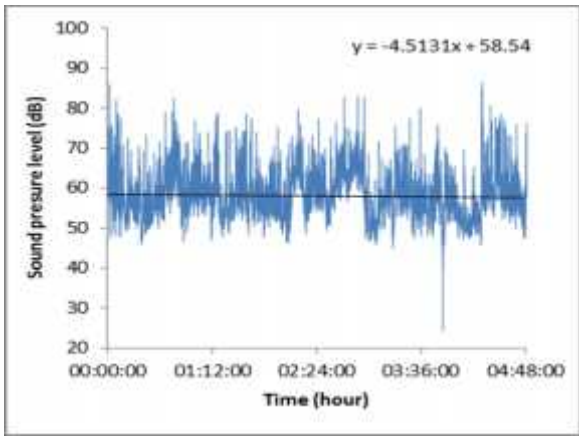

Fig.(2):- *The values of SPL and best linear fit of the means as a function of time in Shelan hospital*

Studied variable

In order to analyze the impact of Sound Pressure Level (SPL) on four dependent variable, which were systolic, diastolic blood pressure, heart rate and oxygen saturation, SPSS program was used. Minimum (Min),Maximum (Max) and average value, were expressed as mean + standard deviation (S.D). Tables 1 show the change occurred on the studied variable before and after expose to noise in both hospitals.

Table (1):- shows the values of Min, Max, Average and S.D of studied variables, before (b) and after (a) exposure to noise, for selected samples at Azadi and Shilan Hospitals in Duhok city from 8:30am - 1:30pm

Variable		Azadi hospitals				Shylan hospitals			
		Min	Max	Average	S.D	Min	Max	Average	S.D
Age		18	43	28	6.2	20	41	29	5.8
Duration of employment		2	23	6	6	2	15	5	4
SpO2%	b	92	99	96.7	1.7	92	99	97	1.6
SpO2%	a	85	99	96	2.7	92	99	96.5	2.2
SBP (mm Hg)	b	99	142	125	12	102	147	124	10
SBP(mm Hg)	a	106	171	134	16	109	162	130	14.7
DBP(mm Hg)	b	65	114	82.9	11	66	122	82	13
DBP(mm Hg)	a	61	151	97	16	65	128	85	13.5
HPR (beats/min)	b	67	109	82	11	67	111	87	11
HPR (beats/min)	a	56	113	88	13	65	112	88	14

Table 1 showed that the averages of studied variable were increased after exposure to noise (at the end of the shift) than before. This indicate that the results were acceptable because there is an association between noise and SBP, DBP and HPR, by increasing the noise level the studied variable increase accordingly (Regecov and Kellerova, 1995).

Systolic (SBP) and Diastolic blood pressure (DBP)

SBP and DBP during working hours for all nurses in both selected Hospitals were recorded. Linear fit of mean were calculated for each of them. The data of systolic and diastolic blood pressure before and after exposed to noise for Azadi hospital was plotted in Figure 3 and Figure 4 While for Shelan hospital was plotted in Figure 5 and 6 respectively.

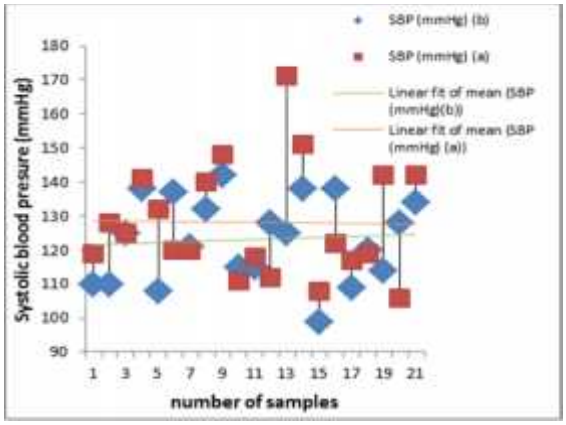

Fig.(3): - *The value of systolic blood pressure of nurses before (b) and after (a) exposure to noise and best Linear fit of mean in Azadi Hospital.*

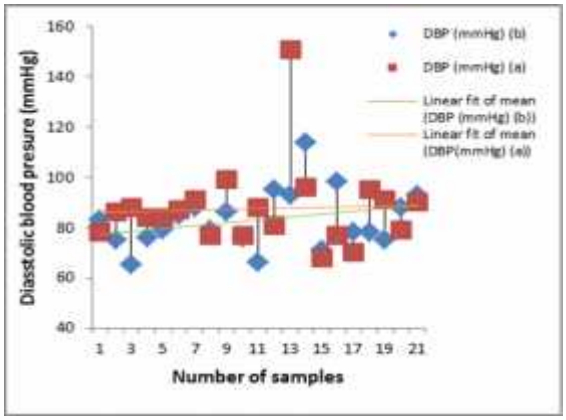

Fig.(4) *The value of diastolic blood pressure of nurses before (b) and after (a) exposure to noise and best Linear fit of mean in Azadi Hospital.*

Fig.3, 4, 5 and 6 illustrate that, the behavior of systolic and diastolic blood pressure of most nurses in both hospitals increased slightly after exposed to noise. While all samples do not have same value because blood pressure does not have constant value, it is affected by the human situation, sex and age (Green *et al*, 1995). The normal blood pressure is 120/80mmHg while above that considered as hypertension (Giuseppe *et al*, 1991). After the percentage concentrations of nurses were calculated, it was found that total number of nurses in both Hospitals, after exposed to noise, having SBP more than 140mmHg was 13 (32%) which cause hypertension. Out of 13 nurses 8 (64%) were female and 5 (36%) were male. While, from 41 nurses of both selected sample hospital 23 (52%) nurses had DBP higher than 81-88 mmHg. Out of 23 (52%) nurses, 8 (40%) were male and 15 (60%) were female. This means that female are affected by noise pollution more than male. Also, one can note that the maximum number of nurses

suffered high (more than normal range) SBP and DBP was greatest in Azadi Hospital than Shelan Hospital. The percentage effect of both SBP and DBP as a function of genders had shown in Fig. 7 and Fig. 8

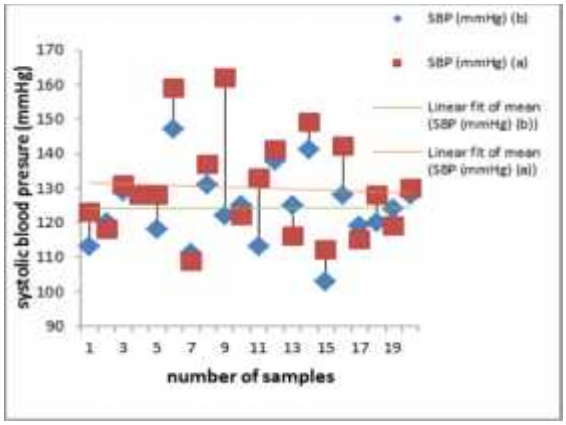

Fig.(5):- *The value of systolic blood pressure of nurses before (b) and after (a) exposure to noise and best Linear fit of mean in Shelan Hospital*

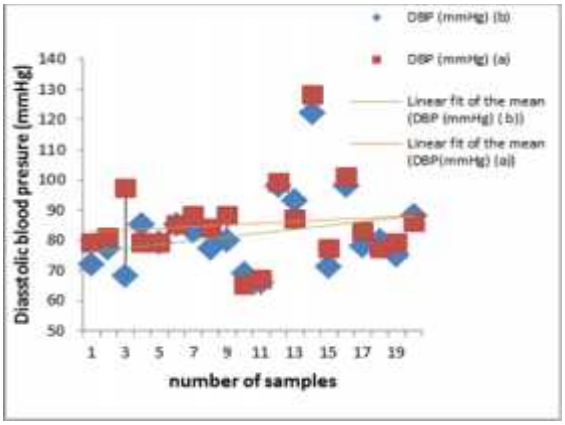

Fig.(6):- *The value of diastolic blood pressure of nurses before (b) and after (a) exposure to noise and best Linear fit of mean in Shelan Hospital*

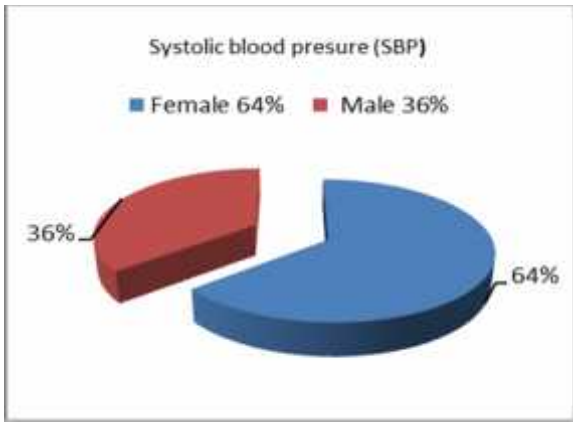

Fig.(7):- Show the results of effect on systolic blood pressure in samples hospitals.

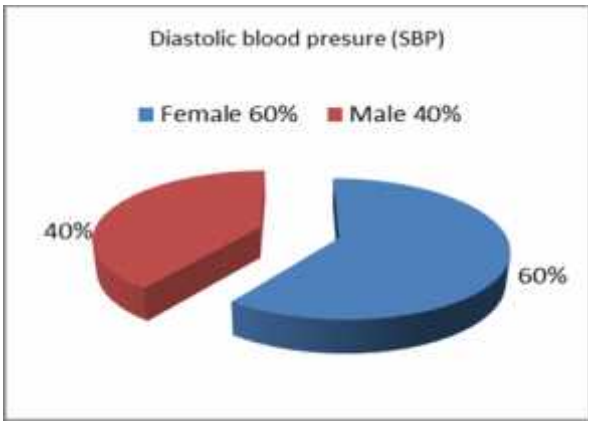

Fig.(8): *-Show the results of effect on Diastolic blood pressure in samples hospitals.*

It is argued that exposure to high noise cause stress reaction that raises both systolic blood pressure and diastolic blood pressure (Noorhan, 2013). This process cause negative effect on human health. It consistent to the behavior of blood pressure, mean heart rate of nurses of both hospitals increase by increasing noise pollution.

Person's correlation(r) and P-value between independent data, sound pressure level and dependent variable systolic and diastolic blood pressure (SBP and DBP), were 0.141, 0.091 and 0.212, 0.067. One can note that P-value for SBP and DBP ($P > 0.05$) which statistically mean that there is no significant relation between the mean sound pressure level and (systolic and diastolic) blood pressure.

Heart Rate (HR) and Oxygen saturation (SpO2%)

In this study, the effect of high sound level on heart pulse rate can be shown by comparing mean of HR of selected nurses in both hospitals before and after exposure to noise. Measurements of heart rate (HR) in selected hospitals are plotted in Fig.9 that shows a slight decrease of heart rate of the samples in two Hospitals.

Also, the mean of the data of oxygen concentration (SpO2) of nurses in both Hospitals before and after exposure to noise were plotted in Fig. 10. In contrast to the results of heart pulse rate, oxygen concentration will reduce by increasing sound level. Fig 10 show that the reduction in SpO2 after exposure to noise in Azadi Hospital more than Shelan Hospital.

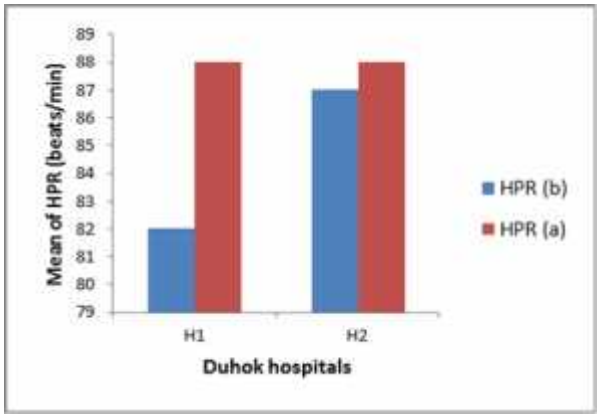

Fig.(9): *-Mean values of heart rate before (b) and after (a) exposure to noise level in Azadi (H1) and Shylan (H2) Hospitals.*

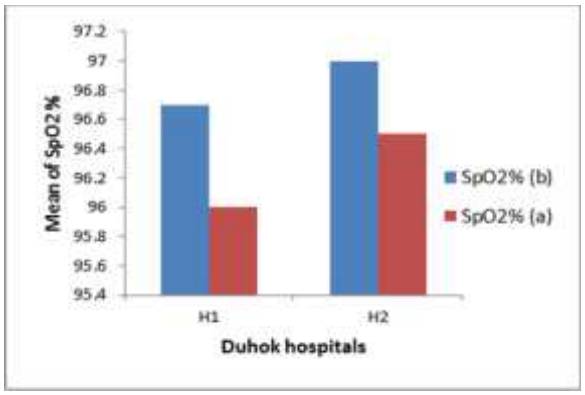

Fig.(10): *-Mean values of the percentage of oxygen concentration (SPO2) before (b) and after (a) exposure to occupational noise in Azadi (H1) and Shelan (H2) hospitals.*

The overall comparison of SBP, DBP, HPR and SpO2 before and after exposure to noise concludes that there were a good relation between studied variables and noise level. Person's correlation coefficient (r) and P-value for heart pulse rate (HPR) before and after exposure to noise 0.511, 0.21 and finally for oxygen concentration (SpO2) were 0.412, 0.091 respectively. P-value for both of them $P > 0.05$ this results indicate that there is no strong association between the independent variables and (HR, SpO2).

Conclusion

The noise level measurement in both sample hospitals showed that the systolic blood pressure (SBP), diastolic blood pressure (DBP), heart rate (HR) and oxygen saturation (SpO2) of nurses were affected by excessive noise continuously. The average value of noise measured during five daily working hours in Azadi Hospital was 66.5 dB While in Shelan Hospital was 58.5dB. This gives some warring about noise pollution in Duhok City hospitals. From analyses of the data it was shown that the maximum and minimum level of noise pollution is different from hospital to another the maximum sound level in Duhok main hospital is (94dB) and the maximum sound level in Shelan hospital is (86dB) which means that the noise pollution level some time is higher than WHO permissible limits for hospitals. Because the acceptable sound pressure level by human ear located between the range 65 to 70 dB (WHO, 1999).

ACKNOWLEDGEMENTS

I would like to express my sincere thanks to all nurses in both studied hospitals for their patient with us to take the data and who help us to complete this research.

REFERENCE

-Alexandros S. H., Konstantina D., Federica V.T., Matteo G., Alessandro B., Marie L.D., Goran P., Gosta B., Danny H., Wolfgang B., Manolis V., Klea K. and Lars J. (2008). European Heart Journal. 29, 658-664

-Ta-Yuan M, Ruei-Man J., Chiu-Sen W. and Chang C.C (2003).Effect of occupational noise exposure on blood pressure. 12(45): 1289-1296.

-Shahid M. A. K., Bashir H., Sabir R. and Awan M. S. (2013).Noise level in the hospital environment of Faisalabad (Pakistan) and its impact on patients.Peak Journal of Medicine and Medical Science. (3):19-31.

-Tomei F, Fantini S, Tomao E, Baccolo T P, Rostai M.V (2000). Hypertension and chronic exposure to noise.Arch Envir. 55 (5): 319-325.

-Oyedepo and Saadu A. A. (2009).A comparative study of noise pollution level in some selected area in Ilorin Metropolis Nigeria. Environmental Monitoring and Assessment. (158): 155-167.

-Khadija, S.M.D. (2012).Effects of Noise Pollution on Arterial BloodPressure, Heart Pulse Rate, Hearing threshold and Blood Oxygen Saturation of Schools' Children in Ramalla Country in Palestine.[Online] Available from: http://scholar.google.com/scholar?q=effect+of+noise+pollution+on+arterial+blood+pressure,+heart+pulse+rate,+hearing&hl=ar&as_sdt=0&as_vis=1&oi=scholart&sa=X&ei=zs07VZ7ZGM74aIOygIgB&ved=0CB4QgQMwAA. [Accessed 15 February 2014].

-Elise EMM, Kempen V, Kruize H, Hendrick C, Boshuizen CB (2002). The association between noise exposure and blood pressure and ischaemic heart disease. Envir Heal Pros. 110:307-317.

-Rashid M., Ghulam J.K., Shamim A., Abdul Jalal S. (2014). Effect of 90 Decibel of 4000 Hertz on Blood Pressure in Young Adults. Department of physiology and department of biochemistry, medical college, Peshawar.

-Maurin, M., and Lambert, J. (1990). Exposure of the French

population to transport noise. Noise Control Engineering Journal 35:5–18.

- Green M.S., Schwartz K., Harari G., Najenson T (1995). Industrial noise exposure and ambulatory blood pressure and heart rate.J Hypertension. 13(4):72-86.
- Noorhan F. A. (2013). The Effects of Light Intensity on Day and Night Shift Nurses' Health Performance. [Online] Available from: https://www.google.iq/search?hl=en-IQ&source=hp&q=the+effect+of+light+intensity+on+day+and+night+shift+nurses%27+health+performance&gbv=2&oq=the+effect+of+light+intensity+on+day+and+night+shift+nurses%27+health+performance&gs_l=heirloom-hp.12...31.59220.0.66926.70.20.0.49.4.0.250.718.2-3.3.0.msedr...0...1ac.1.34.heirloom-hp..64.6.593.Xs93IvZklUM [Accessed 30 May 2014].
- Badal. H. E., Sayran. A. A. and ,Shylan.I (2013). Abo.Effect of Noise Pollution on Arterial Blood Pressure and Heart Pulse Rate of Dentists in there Dental Offices in Duhok city-Iraq.International Journal of Advancements in Research & Technology. (2): 59-64
- Regecov, V. and Kellerova, E. (1995). Effect of urban noise pollution on blood pressure and heart rate in preschool children. Hypertension. 13: 405-412.
- Giuseppe Germano. M.D., Silvio Damiani, Umberto Milito M.D., UgoGermano. M.D., CesareGiarrizzo. M.D. and Anna Santucci.M.D. (1991). Noise in Normal Subject: Time-Dependent Blood Pressure Pattern Assessment. Clin cardiol, (14)321-325
- World Health Organization (WHO), "Noise Report on a WHO Coordination Meeting of the Experts Budapest, Hungary", Journal Occup. Med., 1-14, (1999).

-POLYNOMIAL INVERSE INTEGRATING FACTORS FOR CUBIC SYSTEMS

AZAD **I**. **A**MEN[*] and **A**HMED **M**. **H**USSIEN[**]
[*]Dept. of Mathematics, College of Basic Education, Salahaddin University, Kurdistan region-Iraq
[**]Dept. of Mathematics, College of Science, University of Duhok, Kurdistan region-Iraq

(Received: April 22, 2015; Accepted for publication: October 10, 2015)

ABSTRACT

The main purpose of this paper is to study qualitative properties of existence or non- existence of polynomial inverse integrating factor for some cubic polynomials in two-dimensional autonomous systems. Moreover, we apply these results for studying limit cycles.

KEYWORDS: Polynomial inverse integrating factors, Non-existence polynomial inverse integrating factor.

1. INTRODUCTION TO PLANAR DIFFERENTIAL SYSTEM

First we give some basic concepts and results about qualitative behavior for autonomous ordinary differential equations

$$\begin{aligned} \dot{x} &= P(x,y), \\ \dot{y} &= Q(x,y), \end{aligned} \tag{1.1}$$

where $P(x,y)$ and $Q(x,y)$ are functions of class $C^1(U)$ and $U \subseteq \mathbb{R}^2$. The periodic solution γ of system (1.1) is an algebraic limit cycle if it is a limit cycle and contained in some irreducible invariant algebraic curve $\gamma = 0$ of system (1.1), otherwise it's called non-algebraic limit cycle, (Calanchi, M. and Ruf , B., 2002) and (Chavarriga, J., Giacomini, H. and Gine , J., 1997).

Definition 1.1: A non-zero function $V: U \to R$ is said to be an inverse integrating factor of system (1.1) if of class $C^1(U,\mathbb{R})$, not locally null and satisfies the following linear partial differential equation:

$$P\frac{\partial V}{\partial x} + Q\frac{\partial V}{\partial y} = \left(\frac{\partial P}{\partial x} + \frac{\partial Q}{\partial y}\right)V . \tag{1.2}$$

The inverse integrating factor is the most important tool in this work. We now give necessary conditions for a polynomial vector field to have a polynomial inverse integrating factor.

Theorem 1.2: (Arrow Smith, D.K. and Place , C.M., 1982) and (Chavarriga, 2004.) Two necessary conditions for system (1.1) to have a polynomial inverse integrating factor $V(x,y) = V_r(x,y) + V_{r+1}(x,y) + \cdots + V_m(x,y)$ are

$$\sum_{i=1}^{n+1} l_i M_i(x,y) = \left(\frac{\partial P_n}{\partial x} + \frac{\partial Q_n}{\partial y}\right), \tag{1.3}$$

$$\sum_{j=1}^{s+1} e_j m_j(x,y) = \left(\frac{\partial P_s}{\partial x} + \frac{\partial Q_s}{\partial y}\right), \tag{1.4}$$

where $l_i,\ e_j \in \mathbb{N}$ for $i = 1,\dots,n+1; j = 1,\dots,s+1$,and $m = \sum_{i=1}^{n+1} l_i$, $r = \sum_{j=1}^{s+1} e_j$.

The following theorem, proved in (Chavarriga, J., Giacomini, H. and Gine , J., 1999), gives an important relation between a limit cycle and an inverse integrating factor.

Theorem 1.3: (Chavarriga, J., Giacomini, H. and Gine , J., 1999) Let $V: U \to \mathbb{R}$ be an inverse integrating factor of (1.1). If $\gamma \subset U$ is a limit cycle of (1.1), then γ is contained in the set $\sum = \{(x,y) \in U : V(x,y) = 0\}$.

In (Chavarriga, J., Giacomini, H. and Gine , J., 2000) , the authors proved some results about the non-existence of algebraic limit cycles for quadratic system using inverse integrating factors. In (Chavarriga, J., Llibre , J. and Sorolla , J., 2001), they provided a classification of all the quadratic systems that can

have an algebraic limit cycles. In (Calanchi, M. and Ruf , B., 2002) and (Ferragut, A., 2006) The construction of polynomial inverse integrating factor of quadratic system is used to study the non-existence algebraic limit cycles. (Chavarriga, J., Giacomini, H. and Gine , J., 1999), studied the existence and non-existence of algebraic limit cycles for a planar cubic system by using inverse integrating factor.

2. POLYNOMIAL INVERSE INTEGRATING FACTORS FOR CUBIC SYSTEM.

We consider the real planar cubic system

$$\dot{x} = \sum_{j=0}^{3}\sum_{i=0}^{j} a_{i,j-i}\, x^i y^{j-i} = P_3(x,y)$$
$$\dot{y} = d + ax + by + lx^2 + mxy + ny^2 + zx^3 + rx^2y + sy^2x + wy^3 = Q_3(x,y) \tag{2.1}$$

we assume that P_3 and Q_3 have no common factors. First we explain the method we use to find polynomial inverse integrating factors of degree $k > 0$. Suppose that $V(x,y) = \sum_{i+j=0}^{k} V_{i,j}x^i y^j$, is a polynomial inverse integrating factors of (2.1). Since $P_3(x,y), Q_3(x,y)$ and V are polynomial functions, and it can be written as a linear system with unknowns $V_{i,j}, i+j = 0, \dots, k$. If $k > 1$, we define the matrix $A_{j,k}$,

$$A_{j,k} = \begin{pmatrix} \mathbf{0} & \\ A_{j,k-1} & C_{1,k} \\ & C_{2,k} \\ & C_{3,k} \\ \mathbf{0} & C_{4,k} \end{pmatrix}_{\frac{(k+3)(k+4)}{2}\times\frac{(k+1)(k+2)}{2}} \tag{2.2}$$

where

$$C_{1,k} = \begin{pmatrix} ka_{0,0} & d & & & \\ & (k-1)a_{0,0} & 2d & & \\ & & \ddots & \ddots & \\ & & & a_{0,0} & kd \end{pmatrix}_{k\times(k+1)} \tag{2.3}$$

$$C_{2,k} = \begin{pmatrix} (k-1)a_{1,0} - b & a & & & \\ k\ a_{0,1} & (k-2)a_{1,0} & 2a & & \\ & (k-1)a_{0,1} & \ddots & \ddots & \\ & & \ddots & \ddots & ka \\ & & & a_{0,1} & -a_{1,0} + (k-1)b \end{pmatrix}_{(k+1)\times(k+1)} \tag{2.4}$$

$$C_{3,k} = \begin{pmatrix} (k-2)a_{2,0} - m & l & & & \\ (k-1)a_{1,1} - 2n & (k-3)a_{2,0} & 2l & & \\ ka_{0,2} & (k-2)a_{1,1} - n & \ddots & \ddots & \\ & (k-1)a_{0,2} & \ddots & \ddots & kl \\ & & \ddots & \ddots & -2a_{2,0} + (k-1)m \\ & & & a_{0,2} & -a_{1,1} + (k-2)n \end{pmatrix}_{(k+2)\times(k+1)} \tag{2.5}$$

$$C_{4,k}=\begin{pmatrix} (k-3)a_{3,0}-r & z & & & \\ (k-2)a_{2,1}-2s & (k-4)a_{3,0} & 2z & & \\ (k-1)a_{1,2}-3w & (k-3)a_{2,1}-s & \ddots & \ddots & kz \\ & (k-2)a_{1,2}-2w & \ddots & -3a_{3,0}+(k-1)r & \\ & & \ddots & -2a_{2,1}+(k-2)s & \\ & & & -a_{1,2}+(k-3)w & \end{pmatrix}_{(k+3)\times(k+1)} \tag{2.6}$$

and

$$A_{0,1}=\begin{pmatrix} -a_{1,0}-b & a_{0,0} & d \\ -2a_{2,0}-m & -b & a \\ -a_{1,1}-2n & a_{0,1} & -a_{1,0} \\ -3a_{3,0}-r & -a_{2,0}-m & l \\ -2a_{2,1}-2s & -2n & -2a_{2,0} \\ -a_{1,2}-3w & a_{0,2} & -a_{1,1}-n \\ 0 & -2a_{3,0}-r & z \\ 0 & -a_{2,1}-2s & -3a_{3,0} \\ 0 & -3w & -2a_{2,1}-s \\ 0 & 0 & -a_{1,2}-2w \end{pmatrix}_{10\times 3} \tag{2.7}$$

First we state the following result about inverse integrating factor of system (2.1).

Theorem 2.1: Let $V(x,y)$ be a polynomial inverse integrating factor of degree k of system (2.1). Then, equation (1.2) is equivalent to the homogeneous linear system

$$A_k V^k = 0, \tag{2.8}$$

where A_k *is* the matrix defined in (2.2) and

$$V^k=(V_{0,0},V_{1,0},V_{0,1},V_{2,0},V_{1,1},V_{0,2},\dots,V_{k,0},V_{k-1,1},\dots,V_{1,k-1},V_{0,k})^T$$

is the vector of the coefficients of $V(x,y)$.

Proof: Equation (1.2) is a polynomial of degree $k+2$ in two variables, then it can be written as

$$\sum_{i+j=0}^{k+2}\Big[\Big(a_{1,1}(i-1)+n(j-3)\Big)V_{i,j-1}+\Big(a_{2,0}(i-3)+m(j-1)\Big)V_{i-1,j}+l(j+1)V_{i-2,j+1}$$
$$+a_{0,0}(i+1)V_{i+1,j}+\Big(a_{1,0}(i-1)+b(j-1)\Big)V_{i,j}+a_{0,1}(i+1)V_{i+1,j-1}$$
$$+d(j+1)V_{i,j+1}+z(i-1)V_{j-1,i-1}+a(j+1)V_{i-1,j+1}$$
$$+\Big(a_{2,1}(i-3)+s(j-3)\Big)V_{i-1,j-1}+\Big(a_{3,0}(j-1)+r(i-3)\Big)V_{j,i-2}$$
$$+a_{0,2}(i+1)V_{i+1,j-2}+\Big(a_{1,2}(i-1)+w(j-5)\Big)V_{i,j-2}\Big]x^iy^j=0,$$

where $V_{r,s}=0$ if $r,s,r+s\notin\{0,\dots,k\}$. As all the coefficients of this polynomial must be zero, we must take

$$\Big(a_{1,1}(i-1)+n(j-3)\Big)V_{i,j-1}+\Big(a_{2,0}(i-3)+m(j-1)\Big)V_{i-1,j}+l(j+1)V_{i-2,j+1}+a_{0,0}(i+1)V_{i+1,j}+\Big(a_{1,0}(i-1)+b(j-1)\Big)V_{i,j}+a_{0,1}(i+1)V_{i+1,j-1}+d(j+1)V_{i,j+1}+z(i-1)V_{j-1,i-1}+a(j+1)V_{i-1,j+1}+\Big(a_{2,1}(i-3)+s(j-3)\Big)V_{i-1,j-1}+\Big(a_{3,0}(j-1)+r(i-3)\Big)V_{j,i-2}+a_{0,2}(i+1)V_{i+1,j-2}+\Big(a_{1,2}(i-1)+w(j-5)\Big)V_{i,j-2}=0,$$

for $0\le i+j\le k+2$. In order to obtain equation (2.8), we just have to write these equalities as a linear system with unknowns' $V_{i,j}$.

Proposition 2.2. Consider the cubic system

$$\begin{aligned}\dot{x}&=a_{0,0}+a_{1,2}y^2x+x^3=P_3(x,y),\\ \dot{y}&=d+ax+by+lx^2+mxy+ny^2+zx^3+rx^2y+sy^2x+wy^3=Q_3(x,y),\end{aligned} \tag{2.9}$$

The following statements hold.

1) Assume that $a_{0,0}\in\{0,1,-1\}, a_{1,2}\in\{0,1\}$, and $w\neq 0$. Let $V(x,y)$ be a polynomial inverse integrating factor of (2.9). Then, the degree of $V(x,y)$ with respect to y is three.

2) Assume $a_{0,0}=0, a_{1,2}\in\{0,1\}$, and $w=0$, let $V(x,y)$ be a polynomial inverse integrating factor of degree $k>5$ of (2.9). Then $r=1-\frac{(k-4)}{p}$, where $p\in\{-1,\ 1,\ 2,\ 3,\dots,\ k-1\}$.

Proof: We write $V(x,y)=\sum_{i=0}^{\alpha}W_i(x)y^i$, then equation (1.2) is a polynomial equation in y. The equation corresponding to $y^{\alpha+2}$ is

$$a_{1,2}xW_\alpha{}'(x)+\big(w(\alpha-3)-a_{1,2}\big)W_\alpha(x)=0.$$

If $a_{1,2}=1$, then we obtain $W_\alpha(x)=cx^{-(w(\alpha-3)-1)}, W_\alpha(x)=x^{-(w(\alpha-3)-1)}$, where $\alpha\neq 3$. Since $W_\alpha(x)$ is a polynomial and $w\neq 0$, we take $\alpha=3$, $w\in\mathbb{R}$ and then $W_\alpha(x)=W_3(x)=x$. If $a_{1,2}=0$ as $w\neq 0$ and $W_\alpha(x)\neq 0$ again we must take $\alpha=3$. Next we prove statement 2. We write $V(x,y)$ as in (1.15). The homogeneous equation of degree $k+2$ of equation (1.2) is

$$-(r+3)x^2V_k(x,y)+x^2(zx+ry)\frac{\partial V_k(x,y)}{\partial y}+x^3\frac{\partial V_k(x,y)}{\partial x}=0$$

If $r=1$ then $V_k(x,y)=x^4F(\frac{y}{x}-z\log x)$, so $\deg(V_k(x,y))=4$, this is a contradiction with the assumption $k>5$. If $r\neq 1$, then $V_k(x,y)=x^{r+3}F\left(\frac{z}{r-1}x^{1-r}+x^{-r}y\right)$, where F is an arbitrary function. As $V_k(x,y)$ is a homogeneous polynomial of degree k, the function F must be of the form $F(\delta)=\delta^{p+1}$, with $p\in\mathbb{N}\cup\{-1\}$. We discard $p=0$ because, in this case we would get $k=4$. So let $\delta=\frac{z}{r-1}x^{1-r}+x^{-r}y=x^{-r}(\frac{z}{r-1}x+y)\ \rightarrow F(\delta)=\delta^{p+1}=(x^{-r}(\frac{z}{r-1}x+y))^{p+1}=x^{-rp-r}(\frac{z}{r-1}x+y)^{p+1}$, then

$$V_k(x,y)=x^{r+3}F\left(\frac{z}{r-1}x^{1-r}+x^{-r}y\right)=x^{r+3}F(\delta)=x^{r+3}x^{-rp-r}(\frac{z}{r-1}x+y)^{p+1}$$
$$=x^{3-rp}(\frac{z}{r-1}x+y)^{p+1}$$

Then $k=4-p(r-1)$, and from this equality we get $r=1-\frac{(k-4)}{p}$, $p\in\mathbb{N}\cup\{-1\}$. We must also take $p<k$, because $V_k(x,y)$ contains the monomial $x^{k-p-1}y^{p+1}$.

We now consider the cubic system ◘

$$\begin{aligned}\dot{x}&=x\\ \dot{y}&=d+ax+by+lx^2+mxy+ny^2+zx^3+rx^2y+sy^2x+wy^3,\end{aligned}\tag{2.10}$$

where $d,a,b,l,m,n,z,r,s,w\in\mathbb{R}$. If $a=l=m=n=z=r=w=0$ and $s\neq 0$ then this system is transformed into

$$\begin{aligned}\dot{x}&=x,\\ \dot{y}&=b_{0,0}+by+xy^2,\end{aligned}\tag{2.11}$$

where $b_{0,0}=d$ by the affine change $sx\rightarrow x, \frac{x}{s}+y\rightarrow y$. If $w\neq 0$ then system (2.10) becomes

$$\begin{aligned}\dot{x}&=x,\\ \dot{y}&=\frac{b_{0,0}}{4}-\frac{b_{1,0}}{2}x+\frac{b_{3,0}}{4}x^3+y^3.\end{aligned}\tag{2.12}$$

By the affine change $\sqrt{w}\,y\rightarrow y$, where $b_{0,0}=4\sqrt{w}d$, $b_{1,0}=-2\sqrt{w}a$, $b_{3,0}=4\sqrt{w}z$ and $w\in\mathbb{R}^+$ $b=l=m=n=r=s=0$.

Theorem 2.3: The system (2.10) with $l=m=n=r=s=w=0$ and $z\neq 0$ has always a polynomial inverse integrating factor $V(x,y)$. The system can be written, after an affine change of variables and a rescaling of the time if it is necessary, as $\dot{x}=x$, $\dot{y}=Q_3(x,y)$ where $Q_3(x,y)$ is one of the polynomials below.

(1) $Q_3(x,y)=-y+x^3$. $V(x,y)=1$ the system is Hamiltonian,
(2) $Q_3(x,y)=\delta+x^3$, where $\delta=\pm 1$, and we get $V(x,y)=x$,
(3) $Q_3(x,y)=\delta x+y+x^3$, where $\delta=0,1$, and we get $V(x,y)=x^2$
(4) $Q_3(x,y)=by+x^3$, with $b\neq -1,0,1$, and we get $V(x,y)=x^3$

Proof: We apply Theorem 2.1 to construct a polynomial inverse integrating factor. If $b=-1$, then the system is Hamiltonian. By the change $\frac{-ax}{2z}+\frac{y}{z}-\frac{d}{z}\rightarrow y$, we get (1). From system $A_1V^1=0$,

$$\begin{pmatrix} -b-1 & 0 & d \\ 0 & -b & a \\ 0 & 0 & -1 \\ 0 & 0 & z \end{pmatrix}_{4\times 3} \begin{pmatrix} V_{0,0} \\ V_{1,0} \\ V_{0,1} \end{pmatrix}_{3\times 1} = 0,$$

We get $V(x,y) = x$ and $b = 0$. So statement (2) follows after the change $(zx, -az^2x + z^2y) \to (x,y)$, where δ is the sign of $z^2d \neq 0$. From system $A_2V^2 = 0$, then

$$\begin{pmatrix} -1-b & 0 & d & 0 & 0 & 0 \\ 0 & -b & a & 0 & d & 0 \\ 0 & 0 & -1 & 0 & 0 & 2d \\ 0 & 0 & 0 & 1-b & a & 0 \\ 0 & 0 & 0 & 0 & 0 & 2a \\ 0 & 0 & 0 & 0 & 0 & b-1 \\ 0 & 0 & z & 0 & 0 & 0 \\ 0 & 0 & 0 & 0 & z & 0 \\ 0 & 0 & 0 & 0 & 0 & 2z \end{pmatrix} \begin{pmatrix} V_{0,0} \\ V_{1,0} \\ V_{0,1} \\ V_{2,0} \\ V_{1,1} \\ V_{0,2} \end{pmatrix} = 0.$$

we get $V(x,y) = x^2$and the condition $b = 1$. So statement (3) follows after applying either the change $\left(\frac{zx}{a}, \frac{z^2y}{a^3} + \frac{dz^2}{a^2}\right) \to (x,y)$, if $a \neq 0$ or the change $(zx, z^2y + dz^2) \to (x,y)$, if $a = 0$. Finally, assuming $b \neq -1,0,1$, we consider system $A_3V^3 = 0$,

$$\begin{pmatrix} -1-b & 0 & d & 0 & 0 & 0 & 0 & 0 & 0 & 0 \\ 0 & -b & a & 0 & d & 0 & 0 & 0 & 0 & 0 \\ 0 & 0 & -1 & 0 & 0 & 2d & 0 & 0 & 0 & 0 \\ 0 & 0 & 0 & 1-b & a & 0 & 0 & d & 0 & 0 \\ 0 & 0 & 0 & 0 & 0 & 2a & 0 & 0 & 2d & 0 \\ 0 & 0 & 0 & 0 & 0 & b-1 & 0 & 0 & 0 & 3d \\ 0 & 0 & z & 0 & 0 & 0 & 2-b & a & 0 & 0 \\ 0 & 0 & 0 & 0 & 0 & 0 & 0 & 1 & 2a & 0 \\ 0 & 0 & 0 & 0 & 0 & 0 & 0 & 0 & b & 3a \\ 0 & 0 & 0 & 0 & 0 & 0 & 0 & 0 & 0 & 2b-1 \\ 0 & 0 & 0 & 0 & z & 0 & 0 & 0 & 0 & 0 \\ 0 & 0 & 0 & 0 & 0 & 2z & 0 & 0 & 0 & 0 \\ 0 & 0 & 0 & 0 & 0 & 0 & 0 & z & 0 & 0 \\ 0 & 0 & 0 & 0 & 0 & 0 & 0 & 0 & 2z & 0 \\ 0 & 0 & 0 & 0 & 0 & 0 & 0 & 0 & 0 & 3z \end{pmatrix}_{15\times 10} \begin{pmatrix} V_{0,0} \\ V_{1,0} \\ V_{0,1} \\ V_{2,0} \\ V_{1,1} \\ V_{0,2} \\ V_{3,0} \\ V_{2,1} \\ V_{1,2} \\ V_{0,3} \end{pmatrix}_{10\times 1} = 0,$$

we get the solution shown in statement (4) after the change of variables $\left(zx, \frac{az^2x}{(b-1)} + z^2y + \frac{dz^2}{b}\right) \to (x,y)$. ◘

Theorem 2.4: A system of type (2.11) have a polynomial inverse integrating factor $V(x,y)$ can be written, after an affine change of variables and a rescaling of the time if it is necessary, as $\dot{x} = x$, $\dot{y} = Q_3(x,y)$, where $Q_3(x,y)$ is one of the polynomials below.

(5) $Q_3(x,y) = y + xy^2$, where $\delta \neq -1,0,1$ we get $V(x,y) = \frac{\delta^3(\delta-1)}{(\delta+1)}y^2$.

(6) $Q_3(x,y) = xy^2$, we have $V(x,y) = xy^2$.

Proof: We write $V(x,y) = \sum_{i=0}^{k} V_i(x,y)$, the homogeneous equation of degree $k+2$ of equation (1.2) is

$$-2xyV_k(x,y) + xy^2\frac{\partial V_k(x,y)}{\partial y} = 0.$$

We get $V_k(x,y) = x^{k-2}y^2$.

The homogeneous equation of degree $k+1$ is $-2xy\,V_{k-1}(x,y) + xy^2\frac{\partial V_{k-1}(x,y)}{\partial y} = 0$. From this equation, $V_{k-1}(x,y) = C_{k-1}x^{k-3}y^2$,

$C_{k-1} \in \mathbb{R}$. Then, a polynomial solution $V(x,y)$ must have degree $k = 3$. Now system $A_3V^3 = 0$ is

$$\begin{pmatrix} -1-b & 0 & b_{0,0} & 0 & 0 & 0 & 0 & 0 & 0 & 0 \\ 0 & -b & 0 & 0 & b_{0,0} & 0 & 0 & 0 & 0 & 0 \\ 0 & 0 & -1 & 0 & 0 & 2b_{0,0} & 0 & 0 & 0 & 0 \\ 0 & 0 & 0 & 1-b & 0 & 0 & 0 & b_{0,0} & 0 & 0 \\ -2 & 0 & 0 & 0 & 0 & 0 & 0 & 0 & 2b_{0,0} & 0 \\ 0 & 0 & 0 & 0 & 0 & b-1 & 0 & 0 & 0 & 3b_{0,0} \\ 0 & 0 & 0 & 0 & 0 & 0 & 2-b & 0 & 0 & 0 \\ 0 & -2 & 0 & 0 & 0 & 0 & 0 & 1 & 0 & 0 \\ 0 & 0 & -1 & 0 & 0 & 0 & 0 & 0 & b & 0 \\ 0 & 0 & 0 & 0 & 0 & 0 & 0 & 0 & 0 & 2b-1 \\ 0 & 0 & 0 & -2 & 0 & 0 & 0 & 0 & 0 & 0 \\ 0 & 0 & 0 & 0 & -1 & 0 & 0 & 0 & 0 & 0 \\ 0 & 0 & 0 & 0 & 0 & 0 & -2 & 0 & 0 & 0 \\ 0 & 0 & 0 & 0 & 0 & 0 & 0 & -1 & 0 & 0 \\ 0 & 0 & 0 & 0 & 0 & 0 & 0 & 0 & 0 & 1 \end{pmatrix}_{15\times 10} \begin{pmatrix} V_{0,0} \\ V_{1,0} \\ V_{0,1} \\ V_{2,0} \\ V_{1,1} \\ V_{0,2} \\ V_{3,0} \\ V_{2,1} \\ V_{1,2} \\ V_{0,3} \end{pmatrix}_{10\times 1} = 0.$$

from this system we get the polynomial $V(x,y) = b_{0,0} + \frac{\delta^3(\delta-1)}{\delta+1}y^2 + V_{1,2}xy^2$, $V_{0,0} = b_{0,0}V_{1,2}$ and the condition $(b+1)b_{0,0}V_{1,2} = 0$. If $b_{0,0} = 0, b = 1$ and $V_{1,2} = 0$ then we obtain statement (5). If $b = b_{0,0} = 0$ and $V_{1,2} = 1$ then the system has a common factor, we get statement (6).

Theorem 2.5: A system of type (2.12) have a polynomial inverse integrating factor $V(x,y)$ which can be written, after an affine change of variables and a rescaling of the time if it is necessary, as $\dot{x} = x$, $\dot{y} = Q_3(x,y)$, where $Q_3(x,y)$ is the following polynomial

(7) $Q_3(x,y) = \frac{b_{0,0}}{4} + y^3$, where $b_{0,0} \in \mathbb{R}$, and we have $V(x,y) = x(b_{0,0} + 4y^3)$.

Proof: We write $V(x,y) = \sum_{i=0}^{k} V_i(x,y)$, equation (1.2) can be written as a system of $k+2$ homogeneous equations. If $b_{3,0} \neq 0$ then from homogeneous equation of degree $k+2$, is

$$-12y^2V_k(x,y) + \left(b_{3,0}x^3 + 4y^3\right)\frac{\partial V_k(x,y)}{\partial y} = 0.$$

Solving this equation we obtain $V_k(x,y) = \left(b_{3,0}x^3 + 4y^3\right)f_k(x)$, where $f_k(x)$ is an arbitrary non-zero function of x. As $V_k(x,y)$ is an homogeneous polynomial of degree k we take $f_k(x) = x^{k-3}$, and then $V_k(x,y) = \left(b_{3,0}x^3 + 4y^3\right)x^{k-3}$. The homogeneous equation of degree $k+1$ is $-12y^2V_{k-1}(x,y) + \left(b_{3,0}x^3 + 4y^3\right)\frac{\partial V_{k-1}(x,y)}{\partial y} = 0$.

From which we obtain

$V_{k-1}(x,y) = C_{k-1}x^{k-4}\left(b_{3,0}x^3 + 4y^3\right)$ with $C_{k-1} \in \mathbb{R}$, if $b_{3,0} = 0$ then the homogeneous equation of degree $k+2$ is $-3y^2V_k(x,y) + y^3\frac{\partial V_k(x,y)}{\partial y} = 0$.

Solving this equation we obtain $V_k(x,y) = y^3f_k(x)$, where $f_k(x)$ is an arbitrary non-zero function of x. As $V_k(x,y)$ is an homogeneous polynomial of degree k we take $f_k(x) = x^{k-3}$, and then $V_k(x,y) = y^3x^{k-3}$. The homogeneous equation of degree $k+1$ is

$$-3y^2V_{k-1}(x,y) + y^3\frac{\partial V_{k-1}(x,y)}{\partial y} = 0.$$

From which we get $V_{k-1}(x,y) = C_{k-1}x^{k-4}y^3$, if $b_{3,0} = 0$. In all cases, $C_{k-1} \in \mathbb{R}$. If $k \leq 3$ then system $A_3V^3 = 0$ is

$$\begin{pmatrix} -1 & 0 & 0.25b_{0,0} & 0 & 0 & 0 & 0 & 0 & 0 & 0 \\ 0 & 0 & -0.5b_{1,0} & 0 & 0.25b_{0,0} & 0 & 0 & 0 & 0 & 0 \\ 0 & 0 & -1 & 0 & 0 & 0.5b_{0,0} & 0 & 0 & 0 & 0 \\ 0 & 0 & 0 & 1 & -0.5b_{1,0} & 0 & 0 & 0.25b_{0,0} & 0 & 0 \\ 0 & 0 & 0 & 0 & 0 & -b_{1,0} & 0 & 0 & 0.5b_{0,0} & 0 \\ -3 & 0 & 0 & 0 & 0 & -1 & 0 & 0 & 0 & 0.75b_{0,0} \\ 0 & 0 & 0.25b_{3,0} & 0 & 0 & 0 & 2 & -0.5b_{1,0} & 0 & 0 \\ 0 & 0 & 0 & 0 & 0 & 0 & 0 & 1 & -b_{1,0} & 0 \\ 0 & -3 & 0 & 0 & 0 & 0 & 0 & 0 & 0 & -1.5b_{1,0} \\ 0 & 0 & -2 & 0 & 0 & 0 & 0 & 0 & 0 & -1 \\ 0 & 0 & 0 & 0 & 0.25b_{3,0} & 0 & 0 & 0 & 0 & 0 \\ 0 & 0 & 0 & 0 & 0 & 0.5b_{3,0} & 0 & 0 & 0 & 0 \\ 0 & 0 & 0 & -3 & 0 & 0 & 0 & 0 & 0 & 0 \\ 0 & 0 & 0 & 0 & -2 & 0 & 0 & 0 & 0 & 0 \\ 0 & 0 & 0 & 0 & 0 & -1 & 0 & 0 & 0 & 0 \\ 0 & 0 & 0 & 0 & 0 & 0 & 0 & 0.25b_{3,0} & 0 & 0 \\ 0 & 0 & 0 & 0 & 0 & 0 & 0 & 0 & 0.5b_{3,0} & 0 \\ 0 & 0 & 0 & 0 & 0 & 0 & -3 & 0 & 0 & 0.75b_{3,0} \\ 0 & 0 & 0 & 0 & 0 & 0 & 0 & -2 & 0 & 0 \\ 0 & 0 & 0 & 0 & 0 & 0 & 0 & 0 & -1 & 0 \end{pmatrix}_{20\times 10} \begin{pmatrix} V_{0,0} \\ V_{1,0} \\ V_{0,1} \\ V_{2,0} \\ V_{1,1} \\ V_{0,2} \\ V_{3,0} \\ V_{2,1} \\ V_{1,2} \\ V_{0,3} \end{pmatrix}_{10\times 1} = 0,$$

if $k > 3$, then we must take $b_{3,0} = 0$. From the homogeneous equation of degree k, we obtain the expression of $V_{k-2}(x, y)$,

$$x^{k-3}(k-3)y^3 - \frac{3}{2}b_{1,0}x^{k-2}y^2 - x^{k-3}y^3 - 3y^2V_{k-2}(x,y) + y^3\frac{\partial V_{k-2}(x,y)}{\partial y} = 0.$$

we get

$$V_{k-2}(x,y) = C_{k-2}x^{k-5}y^3 + \frac{1}{2}x^{k-3}\big(-b_{1,0}x + (k-4)y\big),$$

with $C_{k-2} \in \mathbb{R}$. In order to obtain a polynomial, we must take $b_{1,0} = 0$. Then $\dot{y} = \frac{b_{0,0}}{4} + y^3$. In this case the polynomial inverse integrating factor of degree 4 stated in (7) is a solution of (1.2).

□

Similarly by the above cases we obtain the following results:

Theorem 2.6: A system $\dot{x} = y$, $\dot{y} = Q_3(x, y)$, have a polynomial inverse integrating factor $V(x, y)$, where Q_3 is one of the polynomials below.

(1) $Q_3(x,y) = \frac{1}{n(mn-r)}\big(dn^4(m+rx)x^2 + (dx+y^2)(m+rx)n^3 + y(mrx^2 + m^2x - ry)n^2 - nrxy(m+rx)\big)$, an inverse integrating factor

$$V(x,y) = d + 2ndx + \frac{(mn-r)}{n^2}y + dn^2x^2 + \frac{(mn-r)}{n}xy + ny^2.$$

(2) $Q_3(x,y) = rx^2y - n^2xy^2 + ny^2$, an inverse integrating factor

$$V(x,y) = -\frac{r}{n^2}y - \frac{r}{n}xy + ny^2.$$

(3) $Q_3(x,y) = -dn^3x^3 - dn^2x^2 - n^2xy^2 + ny^2$, an inverse integrating factor

$$V(x,y) = d(nx+1)^2 + ny^2.$$

(4) $Q_3(x,y) = bnxy + wb^2x^2y + 2wbxy^2 + ny^2 + wy^3$, an inverse integrating factor

$$V(x,y) = \frac{y\big(w^2y^2 + (2bwxy + b + ny)w + wbx(wbx+n)\big)}{w}.$$

(5) $Q_3(x,y) = d + ax + lx^2 + ny^2 + \big(-\frac{4}{3}n^3d - \frac{2}{3}n^2a - \frac{2}{3}nl\big)x^3$,

an inverse integrating factor

$$V(x,y) = -2ndx - \frac{1}{3}n(3a+6nd)x^2 + ny^2 - \frac{1}{3}n(2na + 4n^2d + 2l)x^3.$$

(6) $Q_3(x,y)=\frac{4n}{(n-1)^2}x-2by-cx^2+\left(\frac{bc}{3n}+\frac{bcn}{3}-\frac{2bc}{3}\right)xy+\frac{c^2(n-1)^2}{18n}x^3$, an inverse integrating factor

$V(x,y)=lx^2-\frac{bl(n-1)^2}{2n}xy-\frac{l(n-1)^2}{4n}y^2-\frac{cl(n-1)^2}{6n}x^3+\frac{cbl(n-1)^4}{24n^2}x^2y+\frac{c^2l(n-1)^4}{144n^2}x^4$. ◘

Theorem 2.7: Having a polynomial inverse integrating factor $V(x,y)$. If $\dot{x}=y+x^2$, $\dot{y}=Q_3(x,y)$, where Q_3 is one of the polynomials below.

(1) $Q_3(x,y)=d+mxy+\frac{1}{3}(m-1)x^3-\frac{1}{9}\frac{(m^2+m-2)}{m}y^3$, an inverse integrating factor

$$V(x,y)=\frac{1}{3}\frac{d\left(3d^2+d(m+2)(3y+x^2)x-\frac{1}{3}(m+2)^2y^3\right)}{d^2}.$$

(2) $Q_3(x,y)=\left(\frac{1}{4}\frac{m^2}{s}-\frac{1}{s}\right)x+mxy+sxy^2$,an inverse integrating factor $V(x,y)=\frac{n\left(\frac{1}{2}m+sy-1\right)^2}{s^2}$.

(3) $Q_3(x,y)=d\left(\frac{m+2}{b}\right)x+mxy+mx^3$, an inverse integrating $V(x,y)=d+b(y+x^2)$.

(4) $Q_3(x,y)=-\frac{s}{2w}x^2-2xy-x^3+\frac{s^2}{4w}x^2y+sxy^2+wy^3$, an inverse integrating factor

$$V(x,y)=-\frac{\left(-w^2y^3+x(x^2+3y-sy^2)w-\frac{1}{4}(2+sx^2)(-2+sy)\right)}{w}.$$

(5) $Q_3(x,y)=d+ax+lx^2-2xy+ny^2+2nx^2y+\frac{1}{3}(-4n^3d-2n^2a-2nl)x^3$, an inverse integrating factor

$$V(x,y)=-2ndx+n(-2nd-a)x^2+ny^2+\frac{1}{3}n(-4n^2d-2na-2l)x^3+2nx^2y$$ ◘

Theorem 2.8: Having a polynomial inverse integrating factor $V(x,y)$ if $\dot{x}=x^3$, $\dot{y}=Q_3(x,y)$, where Q_3 is one of the polynomials below.

(1) $Q_3(x,y)=lx^2+mxy+\frac{1}{4}\frac{m^2}{l}y^2+\frac{2l}{m^2}(m+2ls)\,x^3+\frac{2}{m}(m+2ls)\,x^2y+sxy^2$, an inverse integrating factor $V(x,y)=\frac{4sx\left(lx+\frac{1}{2}my\right)^2}{m^2}$.

(2) $Q_3(x,y)=\frac{1}{3}\frac{b^2}{n}+\frac{b^2s}{b_{0,2}^2}x+by+\left(\frac{b^2s^2}{n^3}+\frac{3}{2}\frac{b}{n}\right)x^2+\frac{2bs}{n}xy+ny^2+\left(\frac{1}{3}\frac{b^2s^3}{n^4}+\frac{bs}{2n^2}\right)x^3+\left(\frac{bs^2}{n^2}+\frac{3}{2}\right)x^2y+sxy^2+\frac{1}{3}\frac{n^2}{b}y^3$, an inverse integrating factor $V(x,y)=\frac{\left((sx+n)b+n^2y\right)^3}{3n^4b}$.

(3) $Q_3(x,y)=\frac{1}{54}\frac{s(9w+2s^2)}{w^2}x^3+\frac{1}{6}\frac{(9w+2s^2)}{w}x^2y+sxy^2+wy^3$,

an inverse integrating factor $V(x,y)=\frac{(sx+3wy)^3}{27w^2}$.

(4) $Q_3(x,y)=d+ax+lx^2-2x^2y+zx^3$, an inverse integrating factor $V(x,y)=ax$.

(5) $Q_3(x,y)=d+ax+lx^2-x^2y+zx^3$,an inverse integrating factor $V(x,y)=lx^2$.

(6) $Q_3(x,y)=d+ax+lx^2+zx^3$, an inverse integrating factor $V(x,y)=zx^3$. ◘

Theorem 2.9: Having a polynomial inverse integrating factor $V(x,y)$ if $\dot{x}=y+x^3$, $\dot{y}=Q_3(x,y)$, where Q_3 is one of the polynomials below.

(1) $Q_3(x,y)=\frac{1}{9}\frac{bn}{w}+\left(-\frac{2}{27}\frac{n^2b}{w}+\frac{4}{81}\frac{n^4}{w^2}-\frac{2}{9}b^2\right)x+by+\left(\frac{4}{81}\frac{n^5}{w^2}+\frac{4}{9}nb^2-\frac{8}{27}\frac{n^3b}{w}+\frac{1}{2}\frac{n}{w}\right)x^2+\left(\frac{4}{9}\frac{n^3}{w}-\frac{4}{3}bn\right)xy+ny^2+\left(\frac{8}{729}\frac{n^6}{w^2}-\frac{8}{81}\frac{n^4b}{w}+\frac{1}{9}\frac{n^2}{w}+\frac{8}{27}n^2b^2-\frac{8}{27}wb^3-\frac{1}{3}b\right)x^3+\left(\frac{4}{27}\frac{n^4}{w}-\frac{8}{9}n^2b+\frac{4}{3}wb^2+\frac{3}{2}\right)x^2y+\left(\frac{2}{3}n^2-2bw\right)xy^2+wy^3$, an inverse integrating factor and a first integral

$$V(x,y)=-\frac{8}{27}\frac{\left(\left(bx-\frac{3}{2}y\right)w^2-\frac{1}{2}nw-\frac{1}{3}wn^2x\right)^3}{w^5}.$$

(2) $Q_3(x,y)=\frac{1}{4}\frac{b^2}{n}+by+\frac{3}{2}\frac{b}{n}x^2+ny^2+3x^2y$, an inverse integrating factor

$$V(x,y)=\frac{(b+2ny)^2}{4n}.$$

(3) $Q_3(x,y)=-\frac{1}{4}b^2x+by+\frac{1}{4}nb^2x^2-nbxy+ny^2+\left(\frac{1}{4}sb^2-b\right)x^3+(3-bs)x^2y+sxy^2$, an inverse integrating factor $V(x,y)=\frac{1}{4}n(bx-2y)^2$.

(4) $Q_3(x,y)=\frac{1}{3}bl+by+lx^2+bx^3$, an inverse integrating factor $V(x,y)=\frac{1}{3}b(l+3y+3x^3)$. ◘

Theorem 2.10: Cubic systems in Theorems 2.2, 2.3 and 2.5 cannot have limit cycles.

Proof: The result follows directly by Theorem 1.3, because the expression of inverse integrating factors does not have closed level.

3. Non-existence polynomial inverse integrating factor of cubic polynomial systems:

Theorem 3.1: The cubic system

$$\begin{aligned}\dot{x}&=x-x^3+2x^2y-2xy^2+y^3\\ \dot{y}&=y-x^3-y^3,\end{aligned}\tag{3.1}$$

has only a non-zero polynomial inverse integrating factor.

Proof: Suppose that system (3.1) has a polynomial inverse integrating factor $V(x,y)$. We apply Theorem 1.2, then

$$\bar{V}_4(x,y)=-(x^2+y^2)(x^2-xy+y^2)\tag{3.2}$$

The factors that appear in (3.2) are $(x-iy),(x+iy),\left(x-\left(\frac{1}{2}+\frac{\sqrt{3}}{2}i\right)y\right)$ and $\left(x-\left(\frac{1}{2}-\frac{\sqrt{3}}{2}i\right)y\right)$ that is $\alpha_1=\alpha_2=\alpha_3=\alpha_4=1,\ \beta_1=-i,\ \beta_2=i,\ \beta_3=-\left(\frac{1}{2}+\frac{\sqrt{3}}{2}i\right)$ and $\beta_4=-\left(\frac{1}{2}-\frac{\sqrt{3}}{2}i\right)$. The cofactors M_i are obtained by $P_3\frac{\partial(x-iy)}{\partial x}+Q_3\frac{\partial(x-iy)}{\partial y}=M_1(x-iy)$, for $i=1,2,3,4$. Then $(-x^3+2x^2y-2xy^2+y^3)-(-x^3-y^3)i=M_1(x-iy)$, hence $M_1=-(x^2-xy+y^2)$ and similarly $M_2=-(x^2-xy+y^2), M_3=-\frac{1}{4}(-1+\sqrt{3}\,i)(2x-y+\sqrt{3}\,iy)(-x+\sqrt{3}\,iy)$ and $M_4=\frac{1}{4}(1+\sqrt{3}\,i)(-2x+y+\sqrt{3}\,iy)(x+\sqrt{3}\,iy)$. Obviously, the decomposition of the quadratic factor would give two complex linear factors with two complex conjugate cofactors and $M_1=M_2, M_4$ is complex conjugate cofactor of M_3. In consequence, in order to satisfy equation (1.3) we must take $l_1=l_2$ and $l_3=l_4$. Then equation (1.3) becomes

$\sum_{i=1}^{4}l_iM_i(x,y)=\left(\frac{\partial P_3}{\partial x}+\frac{\partial Q_3}{\partial y}\right)$,

$l_1M_1(x,y)+l_2M_2(x,y)+l_3M_3(x,y)+l_4M_4(x,y)=-3x^2+4xy-5y^2$

From M_1, M_2, M_3andM_4, $l_1=l_2$ and $l_3=l_4$ we get have

$$(-l_3-2l_1+3)x^2+(2l_3+2l_1-4)xy+(-3l_3-2l_1+5)y^2=0.$$

This implies the following system of three linear equations on the natural numbers l_1 and l_3

$-l_3-2l_1+3=0,\ 2l_3+2l_1-4=0, -3l_3-2l_1+5=0.$

The only solution of these equations is $l_1=l_2=l_3=l_4=1$.Thus, equation (1.2) may have only a polynomial solution of degree 4, $V_4(x,y)$ which is proportion to $\bar{V}_4(x,y)$. A direct calculation shows that this polynomial solution does not exist.

Theorem 3.2.: The cubic system

$$\begin{aligned}\dot{x}&=y+x^2\\ \dot{y}&=-y^3,\end{aligned}\tag{3.3}$$

has only a non-zero polynomial inverse integrating factor.

Proof: The proof is similar to proof of Theorem 3.1.

The oscillation of a violin string (Rayleigh) equation is given by $x''+\varepsilon\left(\frac{1}{3}(x')^2-1\right)x'+x=0$, is equivalent to the system

$$\begin{aligned}\dot{x}&=y,\\ \dot{y}&=-x-\varepsilon(\frac{1}{3}y^2-1)y,\end{aligned}\tag{3.4}$$

Theorem 3.3: The system (3.4) has only a non-zero polynomial inverse integrating factor.

Proof: The application of the method described in Theorem 1.2, then $\bar{V}_4(x,y) = \frac{-\varepsilon}{3}xy^3$.The factors that appear in $\bar{V}_4(x,y)$ are, x and y that is $\alpha_1 = 1, \alpha_2 = \alpha_3 = \alpha_4 = 0, \beta_1 = 0, \beta_2 = \beta_3 = \beta_4 = 1$. The cofactors M_i are obtained from $P_3\frac{\partial(\alpha_i x+\beta_i y)}{\partial x} + Q_3\frac{\partial(\alpha_i x+\beta_i y)}{\partial y} = M_i(\alpha_i x + \beta_i y)$, for $i = 1,2,3,4$, then $M_1 = 0$ and similarly $M_2 = M_3 = M_4 = \frac{-\varepsilon}{3}y^2$.

Inconsequence, in order to satisfy equation (1.3) we must take l_1 any real numbers and $l_2 = l_3 = l_4$. Then, for this case equation (1.3) becomes

$l_1M_1(x,y) + l_2M_2(x,y) + l_3M_3(x,y) + l_4M_4(x,y) = -\varepsilon y^2$.

From $M_1 = 0, M_2 = M_3 = M_4, l_2 = l_3 = l_4$, we get have $(-\varepsilon l_2 + \varepsilon)y^2 = 0$

This implies the following system of one linear equation on the natural numbers l_2, $-\varepsilon l_2 + \varepsilon = 0$. The only solution of these equations is $l_1 = l_2 = l_3 = l_4 = 1$.

Since $\bar{V}_2(x,y) = x(-x + \varepsilon y) - y^2 = -x^2 + \varepsilon xy - y^2$, then linear factors which appear in $\bar{V}_2(x,y)$ are, $\left(x - \left(\frac{\varepsilon}{2} + \frac{\sqrt{\varepsilon^2-4}}{2}\right)y\right)$ and $\left(x - \left(\frac{\varepsilon}{2} - \frac{\sqrt{\varepsilon^2-4}}{2}\right)y\right)$ that is $\delta_1 = \delta_2 = 1$ and $\gamma_1 = -\left(\frac{\varepsilon}{2} + \frac{\sqrt{\varepsilon^2-4}}{2}\right)$, $\gamma_2 = -\left(\frac{\varepsilon}{2} - \frac{\sqrt{\varepsilon^2-4}}{2}\right)$. The cofactors m_1 and m_2 are obtained from equations

$$y\frac{\partial\left(x - \left(\frac{\varepsilon}{2} + \frac{\sqrt{\varepsilon^2-4}}{2}\right)y\right)}{\partial x} + (-x + \varepsilon y)\frac{\partial\left(x - \left(\frac{\varepsilon}{2} + \frac{\sqrt{\varepsilon^2-4}}{2}\right)y\right)}{\partial y} = m_1\left(x - \left(\frac{\varepsilon}{2} + \frac{\sqrt{\varepsilon^2-4}}{2}\right)y\right),$$

$y + (-x + \varepsilon y)\left(-\left(\frac{\varepsilon}{2} + \frac{\sqrt{\varepsilon^2-4}}{2}\right)\right) = m_1\left(x - \left(\frac{\varepsilon}{2} + \frac{\sqrt{\varepsilon^2-4}}{2}\right)y\right)$, then

$m_1 = -\frac{(\varepsilon+\sqrt{\varepsilon^2-4})x+(2-\varepsilon^2-\varepsilon\sqrt{\varepsilon^2-4})y}{-2x+(\varepsilon+\sqrt{\varepsilon^2-4})y}$. Similarly, $m_2 = -\frac{(-\varepsilon+\sqrt{\varepsilon^2-4})x+(-2+\varepsilon^2-\varepsilon\sqrt{\varepsilon^2-4})y}{2x+(-\varepsilon+\sqrt{\varepsilon^2-4})y}$.

In order to satisfy equation (1.4). Then, for this case equation (1.32) becomes

$$e_1\left(-\frac{(\varepsilon+\sqrt{\varepsilon^2-4})x+(2-\varepsilon^2-\varepsilon\sqrt{\varepsilon^2-4})y}{-2x+(\varepsilon+\sqrt{\varepsilon^2-4})y}\right) + e_2\left(-\frac{(-\varepsilon+\sqrt{\varepsilon^2-4})x+(-2+\varepsilon^2-\varepsilon\sqrt{\varepsilon^2-4})y}{2x+(-\varepsilon+\sqrt{\varepsilon^2-4})y}\right) = \varepsilon. \quad (3.5)$$

$$e_1 = -\frac{1}{4}\left(-2 + \varepsilon^2 - \varepsilon\sqrt{\varepsilon^2-4}\right)\left(2e_2 - \varepsilon^2 - \varepsilon\sqrt{\varepsilon^2-4}\right)$$

Therefore, the exponents e_1 and e_2 must satisfy the equation $e_1 = e_2 = 1$. Taking into account that $e_i \in \mathbb{N}$ we have an infinite number of polynomial solutions of equation (3.5). Thus, equation (1.2) may have only a polynomial solution of degree 2 and 4, $V_2(x,y)$and $V_4(x,y)$ which is proportion to $\bar{V}_2(x,y)$ and $\bar{V}_4(x,y)$.

A direct calculation shows that these polynomial solutions do not exist. Then, this system has non-zero polynomial inverse integrating factor. ◘

Vander pol obtained the following differential equation $x'' + \varepsilon(x^2-1)x' + x = 0$, which is equivalent to the system

$$\begin{aligned} \dot{x} &= y, \\ \dot{y} &= -x - \varepsilon(x^2-1)y, \end{aligned} \quad (3.5)$$

The proof of the following theorem is similar to Theorem 3.3.

Theorem 3.4: The system (3.5) has only a non-zero polynomial inverse integrating factor.

REFERENCES

– Arrow Smith, D.K. and Place , C.M. (1982). *Ordinary differential equations.* Mathematics series.

– Calanchi, M. and Ruf , B. (2002). On the number of closed solutions polynomial ODE and a special case of Hilberts. *Adv.Diff.Eq*, 1978-2016.

– Chavarriga, J. (2004.). On the algebraic limit cycles of quadratic systems,. *University Autonoma de Barcelona, .*

– Chavarriga, J., Giacomini, H. and Gine , J. (1997). The null divergence factor. *Publicacions Matematiques*, 41-56.

– Chavarriga, J., Giacomini, H. and Gine , J. (1999). On a new of bifurcation of limit cycles for a planar cubic system. *Nonlinear Analysis*, 139-149.

– Chavarriga, J., Giacomini, H. and Gine , J. (2000). Polynomial inverse integrating factors. *Ann.of Diff.Eqs*, 320-329.

– Chavarriga, J., Llibre , J. and Sorolla , J. (2001). Algebraic limit cycles for quadratic systems. *preprint Universitat de Lleida*.

– Ferragut, A. (2006). Polynomial inverse integrating factors of quadratic differential systems and other results. *Ph.D. thesis, University Autonoma de Barcelona*.

پوختە

ئامانجی سەرەکی لەم توێژینەدا لێکۆلینەوەیە دەربارەی تایبەتمەندیەکانی جۆری، وەك بوونی یان نەبوونی زۆر رادەدارانی هەلگەراوەی هاوکۆلکەی تەواوکاری بۆ هەندێك زۆر رادەدارانی سێ یی لە سیستەمە خوبەخۆیەکانی دوو دووری . لەگەڵ ئەوەدا، ئەنجامەکانمان پراکتیك کردووە بۆ لێکولینەوە دەربارەی ئامانجە خولەیەکان.

الخلاصة

الهدف الرئيسى لهذا البحث هو دراسة الخواص النوعية، مثل وجودية اوعدم وجودية معكوس عامل التكامل المتعدد لبعض متعددات الحدود الثلاثيةفي الانظمة الذاتية ثنائية الابعاد. بالاضافة الى ذلك، تم تطبق هذه النتائج لدراسة الدارات الغائية.

EFFECT OF NOZZLE DİAMETER ON STEAM EJECTOR PERFORMANCE

RİZGAR **B**.**W**ELİ, **M**OHAMMED **J**. **I**BRAHİM and **M**AHDE **A**. **M**OLAN
Dept. of Mechanic, College of Engineering, University of Salahaddin, Kurdistan Region-Iraq

(Received: April 22, 2015; Accepted for publication: June 9, 2015)

ABSTRACT

Single stage steam ejectors with different nozzle diameters between 1 to 4mm have been used to pump secondary fluid (liquid water). The procedure is held at different steam pressures from 1 to 4 bars to optimize the best diameter to be used for the nozzle inside the steam ejector chamber. The nozzle of 3mm diameter gives more reasonable results for delivery water temperature, and ejector performance. The pressure and nozzle diameter dependence on water temperature is represented by empirical function over the ranges, delivery water temperature Tw from (28) to (35) ºC, pressure P from (1) to (4.5), and nozzle diameter from (1) to (4) mm. In overlapping ranges, the results agree well with those previously published.

KEYWORDS: Delivery water temperature, Ejector efficiency, Nozzle diameter, Steam ejector.

INTRODUCTION

Steam ejectors are based on the ejector-venture principal and operate by passing motive steam (primary fluid) through an expanding nozzle. The nozzle provides controlled expansion of the motive steam to convert pressure into velocity which creates a vacuum within the body chamber to draw in and entrain another fluid (secondary fluid)[1].

Steam ejectors are designed to convert pressure energy of a motive fluid to a velocity energy to entrain suction fluid, and then to recompress the mixed fluids by converting velocity energy back into pressure energy[2].

It works on the principle of convergent /divergent nozzle as it provides the venture effect at the point of diffusion, as the tube gets narrowing at the throat the velocity of the fluid increases and because of the venture effect it's pressure decreases, vacuum will occur in the diffuser throat where the suction line will be provided.

Primary advantages of ejectors are exceedingly simple and reliable. There are no moving parts, low Cost, versatile, easy to install, relatively light in weight, corrosion and erosion resistant and high vacuum.

Steam Ejectors are used in a variety of applications in the process, food, steel and petrochemical industries. Typical duties involve filtration, distillation, absorption, mixing, vacuum packaging, freeze drying, dehydrating and degassing. It works us a steam pump, heat exchanger, vacuum pump, thermo compressor, feed water heater… etc.

A. S. Hassan presented a new approach of mathematical correlations performance of thermal vapor compressor (TVC). The performance of TVC is studied. The results of the mathematical model of TVC mixing ratios and performance diagram were very close approach to the power lines [3].

N. Sharifi and M. Sharifi studied a malfunctioning experimental ejector numerically to reveal the source of low evacuation rate from a suction chamber. The steam ejector was designed to operate under a motive pressure of 6 bars. The optimization procedure was performed through using numerical CFD (Computational Fluid Dynamics) simulations. The shape of internal supersonic nozzle was changed in many CFD analyses and the most optimized nozzle was selected for manufacturing. After installing the designed nozzle, an improved entrainment capability under the nominal pressure of 6 bars was observed and the desired vacuum level was attained [4].

J. Yan and others describes the development of a combined ejector-vapor compression cycle (EVCC) that uses working fluid R134a and air-cooled condensers for both sub-cycles. A large amount of experiments have been conducted to test the influence of the evaporating, generating and condensing temperatures of the ejector sub-cycle (ESC) on the performances of EVCC. The

test results show that the performance of the combined cycle is very sensitive to the three temperatures of ESC, and the variation of the degree of sub-cooling at the vapor compression sub-cycle (VCSC) is similar to that of COP improvement at EVCC over VCSC [5].

H. Vidal and S. Colle described the hourly simulation and optimization of a thermally driven cooling cycle assisted by solar energy. The double stage solar ejector cooling cycle is modeled using the TRNSYS-EES simulation tool and the typical meteorological year file containing the weather data of Florianópolis, Brazil. The first stage is performed by a mechanical compression system with R134a as the working fluid; while the second stage is performed by a thermally driven ejector cycle with R141b. Upper bounds for economical feasibility in terms of the costs of the auxiliary energy and electric energy are also presented [6].

P. Chaiwongsa and S. Wongwises investigated experimentally the performance of the refrigeration cycle using a two-phase ejector as an expansion device. Refrigerant R-134a is used as working fluid. Motive nozzles having three different outlet diameters are tested. New experimental data that have never been seen before are presented on the effects of the external parameters i.e. heat sink and heat source temperatures on the coefficient of performance and various relevant parameters i.e. primary mass flow rate of the refrigerant, secondary mass flow rate of the refrigerant, recirculation ratio, average evaporator pressure, compressor ratio, discharge temperature and cooling capacity. The effects of size of the motive nozzle outlet on the system performance are also discussed [7].

THEORY

Ejectors are composed of three basic parts: a nozzle, a mixing chamber and a diffuser. Figure 1 shows the ejector components, its pressure and velocity diagram; the primary fluid (steam) enters the nozzle at point (1) with high pressure, its pressure decreases and reaches its minimum value (less than atmospheric pressure) as it expands when exits from the nozzle (point 3). This low pressure produces vacuum and sucks the secondary fluid (liquid water) at point 2 and it mixes with the steam totally at point 4. The mixture passes through the throat region which is a transient path before enter the diffuser. When the mixture enters the diffuser its pressure begun to increase and its temperature is increases consequently, it reaches the maximum as exits from the diffuser (point 7). The ejector works as a pump when pumps the liquid water and as a heat exchanger when the liquid water's temperature increases as it mixes with the steam. The figure shows also velocity diagram of the steam, liquid water and the mixture. suction[8].

In this paper the amount of water delivered (pumped) and its temperature was measured, furthermore heat exchanging efficiency was calculated with the aid of the below equations[9]:

$$\eta_{HE} = \frac{\dot{m}_w C_{pw} (T_{w2} - T_{w1})}{\dot{m}_s [x.h_{fg} + C_{pw} (T - T_{w2})]} \quad (1)$$

[10]

$$\eta_p = \frac{\dot{m}_w \, g \, H}{\dot{m}_s [x.h_{fg} + C_{pw} (T - T_{w2})]} \quad (2) \quad [11]$$

Where

$$\dot{m}_s = \frac{A_t P_{abs}}{\sqrt{T_s}} \sqrt{\frac{k}{P} \left(\frac{2}{k+1}\right)^{\frac{k+1}{k-1}}}$$

(3) Steam Index k and Specific steam Constant R changes with respect to the steam pressures. And H is the head of the steam ejector acts as a pump, can be calculated by the equation:

$H = P_{abs} \times 10.2 + 0.75$ [11]

$P_{abs} = P_{gauge} + P_{atm}$ [11]

$A_t = (\pi/4)\, d^2$ [11]

EXPERIMENTAL WORK

Present work presents the effect of the steam ejectors nozzle diameter on efficiency of the ejector acts as a pump when it pumps the secondary fluid (liquid water) due to the steam ejectors vacuum and it acts as a heat exchanger when it raise the secondary fluid (liquid water) when it mixes with the steam in the ejectors mixing chamber and absorb heat from it, furthermore the delivery water temperature (steam and the liquid water) and amount of liquid water flow rate. For each nozzle diameter the procedure repeated for a range of pressures (1 to 4 bar gauge).

Single stage Vacuum Ejectors generally covers vacuum ranges from 30mm Hg up to atmospheric pressure. In the current study for comparison performance of the ejector, four different nozzle diameters have been fitted. Various nozzle diameter ejector holding in their case fitted on the CUSSONS testing equipment which consists from a steam boiler, water tanks, and measurement

instrumants (tested and recalibrated prior taking any data by dead weight tester and Fluke Multifunction Calibrators). The ejector was work as a pump when pumped the secondary fluid to the delivery pressure and works as a heat exchanger raising the secondary fluid's temperature as it mixes with the primary fluid (steam) in the mixing chamber. The data which taken each 90 seconds from the device are: Pg, T, T_{W1}, T_{W2}, and V_W are tabulated; atmospheric pressure estimated 1bar, T_s and P_s is saturated temperature and pressure.

To extend the received data from the experiments and create or form more fine figures out of the primary value limits (diameter and pressure limits), a polynomial relation can be created using interpolation or regression method. Multivariable Lagrange techniques used for this purpose. Pressure and diameter were two inputs used to evaluate delivery water temperature, pumping efficiency …etc figures.

RESULTS

After applying the taken data to equations 1to 6 the ejector efficiency was calculated. The efficiency of the ejector when it is act as the pump is estimated. The ejector efficiency when it is work as a heat exchanger is calculated too. Temperature of the delivered water (steam and the liquid water) is taken into account as one of ejectors primary figure; the figures (3-6) show the obtained result As mentioned by creating a polynomial it can be guessed more data; a second degree multivariable polynomial been formulated by a Lagrange method. For the second degree polynomial three data points or input variables needed for each variable (steam pressure and nozzle diameter); the 2, 3, and 4mm diameters chosen to expand the data for larger nozzle diameters and the pressures 2, 2.5, and 3 bars are chosen because all results have reasonable data in this range as in the results. If the Delivery Water Temperature polynomial be stated using the data that shown in table (5), the following second order multivariable will be obtained:

$$f_2(x,y) = 0.8\,x^2y^2 + 10.4\,x^2 + 8.35\,y^2 - 5.8\,x^2y - 4.7xy^2 + 34.2\,xy - 63x - 61.05\,y + 144.3$$

or:

$$T_2(P,D) = 0.8\times P^2\times D^2 + 10.4\times P^2 + 8.35\times D^2 - 5.8\,P^2\times D - 4.7\times P\times D^2 + 34.2\times P\times D - 63\times P - 61.05\times D + 144.3$$

The above polynomial equation can be used to estimate delivery water temperature for diameters higher than 4 mm in the mentioned pressure limit or another pressure. Same procedure can be repeated for stating polynomials for exchanging efficiency, pumping efficiency, and delivery water flow rate.

DISCUSSION

The first curve, figure (3) shows variation of the delivered water temperature with the steam pressure. Values in the beginning are greatest, the steam didn't produce a certain vacuum and amount of pumped water is low. When the test repeated in higher pressure values the delivered water temperature decreases due to increasing the vacuum and subsequently amount of delivered water. The test was done on four different nozzle diameters and figure (3) shows that in the all tests the trend of variation of the delivered water temperature was the same but in the low nozzle diameters (1 &2 mm) the curve slope angle was higher or the average slope of the curves were higher than that in the (3 & 4 mm) nozzle diameters and the delivered water temperature of the former nozzles drops rapidly as pressure is increased.

It is pointed out that the ejector operates as a pump to move the secondary fluid (water). Figure no. 4 shows variation of the pump efficiency with the steam pressure. The 4mm nozzle diameter ejector has the maximum efficiency with respect to other nozzles in low pressure values, but its slope is steep and its value will not increase in a significant amount in higher pressures, furthermore its value will decrease from pressure of 3 bars and over. Other ejectors with nozzle diameters (1, 2, and 3) has lower pumping efficiency with respect to the (4 mm) diameter in the low steam pressure but they increase as pressure increases in different ranges. The (3mm) nozzle diameter has best values in all pressures and its value increases more rapidly (with respect to other diameters) as pressure increases.

Figure no. 5 shows the variation of delivered (transported) water flow rate with the steam pressure. Amount of the delivered water from the suction tank in the small nozzle ejectors (1&2 mm) are nearly the same and rather low although their values is raised due to pressure increasing. Like the pumping efficiency the amount of the deilivered water in the (4 mm) nozzle has the

greatest value but its amount decreases from 3 bars and higher. Although the (3mm) diameter nozzle has amount of the supplied water is less than (4mm) diameter nozzle but is higher than (1&2 mm) values and its value increased regularly as pressure values raised.

Figures of no. 6 are variation of steam ejector efficiency while acts as a heat exchanger with the steam pressure. In the (4mm) diameter nozzle, the ejector has highest efficiency in low pressure values with respect to other nozzle diameter, but it decreases rapidly. The reason is belongs to a large quantity of supplied water that pumped in the higher pressure values and the water can't exchanging heat with the steam sufficiently due to the small size of the ejector and short duration of contacting the two fluids (steam and the supplied water).

The (3mm) diameter nozzle ejector has a significant amount of exchanging efficiency in a wide range, but its value decrease after passing half path duration. A sinusoidal variation of the efficiency with the pressure difference observed in a (2mm) nozzle diameter ejector that it is recommended to use this size if high heat exchanging is required.A (1mm) diameter nozzle has low efficiency in the beginning but it increase decrease subsequently.

CONCLUSION

Four different nozzle small diameter ejectors used to appoint the size that has best value of heat exchanging and fluid pumping efficiency and delivered water temperature. Although small size nozzle ejectors have higher delivery water temperatures but their value decreases rapidly as steam pressure raised unlike large nozzle sizes has lower average slope and their value decrease more smoothly (especially nozzle diameter of 3mm) and they are recommended to be used for wide pressure ranges. The nozzle diameter of 3mm has a significant heating exchange too although its value it decreases finally to about 22% and it’s a significant value with respect to other types.

Ejectors has a low pumping efficiency and when the four nozzles pumping efficiency estimated the 3mm diameter one has a more reasonable figures compared with others and amount of supplied water (secondary fluid) transmitted was more excellent.

REFERENCES

– K. Pranav, H. K. Ranjan, and M.P. Singh, A Study and Analyze of an Ejector in Steam Power Plant, International Journal of Engineering and Management Research, Volume-4, Issue-3, June-2014, Page Number: 195-199

– S. F. Dahkil, T. A. Gabbar and D. K. Jaber , Numerical Study of the Initial Pressure and Diameters Ratio Effect on the Jet Ejector Performance, Basrah Journal for Engineering Science,vol.14, No.1, 2014, page122-135.

– A. S. Hassan, M. A. Darwish, Performance of thermal vapor compression, Desalination, Volume 335, Feb. 2013, Pages 41–46.

– N. Sharifi, M. Sharifi, Reducing energy consumption of a steam ejector through experimental optimization of the nozzle geometry, Energy, Volume 66, Mar. 2014, Pages 860–867.

– Jia Yana, Wenjian Cai, Lei Zhao, Yanzhong Li, Chen Lin, Performance evaluation of a combined ejector-vapor compression cycle, Renewable Energy, Volume 55, July 2013, Pages 331–337.

– S. Colle, H. Vidal, G. Pereira, Simulation and economic optimization of a solar assisted combined ejector–vapor compression cycle for cooling applications, Applied Thermal Engineering, Volume 30, Apr. 2010, Pages 478–486.

– P. Chaiwongsa, S. Wongwises, Effect of throat diameters of the ejector on the performance of the refrigeration cycle using a two-phase ejector as an expansion device, International Journal of Refrigeration, Volume 30, Jun. 2007, Pages 601–608.

– Optimization of A High-Efficiency Jet Ejector by Computational Fluid Dynamics Software, Somsak Watanawanavet, Texas A&M University,May 2005, page 11.

– P. Srisastra, S. Aphornratana, A circulating system for a steam jet refrigeration system, Applied Thermal Engineering, Volume 25, Oct. 2005, Pages 2247-2257.

– Catalogue manual, Cussons Co., 2000.

– Dr J. F. Douglas and others, "Fluid Mechanics", 5th ed, Pearson/ Prentice Hall, 2005.

Table (1): Data recording for 1mm diameter nozzle

P_g	P_{abs}	T	Ts	T_{w1}	T_{w2}	V	t
1.0	2.0	117	120.2	26.7	42.0	160	90
1.5	2.5	123	127.4	27.4	40.2	450	90
2.0	3.0	137	133.6	27.1	39.2	500	90
2.5	3.5	141	138.9	26.9	36.5	535	90
3.0	4.0	150	143.6	27.0	34.5	690	90
3.5	4.5	153	147.9	26.8	33.0	740	90
4.0	5.0	153	151.9	27.0	31.8	930	90

Table (2): Data RECORDING FOR 2MM DIAMETER NOZZLE

P_g	P_{abs}	T	Ts	T_{w1}	T_{w2}	V	t
1.0	2.0	137	120.2	26.1	39.5	1120	90
1.5	2.5	137	127.4	26.0	38.1	1750	90
2.0	3.0	143	133.6	25.7	36.8	2120	90
2.5	3.5	144	138.9	26.0	34.6	2950	90
3.0	4.0	150	143.6	26.0	33.4	3800	90
3.5	4.5	152	147.9	25.6	32.0	5250	90
4.0	5.0	152	151.9	25.6	30.6	6100	90

Table (3): Data recording for 3mm diameter nozzle

P_g	P_{abs}	T	Ts	T_{w1}	T_{w2}	V	t
1.0	2.0	117	120.2	25.7	33.1	5650	90
1.5	2.5	140	127.4	25.7	32.3	7600	90
2.0	3.0	142	133.6	26.0	31.7	10650	90
2.5	3.5	146	138.9	26.1	30.8	13600	90
3.0	4.0	153	143.6	26.1	30.0	14700	90
3.5	4.5	154	147.9	26.0	29.2	15400	90
4.0	5.0	154	151.9	26.0	28.8	16200	90

Table (4): Data recording for 4mm diameter nozzle

P_g	P_{abs}	T	Ts	T_{w1}	T_{w2}	V	t
1.0	2.0	137	120.2	26.3	32.2	14500	90
1.5	2.5	140	127.4	26.0	31.6	17200	90
2.0	3.0	143	133.6	26.9	30.9	18400	90
2.5	3.5	149	138.9	27.1	30.2	19750	90
3.0	4.0	152	143.6	27.1	29.5	20800	90
3.5	4.5	153	147.9	27.0	28.8	18000	90
4.0	5.0	153	151.9	27.0	28.0	17500	90

Table (5): Delivery eater temperature at various pressure and nozzle diameter

Nozzle Diameter mm	Delivery Water Temperature (Tw_2) ℃		
	Steam Pressure (P) bar		
	2.0	2.5	3.0
2.0	36.8	34.6	33.4
3.0	31.7	30.8	30.0
4.0	30.9	30.2	29.5

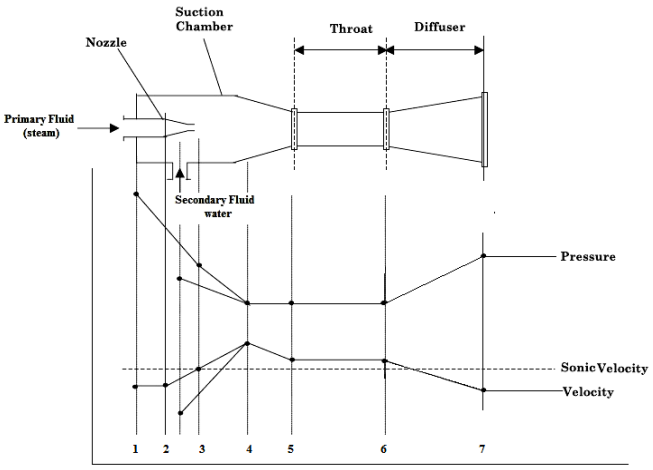

Fig. (1): shows the ejector components, the pressure and velocity diagram of the steam, liquid water and the mixture[8]

Fig. (2): shows the used device

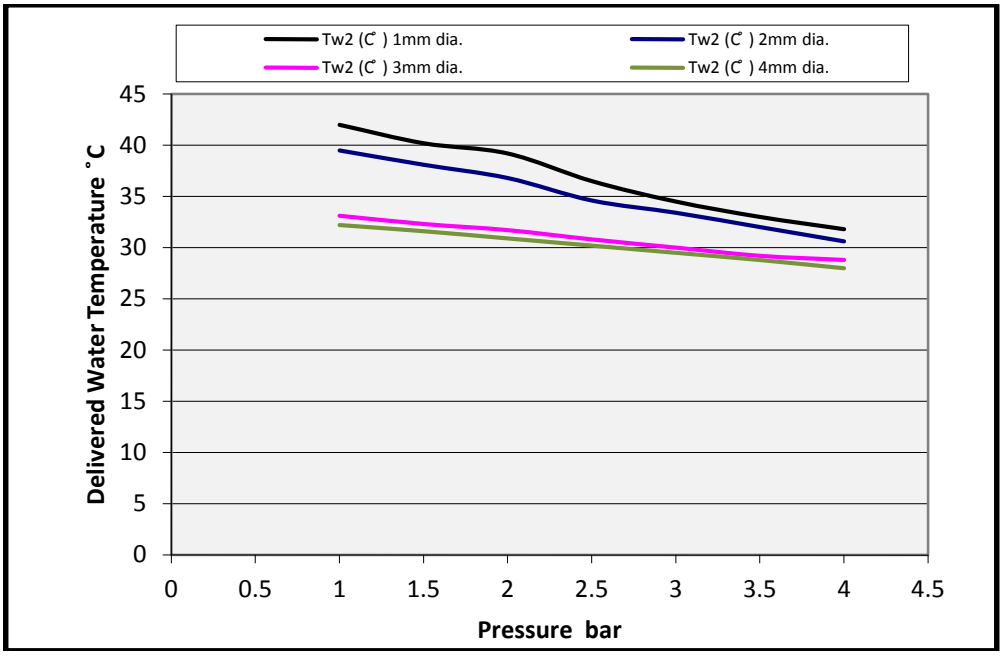

Fig. (3): Effect of Steam Pressure on Delivered Water Temperature

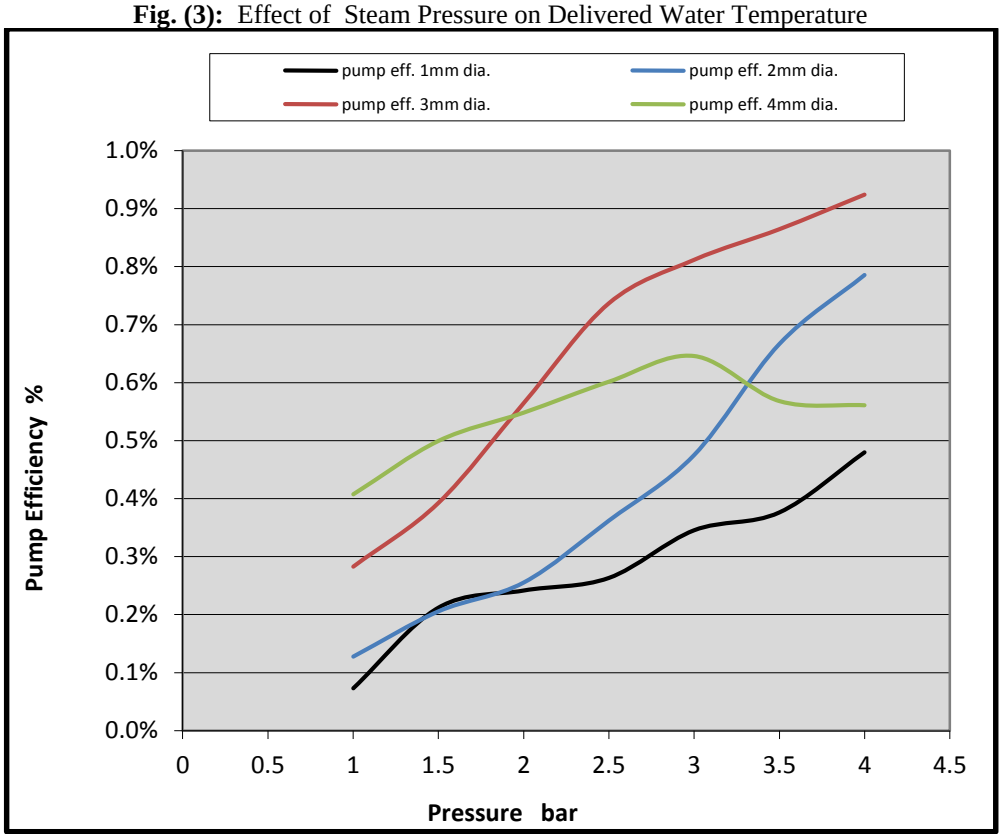

Fig. (4): Effect of Steam Pressure on Ejector Pumping Efficiency

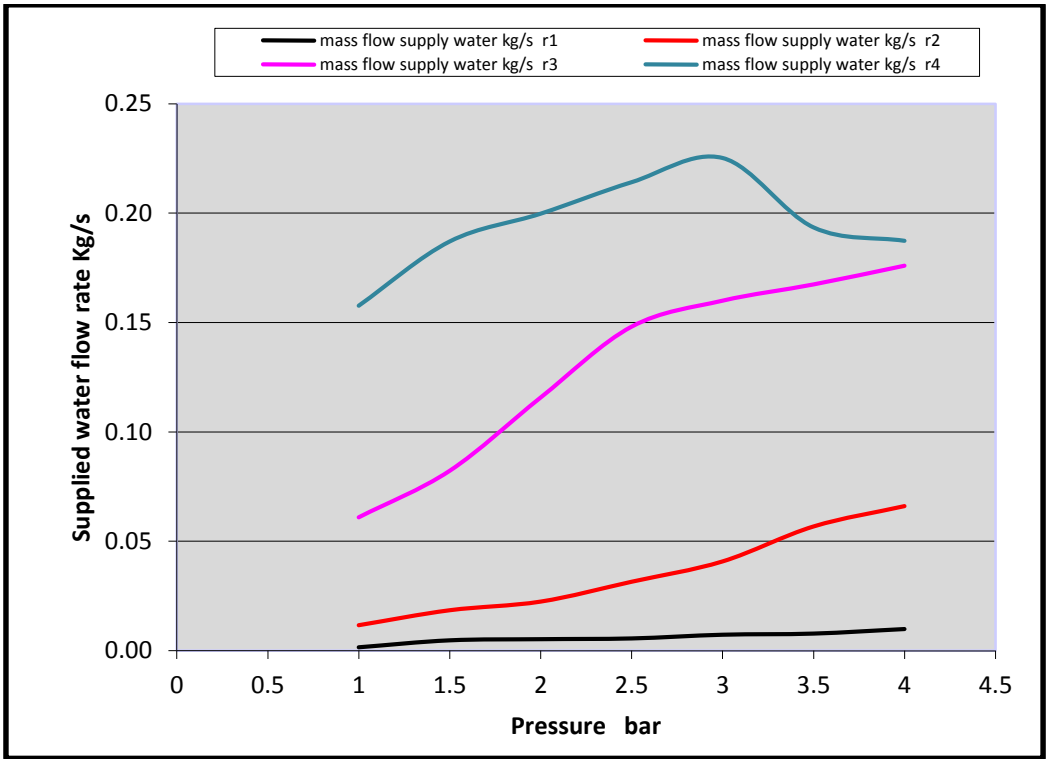

Fig. (5): Effect of Steam Pressure on Supplied Water Flow rate

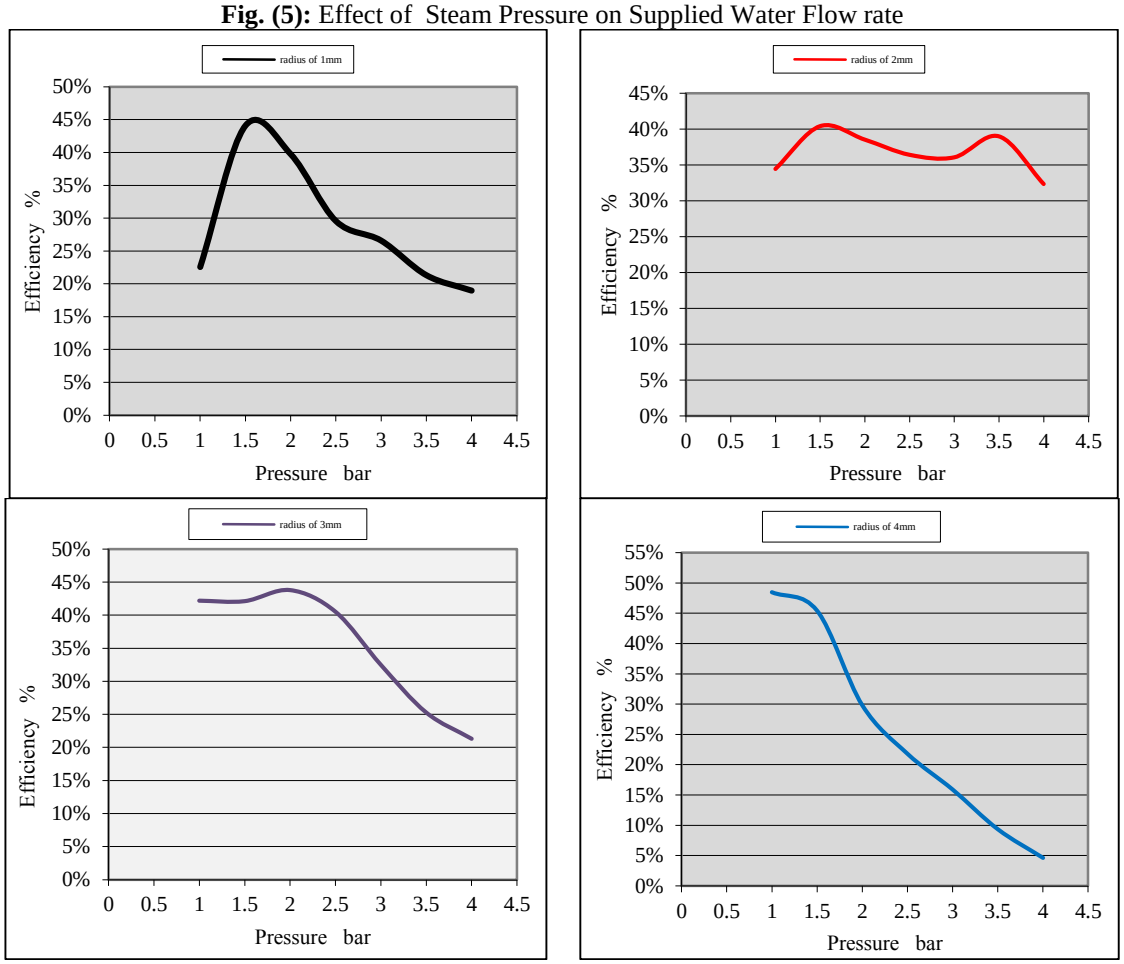

Fig. (6): Effect of Steam Pressure on Efficiency of Ejector for nozzle 1,2,3, and 4mm diameters.

Table (6): Units and symbols used in the calculation

Symbol	Meaning	Unit /
P_g	Steam (Primary Fluid) gauge Pressure	bar
P_{abs}	Steam (Primary Fluid) absolute Pressure	bar
T	Steam (Primary Fluid) Temperature	℃
T_S	Saturated Temperature of Steam	℃
T_{W1}	Water (Secondary Fluid) Temperature	℃
T_{W2}	Delivery (Mixing Steam-Water) Temperature	℃
V_W	Delivery (Mixing Steam-Water) Volume	ml
$\dot{m}_s$	Steam (Primary Fluid) mass flow rate	kg/s
$\dot{m}_w$	Water (Secondary Fluid) mass flow rate	kg/s
C_{PW}	Specific heat capacity of water	=
X	Steam quality	≈ 0.935
K	Steam Index	
R	Specific steam Constant	kJ/kg.K
A_t	Nozzle Throat Area	m^2
T	Time	sec.

الخلاصة

تم استخدام لافظة (نافذ) بخار احادية الطور ذات فوهة قذف متباينة الأقطار الداخلية من (١ - ٤) مليمتر لغرض ضخ المانع الثانوي (الماء) داخل المنظومة .تمت الإجراءات بتسليط قيم مختلفة من ضغط البخار يتراوح مابين (١ -٤) بار لبيان القطر الأفضل والأمثل الفوهة المجهزة داخل حجرة احتراق القاذف .تمتلك فوهة القذف ذات القطر ٣ مليمتر أفضل النتائج لدرجة حرارة ماء التجهيز ولأداء اللافظة بشكل عام .ان اعتماد خاصيتي الضغط المسلط وقطر فوهة القذف على درجة حرارة الماء ممثلة بدالة تجريبية تعمل ضمن المديات التالية :درجة حرارة تجهيز (٢٨- ٣٥) درجة مئوية، ضغط (١ - ٤) بار مع أقطار تتراوح مابين (١ - ٤) مليمتر لفوهة القاذف .عند تشابك المديات، فان النتائج المستحصلة في البحث تتوافق لحد كبير مع مامنشور آنفا .

پوختە

هاوێژەری هەڵمی یەك قۆناغبە بەکارهێنانی تیرەی جیاواز لە **1** تا **4** ملیمەتر بەکارهێنرا بۆ پاڵهێنانی شلەی لاوەکی (ئاو)، کارەکە ئەنجامدرا بە بەکارهێنانی پاڵەپەستۆی هەڵمی جیاوازی لە نێوان **1** تا **4** بار (گێج) بۆ دۆزینەوەی باشترین تیرەی بەکارهێنراو کە باشترین چوستی هەبێت وە زۆرترین ئاو بگوازێتەوە. لە ئەنجامی تۆژینەوەکە بۆمان دەرکەوت کە تیرەی نۆزڵی **3** ملیمەتری باشترین و گونجاوترینە بۆگواستنەوەی ئاو وە پری بەرزکردنەوەی پلەی ئاوی گواستراوەو چوستە سیستەمەکە.

کاریگەری پاڵەپەستۆی هەڵمی بەکارهاتوو و تیرەی نۆزڵەکە لەسەر پلەی گەرمی گواستراوە بەشێوەی پەیوەندیەکی ماتماتیکی دۆزرایەوە بۆ مەودای جیاواز لە پلەی گەرمی ئاوی گواستراوە لە **28** سە بۆ **35** سەدی و پاڵەپەستۆی بەکار هاتوو (**1**تا **4,5** بار گێج). لەگەڵا تیرەی نۆزڵا لە ا تا **4** ملم. وە ئەنجامەکان گونجاون لەگەڵا ئەو ئەنجامانەی لەلایەن توێژەری تر بڵاوکراوەنەتەوە.

NURSE'S KNOWLEDGE REGARDING POST OPERATIVE CARE FOR CHILDREN WITH CARDIAC SURGERY IN SURGICAL SPECIALTY HOSPITAL-CARDIAC CENTER IN ERBIL CITY

NAZAR RAMADHAN OTHMAN
Pediatric Nursing Unit, Nursing College, Hawler Medical University, Erbil-Kurdistan Region-Iraq

(Received: April 28, 2015; Accepted for publication: December 29, 2015)

ABSTRACT

Background: Heart disease in children is mostly congenital it is the most common single group of structural malformation in children. Postoperative care includes evaluating the patient's recovery process by checking vital signs, administering intravenous lines, ordering medications and laboratory tests as needed and monitoring the patient to ensure there are no complications after Surgery. The study aims to assess nurse's knowledge for post-operative care of children with cardiac surgery.

Method: A descriptive study was conducted in Surgical Specialty Hospital Cardiac Center, in period from (15th) of November 2011 to (30th) of April 2012. The samples consist of 28 nurses' who were giving Post-Operative care for Children with cardiac surgery and working in pediatric and Intensive care unit in Surgical Specialty Hospital-Cardiac Center. Data was gathered through the use of questionnaire format which consist of Socio demographic characteristics of selected sample and Nurses' knowledge regarding Postoperative Care of Children with Cardiac Surgery.

Results: Researcher has concluded that most of the nurses were from age group between (26-30) years old, and most of them were male. More than half of them were graduated in nursing college, and most of the nurses have (1-3) years of experience. There was significant association between years of experience and their knowledge.

Conclusion: Based on the result the researcher has concluded that most of the nurses were male, their age were between (26-30) years old, have (1-3) years of experience, were graduated from nursing college, and there was significant association between years of experience and their knowledge.

***KEY WORD*:** Assessment, Nurses Knowledge, Post operative care, Cardiac surgery.

INTRODUCTION

Heart disease in children is mostly congenital it is the most common single group of structural malformation in children,The incidence of congenital heart disease (CHD)is about 8per 1000live-born infant have significant cardiac malformation[1] . High demand for acute care nurse practitioners (ACNPs) in Canadian postoperative cardiac surgery settings has outpaced methodologically rigorous research to support the role[2]. Many patients with complex CHD, such as hypo plastic left heart syndrome, undergo a series of complex surgeries before final palliation or repair is achieved. Surgical and technological advances have resulted in markedly improved survival and life expectancy in patients with CHD since the first surgery for CHD ligation of a patent ductus arteriosus (was performed in 1938.3 Postoperative recovery of these children can be one of the most technical and rewarding challenges confronted by critical care nurses[3]. High quality nursing care for children in cardiac intensive care units (ICU) demands professional nursing knowledge and practical skills, due to its specificity and complexity. Nurses must be knowledgeable about the human responses of these children; many of their responses are physiological, yet there are a multitude of psychosocial, behavioral and family responses that are also very important for the nurse to understand, diagnose and treat Standardized nursing terminologies can support clinical reasoning and decision-making processes used for quality patient care. Therefore, we describe the nursing clinical judgment as a basis for nursing diagnosis ND identification and development of a neonatal intensive care (NIC)treatment plan for a child after cardiac surgery under intensive care[4]. Among 6,314 patients with CHD after cardiac surgeries, aged 1 to 18 years, 197 had postoperative infections. Out of these, three had more than one type of infection and the mortality rate was 25.38% compared with 3.91% in patients without infections[5]. The transportation of the child from the theatre to the intensive care unit requires special care. A member of both the surgical and anesthetic teams should accompany the child; Nurses should remain alert to the possibility of lost drains, catheters and probes, hypoventilation or accidental extubation[6]. Post-operative care includes evaluating the patient's recovery process by checking vital signs, administering intravenous lines, ordering medications and laboratory tests as needed and monitoring the patient to ensure there are no complications after Surgery[7].The complications of cardiac surgery are including Shock, Hemorrhage, Femoral phlebitis, or

thrombosis, Plural effusion, Anemia, Pulmonary edema, Cerebrovascular accident, Atelectasis, Urinary retention, Urinary incontinence and Chest infection[8]. Parents and family members of the child undergoing cardiac surgery are in a very emotionally stressful situation; Nurse can help family members cope by explaining the use of all monitoring and medical equipment attached to their child[3].

Objective of the study:

The study aims to assess nurse's knowledge regarding post-operative care of children with cardiac surgery, determine socio-demographic characteristics of nurse's and to find out the association between nurse's knowledge toward postoperative care of children with cardiac surgery and their socio-demographic characteristics.

Subjects and Methods

Design of the study:

A descriptive study was conducted to assess the nurse's knowledge for post-operative care of children with cardiac surgery at Surgical Specialty Hospital Cardiac Center in Erbil city from 15th of November 2011 to 30 of April 2012.The sample consists of all nurses' who was giving Post-Operative care for Children with Cardiac Surgery and who were working in pediatric unit and ICU in Surgical Specialty Hospital-Cardiac Center. Questionnaire was prepared by the researcher which consists of two parts, First part is about socio-demographic characteristics of nurses such as (age, level of education, number of years of experiences) and second part some items are about nurses' knowledge like (assessment of vital signs, oxygen saturation, dressing, drain site care)9. The data was being analyzed by using the social package of statistical Science (SPSS version 18) and using frequency, percentage and Chi square at P value ≤ 0.05. Ethical consideration was a main principle in data collection. Permission has been taken from the nurses before starting interview. The answers and information raised from the study were kept confidentially and used for the purpose of this study only. In addition, Researcher provided opportunities for participants to ask questions or express concerns at any point.

Result:

Below table shows that (67.9%) of the nurses were from the age group between (26-30) years old, (75.0%) of them were male, (60.7%) of them were single, (53.6%) of them were graduated in nursing college, (60.7%) of the nurses have (1-3) years of experience, (71.4%) were working in ICU Unit. and (71.4%) of them were in middle socioeconomic status.

Table (1) Socio-Demographical Characteristics of the Nurse's.

Variable	**N= 28 Percent**
20-25 years old	(7) 25.0
26-30 years old	(19) 67.9
31-35 years old	(2) 7.1
Total	**100**
Male	(21) 75.0
Female	(7) 25.0
Total	100
Nursing college graduate	(15) 53.6
Nursing institution graduate	(13) 46.4
Total	**100**
Married	(11) 39.3
Single	(17) 60.7
Total	**100**
1-3	(17) 60.7
4-6	(7) 25.0
7-10	(4) 14.3
Total	**100**
ICU unit	(20) 71.4
Pediatric unit	(8) 28.6
Total	**100**
High	(4) 14.3
Middle	(20) 71.4
Low	(4) 14.3
Total	**100**

The below table shows that the nurses gave the correct answer about (96.4%) regarding respiratory assessment every hour, (89.2%) The drainage must be checked by nurse every hour for color only,(75%) The heart rate is normally decreased after surgery. While they gave incorrect answer about (75%) giving analgesic during chest tube remove, (71.4%) children with pulmonary hypertension should remain sedately for the first 24 hours, (54.1%) Urine output should be checked every 2 hours.

Table (2) Nurse's Knowledge Regarding Post Operative Care.

No.	Items	Correct answers		Incorrect answers		Total	
		No.	%	No.	%	No.	%
1.	The nurse should assess respiratory status every hour.**(True)**	27	96.4	1	3.6	28	100
2.	Urine out put should be checked every 2 hour.**(False)**	12	42.9	16	57.1	28	100
3.	Chest tube drainage less than 3 ml/kg/hrs for more than 3 consecutive hour may indicate postoperative hemorrhage.**(False)**	10	35.7	18	64.2	28	100
4.	The nurse must assess the dressing site for conclusiveness, fullness and any drainage generally at the edge around the neck.**(False)**	8	28.5	20	71.4	28	100
5.	Always use analgesics during removing of the chest tube.**(False)**	21	75.0	7	25.0	28	100
6.	The nurse should do the suctioning within 5 second to prevent depleting the O2 supply.**(True)**	23	82.1	5	17.8	28	100
7.	Extubate patient in late post operative period.**(False)**	13	46.42	15	53.57	28	100
8.	The nurse should restrict fluid during the immediate postoperative period to prevent hypovolemia.**(True)**	21	75.0	7	25.0	28	100
9.	The drainage must be checked by nurse hourly for color only.**(False)**	25	89.2	3	10.7	28	100
10.	Decreased urine out put(less than 5 ml/kg/hrs) ,and elevate levels of blood urea nitrogen and serum creatinine are the signs of renal failure.**(False)**	11	39.2	17	60.7	28	100
11.	All patients need IV analgesics for pain control during the immediate postoperative period.**(False)**	16	57.1	12	42.8	28	100
12.	During chest tube drainage remove after the suture is cut, the tubes are quickly pulled out, at the end of full expiration to prevent intake of air into the pleural cavity.**(False)**	12	42.8	16	57.1	28	100
13.	Diminished or absent breath sound is most likely to indicate an area of pneumonia.**(False)**	11	39.2	17	60.7	28	100
14.	Hyperthermia is expected immediately after surgery.**(False)**	22	78.5	6	21.4	28	100
15.	The heart rate is normally decreased after surgery.**(False)**	21	75.0	7	25.0	28	100
16.	The nurse should always removed the chest tubes on the first to third postoperative day.**(True)**	16	57.1	12	42.8	28	100
17.	The patient should be put in lateral position until hemodynamic status is stable.**(False)**	20	71.4	8	28.5	28	100
18.	The nurse should monitor any fluid retention by weighining child daily.(**True)**	20	71.4	8	28.5	28	100
19.	When pulmonary hypertension is to be expected, the children should remain sedated for the first 24 hours until they have been stabilized. **(False)**	8	28.5	20	71.4	28	100
20.	The children need ambulation usually by the second post operative day to prevent any complication.**(True)**	20	71.4	8	28.5	28	100

Below table shows the significant association between nurse's knowledge and their levels of education at P. value (≤ 0.05), also there is a highly significant association between nurse's knowledge and their years of experience at P. value (≤ 0.009), while non-significant association is found with other variable.

Table (3). Association between Knowledge &Socio-demographic characteristics:

No.	Variable	Category	Frequency	Percent	P.value
1.	**Age**				
		20-25 Years	7	25.0	0.152
		26-30 Years	19	67.9	
		31-35 Years	2	7.1	
2.	**Gender**				
		Female	21	75.0	0.769
		Male	7	25.0	
3.	**Nurse's level of education**	Nursing institution graduate	15	53.6	0.04
		Nursing college graduate	13	46.4	
4.	**Marital status**				
		Single	11	39.3	0.488
		Married	17	60.7	
5.	**Years of experience**				
		7-10 Years	17	60.7	0.009
		1-3 Years	7	25.0	
		4-6 Years	4	14.3	
6.	**Unit of work;**				
		Pediatric unit	20	71.4	0.324
		ICU	8	28.6	
7.	**Socioeconomic status;**	Low	4	14.3	0.080
		High	20	71.4	
		Middle	4	14.3	

DISCUSSION

A compassionate, knowledge, and skilled nurse caring for the patient after opening heart surgery are an asset achievement of positive outcomes for the patient and his/her significant others[10], this comes with line of our study that most of the nurses answered truly during the interview. Regarding the group age about 25% of nurses were between (20-25) years old, this finding is agreeable with the study that had done in Iraq that had found respectively about (22.0 %) of the age between (26-30) and (21-25) years[13]. This study have found that there is no significant association between the nurses' age groups and their knowledge at P. value (0.152), our finding is agree with the study in India that had found that there was no significant association between the nurses' age groups and their knowledge at P. value (0.4). There was no significant association between nurses' knowledge and their gender at P. value (0.769). Our finding is agree with study done in India that found there was no significant association between nurses' knowledge and their gender (C.3.08), (T 5.99)[14]. There is no significant association between nurses' knowledge and marital status p. value (0.488). Our finding is agree with the study that had done in Egypt and detected that there was no significant association between nurses' knowledge and their marital status at p. value (>0.05)[15]. There is a highly significant association between nurses' knowledge and their years of experience at p. value (≤ 0.009) this is agree with study that had done in Egypt which found that there was highly significant association between nurses' knowledge and their education level at p. value (≤ 0.0001)[15,17]. Also there is a highly significant association between nurses' knowledge and their years of experience. The finding of present study is agree with the

study in Egypt which found that the significant difference between total nurses' knowledge score with their duration of experiences, normally with increased years of experiences the knowledge will be improved, also they reported that the majority of nurses were aged from 20 - 40 years and the majority of nurses were getting diploma of nursing which was the highest proportion and highly accepted with our study[12], and also agree with the study that had done in Egypt which found that years of experience are positively correlated with knowledge and practice scores of nurses with highly statistical significant differences with p. values of (<0.001) [15]. There is no significant association between nurses' knowledge and their unit of works with p. value (0.324). this result agree with the study that had done in India that found there was no significant relation between the area of work and the knowledge score of the samples p. value (0.09) accordingly[11]. Also agree with the study that had done in Israel that found there was no association between nurses' knowledge and their unit of work at p value (0.55) [16].

CONCLUSIONS AND RECOMMENDATIONS

Based on the results the researcher has concluded that most of the nurses were male, most of their ages were between (26-30) years old, most of the nurses have (1-3) years of experience and were graduated from nursing college, and there was a significant association between years of experience and their knowledge. The researcher Recommends to engage a highly qualified of head nurses and nursing supervision to the nursing service, opening specific training courses or sessions to those nurses, encourage nurses who are graduated college of nursing to work in intensive care unit, provide special significant, get a good salary or reward in order to make traction nurses for this unit.

REFERENCES

-Tom L and Graham C. (2007). Illustrated Text book of Pediatrics.3rd Edition. London. Elsevier.p.285.

- Goldie CL, Prodan-Bhalla N and Mackay M (2012). Nurse practitioners in postoperative cardiac surgery: are they effective. ***Can J Cardiovasc Nurs***.22(4):8-15.

-Pye S. and Donnell M (2010). Nursing considerations for children undergoing delayed Sternal closure after surgery for congenital heart disease .***aacn journal***.30 (50 -61).

- CavalcanteI A. Maria, Brunori E. Helena *etal* (2014).Nursing diagnoses and interventions for a child after cardiac surgery in an intensive care unit. ***Rev. Bras. Enferm.***68. (1).

-Kansy A, Jacobs JP, Pastuszko A, Mirkowicz-Małek M, Manowska M, Jezierska E, *etal* (2012)Major infection after pediatric cardiac surgery: external validation of risk estimation model**.** ***Ann Thorac Surg*** [16];94(6):2091-5.

- Junior F. Faria and David P. Ramos (2003). Immediate post-operative care following cardiac surgery.***J. Pediatr***.79(2).

- Friend L (2011).Role of Nurses for Cardiac Surgery Patients. Amarican HeartAssociation.

- Hockenberry M, Wilson D and Winkelstein M.Wong's.(2005).Essential of Pediatric Nursing.7th Edition. New York. Elsevier..Pp.(920-922,1465,1471-1472).

- Frederick A. Hensley, Jr., MD; Donald E. Martin, MD; and Glenn P. Gravlee, MD 2003. A Practical Approach to Cardiac Anesthesia, 3rd Edition.Russell P. Woda and Robert E. Michler .Postoperative Care .

-Caron G. Martin and Sandra L. Turkelson (2006).Nursing care of the patient undergoing coronary artery bypass grafting **. *J Cardiovasc Nurs***. (21) 2: (109 – 117).

-Aswathy V (2011).A study to assess the knowledge and Practices of staff nurses regarding fluid And electrolyte administration in post operative cardiac surgical patients Admitted in cardiac surgical icu and Cardiac surgical ward.

-Hala M. Ghanem and Roshdy Abd El-Aziz El-khayat (2012). Chronic Subdural Hematoma: Effect of Developing and Implementing Postoperative Nursing Care Standards on Nurses Performance for Reduction or Prevention Postoperative Complications**.** ***J Am Sci***. 8(2).

-Al-Ganmi A. Hussein (2014). Assessment of Nurses' Knowledge Concerning Cardiogenic Shock for Patients' in Cardiac Care Unit at Baghdad Hospitals. *kufa* ***Journal for Nursing sciences***. 4 (2): 215-222.

- Prasanna K, Radhika M (2015). Knowledge regarding Catheter care among Staff Nurses. ***IJAR***; 1(8): 182-186.

- Mohammed1 E. Kamel and Taha A. Said (2014). Critical Care Nurses' Knowledge and Practice Regarding Administration of Total Parenteral Nutrition at Critical CareAreas in Egypt. ***JBAH*** .4.(13).

- Topaz M. and Doron I (2013). Nurses' Attitudes Toward Older Patients in Acute Care in Israel .*OJIN* .2(18).???

-Mahmoud A. Shahin, Mohamed W. Yousef and Saye M (2012). Nurses' Knowledge and Practices regarding Enteral Nutrition at the Critical Care Department of Al- Manial University Hospital in Egypt: Impact of a Designed Instructional Program**.** ***JOAS***.8(11).

زانیاری پەرستاران سەبارەت بە چارەسەر ی دوای نەشتەر گەری دڵی منداڵان لە نەخۆشخانەی دل/سەنتەری نەشتەر گەری دڵ لە هەولیر

پوختە

پێشە کی : نەخوشی دڵ لە منداڵان زۆربەیان زکماکیە و یە کیکە لە باوترین نەخۆشی لەمنداڵان چارەسەر ی دوای نەشتەر گەری بریتیە لە هە لسەنگاندنی نەخۆش گرتنەوەی نیشانەکانی زیندوویو دانانی بۆری ناوەندی وپێدانی دەرمان و تێستی تاقێگەو چاودێریکرنی نەخۆش بۆ دڵنیابوونەوە لە کاریگەری لاوەکی وزیانبەخش لە دوای نەشتەر

ئارمانج: هەلسەنگاندنی ئاستی زانیاری پەرستاران سەبارەت بە چارەسەر ی دوای نەشتەر گەری دل رێکێن ڤەکولێنێ:تویژینەوەیەکی وەسفی لە سەنتەری نەشتەر گەری دڵ لە شاری هەولیر ئەنجامدرا بۆ هەلسەنگاندنی ئاستی زانیاری پەرستاران سەبارەت بە چارەسەر ی دوای نەشتەر گەری دل لە ماوەی نیوان**15**ی**11**ی**2011**تاکو **30**ی**3**ی **2012** نمونەی تویژینەوە بریتییە(**28**) لە پەرستاران کۆکرایەوە کە لە سەنتەری نەشتەر گەری دڵ لە بەشی منداڵان و چارەسەری چر .زانیاریەکان لەریگەی پرسیار نامە(روبەروو گفتووگۆ کردن)بوو کە پیك هاتبوو لە زانیاری کەسیتی پەرستاران و زانیاریان دەربارەی کاریگەریەکان .ئەنجام زانیاریەکان شیکرانەوە لەریگەی بەرنامەی تویژەرەوان گەیشتنە ئەو ئەنجامەی کەوا باری کەسیتی و کۆمەلایەتی پەرستاران لە سەنتەری نەشتەر گەری دڵ جیاوازیەکی زۆر هەیە لە نیوانیان.زۆربەی پەرستاران لە تەمەنی ناوەراست بوون , زۆربەیان لە رەگەزی نێر بوون , زیاتر لە نیوەیان دەرچووی کۆلیژ بوون و زۆربەیان **(3-1)** سالّ خزمەتیان لەو بارە هەبوو.هەروەها

دەرئەنجام :تویژینەوە ئەوە دەردەخات کەوا پەتوەندییەکی توند لە نیوان سالّ خزمەتی پەرستاران زانیارییەکانیاندا هە یە

ووشەکانی سەرەکی : هە لسەنگاندن, زانیاریی پەرستاران ,چارەسەری دوای نەشتەر گەری, نەشتەر گەری دل

معرفة الممرضين عن عناية بعد العمليات القلبية للاطفال في المستشفى القلبية \مركز القلبية في مدينة اربيل

الخلاصة

خلفية البحث : الامراض القلبية تعتبر من أكثر الأمراض لدى ألاطفال وهذه الامراض أكثريتهم تشوهات خلقية قلبية .ان العناية بعد العمليات يتكون من مراقبة العلامات الحيوية واخال كانيولا مركزي وفحوصات مختبريةو مراقبة المضاعفات بعد العمليات .

الأهداف: تهدف الدراسة لتقييم معرفة الممرضين لعناية بعد العمليات قلبية للاطفال المصابين بالامراض تشوهات خلقية القلبية.

طرق ألبحث :أجريت دراسة وصفية في مركزاربيل للعمليات القلبية للفترة **15-11-20111** الى **30-3-2012-** اختيرت عينة من**(28)** الممرضيين, تم تصميم استمارة استبيان تتضمن جزئين لجمع البيانات من خلال استخدام أداة الاستبيان باعتماد تقنيات المقابلة المباشرة كوسيلة لجمع البيانات.

ألنتائج :اظهرت النتائج ان غالبية الممرضيين اعمارهم تتراوح بين**(26-30)** سنة وذكور واكثر من نصفهم من خريجو كلية تلتمريض و واكثريتهم لديهم خبرة بين **(1-3)**سنوات.

الاستنتاجات : استنتج البحث بوجد علاقة طردية قوية بين معلومت الممرضين و سنوات خبرة لديهم في مركز اربيل للعمليات القلبية.

RISK FACTORS FOR MDR-TB OF AFGHAN IMMIGRANTS IN A SPECIALIZED REFERRAL HOSPITAL IN IRAN

MUAYAD **A**. **M**ERZA*
Dept. of Internal Medicine Medical School, University of Duhok, Duhok, Kurdistan Region-Iraq

(Received: May 21, 2015; Accepted for publication: October 4, 2015)

ABSTRACT

The study aimed to identify risk factors for multidrug-resistant tuberculosis (MDR-TB) among Afghan immigrant patients at a tertiary care hospital in Iran. This was a retrospective analysis of all confirmed Afghan immigrant TB patients from December 2000 – June 2005. Drug susceptibility testing (DST) to isoniazid, rifampicin, streptomycin, ethambutol, and pyrazinamide was performed on Lowenstein–Jensen media according to proportion method. The risk factors associated with MDR-TB were investigated. *Mycobacterium tuberculosis* strains were isolated from 668 Afghan immigrant patients. There were 397 males and 271 females and the mean age was 35.2 ± 16.3 (SD). Based on DST, Afghan immigrant patients were divided into two groups: 493 patients were non-MDR and 175 patients were MDR-TB. The parameters significantly associated with MDR were under 45 years of age, male sex, previous TB treatment, poor socio-economic conditions, and smoking. Site of TB disease whether pulmonary or extra-pulmonary, and drug abuse habit were not associated with MDR TB. In conclusion, based on our results an improved TB control programme, which must be coupled with early detection of MDR-TB among Afghan immigrant patients particularly in those with high risk factors, is highly recommended.

KEYWORDS: Mycobacterium tuberculosis, Afghan immigrants, Multidrug-resistant tuberculosis, Risk factors.

INTRODUCTION

Multidrug-resistant tuberculosis (MDR-TB) is defined as *Mycobacterium tuberculosis* resistant to at least rifampicin (RIF) and isoniazid (INH). MDR-TB poses a significant global and public health concern, because of low efficacy rates for first line treatment regimens, requires 18 to 24 months of treatment, and associated with considerable mortality worldwide (Gupta *et al.*, 2001; Drobniewski *et al.*, 2005). An additional concern was the persistence of high or increasing incidence and spread of MDR-TB in developed and the developing world, related to poverty, migration, ethnic conflicts, substance abuse and the increase in human immunodeficiency virus (HIV) infection, sometimes coupled with the poor performance of national programmes. These factors may lead to the development or increase of MDR-TB, which is susceptible to proper health control measures (Antunes *et al.*, 2000). These measures are directed at reducing the transmission by identifying infectious patients quickly and through fast appropriate diagnostic measures. This would be followed by immediate treatment with effective anti-TB drugs according to resistance pattern, so long as adequate protective vaccine is no available (Loddenkemper *et al.*, 2002). In 2006, the World Health Organization (WHO) has estimated that around 500,000 cases of MDR-TB occurred worldwide (World Health Organization, 2008a). Although MDR-TB is present in almost all the world, but the highest proportion of MDR-TB among new cases has been reported from former Soviet Union, China, and India (World Health Organization, 2008b).

In Iran, TB remains endemic; however the TB incidence and prevalence rates are in decline. The TB incidence and prevalence per 100,000 populations was respectively declined from 36 and 50 cases in 1990 to 22 and 28 cases in 2006. Until now, there is no precise representative survey of drug resistance rate in Iran. However according to a national wide survey performed in 1999, among all TB patients who underwent drug susceptibility testing (DST), 10.9% showed resistance to ≥ 1 anti-TB drug, and 6.7% showed MDR-TB strains (World Health Organization, 2000). In subsequent studies, the presence and circulation of extensively drug resistant TB (XDR-TB) strains (i.e., MDR-TB isolates with additional resistance to fluoroquinolones plus resistance to at least 1 of the 3 injectable second line anti-drugs) in epidemiologically linked

MDR-TB patients have been documented (Masjedi *et al.*, 2006). Many studies have been conducted on *M. tuberculosis* clinical isolates genotyping and drug resistance encompassing MDR-TB, in Iran. But only few investigations focused separately on MDR in immigrant TB patients. Here, I tried to determine risk factors of MDR-TB and develop a policy and plan for public health TB control for immigrant patients.

MATERIALS AND METHODS

Setting:

The Mycobacteriology Research Center (MRC) at National Research Institute of Tuberculosis and Lung Diseases (NRITLD) is the main health facilities in Iran for performing cultures and drug susceptibility testing (DST) for *M. tuberculosis*. The NRITLD is the only tertiary referral hospital for TB patients in Iran.

Study population:

The Aghan immigrant patients, who had positive TB culture, were retrospectively studied between December 2000 and June 2005. Exclusion criteria were patients with negative culture, culture contamination, only smear examination, atypical tuberculosis culture, and patients without DST test. Hence, our studied population deemed to be representative of Afghan immigrants TB patients in Iran. Based on drug resistance pattern, TB patients were categorized into two groups: Multidrug resistant and non multidrug resistant tuberculosis patients. Patient case sheets were reviewed and relevant data were gathered by using a standardized questionnaire. Accordingly, the demographic and risk factor data were registered. The parameters investigated in this study were age, sex, TB treatment history, site of TB disease (i.e. pulmonary/extra-pulmonary), and socioeconomic status. Smoking and drug abuse history were also included.

Bacteriological study:

The diagnosis of *M. tuberculosis* was performed by smear microscopy and culture examination. Identification of Mycobacterial species was made by conventional biochemical tests (Kent and Kubica, 1985). Based on the production of niacin, nitrate reduction, catalase activity, pigment production and growth rate, *M. tuberculosis* complex was identified. Susceptibility testing of anti-TB drug was routinely performed using the proportion technique on Lowenstein Jensen (LJ) culture for the isolation of *M. Tuberculosis*. The anti-mycobacterial drugs concentrations were as follows:

1- RIF concentration was 40.0 µg/ml, which was prepared from a stock solution made by dissolving 40 mg of RIF in 10 ml of DMSO.

2- INH concentration was 0.2 µg/ml, which was prepared from a stock solution made by dissolving 50 mg of INH in 2 ml of DW.

3- Ethambutol [ETM] concentration was 2.0 µg/ml, which was prepared from a stock solution made by dissolving 50 mg of ETM in 25 ml of DW.

4- Streptomycin [SM] concentration was 4.0 µg/ml, which was prepared from a stock solution made by dissolving 128.7 mg of SM in 10 ml of DW.

5- Pyrazinamide [PZA] concentration was 100 µg/ml, which was prepared from a stock solution made by dissolving 100 mg of PZA in 10 ml of DW. DST to PZA was performed by using two phase medium. Pyrazinamide resistant strain of *M. tuberculosis* was defined when the percentage of resistant colonies was higher than the critical proportion on the 21st day of incubation.

Definitions:

Multidrug-resistant tuberculosis was indicated as *M. tuberculosis* strains with simultaneous resistance to INH and RIF (World Health Organization, 2009).

Data analysis:

Data analysis was carried out by using the SPSS software programme, version 11.0. Statistical significance was reported whenever p value was less than 0.05.

Ethics approval:

Following ethical consideration by NRITLD committee, the practice in this study was considered to be ethical.

RESULTS

Patients

A total of 3812 patients with TB disease from December 2000 to June 2005 were referred to NRITLD. Out of 3812 TB patients, 1583 (41.5%) were ruled out because their culture result were negative (916) (24.0%) or they had positive smear microscopy without culture (667) (17.5%). Additional 394 TB patients (10.4%) were ruled out due to contaminated culture. Further, 93 patients (2.4%) were infected with MOTT. Another 1074 (28.2%) were Iranian and they were excluded. The study therefore included 668 (17.5%) Afghan immigrant

patients. Table 1 demonstrates the characteristic features of studied population.

Table (1): Characteristics of the study population (no = 668)

Variable		No (%)
Mean age	35.2 ± 16.3 (SD)	
Sex	Male	397 (59.4)
	Female	271 (40.6)
History of TB treatment	New cases	408 (61.1)
	Previous TB treatment	260 (38.9)
Manifestation of TB	Pulmonary	612 (91.6)
	Extra-pulmonary	56 (8.4)
Socio-economic condition	Acceptable	333 (49.8)
	Poor	335 (50.2)
Smoking	Smoker	466 (69.8)
	Non smoker	202 (30.2)
Drug abuse	Abuser	66 (9.9)
	Non-abuser	602 (90.1)

Associated risk factors of MDR-TB patients

According to the DST, the 668 Afghan immigrants were divided into two patients groups. There were 493 patients with non-MDR and 175 patients with MDR-TB. The number of MDR-TB patients for each of the parameters analysed and also the crude odds ratios for MDR TB were shown in table 2. Certain parameters demonstrated significant association with MDR-TB, which included: age less than 45 years (OR, 2.048; 95% CI, 1.388-3.027; *p*=0.000), male sex (OR, 1.535; 95% CI, 1.052-2.240; p=0.020), previous TB treatment (OR, 7.162; 95% CI, 4.779-10.754; p=0.000), poor socio-economic conditions (OR, 6.113; 95% CI, 3.974-9.436; p=0.000), and smoking (OR, 1.722; 95% CI, 1.131-2.630; p=0.007) (Table 2).

Table (2): -Associated risk factors of multidrug-resistant tuberculosis.

Variable		Non-MDR-TB (493) no (%)	MDR-TB (175) no (%)	Odd ratio (95% CI)	P value
Age	Age < 45 yr	271 (55.0)	125 (71.4)	2.048 (1.388-3.027)	0.000
	Age > 45 yr	222 (45.0)	50 (28.6)		
Sex	Male	280 (56.8)	117 (66.9)	1.535 (1.052-2.240)	0.020
	Female	213 (43.2)	58 (33.1)		
History of TB treatment	New cases	360 (73.0)	48 (27.4)	7.162 (4.779-10.754)	0.000
	Previous TB treatment	133 (27.0)	127 (72.6)		
Manifestation of TB	Pulmonary	457 (92.7)	155 (88.6)	1.638 (0.884-3.017)	0.111
	Extra-pulmonary	36 (7.3)	20 (11.4)		
Socio-economic condition	Acceptable	298 (60.4)	35 (20.0)	6.113 (3.974-9.436)	0.000
	Poor	195 (39.6)	140 (80.0)		
Smoking	Smoker	330 (66.9)	136 (77.7)	1.722 (1.131-2.630)	0.007
	Non smoker	163 (33.1)	39 (22.3)		
Drug abuse	Abuser	46 (9.3)	20 (11.4)	1.254 (0.692-2.256)	0.461
	Non-abuser	447 (90.7)	155 (88.6)		

DISCUSSION

Global surveillance documents that drug resistance is a serious problem and extensively widespread, and furthermore there are high percentage of TB isolates resistant to 3 or 4 drugs (World Health Organization, 2007). Worldwide, it is estimated that 1 to 1.5 million people are living with MDR-TB. In 2006, one per 20 new TB cases was MDR. Of the nearly 500,000 people who became ill with MDR-TB, 50% were living in China and India, and 7% were living in the Russian Federation (World Health Organization, 2008b). The high percentage of drug-resistant TB among new cases suggests an alarm with regard to transmission of drug-resistant strains (World Health Organization, 2008b). Accordingly; careful follow up and monitoring of transmission trends of drug resistance TB strains is priority to ensure effective TB control programme.

In this study population, age less than 45 years and male sex were significantly associated with MDR-TB, which was in concordance with other studies (Granich *et al.*, 2005; Surucuoglu *et al.*, 2005; Choi *et al.*, 2007). The finding of high frequency of MDR-TB strains in young age group is highly suggestive of recent transmission in the current study. Accordingly, in order to ensure successful TB control programme, strict protocols to monitor and control trend of transmission of MDR-TB strains must be considered a real priority. This can be done through cautious management of relapsed TB patients within Afghan immigrant cases until obtaining results of DST. In contrast to this study, in old age group patients, recent transmission is unlikely and the infection has been acquired previously. Faustini *et al.* (2006) in their review documented that although multidrug resistance was more frequent in patients with age group less than 65 years, the association was not strong and more diverse in patients with age group less than 45 years. In this study, the higher frequency of MDR-TB in male over female may be clarified by that males are more likely to be outside and hence more vulnerable to community acquired drug resistance TB. Additional factor for male susceptibility to MDR-TB is that females are more adherent with long course anti-TB drugs and hence they unlikely to have insufficient treatment than males (Faustini *et al.*, 2006; Mirsaeidi *et al.*, 2007).

In the current study, there was statistically significant association between MDR-TB and previous treatment of TB patients. This finding necessitates performance of urgent DST for all smear positive treatment failure cases so that to identify proper anti-TB regimen for such cases and subsequent prevention of emergence of drug resistance. Hence, the WHO category II regimen should be revised particularly for countries with high burden drug resistance. The association between MDR-TB and retreatment had been well confirmed in the literature (Antunes *et al.*, 2000; Caminero, 2005; He *et al.*, 2008; Shamaei *et al.*, 2009; Suárez-García *et al.*, 2009). The high rate of drug resistance in previously treated patient could result from improper anti-TB regimen, suboptimal or erratic drug delivery, unpleasant compliance by TB patients or physician, inappropriate follow up of treatment, and poor performance of proper infection control practices in health care facilities. It has been reported that drug resistance particularly MDR-TB is ten times more in patients with previous treatment (Merza and Masjedi, 2010).

In the present study, the prevalence of multidrug resistance was higher in patients with poor socio-economic status than non poor living condition, which is in line with other studies (Rubel and Garro, 1992; Sumartojo, 1993; Antunes *et al.*, 2000). Generally, patients with poor socio-economic status such as poverty and homelessness assumed to be higher consumers of medicines; however, they are less compliant with treatment that may induce treatment failure and subsequent MDR-TB. Furthermore, in this study, smoking was found to be significantly associated with drug resistance TB. Although, this is uncommon finding in other studies, it has been documented in few reports (Barroso *et al.*, 2003).

There were certain limitations in this study such as HIV co-infection, cavitary pulmonary TB, diabetes mellitus and other risk factors were not included because sufficient information on these parameters were not recorded for all patients.

Conclusion: in concordance with reported studies, MDR-TB is a serious global health issue particularly in immigrants. The MDR-TB rate was significantly higher in the younger age less than 45 yr, male gender, previous TB treatment, poor socio-economic conditions, and smokers. Therefore, an improved TB control programme, which must be coupled with early detection of MDR-TB among Afghan immigrants

particularly in those with high risk factors, is highly recommended.

ACKNOWLEDGMENTS

I highly appreciate help of health staff at the Mycobacteriology Research Center in Iran for providing necessary information for performing this study.

REFERENCES

- Antunes, M. L., Aleixo-Dias, J., Antunes, A. F., Pereira, M. F., Raymundo, E., Rodrigues, M. F. (2000). Anti-tuberculosis drug resistance in Portugal. Int J Tuberc Lung Dis., 4: 223-231.
- Barroso, E. C., Mota, R. M. S., Santos, R. O., Sousa, A. L. O., Barroso, J. B., Rodrigues, J. L. N. (2003). Risk factors for acquired multidrug-resistant tuberculosis. J Penumol., 29: 89–97.
- Caminero, J. A. (2005). Management of multidrug-resistant tuberculosis and patients in retreatment. Eur Respir J., 25: 928-936.
- Choi, J. C., Lim, S. Y., Suh, G. Y., Chung, M. P., Kim, H., Kwon, O. J., Lee, N. Y., Park, Y. K., Bai, G. H., Koh, W. J.(2007). Drug resistance rates of Mycobacterium tuberculosis at a private referral center in Korea. J Korean Med Sci., 22: 677-681.
- Drobniewski, F., Balabanova, Y., Nikolayevsky, V., Ruddy, M., Kuznetzov, S., Zakharova, S., Melentyev, A., Fedorin, I. (2005). Drug-resistant tuberculosis, clinical virulence, and the dominance of the Beijing strain family in Russia. *JAMA*., 293: 2726-2731.
- Faustini, A., Hall, A. J., Perucci, C. A.(2006). Risk factors for multidrug resistant tuberculosis in Europe: a systematic review. Thorax., 61: 158-163.
- Granich, R. M., Oh, P., Lewis, B., Porco, T. C., Flood, J. (2005). Multidrug resistance among persons with tuberculosis in California, 1994-2003. JAMA., 293: 2732-2739.
- Gupta, R., Kim, J. Y., Espinal, M. A., Caudron, J. M., Pecoul, B., Farmer, P. E., et al. (2001). Responding to market failures in tuberculosis control: a model to increase access to drugs and treatment. Science., 293: 1049-1051.
- He, G. X., Zhao, Y. L., Jiang, G. L., Liu, Y. H., Xia, H., Wang, S. F., Wang, L. X., Borgdorff, M. W., van der Werf, M. J., van den Hof, S. (2008). Prevalence of tuberculosis drug resistance in 10 provinces of China. BMC Infect Dis.,8:166.
- Kent, P. T., Kubica, G. P. (1985). Public Health Mycobacteriology: A guide for level II laboratory. Atlanta, GA. Public Health Services, US Department of Health and Human Services.
- Lee, S. W., Jeon, K., Kim, K. H., Min, K. H. (2009). Multi-drug resistant pulmonary tuberculosis among young Korean soldiers in a communal setting. J Korean Med Sci., 24: 592-595.
- Loddenkemper, R., Sagebiel, D., Brendel, A. (2002). Strategies against multidrug-resistant tuberculosis. Eur Respir J Suppl. , 36: 66s-77s.- Masjedi, M. R., Farnia, P., Sorooch, S., Pooramiri, M. V., Mansoori, S. D., Zarifi, A., Velayati, A. A., Hoffner, S. (2006). Extensively drug resistant tuberculosis: 2 years of surveillance in Iran. Clin Infect Dis., 43: 840-847.
- Merza, M., Masjedi, M. R. (2010). Extensively drug-resistant tuberculosis (XDR) and extremely drug-resistant tuberculosis (XXDR): risk factors and molecular perspectives. Iranian Journal of Clinical Infectious Diseases, 5: 174-188.
- Mirsaeidi, M. S., Tabarsi, P., Farnia, P., Ebrahimi, G., Morris, M. W., Masjedi, M. R., Velayati, A. A., Mansouri, D. (2007). Trends of drug resistant *Mycobacterium tuberculosis* in a tertiary tuberculosis center in Iran. Saudi Med J., 28: 544-550.
- Rubel, A. J., Garro, L. C. (1992). Social and cultural factors in the successful control of tuberculosis. Public Health Rep., 107: 626-36.
- Shamaei, M., Marjani, M., Chitsaz, E., Kazempour, M., Esmaeili, M., Farnia, P., Tabarsi, P., Amiri, M. V., Mirsaeidi, M., Mansouri, D., Masjedi, M. R., Velayati, A. A. (2009). First-line anti-tuberculosis drug resistance patterns and trends at the national TB referral center in Iran--eight years of surveillance. Int J Infect Dis.,3:e236-240.
- Suárez-García, I., Rodríguez-Blanco, A., Vidal-Pérez, J. L., García-Viejo, M. A., Jaras-Hernández, M. J., López, O., Noguerado-Asensio, A. (2009). Risk factors for multidrug-resistant tuberculosis in a tuberculosis unit in Madrid, Spain. Eur J Clin Microbiol Infect Dis.,28: 325-330.
- Sumartojo, E. (1993). When tuberculosis treatment fails. A social behavioral account of patient adherence. Am Rev Respir Dis., 147: 1311-1320.
- Surucuoglu, S., Ozkutuk, N., Celik, P., Gazi, H., Dinc, G., Kurutepe, S., Koroglu, G., Havlucu, Y., Tuncay, G. (2005). Drug-resistant pulmonary tuberculosis in western Turkey: prevalence, clinical characteristics and treatment outcome. Ann Saudi Med., 25: 313-318.
- World Health Organization. (2000). The WHO/IUATLD global project to anti-tuberculosis drug resistance surveillance. *Volume 278*. WHO. Geneva, Switzerland, 2000: 1-250.
- World Health Organization. (2007). Global tuberculosis control: surveillance, planning and financing. WHO report. WHO/HTM/TB/2004.343. Geneva, Switzerland: WHO.
- World Health Organization. (2008a). Global tuberculosis control: surveillance, planning and financing. WHO report. WHO/HTM/TB/2008.393. Geneva, Switzerland: WHO.
- World Health Organization. (2008b). The WHO/IUATLD global project on anti-tuberculosis drug resistance surveillance 2002-2007. WHO/HTM/TB/2008.394. Geneva, Switzerland: WHO.
- World Health Organization. (2009). Guidelines for surveillance of drug resistance in tuberculosis-4th ed. WHO/HTM/TB/2009.422. Geneva, Switzerland: WHO.

A NEW INVESTIGATION OF MININET EMULATOR FOR EVALUATING SOFTWARE DEFINED NETWORKS PERFORMANCE

FARIS **K**ETI and **S**HAVAN **A**SKAR
Dept. Of Electrical and Computer Engineering, College of Engineering, University of Duhok, Kurdistan Region-Iraq

(Received: June 8, 2015; Accepted for publication: September 15, 2015)

ABSTRACT

In this paper an evaluation of a Software Defined Networks emulation tool called Mininet is conducted. Tests were conducted to study the performance of Mininet in emulating software defined network layers which are; the network infrastructure layer, southbound (OpenFlow Protocol) interface layer, software defined network's centralized controller platform layer, and finally the real- time software defined network applications and northbound interface layer. In addition, Mininnet limitations related to the simulation environment, resource capabilities are tested. To evaluate the later, the scalability of Mininet in term of creating many topologies is tested with varying number of nodes and two different environment scenarios. Results show that the simulation environment has a remarkable effect on the required time for building a topology, for instance, the powerful resources scenario needed only 0.19 sec, whereas, 5.611 sec were needed when the resources were less. However, the required time were increased in both scenarios when the number of nodes was increased into 242.842 and 3718.117 sec for the powerful and less capabilities resources respectively.

KEYWORDS:- Software Defined Networking, Emulation,OpenFlow, Pox controller, Mininet.

I. INTRODUCTION

Because of the astronomic number of users each with different applications or services which also increase continuously, the Internet has already become a kind of global communication infrastructure. But, the Internet with its current capabilities is still suffering from variety of great challenges in network control, configuration, and management issues. Research on Internet application, service, network control and management is one of the hot and interesting topics in recent years. Many of research projects have been initiated in this subject's area [1, 2].

The research community of computer networks has been searching for solutions that enable the use of networks with more programming resources and less need for replacement of hardware elements, so that new technologies designed to solve new problems can be inserted gradually into the network and without significant costs [3, 4]. Software-Defined Networking (SDN) is a new network paradigm that virtualizes network infrastructure by decoupling the control and data plane logic of traditional network devices, creating a dynamic, flexible, automated and manageable architecture [2].

SDN is implemented through a protocol known as OpenFlow that lets administrators select the path through which data will flow through a network [5].

Section II of this paper discusses the SDN paradigm by describing its motivation, network elements, and the operation among the elements. Section III describes the utilized simulation tool which is called Mininet, in addition, it presents Mininet characteristics. In section IV, the performance of Mininet tool in emulating software defined networks is evaluated, this includes the creation of network infrastructure and southbound interface (openflow protocol) messages between the controller and the network infrastructure in order to insert entries and create flow tables in the openflow based switches. The role of controller in SDN networks was proposed utilizing SDN tools, and also one of Mininet performance related to the simulation's environment was tested. Section V concludes the paper.

II. SOFTWARE-DEFINED NETWORKS

Experienced IT personnel are inevitable when it comes to configuring and installing network's elements. Accurate and complicated simulators are needed when the simulating networks in which interactions among its elements are needed such as switches, routers, etc. Supporting this is highly difficult to achieve. Therefore; a new network model is required to support these agility requirements [4].

There are four factors that SDN focuses on which are namely [6];

A. *Control plane and data plane Separation*

B. *A centralized controller and view of the network*

C. *Open interfaces between the devices in the control plane and the data plane*

D. *Use of external application to support the programmability feature of the network*

A. Control plane and data plane separation:

One of the tenets expressed early in the introduction of SDN is the potential advantage of the separation of a network device's control and data planes. This separation affords a network operator certain advantages in terms of centralized or semi-centralized programmatic control. It also has a potential economic advantage based on the ability to consolidate in one or a few places what is often a considerably complex piece of software to configure and control onto less expensive, so-called commodity hardware [6,7,8,9].

B. A centralized controller and view of the network

The most important characteristic of SDN is the use of a centralized control plane, which transfer the decision-making logic from the network devices into external controllers [5]. Because of this, an awareness of network elements and characteristics will be attained.

C. Open interfaces between the devices in the control plane and the data plane (OpenFlow):

In the OpenFlow architecture, an OpenFlow switch consists of many flow tables in addition to an abstraction layer which communicates with a controller in a secure manner via OpenFlow protocol [10]. Flow tables contain forwarding flow entries, each one match packets to its correspondent flow, then processed and forwarded. Forwarding flow entries consist of the following parameters; match fields, counters, and a set of instructions. Match fields are used for the purpose of matching the incoming packets by using specific information such as; packet header, ingress port, and metadata. Counters are used to build up statistic data for each flow such as; the number of received packets, the number of received bytes, and duration of a particular flow. A set of instructions apply when there is a match; they dictate how to handle matched packets [11].

D. Use of external application to support the programmability feature of the network:

In SDN environment, it is possible to control and program network devices, there is a capability of utilizing software applications that are developed from hardware for the purpose of controlling the policies of packet forwarding [8]. With SDN, it is possible to deploy network applications that have precise traffic monitoring and processing capabilities. This will consequently support; a dynamic QoS provisioning, load balancing, and access control.

SDN has many advantages [12]; it supports a faster response to changing traffic conditions. In addition, it allows for more options for dynamic provisioning, better

load balancing, more preferred traffic engineering, improved network resource utilization, and enhanced opportunities to implement many new types of services.

III. MININET

There are many reasons that trigger the use of a new emulator called Mininet; first, there are only few network devices available for the purpose of implementing SDN standard as it is yet not widespread technology from the industrial perspective. In addition, implementing network with large number of network devices is very difficult and costly. Therefore, to overcome these problems, virtual mode strategy has been conducted for the purpose of prototyping and emulating there kind of network technologies and the most important one is Mininet [1].

Mininet has the capability to emulate different kinds of network elements such as; host, layer-2 switches, layer-3 routers, and links. It works on a single Linux kernel and it utilizes virtualization for the purpose of emulating a complete network utilizing only a single system. However, the created hosts, switches, routers, and links are real-world elements although they are created by means of software [13].

A. Some characteristics guided the creation of Mininet are [14]:

- Flexibility, that is, new topologies and new features can be set in software, using programming languages and common operating systems.
- Applicability, correctly implementations conducted in prototypes should also be usable in real networks based on hardware without any changes in source codes.
- Interactivity, management and running the simulated network must occur in real time as if it happens in real networks.
- Scalability, the prototyping environment must be scaling to large networks with the hundreds or thousands of switches on only a computer.
- Realistic, the prototype behavior should represent real time behavior with a high degree of confidence, so applications and protocols stacks should be usable without any code modification.
- Share-able, the created prototypes should be easily shared with other collaborators, which can then run and modify the experiments.

B. MININET Workflow

Mininet has the capabilities that enable researchers or network programmers to create software defined network prototype in a simple manner. With the capability to interact, customize and share it, and provides a smooth path to running it on hardware [14].

IV. SDN SIMULATION USING MININET AND POX CONTROLLER

In order to evaluate the performance of Mininet tool in emulating software defined networks, main layers of a software defined network are investigated, described, and tested individually utilizing Mininet.

Any software defined network consists of three main planes, namely; data plane, control plane, and management plane. Figure 1 shows the main software defined network planes.

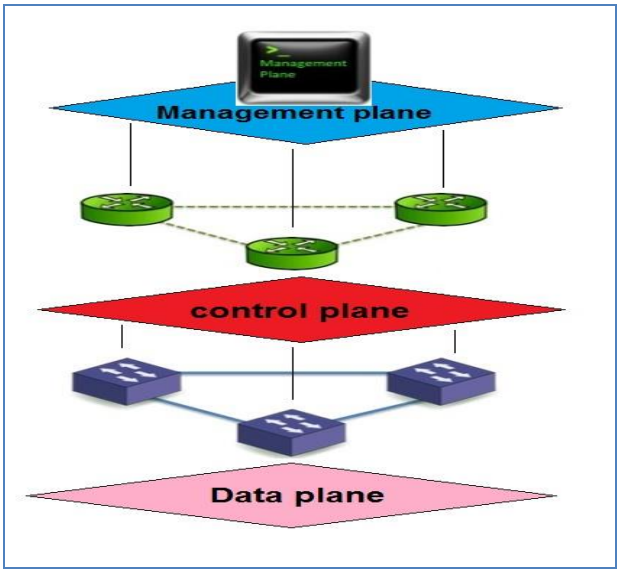

Fig. (1): SDN Planes

Before delving into describing the results of evaluating the performance of the Mininet tool in emulating software defined networks, an insight into the layers of those kinds of networks is given. Each plane is represented by means of two or more layers. In other words, our suggested emulation tool is used to test the entire software defined network in a precise way by testing it layer by layer rather than plane by plane.

Main layers of a software defined network in relation to corresponding planes are displayed in Figure 2.

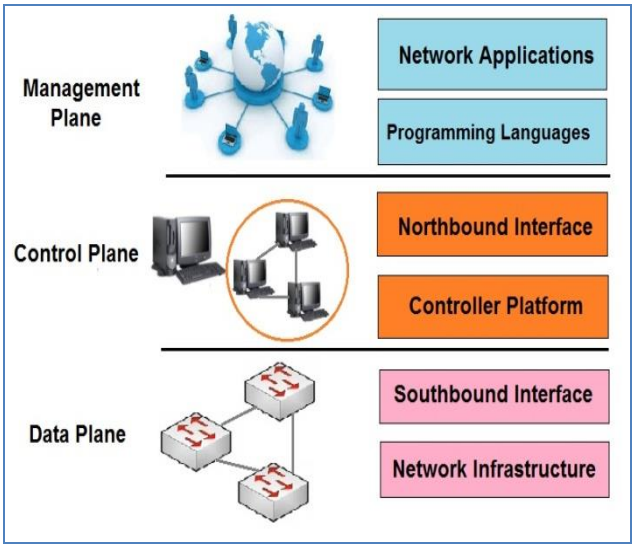

Fig. (2): SDN layers

Figure 2 shows the main software defined network's layers. The layers are described separately to indicate how they interact with each

other. Figure 3 show the functionality of each layer in a more detailed manner to emphasize the relations between layers in Mininet tool [14, 15].

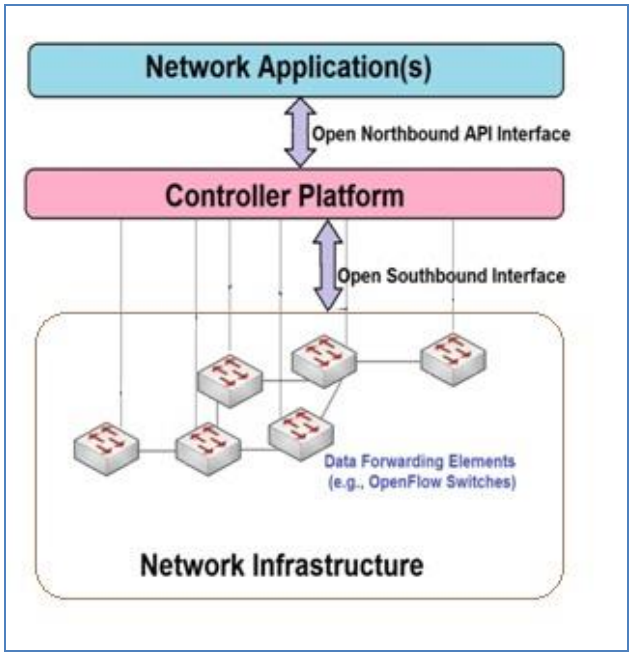

Fig. (3): SDN architecture

There are many SDN controllers exist, however, POX is the selected controller for our test. POX is a software platform developed in Python [16, 17].POX began early as a controller for an OpenFlow protocol. However, it can, nowadays, act as an OpenFlow switch, and can be used for developing networking software.

POX work with Python 2.7 (it can also work fine with Python 2.6), and can run under Linux OS, Mac OS, and Windows. The core and main modules are developed in python [16].

In this section many tests are presented which explain some features and capabilities of Mininet emulator along with POX controller software in order to test the performance of Mininet tool in emulating software defined network by evaluating its performance on the network from down layer to top layer. The functionality of each layer is now shown with SDN networking paradigm. At first all the tests are conducted with the same simulation environment described in part A in this section. Thereafter, some additional tests are conducted for the purpose of comparing results obtained by Mininnet in two different simulation environments in order to explain its effect on the performance of Mininet in emulating software defined networks.

***A*. MININET environment specifications.**

In all the tests or experiments a computer DELL Inc. Inspiron1525 PC with the following specifications was used; processor Intel ® Core ™ 2 Duo CPU 2.00 GHZ,3072 MB of RAM running the operating system Windows 7 32bits and VirtualBox Oracle VM version 4.3.18.

The guest operating system: Mininet Emulator version 2.1 on Linux operating system Ubuntu14.0432bits with 1 GB of RAM and POX 0.2.0(carp) Controller are installed on this computer, under the management of VirtualBox.

***B*. Emulation of SDN Network Infrastructure**

In this section, the ability of Mininet tool in creating SDN network topology infrastructure is assessed. Mininet tool has the ability to create different network topologies. In addition, custom topologies can also be created by Mininet. One of those many topologies is created for the sake of showing how SDN network infrastructure is formed utilizing Mininet.

In SSH terminal, a topology with four hosts, one switch, and one remote controller was created. The connections between nodes were wired links. The created topology is shown in Figure 4 below.

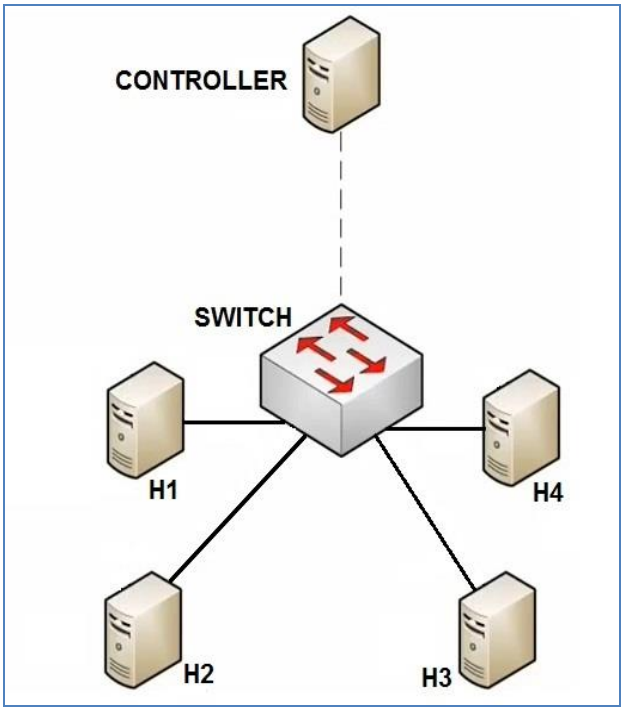

Fig. (4): The Simulated topology

The proposed topology created with the following command line:

$ sudomn - -topo single,4 - - controller remote

After the execution of the above-mentioned command, the script in Figure 5 below is displayed.

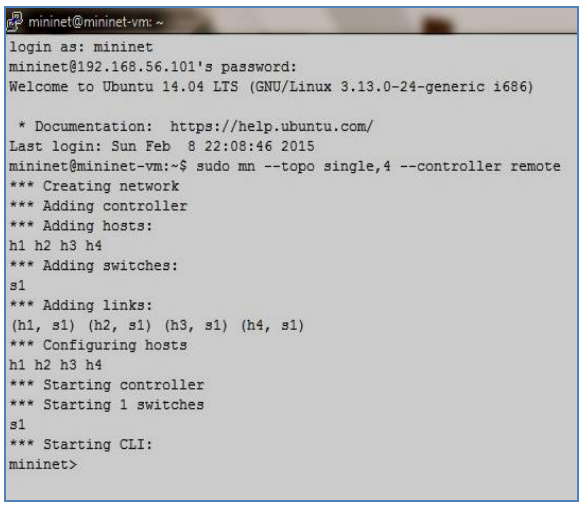

Fig. (5): The Emulated Topology

To test the connectivity of topology, a Ping test can be done:

Mininet>h1 ping –c1h10

The result of the ping test is shown as in Figure 6 below.

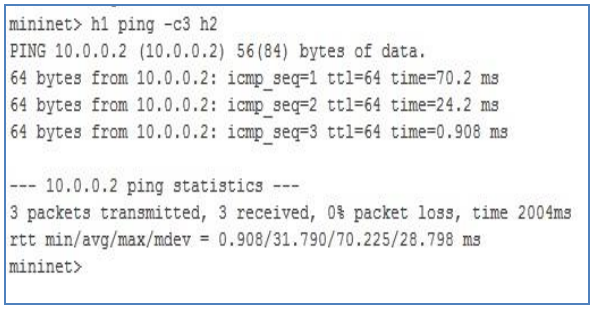

Fig. (6): Ping Connectivity Test

C. Southbound Interface (OpenFlow Protocol) Messages

An openflow-enabled forwarding device consists of flow tables where each entry of the table has three parts: (1) a matching rule, (2) actions to be executed on matching packets, and (3) counters that keep statistics of matching packets as shown in Figure 7.

The function of southbound (OpenFlow protocol) interface is emulated by Mininet and Wireshark analysis tool. It shows how messages are exchanged between the network infrastructure's; client, SDN centralized controller, and the HTTP server, when an HTTP request is issued by one of the clients.

To conduct the above, host (H4) is configured as a simple HTTP server while host (H1) as an HTTP client. The controller conducted a series of synchronized requests and acknowledgments among the HTTP client and the HTTP server utilizing openflow messages such as packet-in, flow modification, and packet-out messages.

At the beginning, there will be no matches in the flow table of the switch, therefore, an entry is created and the contents of this established new entry is shown in Figure 8 which is captured utilizing Wireshark analyzing tool.

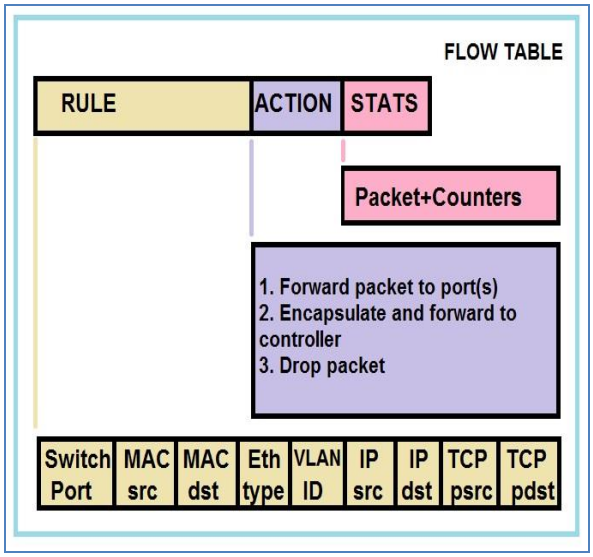

Fig. (7): OpenFlow Switch Flow Table

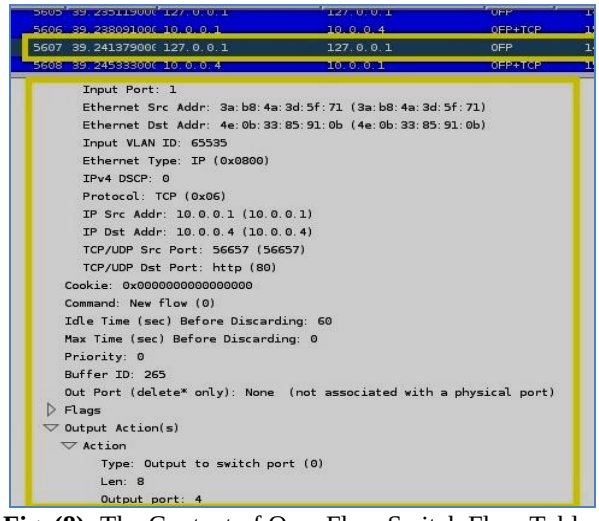

Fig. (8): The Content of OpenFlow Switch Flow Table Captured by Wireshark

The fields of openflow's switch flow table were shown in Figure 7 which is a theoretical representation of how the flow table should look like. Our practically obtained results are shown in Figure 8 which matches with the theoretical fields but with real contents.

D. The SDN Controller Plateform

In this test, the role of the controller in setting forwarding rules in the flow tables is explained. It also shows how it can control the behavior of forwarding hardware in the way of dealing with packets and also what happens in the absence of controller and what should we do alternatively. So, from Mininet console:

$ cd pox

Now the controller will be programmed as a hub:

$./pox.py log.level –DEBUG misc.of_tutorial

This tells POX to enable verbose logging and to start the of_tutorial component (which runs as a hub).

Now to verify the behavior of a hub, that all hosts see the exact same traffic when hosts ping each other, xterms for each host was created, the traffic in each host was viewable. In the Mininet console:

Mininet>xtermh1h2h3h4

In the xterms for h2, h3, and h4, we run tcpdump , a utility that print the packets seen by a host:

tcpdump –xx –n –I h2-eth0
tcpdump –xx –n –I h3-eth0

And respectively

tcpdump –xx –n –I h4-eth0

In the xterm for h1, we sent a ping:

ping -c1 10.0.0.2

The ping packets are now going up to the controller, which floods them out into all interfaces except the sending one. There should be identical ARP and ICMP packets corresponding to the ping in all the xterms running tcpdump. This is the behavior of a hub; it sends all packets to every port on the network as shown in Figure 9.

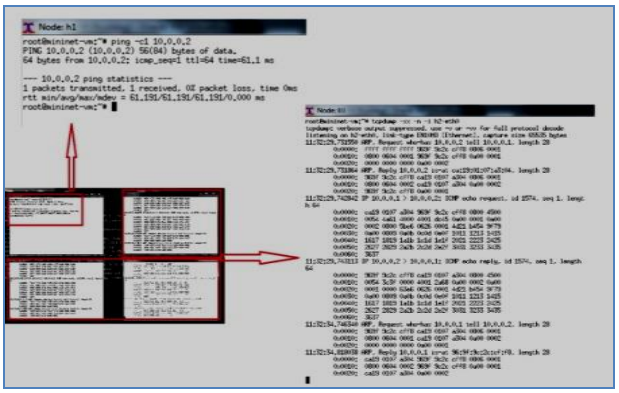

Fig. (9): The controller hub behavior.

The details and output text of controller hub behavior does not appear so clear in Figure 9, however, it was needed to show the real output of the emulator as it is. To make it clearer and readable, we added another two figures; the up arrow in Figure 9 refers to the output that is shown in Figure 10. The right arrow in Figure 9 points to the contents that are shown in Figure 11.

Figure 10 shows more details on the function of controller hub. It depicts the ping request source (node 1) content and successfulness status of receiving it with no loss. Figure 11 shows the ping destination in addition to all the receiving hosts, as it is depicted in Figure 11, all the hosts have the same contents and this is due to the hub behavior of the controller.

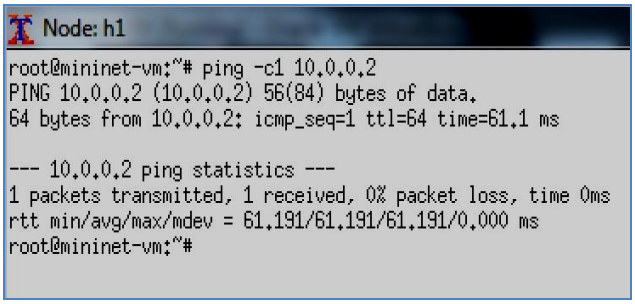

Fig.(10): Ping Request

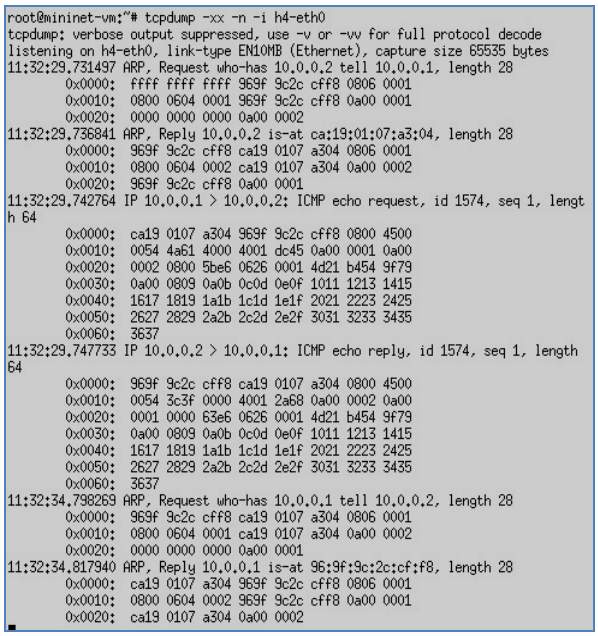

Fig. (11): The Content of Destination and All other Hosts (hub behavior)

Now the previous scenario will be repeated but this time with programming the controller as a learning switch by using the following component:

$ cd pox

$ python ./pox.py forwarding.l2_learning

Again in the xterm for host1a ping request is executed

ping –c1 10.0.0.2

Then as shown in Figure 12 only the destination host will receive the ARP and ICMP packets corresponding to the ping. Hosts that are not the destination for a ping should display no tcpdump traffic after the initial broadcast ARP request.

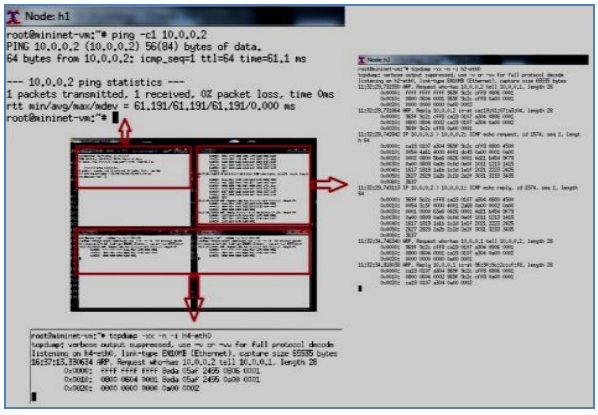

Fig. (12): The behavior of controller as a learning switch.

Contents of Figure 12 are; the ping source which is similar to what was shown in Figure 10, the ping destination which is depicted in Figure 11, and the hosts that are not listed in the destination address of the ping that display only an initial broadcast ARP request that as shown in Figure 13 below.

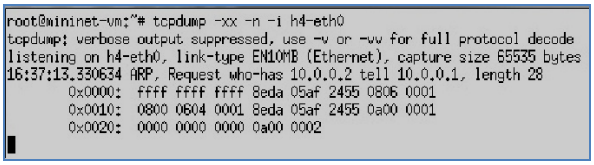

Fig. (13): Non Destination Hosts Content

To further have an insight into the role of controller in inserting fields into the forwarding rules, the controller was disconnected and another ping command was executed. Because switches are only forwarding hardware and there are no flow entries in its flow tables, all the ping packets were lost because of the absence of the controller, therefore; forwarding rules were entered manually as follow:

$ dpctl add-flow tcp:127.0.0.1:6634in_port=1,idle_timeout=120,actions=output:2

$ dpctl add-flow tcp:127.0.0.1:6634in_port=2,idle_timeout=120,actions=output:1

This will forward packets coming at port 1 to port 2 and vice-verca.

To display the flow table installed, this command line is used:

$ dpctl dump-flows tcp:127.0.0.1:6634

The content of manually entered flow table is shown in Figure 14.

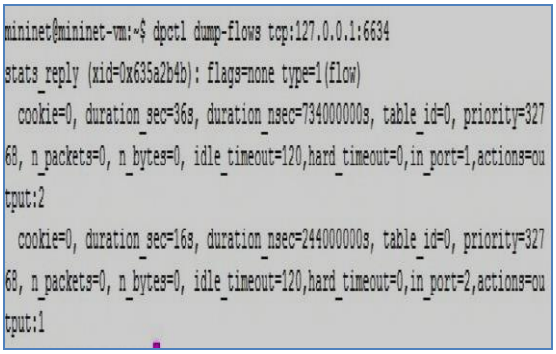

Fig. (14): The content of manually installed flow table

After installing a flow table with few last steps, a ping command could be executed and the destination host expected to receive the ARP and

ICMP packets corresponding to the ping request. It is important to remember that the above task, the manual case, was performed by the controller automatically in SDN paradigm.

E.SDN Applications and Nourthbound Interface

The Internet with its current structure still suffers from a variety of great challenges in network control, configuration, and management. For this reason, it is vital to review current methodologies and protocols available in the present networks for the purpose of QoS reservation for real-time applications or any other higher priority applications [18, 19]. Since the current methods for QoS provisioning in traditional networks are static, coming up with new innovative technologies to deal with this huge amount of traffic and QoS support is inevitable [20].

Therefore; the demand for network resources by critical real-time Internet applications will be supported in a dynamic manner utilizing a new proposed scheme and Software-Defined Networking (SDN) technology. The resource requirement of applications can be issued through polices by the SDN controller at run-time so providing dynamic QoS to the real time applications that matches their requirements and provide better quality of experience (QoE) to the end users than that provided in traditional networks although the available resources are the same in both cases[19].

This SDN topic include so many issues and details, testing one of the SDN layers on its own would not lead to a real indication of the performance, for this reason, Mininet is utilized in such as way so that real time application resources' requirements are programmed to interact with SDN controller[20].

F. Mininet Performance in Two Different Environments

Although Mininet is considered as a great and convenient tool, it still has some limitations. In this experiment the effect of one of its limitations on its scalability was studied. Because Mininet runs on a single system, it imposes resource limitation. Those resources need to be normalized and shared among virtual hosts and switches.

A comparison between two sets of scalability tests were conducted, where, two different environments were tested. Each test environment differs from the other by the resource characteristics. The first set of scalability test was conducted by using the following environment: a microcomputer HP Compaq8200 Elite SFF PC with the following specifications: Processor Intel ® Core ™ i5-2400 3.10GHz, 4GB of RAM running the Operating System Windows 7 64bits and VirtualBox Oracle VM version 4.2.12.

In this microcomputer, under the management of VirtualBox, the following guest operating systems were installed: Mininet Emulator version 2.0 on Linux operating system Ubuntu 10.12 64bits with 1Gb of RAM; Floodlight Controller version 0.90 on Linux operating system Ubuntu 12.10 64bits with 256MB of RAM.

The obtained scalability results are shown in Table I.

Table (I): First Scalability Test Results

Node Numbers	Host Numbers	Switch numbers	Start/stop Time(sec)
3	2	1	0,190
7	4	3	0,525
15	8	7	1,175
31	16	15	2,795
63	32	31	7,088
127	64	63	20,210
255	128	127	64,818
511	256	255	242,842

From the second set of scalability test, which was conducted with the characteristics specified in part (A) of this section, the scalability results displayed in Table 6 were obtained.

Table (2): Second Scalability Test Results

Node numbers	Host numbers	Switch numbers	Start/stop time(sec)
3	2	1	5,611
7	4	3	16,162
15	8	7	35,480
31	16	15	77,304
63	32	31	172,535
127	64	63	410,153
255	128	127	1054,714
511	256	255	3718,117

Comparing results of the two different scenarios mentioned above gives an indication that

the amount of time required to create a virtual network increases with the increase of virtual nodes number in both scenarios, however, there is a remarkable difference in the required time between the first and second scenario which means that the resource limitation has a huge impact on the results as depicted in Figure 15.

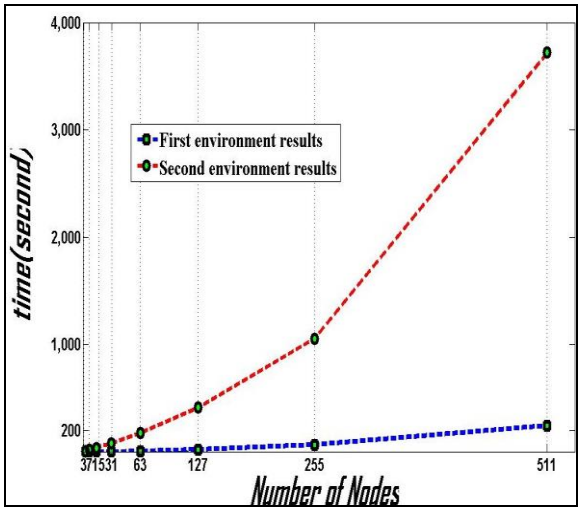

Fig. (15): Comparison between scalability tests results in different environment**.**

V. CONCLUSIONS

In this paper the performance of Mininet tool for emulating SDN networks was evaluated. During this study many capabilities of Mininet emulator in the SDN paradigm evaluation was covered, from the creation of basic topologies with reference controller to the ability of connecting with remote controllers (in this case POX controller).

The effect of simulation environment with limited resources was studied and a comparison between results for two different environments was conducted, it was noted that for small number of nodes, the time required for the creation (start/stop) is increased from 0.190 sec in the environment of better resources to 5.611 sec in the environment of worse resources. The time required for creation (start/stop) in both environments increases with the increase in the number of nodes but with different rates. Therefore, with the large topology (511 nodes), the time increased from 242.842 sec in first the environment to 3718.117sec in the second environment. In other words, with large topology, the second environment is 15 times slower than the first environment. It was concluded that the characteristics and qualifications of simulation environment must be taken into consideration if accurate results are need by mininet. If the above characteristics were carefully selected then Mininet can be utilized as one of the powerful tools in emulating the SDN and virtual networks.

REFERENCES

- WANG Wendong, Yannan HU, XirongQUE, GONG Xiangyang, “Autonomicity Design in OpenFlow Based Software Defined Networking”, GC'12 Workshop: The 4th IEEE International Workshop on Management of Emerging Networks and Services©2012 IEEE.
- Adrian Lara, Anisha Kolasani, Byrav Ramamurthy, “Simplifying network management using Software Defined Networking and OpenFlow”, 2012 IEEE International Conference on Advanced Networks and Telecommunciations Systems (ANTS).
- Guohui Wang, T. S. Eugene Ng, Anees Shaikh, “Programming your network at run-time for big dataapplications”,HotSDN’12, Helsinki, Finland, August 13, 2012.
- RogérioLeão Santos de Oliveira, Ailton Akira Shinoda, Christiane Marie Schweitzer, Ligia Rodrigues Prete, “Using Mininet for Emulation and Prototyping Software-Defined Networks”, Brazil, ©2014 IEEE.
- Kannan Govindarajan, Kong Chee Meng, Hong Ong , Wong Ming Tat,SridharSivanand, Low Swee Leong, “Realizing the Quality of Service (QoS) inSoftware-Defined Networking (SDN) Based Cloud Infrastructure, Kualalumpur, Malaysia, 2014 second international conference on information and communication technology(ICoICT),©2014IEEE.
- Cristian Cleder Machado, Lisandro Zambenedetti Granville, Alberto Schaeffer-Filho,Juliano Araujo Wickboldt, “Towards SLA Policy Refinement for QoSManagement in Software-Defined Networking”, 2014 IEEE 28th International Conference on Advanced Information Networking and Applications.
- S. Sezer, S. Scott-Hayward, P. Chouhan, B. Fraser, D. Lake, J. Finnegan,N. Viljoen, M. Miller, and N. Rao, “Are we ready for sdn? Implementationchallenges for software-defined

networks," CommunicationsMagazine, IEEE, vol. 51, no. 7, pp. 36–43, 2013.

- O. W. Paper, "Software-Defined Networking: The New Norm for Networks," Open Networking Foundation, Tech. Rep., April 2012.
- Thomas D. Nadeau, Ken Gray, "SDN: Software Defined Networks", Published by O'Reilly Media, Inc., 1005 Gravenstein Highway North, Sebastopol, CA 95472, First Edition, August 2013.
- Sugam Agarwal, Murali Kodialam, T. V. Lakshman, "Traffic Engineering in Software Defined Networks", 2013 Proceedings IEEE INFOCOM, Work done at Bell Labs, ©2013 IEEE.
- Bruno Astuto A. Nunes, Marc Mendonca, Xuan-Nam Nguyen, Katia Obraczka, and Thierry Turletti, "A Survey of Software-Defined Networking: Past,Present, and Future of Programmable Networks", hal-00825087,version 5- 19 Jan 2014.
- Joe Mambretti, Jim Chen, FeiYeh, "Software-Defined Network Exchanges (SDXs): Architecture, Services, Capabilities, and Foundation Technologies", Proceedings of the 2014 26th International Teletraffic Congress (ITC), ©2014 ITC.
- Mininet. An Instant Virtual Network on your Laptop.2014, Accessed: Sept. 2014[Online]Available: http://mininet.org.
- B. Lantz, B. Heller, and N. McKeown, "A network in a laptop: rapidprototyping for software-defined networks," in Proceedings of the 9thACMSIGCOMM Workshop on Hot Topics in Networks. ACM, 2010.
- The Openflow Switch, openflowswitch.org.

[16] POX, "Pox openflow controller," 2014, Accessed: Sept.2014. [Online].Available: http://www.noxrepo.org/pox/about-pox.

- Python Software Foundation, "Python language reference, version 2.7," 2014, Accessed: Sept. 2014. [Online].Available: http://www.python.org,.
- Yitzhak Bar-Geva, Jon Crowcroft/Helen Oliver, "Tearing down the Protocol Wall with Software Defined Networking", The work is enabled by generous funding by the EPSRC for the INTERNET project.
- Himal Kumar, Hassan Habibi Gharakheili, Vijay Sivaraman, "User Control of Quality of Experience in Home Networks using SDN", IEEE ANTS 2013 1569797953 .
- Myung-Ki Shin, Ki-Hyuk Nam, Hyoung- Jun Kim, "Software-Defined Networking (SDN): A Reference Architecture and Open APIs", ©2012 IEEE

DISTRIBUTION OF RH. ANTIGENS (D,C,c,E,e) AMONG BLOOD DONORS IN DUHOK PROVINCE – KURDISTAN REGION

MAJEED **K**HAMO **A**HMED
Dept. Blood Bank, Directorate of Health, Duhok, Kurdistan Region

(Received: July 9, 2015 ; Accepted for publication: November 12, 2015)

ABSTRACT

Information of blood antigens and phenotype dissemination is vital for blood donation centers and transfusion administration strategies. The current study aims to evaluate the frequency of Rh. Antigens (D,C,c,E,e) Among Blood Donors in Duhok Province.

Materials and Methods: The study was conducted on 500 blood donors recruited to the blood bank at Duhok province between January to April 2015. Blood samples have been collected from each donor. ABO and Rh phenotype reactivity was dictated by utilizing tube system as indicated by the producer's direction. The Rh antigens investigated were D, C, c, E and e.

Result: The predominant blood group was O(38.6%), then A(37.2%), B(18.6%) and the lowest blood group was AB(5.6%). 450 (90%) 0f the blood donors were Rh(D) +ve and the other 50 (10%) were Rh (D) –ve. Rh antigen phenotype (E,e,C,c,D) was found to be as 474 (94.8%) of the blood donors have had e antigen, 143 (28.6%) have E antigen, 360 (72%) have c antigen and 389 (77.8%) have C antigen.

Conclusion: The study demonstrates that the most continuous Rh antigen in Duhok province is e antigen. Ten Rh-antigen complexes phenotypes of different frequencies were recorded.

KEY WORDS: Rh antigens, blood transfusion, blood groups)

INTRODUCTION

The Rhesus blood bunch framework (ISBT 004) is the normal complex blood bunch framework; involving 46 antigens numbered RH1 to RH53 with seven numbers out of date (Daniels, 2002). It is the most polymorphic human blood bunch, and beside ABO, the clinically noteworthy in transfusion drug (Flegr et al., 2009). In Rh blood framework, 18 phenotypes can be recognized by utilizing five sorts of against D,C,c,E,e (Daniels, 2002). Eight essential haplotypes are framed from primitive haplotype cDe by a progression of duplication, point change and recombination occasions (Gates et al., 2010 and Flegel et al., 2000b). The frequencies of these haplotypes shift among diverse populaces (Daniels et al., 2006). From serological results, it is regularly difficult to focus the genuine genotype of an individual and phenotypes are infrequently symbolized as the most plausible genotypes reasoned from known haplotype frequencies (Daniels, 2002). Serologically comparative phenotypes have diverse atomic foundations (Reid et al., 2004).

The importance of Rhesus antigen was found in 1939 by Levine taking after infusion of human erythrocytes in Rhesus monkeys. The monkeys created particular antibodies which agglutinated the red cells of 85% of ABO good donors (Conteras et ., 1999). The Rhesus framework is considerably more perplexing than the ABO framework; at the present time the Rh blood bunch framework is made out of more than 50 separate specificities. The representation of Rh variable is controlled by two nearly connected qualities on chromosome one; one quality codes for D and the other quality for CcEe (Mollison , 1994 and Issit, 2001). The D-antigen, which is the most immunogenic red cell antigen after A and B and is the most essential in transfusion solution, since hostile to D arrangement ordinarily comes about because of introduction through either pregnancy or transfusion of red cells having the D-antigen to individual who do not have this antigen (Knowles, 2001). The D unwilling phenotype has either rh particular successions positive or rh complete erasure. The aggregate recurrence of different rh alleles in D negative Europeans is 1:1,500 (Wagner et al., 2001). On the other hand, in Africans and Asians, the

frequencies are entirely different. In D miserable Han Chinese, around 19.9%(all C+) have a terribly in place Rh, 168 % convey at minimum one rh exon (Xu et al., 2003), and in D negative African, around 82 % African have RHDW and RHD-CE-D cross breed quality (Singleton et al., 2000). The D-antigen is the most immunogenic of the Rh antigens and the clinically most vital (Daniels, 2002). Hostile to D for the most part is presented after blood transfusion or pregnancy. Around 85 % of D negative beneficiaries produce against D taking after transfusion of 200 ml or a greater amount of D clear red cells (Barry et al. 1999) and as meager as 0.1 ml of D good blood can vaccinate D skeptical beneficiary (Woodrow et al., 1968). Indeed, even feeble D sort 2 (Flegel et al., 2000a) or DEL phenotype (Wagner's et al., 2005) red cells can cause D unwilling beneficiary to create against D. Clinically, hostile to D can possibly cause hemolytic sickness of the infant, transfusion responses and immune system hemolyticus sickness. Information of Rh phenotypes in given populace is important for better arranging and administration of a blood donation center; to discover good blood for patients requiring various blood transfusions, which would resolve the blood transfusion needs of beneficiaries. An irregular study for Rh in Aljouf, Sakaka populace was uncovered rh allele dispersion characters and characterizes its frequencies; it was likewise be advantage for aggregating human hereditary information and valuable rules for transfusion systems (Fathelrahman et al., 2013).

Three strategies for Rh classification were depicted. Fisher and Race suggested that the Rh antigens were controlled by three nearly connected qualities offering ascent to eight quality complex or haplotypes: CDe, cDE, CDE, cde, Cde, cdE , CdE and cDe. At about the same time, Wiener suggested that there was one and only Rh quality, controlling various blood variables, proportionate to C, c, D, E, e5. Rosenfield proposed an arrangement of terminology in view of serologic perception. Images were not expected to pass on hereditary data, only to encourage correspondence of phenotypic information. Every antigen is given a number, by and large in the request of its revelation or its task to the Rh system (Roback et al., 2008). Information of Rh phenotypes in given populace is pertinent for better arranging and administration of blood donation center; the fundamental objective is to discover good blood for patients requiring different blood transfusions (Al-Sheikh et al,. 1998).

Information of Rh phenotypes in given populace is pertinent for better arranging and administration of Blood Banks (Al-Sheikh et al., 1998). Patients requiring numerous blood transfusion like those with sickle cell ailment, thalassemias, and so forth, are not few in our locale, they may create allo-antibodies against Rh antigens. To discover good blood for such patients, we have to know Rh phenotypes of the benefactors and beneficiaries.

The current study aims to evaluate the frequency of Rh. Antigens (D,C,c,E and e) Among Blood Donors in Duhok Province.

Methodology & Subjects

The ABO and Rh serological investigations are conducted in the Blood Bank Department of Health Directorate in Duhok province from January to April 2015. Through this period a sum of 500 male with distinctive ages, gave blood for different reasons were assessed for the ABO and Rh antigens (c,C,e,E and D).

Serology

Two ml of venous blood was taken from every subject into EDTA tubes. The blood tests were done by tube technique utilizing ABO and Rh (D) writing Antisera Seraclone, Biotec Lab, Germany. All D negatives results were affirmed minutely. Albumin and AHG test were utilized as control and for feeble D affirmation. RBCs were phenotyped for C, c, E and e antigens as per standard serologic conventions (tube strategy) using monoclonal antisera from DiaMed-Switzerland.

RESULTS

Five hundred apparently healthy blood donors were enrolled in the current study. Their ages ranged between 18-60 years. The hemoglobin concentration ranged between 13.5 – 17.5 gm/dL. Out of the 500 enrolled blood donors, 193 (38.6%) were blood group O, 186 (37.2%) were blood group A, 93 (18.6%) were blood group B and 28 (5.6%) have AB blood group, table 1. Four hundred fifty (90%) blood donors have had Rh (D) phenotype when they were (Rh +ve), the other 50 (10%) were Rh (D)–ve .

Table (1): The frequency of ABO blood group among the blood donors enrolled in the current study:

ABO blood group	Number of donors
A	186 (37.2%)
B	93 (18.6%)
O	193 (38.6%)
AB	28 (5.6%)
Total	500

The distribution of the Rh antigens (e, E, c and C) are shown in table 2, 474 (94.8%) of the blood donors have had e antigen, 143 (28.6%) have E antigen, 360 (72%) have c antigen and 389 (77.8%) have C antigen.

Table (2): The distribution of (e, E, c, and C) Rh antigens in blood groups of the donors:

Rh antigen phenotype	Number & %
e	474 (94.8%)
E	143 (28.6%)
c	360 (72%)
C	389 (77.8%)

The frequency of the Rh- antigen complexes among the blood donors is shown in table 3.

Table (3): The frequency of the Rh- antigen complexes among the blood donors

Rh-antigen complex	No. & %
DCcEe	142 (28.4%)
DCEe	76 (15.2%)
DCce	57 (11.4%)
DCe	44 (8.8%)
De	21 (4.2 %)
D	101 (20.2%)
Null	33 (6.6 %)
DcE	23 (4.6 %)
ce	3 (0.6 %)
Total	500

DISCUSSION

The Rhesus (Rh)D was, actually, the fourth blood group found, positioned second to ABO framework in terms of clinical significance. (Ahmed, et al., 2009). Both are of equivalent significance in straightforward and criminological prescription. It is so recommendable to figure out the appropriation of Rh phenotypes furthermore, genotypes in Duhok Province of the Kurdistan district in Iraq since there where no prior serological information are accessible. In the current study, blood bunch O was discovered overwhelming and AB was remained on the most reduced side among the 500 blood givers examined Comparative appropriation example of ABO blood gatherings was accounted for in Saudia Arabia, Egypt, Jordon, Nigeria, and Kenya. In any case, different nations, for example, Syria, Lebanon, Israel and Jordan have a surprising ABO conveyance design in which blood bunch A was overwhelming. This may be credited to their particular ethnic foundation, other than examining technical errors. Additionally, in concurrence with past studies (Bashwari et al., 2001; Hanania et al., 2007 and Sakharov et al., 1996). Regarding the frequency of Rh blood group in the current study, the Rh+ve (90%) and Rh-ve (10%) are in favor with those results reported by Jena.

In a study conducted in Baghdad, Iraq, the recurrence of Rh +ve and Rh -ve were 87% and 12.8% individually however the number

contemplated was littler than the present study (Jaff, 2010). As regarding to phenotype in Rh negative subjects, the most predominantly seen in this study was DCcEe which is unlike that reported in studies directed in Iraq, Saudia, Kuwait and West, in which ce was more common (Jaff, 2010 and Al-Shiekh, 1998). This likely attributed to the change in the character of populace amid the previous years, for example, migration, Wars and marriage to non-natives. Precisely 50 years back, R.A.Fisher and R.Race proposed a model for the advancement of the Rh (rhesus) qualities in which the less regular haplotypes were gotten from the ordinary person ones by recombination, and in which the quality request was D-CE. No immediate proof bearing on this model was accessible at that point, and has not been, as of recently (Carritt, et al., 1997). The most likely haplotype frequencies by and large the white gathering demonstrated a nearby likeness to those of the canary islands (Planas et al., 1969) and Southern Spain (Valls, 1975) with a dreadful recurrence of cDe haplotype and a towering recurrence of cde. Negroes had the CDE haplotype, with modestly base recurrence of cDe and lifted CDe recurrence, particular from the lion's share of African tests (Mourant et al., 1976).

REFERENCES

- Ahmed, S.G; M.B. Kangu and U.A.M. Abjah. 2009 . The role of du testing in scaling down the burden of Rhesus-D negative transfusion in Northern Nigeria. Int. J. Third World Med., Vol. 8 (2).
- Al-Sheikh, IM; Zaidi SZA, Islam SIA, 1998. Frequency of various Rh antigens in Dammam Eastern province, Saudi Arabia. Saudi.Med.J.; 19(3):265-68.
- Am. J. of Hem. 1999; 60: 245–247.
- Barry, A.; Aziza T., Joseph E., S. and Gerald S. Successful Prevention of Post-Transfusion Rh Alloimmunization by Intravenous Rho (D) Immune Globulin (WinRho SD),
- Bashwari LA, Al-Mulhim AA, Ahmad MS, Ahmed MA 2001. Frequency of ABO blood groups in Eastern region of Saudi Arabia. Saudi Med J, 22(11): 1008-1012.
- Carritt, B., Kemp T. J., and Poulter M. Evolution of the human RH (rhesus) blood group genes: a 50 year old prediction (partially) fulfilled Human Molecular Genetics, 1997; 6(6): 843–850.
- Conteras M and Lubenko A. Antigen in humen blood. In postgraduate haemotology by Haffbrand AV, Lewis SM and Tuddenham EGD. Fourth ed. Butter Worth-Heinemann, Oxford, 1999, Cahp. 10: 182-214.
- Daniels G et al. The clinical significance of blood group antibodies. Transfusion Medicine 2002;12:287–295.
- Daniels G, Finning K, Martin P, Summers J . "Fetal blood group genotyping: present and future". Annals of the New York Academy of Science, 2006; 1075: 88–95.
- Fathelrahman M. Hassan, Meshref A. Alruwaili and Atef H. Abdelhamid. The frequency of rhesus alleles, haplotypes and genotypes in major Sakaka city population, Aliof region, Saudia Arabia. Asian Journal of Science and Technology 2013, 4: 03;044-048,
- Flegel WA, Khull SR, Wagner FF: Primary anti-D immunization by weak D type 2 RBCs. Transfusion 2000a; 40: 428-434.
- Flegel WA, Wagner FF: Molecular genetics of RH. Vox Sang. 2000b; 2: 109- 1 15.
- Flegel WA: Molecular genetics of RH and its clinical application. Transfus Clin Biol. 2006; 13: 4-12.
- Gates, MA; Wolpin, BM; Cramer, DW; Hankinson, SE; Tworoger, SS. "ABO blood group and incidence of epithelial ovarian cancer.". International journal of cancer.
- Hanania S, Hassawi D, Irshaid N 2007. Allele frequency and molecular genotypes of ABO blood group system in Jordanian population. J Med Sci, 7(1): 51-58.
- Issitt PP. The Rh blood group system: From clumps to clones. Transfusion 1994, 34: 462-63.
- Jaff MS. ABO and Rhesus Blood Group Distribution in Kurds. J of Blood Medicine 2010; 1: 143-6.
- Knowles SM. Red cell blood group antigens and antibodies. In practical haematology by Lewis SM, Bain BJ and Bates I. Ninth ed. London: Churchill Livingstone, 2001: 429-71.

- Mollison PL. The genetic basis of the Rh blood group system. Transfusion 1994, 34: 534-41.
- Mourant, A.E., Koppec, A.C. and Domaniewska-Sobczak, K. 1976. The distribution of the Human Blood Groups and other polymorphisms. 2nd ed. Oxford University Press, London.
- Planas J., Fuste, M., Diaz, J.M. and Pons, J. 1969 Blood groups (Rh, ABO) in thev population of Gran Canaria(Canary Islands, Spain). Hum. Hered. 19: 185 - 189.
- Reid ME, Lomas-Francis C: The blood group antigen factsbook. 2nd Edition. Elsevier Academic Press, California, S.2004; 124 .
- Roback J, Combs MR, Grossman B, et al. Technical Manual. 16th Ed. Bethesda: American Association of Blood Banks (AABB), 2008: 387-409
- Sakharov RS, Nofal'Kh K 1996. The frequency of ABO blood groups and the expression of group antigens and isohemagglutinins in Syrian Arabs. Sud Med Ekspert, 39(2): 34-36.
- Singleton BK, Green CA, Avent ND, Martin PG, Smart E, Daka A, Narter-Olaga EG,Hawthorne LM & Daniels G (2000). The presence of an RHD pseudogene containing a 37 base pair duplication and a nonsense mutation in Africans with the Rh Dnegative blood group phenotype. *Blood*, 95: 12-18.
- Valls, A. Seroantropologia de la poblacion Espanola. Rev. Univ. Complutense XXXIV; 1975(97) 111 -139.
- Wagner FF, Ernst M, Sonneborn HH, Flegel WA: A D(V)-like phenotype is obliterated by A226P in the partialD DBS. Transfusion . 2001 a; 41: 1052-1058 .
- Wagner T, K GF, Buchta C, Vandon M, Lanzer 0, Mayr WR, Legler TJ: Anti-D immunization by DEL red blood cells. Transfusion. 2005; 45: 520-526.
- Woodrow, J. C. and Donohoe, W. T. A. Rh-immunizationby pregnancy: results of a survey and their relevance to prophylactic therapy. British Medical Journal, 1968; 4: 139-144.
- Xu Q, Zhang J, Wang Q, Zhang S, Si 0: RHD gene polymorphism among RIiDnegative Han Chinese. Chin Med J. 2003; 116: 1539-1543.

DATE EXTRACT AS A CARBON SOURCE FOR THE PRODUCTION OF XANTHAN GUM BY THE BACTERIUM XANTHOMONAS CAMPESTRIS

MUSTAFA **M H**AIDER
Dept. of Biology, Faculty of Science, Duhok University, Kurdistan Region, Duhok, Iraq.

(Received: July 26, 2015; Accepted for publication: November 5, 2015)

ABSTRACT

This study was designated to evaluate the influence of incubation periods, different carbon concentrations in the form of date extract and different nitrogen sources, on the production of exopolysaccharide "xantha gum" by previously isolated and characterized bacterium *Xanthomonas campestris* MU1. Maximum xanthan gum accumulated was observed in date extract medium of 4% sugar containing ammonium nitrate as nitrogen source after 4 day of incubation, yielding 0.85g/100ml at agitation rate of 150RPM of rotary incubator. The final pH of the tested media was declined owing to the acidic nature of the accumulated xanthan.

KEYWARDS: *Date extract, Nitrogen sources, Xanthan gum, Xanthomonas campestris*

INTRODUCTION

Xanthan gum (exoplysaccharide) is a natural thickener derived from fermentation of glucose or sucrose or other carbon sources by a bacterium, the *Xanthomonas campestris* (Sutherland, 1990; Galindo, 1994). It was approved as a safe food additive in 1968; it is used primarily as a thickener agent because of its ability to enhance the viscosity of liquids (Kamal and Mehrgan, 2002).

Xanthan is a heteropolysaccharide with a very high molecular weight consisting of repeating pentasacchride units, formed by two glucose units, two mannose units and one glucuronic acid unit in the molar ratio 2.8:2:1 (Cadmus *et al*., 1978).

The glucose is linked to form a 1,4-glucan cellulosic backbone, and alternate glucoses have a short branch consisting of a glucuronic acid located between two mannose units. The side chain consists, therefore, of mannose-1,4-glucuronic acid-1,2- mannose (Cottrell and Kang, 1978; Kennedy and Bradshow, 1984).

The terminal mannose carries pyruvate residues linked to the 4- and 6- positions.The internal mannose unit is acetylated at C-6. Acetyl and pyruvate substituents are linked in different proportion to the side chains, depending upon the isolated *X. campestris* strain and fermentation conditions (Becker *et al.*, 1998). Because of emulsion stabilization, excellent stability and solubility in basic and acidic solution and resistance to degradation at high temperature and at various level of pH, high degree of pseudoplastisity and high viscosity even at low concentration, xanthan has many applications in food, cosmetics, pharmaceutical and oil industries, where it is commonly used in drilling fluids and in enhancing oil recovery (EOR) processes (Galindo, 1994; García-Ochoa *et al.*, 2000; Borges and Vendruscolo, 2007; Anbuselvi *et al*.**,** 2012).

Many investigators reported that the production of xanthan gum by the bacterium *X. campesteris* is affected by the nature, composition and physical properties of fermentation media (Souw and Demain,1979; Prell *et al*. 1995;Tait *et al*., 1986; Lo *et al*., 1997; Carignato *et al*., 2011) and also on the bacterial stain (Vidhyalakshmi *et al.*, 2012).

Different natural carbon sources were used as a fermentation media for biosynthesis of xanthan by different strain of *X. campestris* as hydrolyzed starch, corn syrup, hydrolyzed rice, barley and corn flour, acid whey, sugarcane molasses, coconut juice, sugar cane, beet molasses, date juice palm, corn steep liquor and cheese whey, etc. (De Vuyst and Vermeire, 1994; El-Salam *et al*., 1994; García-Ochoa *et al.*, 2004; Kalogiannis *et al*., 2003; Kongruang, 2005, Rosalam and England, 2006 ; Gilani *et al*., 2011; Ben-Salah *et al*., 2011). Reports on the isolation of wild strains of *X. campestris* having potentiality to produce xanthan gum are very limited. Scamparini and Rosato (1987), and Torrestiana *et al.*, (1990), have reported that the isolation of several wild *Xanthomonas* strains some of which are produced a high quantity of xanthan gum. In this study, the potential activity of local isolates of *X. campestris* MU1with respect to xanthan gum production during different periods of incubation was determined using date extract as a basal medium and carbon source supplemented with different nitrogen sources.

MATERIALS AND METHODS

Microorganism

A local strain of *X. campestris* MU1which was previously isolated from infected cabbage leaves *(Brassica oleracea)* of yellow necrotic lesion and characterized (Kassim, 2011). It was maintained in malt-yeast (MY) extract agar slants which consists of (g/l) glucose, 10; peptone, 5; yeast extract, 3; malt extract, 3; agar15 at 4°C and subcultured for activation every two weeks.

The production of inoculum

The inoculum was prepared by the inoculation of 250ml size conical flasks containing 50ml of MY broth medium from 3days old bacterial slants. The pH of the medium was adjusted to 7.0 before autoclaving at 121°C for 15min. The inoculated flasks were incubated in a rotary incubator at 150rpm and 28 ± 1°C for 72hrs. These cultures were used as a seed for the inoculation of each formulated medium used for the production of xanthan (Kassim, 2011)

Growth medium

Iraqi date syrup was used as a growth medium and as a carbon source, in which the date fruits were washed well and boiled in distilled water for 7-8hours. After cooling, date syrup was separated from the debris by centrifugations. The sugar concentration in the date syrup was 65% from which different carbon concentration were prepared (2, 4, 6, 8, 10 and 12)%. urea was added at a concentration of 0.2% as a nitrogen source unless otherwise stated (Borges and Vendruscolo, 2007). The broth medium was mixed well and completed to the final volume after the adjustment of pH at 7.0

Cultural conditions

The growth medium of each experiment was prepared and distributed into 250 ml Erlenmeyer flasks in triplicate samples each of 45ml of broth medium. Then, they were plugged before autoclaving for 15 minutes at 121ºC. After cooling, the culture flasks were inoculated with 5% of bacterial cell suspension. After that the inoculation culture flasks were incubated in a rotary shaker (150rev/min) for sufficient time at 28±1ºC.

Analytical methods

During fermentation cycles, at regular time intervals, triplicated samples were withdrawn and analyzed for growth, levels of xanthan residual sugar and final sugar. Growth was measured by cell dry mass determination. The samples were, therefore, centrifuged, the centrifuged cells were washed twice with distilled water and centrifuged again. The precipitated cells were dried at 75°C for 24hrs. The crude xanthan gum was precipitated from the supernatant by the addition of two volumes of cold acetone, thereafter, the mixture was centrifuged and the precipitate was collected and repeatedly dissolved in distilled water and reprecipitated with two volumes of cold acetone, then dried at 50°C to constant weight (Davidson, 1978). Initial and residual sugar was determined by the phenol sulphuric acid method (Dubois *et al*., 1956) using glucose as a standard.

RESULTS AND DISCUSSION

Production of xanthan gum at different incubation periods

The results of growth, xanthan production uptake of sugar and final pH of *X. campestris* MU1culturs incubation periods of 7days in fermentation medium are given in table (1). The bacterium produced 0.27g/100ml xanthan within 2days of incubation. Xanthan gum continued to increase with incubation time reaching maximum xanthan production of (0.67 g/100ml) after 4days of incubation, then started to decrease with the time reaching (0.41g/100ml) at the end of the experiment (7days). The results showed that sugar uptake is directly related to the growth of the bacterium and xanthan production. Referring to xanthan production, our result is consistent with the results obtained by Pensrity (2006) who pointed out that maximum xanthan production by the bacterium *X. campestris* 2B 1459 was obtained after 4days of incubation. Moreover, Souw and Demain (1979) stated that, maximum xanthan production was obtained after only 5 days of incubation using the same mentioned bacterial strain.

Torrestiana *et al.,* (1990) showed that, 0.8 g/l xanthan was obtained after 48hrs of incubation by different strains of *X. campestris*, while maximum xanthan production was obtained after three day of incubation (Gilani *et. al*., 2011; Murugesan *et al*., 2012) . The decreases in the amount of xanthan produced after 4 days of incubation might be due to the effects of accumulated toxic lipids that affect the metabolic pathway of xanthan production (Kamal and Mehrgan, 2002). Moreover, the low rate of xanthan acumulation at the beginning of incubation periods may be attributed to the utilization of some sugar for the biosynthesis of required energy for bacterial growth and for anabolic reactions. By increasing the number of bacterial cells, promoted the increase of xanthan production (De Vuyst and Vermeire, 1994).

Table (1): The effect of incubation periods on xanthan production by *X. campestris* MU1

Incubation (days)	Biomass (g/100ml)	xanthan g/100ml	residual (%)	Final pH
2	0.08 (0.002)	0.27 (0.041)	2.93 (0.001)	6.21 (0.000)
3	0.23 (0.014)	0.53 (0.021)	2.17 (0.023)	5.45 (0.004)
4	0.39 (0.028)	0.67 (0.000)	1.88 (0.022)	5.78 (0.001)
5	0.44 (0.009)	0.61 (0.009)	1.48 (0.051)	5.66 (0.001)
6	0.43 (0.002)	0.48(0.209)	1.08 (0.042)	5.52 (0.087)
7	0.38 (0.308)	0.41(0.015)	0.07 (0.200)	5.50 (0.153)

Each number represents the mean of three replicates and the numbers between brackets represent the standard deviation (± SD)

The effect of sugar concentration

Xanthan gum production by different strains of *X. campestris* using different sugar concentration has been investigated by many researchers. As shown in Table 2, the production of xanthan by the bacterium *X. campestris* was affected by the level of sugar added to the culture medium. Gradual increasing of added sugar concentration to the culture media stimulated the biosynthesis of xanthan and the height accumulation of xanthan was achieved in fermentation medium containing 4%sugar, (0.77g/100ml). By increasing sugar level in the culture media above 4% has inhibition effect on the accumulation of xanthan gum.

This result was in agreement with Funahashi *et. al*., (1987) and Niknezhad *et al.,* (2014) who stated that, maximum xanthan production was obtained at sugar concentration of 4% using two different strains of *X. campestris*. Lo *et al.,* (1997) stated that the maximum yield of xanthan was obtained by *X. campestris* when the culture medium containing 5% sugar in the form of glucose, while, Murugesn *et al*., (2012) found the availability of acidified sugar cane molasses at a concentration of 1% in culture medium stimulated xanthan biosynthesis by *X. campestris* MTCC 2286. Moreover, the preseces of cassava starch at a concentration of 3% as acarbon source highly stimulated xanthan production by *X. campestris* 8004 (Li *et al*., 2012). The variation between these results may be attributed to the bacterial strains and nature of the culture media.

Table 2: The effect of sugar concentrations on xanthan production by *X. campestris* MU1

Sugar (%)	Biomass (g/100ml)	Xanthan (g/100ml)	Residual (%)	Final pH
2	0.14 (0.003)	0.24 (0.033)	0.98 (0.000)	5.87 (0.000)
3	0.37 (0.014)	0.66 (0.051)	1.03 (0.001)	5.46 (0.006)
4	0.48 (0.058)	0.77 (0.045)	1.25 (0.062)	5.44 (0.004)
5	0.56 (0.007)	0.68(0.009)	1.88 (0.004)	5.44 (0.005)
6	0.67 (0.001)	0.55 (0.021)	2.58 (0.151)	5.46 (0.003)

Each number represents the mean of three replicates and the numbers between brackets represent the standard deviation (± SD)

The effect of nitrogen sources

This experiment was carried out to determine the best nitrogen source containing the same amount of nitrogen present in 0.2% urea and stimulating the highest production of xanthan by *X. campestris* MU1and the results are presented in table 3. It is clear that most of the applied nitrogen sources to the date extract medium were stimulated biosynthesis of xanthan by *X. campestris* MU1, the most superior one is ammonium nitrate in which the amount of the produced xanthan reached 0.85g/100ml, followed by urea 0.74g/100ml. Among the applied nitrogen sources only the fermentation medium containing NH_4CL has inhibition effect on xanthan production compared with the results of experiment 2.These results are agreed with the results of Kassim (2011) who used urea at a concentration of 4% for a high production of xanthan by the same strain of the bacterium, while Khosravi-Darani *et al*., (2011) and Faria *et al*., (2011) added NH_4NO_3 as a suitable nitrogen source to date extract and sugar cane media for the highest production of xanthan by *X. campestris* PTCC1473 and *X. campestris* NRRl B-1459 respectively. The decline in pH value in the results of this observation after fermentation process is normally due to the accumulation of xanthan gum in culture media because of its acidic nature, as it contains organic acids in its structure (Kassim, 2011).

Table 3:The effect of nitrogen sources on xanthan production by *X. campestris* MU1

N. Sources (%)	Biomass (g/100ml)	Xanthan (g/100ml)	Residual (%)	Final pH
Urea (0.20)	0.47 (0.201)	0.74 (0.002)	1.05 (0.104)	5.5 (0.005)
$(NH_4)_2HPO_4$ (0.33)	0.52 (0.004)	0.72 (0.020)	0.91 (0.005)	5.9 (0.008)
$NH_4H_2PO_4$ (0.58)	0.56 (0.000)	0.67 (0.053)	0.99 (0.008)	5.8 (0.004)
$(NH_4)_2SO_4$ (0.33)	0.43 (0.109)	0.69(0.044)	0.75 (0.006)	5.6 (0.039)
Peptone (0.43)	0.48 (0.201)	0.69 (0.008)	1.20 (0.042)	6.0 (0.044)
NH_4NO_3 (0.20)	0.44 (0.205)	0.85 (0.111)	1.05 (0.006)	5.6 (0.008)
NH_4CL (0.27)	0.48 (0.070)	0.60 (0.005)	1.13 (0.012)	5.3 (0.000)

Each number represents the mean of three replicates and the numbers between brackets represent the standard deviation (± SD)

CONCLUSION

The optimization of xanthan gum biosynthesis using different incubation periods, carbon concentration and nitrogen sources were compared using date extract as a carbon source and as a basal medium. Date extract medium at concentration of 4% sugar and NH_4NO_3 as a nitrogen source stimulated xanthan gum, production by *X. campestris* MU1, yeilding 0.85g/100ml after four days of incubation.

REFERENCES

– Anbuselvi, S., Kumar, M. S. and Padmaja, M. V. (2012). A comparative study on biosynthesis of xanthan gum using three different *Xanthomonas campestris* isolated from diseased plants, Int. J. Pharm. Bio. Sci., 3(3):1-6.

– Becker, A., Katzen, F., Puhler, A. and Lelpi, L. (1998). Xanthan gum biosynthesis and application, Appl. Microbiol Biotechnol., 50: 145-152.

– Ben-Salah,. R., Chaari, K., Besbes, S., Blecker, C. and Attia, H. (2011). Production of xanthan gum from *Xanthomonas campestris* NRRL B-1459 by fermentation of date juice palm by-products, (*Phoenix Dactyllifera.L.*) J. Food Pro. Eng., 34:457–474.

– Borges, C. D. and Vendruscolo, C. T. (2007). Xanthan synthesized by strain of *Xanthomonas campestris* pv.pnni: production, viscosity and chemical composition, Biosci. J. Vberlandia, 23(4):67-73.

– Cadmus, M. C., Knatson, C. A., Lagoda, A. A., Pittsley, J. E. and Burton, K. A. (1978). Synthetic media for production quality xanthan gum in 20 liter fermentation, Biotechnol. Bioeng., 20:1003-1014.

– Carignato, C. R., Oliveira, K. S., Lima, V. M. and Pedro de Oliva-neto, P. (2011). New culture medium to xanthan production by *Xanthomonas campestris*, Indian J. Microbiol., 51: 283-288.

– Cottrell. I. W. and Kang, K. S. (1978). Xanthan gum: A unique bacterial polysaccharide for food application , Develop. Ind. Microbiol., 19:117-131.

– Davidson, I. W. (1978). Production of

– polysaccharide by *xanthomonas Camprestris* in

– continuous culture SEMS, Microbial. lett.,3:347-349.

– De Vuyst L. and Vermeire, A. (1994).Use of industrial medium components for xanthan production by *Xanthomonas campestris*, Appl. Microbiol. Biotechnol., 42:. 187–191

– Dubois, M.A., Gilles, K.A., Hamilton, J.K., Rebers, P.A. and Smith F.(1956). Colorimetric method for determination of sugars and related substances, Anal. Chem., 28:350–356

– El-Salam, M. H., Fadel, M .A. and Murad., H. A. (1994) Bioconversion of sugar cane molasses into xanthan gum, J. Biotechnol., 33:03–106.

– Faria, S., Oliveira, C. L., Morais, S. A., Terrones, M. G., Resende, M. M., France, F. P. and Cardoso, V. L. (2011). Characterization of xanthan gum produced from sugar cane broth, Carb. Poly., 86(2):469-476.

– Funahashi, H. Yoshida, T. and Tagushi, H. (1987). Effect of glucose concentration on xanthan gum production by *Xanthomonas campestris*, J. Ferment. Technol., 65:603-606

– Galindo, E. (1994). Aspect of the processing of xanthan production, Trans. Institute. Chemival Eng., 72: 227- 237.

– García-Ochoa, F., Santos, V. E., Casas, J. A and Gómez. A. (2000). Xanthan gum: production,

recovery, and properties, Biotechnol. Adv., 18:549–579.
– García-Ochoa, F., Santos, V. E. and Alcon, A. (2004). Chemical structured kinetic model for xanthan production, En. Microbial Technol., 35: 284–292.
– Gilani, S. L., Heydarzadeh, H. D., Mokhtarian, N., Alemian, A. and Kolaei, M. (2011). Effect of preparation conditions on xanthan gum production and rheological behavior using cheese whey by *Xanthomonas campestris*, Aust. J. Bas. Appl. Sci., 10: 855-859.
– Kalogiannis, S. Iakovidou, G., Liakopoulou-Kyriakides, M., Kyriakidis, D.A. and Skaracis, G. N. (2003). Optimization of xanthan gum production by *Xanthomonas campestris* grown in molasses, Proc. Biochem., 39:249–256.
– Kamal, F. and Mehrgan, H. (2002). Mutagenesis of *Xanthomonas campestris* and selection of strain with enhanced xanthan production, Tehran university, Biomed. J. (7(3):91-98.
– Kassim, M. B. (2011). Production and characterization of the polysaccharide "xanthan gum" by local isolate of the bacteria *Xanthomonas campestris*, Afr. J. Biotechnol., 10(74):16924-16928.
– Kennedy, J. F. and Bradshaw, I. J. (1984). Production, properties and application of xanthan, Prog. Ind. Microbiol., 9:319-371.
– Khosravi-Darani, K. Reyhani, F. S., Naser-nejad, B. and Farhadi, G. B. (2011). Bench scale production of xanthan from date extract by *Xanthomonas campestris* in submerged fermentation using centrl composite design, Afr. J. Biotechnol., 10(62):13520-13527.
– Kongruang, S. (2005). Growth kinetics of xanthan production from uneconomical agricultural products with *Xanthomonas campestris* TISTR 1100, J. Appl. Sci., 4(2): 78–88.
– Li, Q., yan, W., Yang, K., Wen, Y. and Tang, J. (2012). Xanthan gum production by *Xanthomonas campestris* pv.*campestris* 8004 using cassava starch as carbon source, Afr. J. Biotechnol., 11(73):13809-13813.
– Lo, Y. M., Tang, S. T. and Min, D. B. (1997). Effect of yeast extract and glucose on xanthan production and cell growth in batch culture of *Xanthomonas campestris*, Appl. Microbiol. Biotechnol., 47:689-694.
– Murugesan, A. G., Dhevarhi, B., Gowdhaman, D., Bala, A. K. and Sathesh, P. C. (2012). Production of xanthan employing *Xanthomonas campestris* using sugar cane molasses, Am. J. Env. Eng., 2(2):31-34.
– Niknezhad, S. V., Asadollahi, M. A., Zamani, A. and Biria, D. (2014). Production of xanthan gum by Xa*nthomonas campestris* species using starch as a carbon source. Min. Biotechnol., 26930:191-197.
– Pensrity, N. Y. (2006). Date extract by product recycling for xanthan production by *Xanthomonas campestris* 2B1459. M.Sc. Thesis, Academy of Postgraduate studies, Benghazi, Lybai.
– Prell, A., lasik, J., Sobotka, M. and Sys, J. (1995). Growth and xanthan production by *Xanthomonas campestris* depending on the N-source concentration. Biopro. Eng., 13:280-292.
– Rosalam, S. and England, R. (2006). Review of xanthan gum production from unmodified starches by *Xanthomonas campestris* sp, Enz. Microbial Technol., 39:197–207.
– Scamparini, A. R. and Rosato, Y. B. (1987). Production of xanthan gum by different strain of *Xanthomonas campestris*. Proceeding: 4th European congeress on biotechnology, ed. Niejssel, D. M. vander Meer R. R. and Luybea, K., Ch. A. M. Amesterdam: Elsevier Sci., 1;301-304.
– Souw, P., Demain, A.L. (1979). Nutritional studies on xanthan production by *Xanthomonas campestris* NRRL-B 1459, Appl. Environ. Microbiol., 37:186-1192.
– Sutherland, I. W. (1990). Biotechnology of microbial exopolysaccharides, Cambridge University Press. Cambridge, U.K.
– Torrestiana, B., Fucikovsky, L. and Galindo, E. (1990). Xanthan production by some *Xanthomonas* isolates, Lett. Appl. Microbiol., 10(2):81-85.
– Tait. M. I., Sutherland I.W. and Sturman, A. J. (1986). Effectof growth conditions on the production , composition and viscosity of *Xanthomonas campestris* exopolysaccharide, J. Gen. Microbiol., 132:1483-1492.
– Vidhyalakshmi, R., Vallinachiyar, C. and Radhika, R. (2012). Production of xanthan from agro-industrial waste, J. Adv. Sci. Res., 3(2):56-59.

THE BIVARIATE HAHN POLYNOMIALS

MOHAMMED **A**BDALI **A**BDLHUSEIN[1]
Dept. of Mathematics, College of Education for Pure Sciences, Thiqar University, Thiqar, Iraq

(Received: September 1, 2015; Accepted for publication: December 29, 2015)

ABSTRACT

In this paper, we write the bivariate Hahn polynomials $\varphi_n(a,x)$ by a special representation of the Cauchy operator and the limit technique are used for deriving the basic identities: generating function, Mehler's formula, Rogers formula (with it's special cases), another Rogers-type formula, and linearization formula. Also, we introduce an extensions for generating function, Mehler's formula, Rogers formula and another extended identities for Hahn polynomials.

***KEYWORDS*:** Hahn polynomials, Cauchy operator, generating function, Mehler's formula, Rogers formula, extended Mehler's formula.
AMS Classification: 05A30, 33D45

1. INTRODUCTION AND NOTATION

Chen and Liu [14] developed a method of deriving hypergeometric identities by parameter augmentation, this method has more realizations as in [1, 2, 3, 4, 5, 12, 13, 15, 18, 19]. In this paper, we derive some identities for the bivariate Hahn polynomials $\varphi_n(a,x)$ after represented it by the Cauchy operator, where few of these identities were given by another method (see [7, 9, 10]).

Let us review some common notation and terminology for basic hypergeometric series in [16]. Assume that $|q|<1$. The q-shifted factorial is defined by:

$$(a;q)_0=1,\qquad (a;q)_n=\prod_{k=0}^{n-1}(1-aq^k),$$
$$(a;q)_\infty=\prod_{k=0}^{\infty}(1-aq^k);\qquad n\in\mathbb{Z}^+. \tag{1.1}$$

It is clear

$$(a;q)_n=(a;q)_\infty/(aq^n;q)_\infty\ ,$$
$$(a;q)_{n+k}=(a;q)_k\ \ (aq^k;q)_n\ .$$

We also adopt the following notation for multiple q-shifted factorial:

$$(a_1,a_2,\cdots,a_m;q)_n=(a_1;q)_n(a_2;q)_n\cdots(a_m;q)_n\ ,$$
$$(a_1,a_2,\cdots,a_m;q)_\infty=(a_1;q)_\infty(a_2;q)_\infty\cdots(a_m;q)_\infty\ .$$

The q-binomial coefficient is defined by:

$$\begin{bmatrix}n\\k\end{bmatrix}=\frac{(q;q)_n}{(q;q)_k(q;q)_{n-k}}.$$

The basic hypergeometric series ${}_{r+1}\phi_r$ is defined by:

$${}_{r+1}\phi_r\left(\begin{matrix}a_1,\dots,a_{r+1}\\b_1,\dots,b_r\end{matrix};q,x\right)$$
$$=\sum_{n=0}^{\infty}\frac{(a_1,\dots,a_{r+1};q)_n}{(q,b_1,\dots,b_r;q)_n}\ x^n.$$

The inverse pair is defined for every sequences a_n and b_n as:

$$a_n = \sum_{k=0}^{n} \begin{bmatrix} n \\ k \end{bmatrix} b_k \quad \Leftrightarrow \quad b_n$$
$$= \sum_{k=0}^{n} \begin{bmatrix} n \\ k \end{bmatrix} (-1)^k q^{\binom{k}{2}} a_{n-k} \quad .$$

In this paper, we will use the Cauchy identity:

$$\sum_{k=0}^{\infty} \frac{(a;q)_k}{(q;q)_k} x^k = \frac{(ax;q)_\infty}{(x;q)_\infty}, \qquad |x| < 1.$$

Putting $a = 0$, (1.3) becomes Euler's identity:

$$\sum_{k=0}^{\infty} \frac{x^k}{(q;q)_k} = \frac{1}{(x;q)_\infty}, \qquad |x| < 1,$$

and its inverse relation:

$$\sum_{k=0}^{\infty} \frac{(-1)^k q^{\binom{k}{2}} x^k}{(q;q)_k} = (x;q)_\infty.$$

The classical Rogers-Szegö polynomials [3, 6, 13, 15, 18, 19] was defined in 1926 by Szegö, as:

$$h_n(x|q) = \sum_{k=0}^{n} \begin{bmatrix} n \\ k \end{bmatrix} x^k.$$

Which has the following generating function [3, 13, 19]:

$$\sum_{n=0}^{\infty} h_n(x|q) \frac{t^n}{(q;q)_n} = \frac{1}{(t, xt; q)_\infty} \quad ; \qquad |t| < 1.$$

Also (1.6) has Rogers formula in the form [3, 13, 19]:

$$\sum_{n=0}^{\infty} \sum_{m=0}^{\infty} h_{n+m}(x|q) \frac{t^n}{(q;q)_n} \frac{s^m}{(q;q)_m} = \frac{(xst;q)_\infty}{(t, s, xt, xs; q)_\infty} \quad ,$$

where $max\{|t|, |s|, |xt|, |xs|\} < 1$.

The q-differential operator [13] is defined by:

$$D_q f(a) = \frac{f(a) - f(aq)}{a} \quad .$$

Lemma 1.1 [13].

$$D_q^k \{x^n\} = \frac{(q;q)_n}{(q;q)_{n-k}} \quad x^{n-k}.$$

In 2008, Chen and Gu [12] introduced the Cauchy augmentation operator for basic hypergeometric series, they found that the Cauchy operator is suitable for the study of some terminating summation formulas of basic hypergeometric series and q-integrals, they defined it by:

$T(a,b;D_q)$

$$= \sum_{n=0}^{\infty} \frac{(a;q)_n}{(q;q)_n} (bD_q)^n.$$

They derived three important results for this operator:

Proposition 1.2 [12].

$$T(a,b;D_q)\left\{\frac{1}{(ct;q)_\infty}\right\} = \frac{(abt;q)_\infty}{(bt,ct;q)_\infty}; \qquad |bt| < 1.$$

$$T(a,b;D_q)\left\{\frac{1}{(cs,ct;q)_\infty}\right\}$$

$$= \frac{(abt;q)_\infty}{(bt,cs,ct;q)_\infty} \quad {}_2\phi_1\left(\begin{matrix}a, ct\\ abt\end{matrix};q,bs\right),$$

$where \quad max\{|bs|,|bt|\} < 1.$

$$T(a,b;D_q)\left\{\frac{(cv;q)_\infty}{(cs,ct;q)_\infty}\right\}$$

$$= \frac{(abs,cv;q)_\infty}{(bs,cs,ct;q)_\infty} \quad {}_3\phi_2\left(\begin{matrix}a, cs, v/t\\ abs, cv\end{matrix};q,bt\right),$$

$where \quad max\{|bs|,|bt|\} < 1.$

Notice that when we set $s = 0$ in (1.13), we get the following operator identity (see [17]), which will be used later to derive Rogers-type formula :

$$T(a,b;D_q)\left\{\frac{(cv;q)_\infty}{(ct;q)_\infty}\right\} = \frac{(cv;q)_\infty}{(ct;q)_\infty} \quad {}_2\phi_1\left(\begin{matrix}a, v/t\\ cv\end{matrix};q,bt\right); \qquad |bt| < 1.$$

In 2009, the author [1] derived another six results for the Cauchy operator, he used this operator when he studied the homogeneous Rogers-Szegö polynomials.

Proposition 1.3 [1].

$$T(a,b;D_q)\left\{\frac{c^n}{(ct;q)_\infty}\right\} = \frac{(abt;q)_\infty}{(bt,ct;q)_\infty} \sum_{j=0}^{n} \begin{bmatrix}n\\ j\end{bmatrix} \frac{(a,ct;q)_j}{(abt;q)_j} \quad b^j \quad c^{n-j} \qquad ; |bt| < 1 \tag{1.15}$$

$$T(a,b;D_q)\left\{\frac{c^n}{(cs,ct;q)_\infty}\right\}$$

$$= \frac{(abt;q)_\infty}{(bt,ct,cs;q)_\infty} \sum_{l=0}^{\infty} \sum_{j=0}^{n} \begin{bmatrix}n\\ j\end{bmatrix} \frac{(a,ct;q)_{j+l}(cs;q)_j}{(abt;q)_{j+l}(q;q)_l} \quad b^{j+l} c^{n-j} s^l,$$

$where \quad max\{|bs|,|bt|\} < 1.$

$$T(a,b;D_q)\left\{\frac{c^n(cv;q)_\infty}{(cs,ct;q)_\infty}\right\}$$

$$= \frac{(abs,cv;q)_\infty}{(bs,cs,ct;q)_\infty} \sum_{l=0}^{\infty} \sum_{j=0}^{n} \begin{bmatrix}n\\ j\end{bmatrix} \frac{(a,cs;q)_{j+l}(ct;q)_j(v/t;q)_l}{(abs,cv;q)_{j+l}(q;q)_l} \quad b^{j+l} c^{n-j} t^l, \tag{1.17}$$

$where \quad max\{|bs|,|bt|\} < 1.$

$$T(a,b;D_q)\left\{\frac{1}{(cs,ct,cv;q)_\infty}\right\}$$
$$=\frac{1}{(cv,bt;q)_\infty}\sum_{k=0}^{\infty}\frac{(a;q)_k(bv)^k(abtq^k;q)_\infty}{(q;q)_k(csq^k,ctq^k;q)_\infty}\quad {}_2\phi_1\left(\begin{matrix}aq^k,ctq^k\\abtq^k\end{matrix};q,bs\right), \tag{1.18}$$
$where \quad max\{|bs|,|bt|\}<1.$

$$T(a,b;D_q)\left\{\frac{(cv;q)_\infty}{(cs,ct,cu;q)_\infty}\right\}$$
$$=\sum_{k=0}^{\infty}\frac{(a;q)_k(bu)^k(absq^k,cvq^k;q)_\infty}{(q;q)_k(cu,bs,csq^k,ctq^k;q)_\infty}\quad {}_3\phi_2\left(\begin{matrix}aq^k,csq^k,v/t\\absq^k,cvq^k\end{matrix};q,bt\right), \tag{1.19}$$
$where \quad max\{|bs|,|bt|\}<1.$

$$T(a,b;D_q)\left\{\frac{(cv,cw;q)_\infty}{(cs,ct,cu,cz;q)_\infty}\right\}=\frac{(abs,cv,cw;q)_\infty}{(bs,cs,ct,cu,cz;q)_\infty}$$

$$\times\sum_{j,k,l=0}^{\infty}\frac{(a,cs;q)_{j+k+l}(ct;q)_{k+l}(cu,w/z;q)_k(v/t;q)_j}{(abs,cv;q)_{j+k+l}(cw;q)_k}\frac{(bt)^j}{(q;q)_j}\frac{(bz)^k}{(q;q)_k}\frac{(bu)^l}{(q;q)_l},$$
Where $\max\{|bs|,|bt|\}<1.$

.

2. The Basic Identities

In this section, we recall the definition of bivariate Hahn polynomials $\varphi_n^{(a)}(x)$ and represent this polynomials by the Cauchy operator, then we derive it's generating function, Mehler's formula, Rogers formula and another Rogers-type formula. Also, we give some applications of the Rogers formula such as the linearization formula.

Definition 2.1 [Bivariate Hahn polynomials] [7, 8, 9, 10]:

$$\varphi_n(a;x)=\varphi_n^{(a)}(x)=\sum_{k=0}^{n}\begin{bmatrix}n\\k\end{bmatrix}(a;q)_k\ \ x^k.$$

Notice that, the classical Rogers-Szegö polynomials (1.6) is a $(a=0)$ case of the bivariate Hahn polynomials, therefore when we setting $a=0$ in all identities of $\varphi_n(a;x)$ (which are given in this paper) we will get the corresponding identities for $h_n(x|q)$. Also it is clear that the bivariate Hahn polynomials $\varphi_n(a;x)$ is not symmetric in the variables a and x, therefor $\varphi_n(a;x)\neq\varphi_n(x;a)$.
Now, we represent the polynomials $\varphi_n(a;x)$ by the following case of the Cauchy operator:

Proposition 2.2
$\lim_{c\to 1} \quad T\big(a,x;D_q\big)\{c^n\}$
$=\varphi_n(a;x).$

Proof. By definition of the Cauchy operator (1.10) and lemma (1.1) .

Depending on our representation (2.1) for the bivariate Hahn polynomials $\varphi_n(a;x)$, we can give the following proofs of the generating function, Mehler's formula, Rogers formula and another Rogers-type formula by using the roles (1.11), (1.13), (1.12) and (1.14) of the Cauchy operator respectively.
Firstly, we derive the generating function by using (2.1) and identity (1.11) as follows:

Theorem 2.3 (The generating function for $\varphi_n(a;x)$) Assume (1.11) and (2.1) are satisfied, then:

$$\sum_{n=0}^{\infty} \varphi_n(a;x)\frac{t^n}{(q;q)_n}$$
$$= \frac{(axt;q)_\infty}{(t,xt;q)_\infty},$$
where $|xt|<1$.

Proof.

$$\sum_{n=0}^{\infty} \varphi_n(a;x)\frac{t^n}{(q;q)_n} = \sum_{n=0}^{\infty} \lim_{c\to 1} T(a,x;D_q)\{c^n\} \quad \frac{t^n}{(q;q)_n}$$
$$= \lim_{c\to 1} T(a,x;D_q)\left\{\sum_{n=0}^{\infty}\frac{(ct)^n}{(q;q)_n}\right\}$$
$$= \lim_{c\to 1} T(a,x;D_q)\left\{\frac{1}{(ct;q)_\infty}\right\}$$
$$= \lim_{c\to 1}\left[\frac{(axt;q)_\infty}{(ct,xt;q)_\infty}\right]$$
$$= \frac{(axt;q)_\infty}{(t,xt;q)_\infty} \ .$$

Due to the above generating function (2.2), we can verify the definition (2.1) of the bivariate Hahn polynomials benefitted from the Cauchy identity (1.3) and the inverse pair (1.2) as the following proof:

Proof.

$$\sum_{n=0}^{\infty}\frac{(ax;q)_n}{(q;q)_n}\ t^n = \frac{(axt;q)_\infty}{(t;q)_\infty} = (xt;q)_\infty\frac{(axt;q)_\infty}{(t,xt;q)_\infty}$$
$$= \sum_{k=0}^{\infty}\frac{(-1)^k q^{\binom{k}{2}}(xt)^k}{(q;q)_k}\sum_{n=0}^{\infty}\varphi_n(a;x)\ \frac{t^n}{(q;q)_n}$$
$$= \sum_{k=0}^{\infty}\sum_{n=0}^{\infty}\frac{(-1)^k q^{\binom{k}{2}}x^k}{(q;q)_k}\varphi_n(a;x)\ \frac{t^{n+k}}{(q;q)_n}\ ; \qquad set \quad n=n-k$$
$$= \sum_{k=0}^{\infty}\sum_{n=k}^{\infty}\frac{(-1)^k q^{\binom{k}{2}}x^k}{(q;q)_k}\varphi_{n-k}(a;x)\ \frac{t^n}{(q;q)_{n-k}}$$
$$= \sum_{n=0}^{\infty}\sum_{k=0}^{n}\frac{(-1)^k q^{\binom{k}{2}}x^k}{(q;q)_k}\varphi_{n-k}(a;x)\ \frac{t^n}{(q;q)_{n-k}}.$$

By comparing the coefficients of t^n in the two sides, we get:

$$(ax;q)_n = \sum_{k=0}^{n}\begin{bmatrix}n\\k\end{bmatrix}(-1)^k q^{\binom{k}{2}}x^k\varphi_{n-k}(a;x)$$

$$\Rightarrow \quad \frac{(ax;q)_n}{x^n} = \sum_{k=0}^{n}\begin{bmatrix}n\\k\end{bmatrix}(-1)^k q^{\binom{k}{2}}\frac{\varphi_{n-k}(a;x)}{x^{n-k}}.$$

By using the inverse pair (1.2) we get:

$$\varphi_n(a;x)$$
$$= \sum_{k=0}^{n}\begin{bmatrix}n\\k\end{bmatrix}(ax;q)_k\ \ x^{n-k}.$$

Mehler's formula for the bivariate Hahn polynomials will be derived by applying our representation

(2.1) and the Cauchy operator identity (1.13) as follows:

Theorem 2.4 (Mehler's formula for $\varphi_n(a;x)$) Assume (1.13) and (2.1) are satisfied, then:

$$\sum_{n=0}^{\infty} \varphi_n(a;x)\ \ \varphi_n(b;y)\frac{t^n}{(q;q)_n}$$
$$=\frac{(axt,byt;q)_\infty}{(t,xt,yt;q)_\infty}\ \ {}_3\phi_2\left(\begin{matrix}a,b,t\\ axt,byt\end{matrix};q,xyt\right)\ ,$$

where $\max\{|xt|,|xyt|\}<1$.

Proof.

$$\sum_{n=0}^{\infty} \varphi_n(a;x)\varphi_n(b;y)\frac{t^n}{(q;q)_n}=\sum_{n=0}^{\infty}\lim_{c\to 1}\ T(a,x;D_q)\{c^n\}\ \ \varphi_n(b;y)\ \ \frac{t^n}{(q;q)_n}$$
$$=\lim_{c\to 1}T(a,x;D_q)\left\{\sum_{n=0}^{\infty}\varphi_n(b;y)\ \ \frac{(ct)^n}{(q;q)_n}\right\}$$
$$=\lim_{c\to 1}\ T(a,x;D_q)\left\{\frac{(byct;q)_\infty}{(ct,yct;q)_\infty}\right\}$$
$$=\lim_{c\to 1}\left[\frac{(axt,byct;q)_\infty}{(xt,ct,yct;q)_\infty}\ \ {}_3\phi_2\left(\begin{matrix}a,b,ct\\ axt,byct\end{matrix};q,xyt\right)\right]$$
$$=\frac{(axt,byt;q)_\infty}{(t,xt,yt;q)_\infty}\ \ {}_3\phi_2\left(\begin{matrix}a,b,t\\ axt,byt\end{matrix};q,xyt\right)\ .$$

In the same method, we give the deriving of the Rogers formula for the bivariate Hahn polynomials depending on our representation (2.1) and the Cauchy operator identity (1.12) as follows:

Theorem 2.5 (The Rogers formula for $\varphi_n(a;x)$) Assume (1.12) and (2.1) are satisfied, then:

$$\sum_{n=0}^{\infty}\sum_{m=0}^{\infty}\varphi_{n+m}(a;x)\frac{t^n}{(q;q)_n}\ \ \frac{s^m}{(q;q)_m}$$
$$=\frac{(axs;q)_\infty}{(t,s,xs;q)_\infty}\ \ {}_2\phi_1\left(\begin{matrix}a,s\\ axs\end{matrix};q,xt\right)\ ,$$

where $\max\{|s|,|t|,|xs|,|xt|\}<1$.

Proof.

$$\sum_{n=0}^{\infty}\sum_{m=0}^{\infty}\varphi_{n+m}(a;x)\ \ \frac{t^n}{(q;q)_n}\ \ \frac{s^m}{(q;q)_m}$$
$$=\sum_{n=0}^{\infty}\sum_{m=0}^{\infty}\lim_{c\to 1}\ T(a,x;D_q)\{c^{n+m}\}\ \ \frac{t^n}{(q;q)_n}\ \ \frac{s^m}{(q;q)_m}$$
$$=\lim_{c\to 1}\ T(a,x;D_q)\left\{\sum_{n=0}^{\infty}\frac{(ct)^n}{(q;q)_n}\ \ \sum_{m=0}^{\infty}\frac{(cs)^m}{(q;q)_m}\right\}$$
$$=\lim_{c\to 1}\ T(a,x;D_q)\left\{\frac{1}{(ct,cs;q)_\infty}\right\}$$
$$=\lim_{c\to 1}\left[\frac{(axs;q)_\infty}{(ct,cs,xs;q)_\infty}\ \ {}_2\phi_1\left(\begin{matrix}a,cs\\ axs\end{matrix};q,xt\right)\right]$$
$$=\frac{(axs;q)_\infty}{(t,s,xs;q)_\infty}\ \ {}_2\phi_1\left(\begin{matrix}a,s\\ axs\end{matrix};q,xt\right)\ .$$

In the following theorem, we give another Rogers-type formula for $\varphi_n(a;x)$ by using identity (1.14) of

the Cauchy operator and our representation (2.1).

Theorem 2.6 (Rogers-type formula for $\varphi_n(a;x)$) Assume (1.14) and (2.1) are satisfied, then:

$$\sum_{n=0}^{\infty}\sum_{m=0}^{\infty}\varphi_{n+m}(a;x)\frac{t^n}{(q;q)_n}\ \frac{(-1)^m q^{\binom{m}{2}}s^m}{(q;q)_m}$$
$$=\frac{(s;q)_\infty}{(t;q)_\infty}\ {}_2\phi_1\left(\begin{matrix}a, s/t\\ s\end{matrix};q,xt\right),$$

where $|xt|<1$.

Proof.

$$\sum_{n=0}^{\infty}\sum_{m=0}^{\infty}\varphi_{n+m}(a;x)\ \frac{t^n}{(q;q)_n}\ \frac{(-1)^m q^{\binom{m}{2}}\ s^m}{(q;q)_m}$$
$$=\sum_{n=0}^{\infty}\sum_{m=0}^{\infty}\lim_{c\to 1}T(a,x;D_q)\{c^{n+m}\}\ \frac{t^n}{(q;q)_n}\ \frac{s^m}{(q;q)_m}$$
$$=\lim_{c\to 1}\ T(a,x;D_q)\left\{\sum_{n=0}^{\infty}\frac{(ct)^n}{(q;q)_n}\ \sum_{m=0}^{\infty}\frac{(-1)^m q^{\binom{m}{2}}(cs)^m}{(q;q)_m}\right\}$$
$$=\lim_{c\to 1}\ T(a,x;D_q)\left\{\frac{(cs;q)_\infty}{(ct;q)_\infty}\right\}$$
$$=\lim_{c\to 1}\left[\frac{(cs;q)_\infty}{(ct;q)_\infty}\ {}_2\phi_1\left(\begin{matrix}a, s/t\\ s\end{matrix};q,xt\right)\right]$$
$$=\frac{(s;q)_\infty}{(t;q)_\infty}\ {}_2\phi_1\left(\begin{matrix}a, s/t\\ s\end{matrix};q,xt\right).$$

Now, we introduce some applications of the Rogers formula (2.5) such as the linearization formula and some relations between the bivariate Hahn polynomials and the classical Rogers-Szegö polynomials.

Lemma 2.7 (The Linearization formula for polynomial $\varphi_n(a;x)$) Assume (2.5) is satisfied, then:

$$\sum_{k=0}^{n}\sum_{l=0}^{m}\begin{bmatrix}n\\k\end{bmatrix}\ \begin{bmatrix}m\\l\end{bmatrix}\ (a;q)_k\ (ax;q)_l\ x^k\ \varphi_{n+m-k-l}(a;x)$$

$$=\sum_{k=0}^{n}\sum_{l=0}^{m}\begin{bmatrix}n\\k\end{bmatrix}\ \begin{bmatrix}m\\l\end{bmatrix}\ (a;q)_k\ (ax;q)_l\ (xq^l)^k\ \varphi_{n-k}(a;x)\ \varphi_{m-l}(a;x)\ .$$

Proof. Rewrite the Rogers formula (2.5) in the following form:

$$\frac{(axt,axs;q)_\infty}{(xt,s;q)_\infty}\sum_{n=0}^{\infty}\sum_{m=0}^{\infty}\varphi_{n+m}(a;x)\ \frac{t^n}{(q;q)_n}\ \frac{s^m}{(q;q)_m}$$

$$=\sum_{k=0}^{\infty}\frac{(a;q)_k\ (axsq^k;q)_\infty}{(q;q)_k\ (sq^k;q)_\infty}\ (xt)^k\ \sum_{n=0}^{\infty}\sum_{m=0}^{\infty}\varphi_n(a;x)\ \varphi_m(a;x)\ \frac{t^n}{(q;q)_n}\ \frac{s^m}{(q;q)_m}\ .$$

Expanding $(axt;q)_\infty/(xt;q)_\infty$, $(axs;q)_\infty/(s;q)_\infty$, and $(axsq^k;q)_\infty/(sq^k;q)_\infty$ by the Cauchy identity (1.3) as follows:

$$\frac{(axt;q)_\infty}{(xt;q)_\infty}=\sum_{k=0}^{\infty}\frac{(a;q)_k}{(q;q)_k}\ (xt)^k;\qquad |xt|<1,$$
$$\frac{(axs;q)_\infty}{(s;q)_\infty}=\sum_{l=0}^{\infty}\frac{(ax;q)_l}{(q;q)_l}\ (s)^l;\qquad |s|<1,$$

$$\frac{(axsq^k;q)_\infty}{(sq^k;q)_\infty}=\sum_{l=0}^{\infty}\frac{(ax;q)_l}{(q;q)_l}\ (sq^k)^l.$$

Now substitute these expansions in (2.8):

$$\sum_{n=0}^{\infty}\sum_{m=0}^{\infty}\sum_{k=0}^{\infty}\sum_{l=0}^{\infty}\frac{(a;q)_k\ x^k}{(q;q)_k}\ \frac{(ax;q)_l}{(q;q)_l}\ \varphi_{n+m}(a;x)\ \frac{t^{n+k}}{(q;q)_n}\ \frac{s^{m+l}}{(q;q)_m}$$

$$=\sum_{n=0}^{\infty}\sum_{m=0}^{\infty}\sum_{k=0}^{\infty}\sum_{l=0}^{\infty}\frac{(a;q)_k\ x^k}{(q;q)_k}\ \frac{(ax;q)_l}{(q;q)_l}\ q^{kl}\ \varphi_n(a;x)\ \varphi_m(a;x)\ \frac{t^{n+k}}{(q;q)_n}\ \frac{s^{m+l}}{(q;q)_m}.$$

Set $n\to n-k$ and $m\to m-l$:

$$\sum_{n=k}^{\infty}\sum_{m=l}^{\infty}\sum_{k=0}^{\infty}\sum_{l=0}^{\infty}\frac{(a;q)_k\ x^k}{(q;q)_k}\ \frac{(ax;q)_l}{(q;q)_l}\ \varphi_{n+m-k-l}(a;x)\ \frac{t^n}{(q;q)_{n-k}}\ \frac{s^m}{(q;q)_{m-l}}$$

$$=\sum_{n=k}^{\infty}\sum_{m=l}^{\infty}\sum_{k=0}^{\infty}\sum_{l=0}^{\infty}\frac{(a;q)_k\ x^k}{(q;q)_k}\ \frac{(ax;q)_l}{(q;q)_l}\ q^{kl}\ \varphi_{n-k}(a;x)\ \varphi_{m-l}(a;x)\ \frac{t^n}{(q;q)_{n-k}}\ \frac{s^m}{(q;q)_{m-l}}.$$

By equating the coefficients of $t^n s^m$, we get the required identity.

Lemma 2.8 For $n,m\geq 0$, assume (2.5) is satisfied, then:

$$\sum_{k=0}^{\min\{n,m\}}\begin{bmatrix}n\\k\end{bmatrix}\ \begin{bmatrix}m\\k\end{bmatrix}(q;q)_k\ x^k\ h_{n+m-2k}(x|q)$$

$$=\left(\sum_{k=0}^{n}\begin{bmatrix}n\\k\end{bmatrix}\ (ax)^k\ \varphi_{n-k}(a,x)\right)\left(\sum_{j=0}^{m}\begin{bmatrix}m\\j\end{bmatrix}(ax)^j\ \varphi_{m-j}(a,x)\right),\qquad(2.9)$$

where $max\{|t|,|s|,|xt|,|xs|,|axt|,|axs|,|xts|\}<1$.

Proof. Let $a=0$ in the Rogers formula (2.5), we get:

$$\sum_{n=0}^{\infty}\sum_{m=0}^{\infty}h_{n+m}(x|q)\frac{t^n}{(q;q)_n}\frac{s^m}{(q;q)_m}=\frac{1}{(s,xs,xt;q)_\infty}\sum_{k=0}^{\infty}\frac{(xs;q)_k}{(q;q)_k}t^k$$

$$=\frac{(xst;q)_\infty}{(s,t,xs,xt;q)_\infty}\ =\frac{(xst;q)_\infty}{(axt,axs;q)_\infty}\frac{(axt;q)_\infty}{(t,xt;q)_\infty}\frac{(axs;q)_\infty}{(s,xs;q)_\infty}$$

$$=\frac{(xst;q)_\infty}{(axt,axs;q)_\infty}\sum_{n=0}^{\infty}\varphi_n(a,x)\frac{t^n}{(q;q)_n}\sum_{m=0}^{\infty}\varphi_m(a,x)\frac{s^m}{(q;q)_m}.$$

Then:

$$\frac{1}{(xst;q)_\infty}\sum_{n=0}^{\infty}\sum_{m=0}^{\infty}h_{n+m}(x|q)\frac{t^n}{(q;q)_n}\frac{s^m}{(q;q)_m}$$

$$=\frac{1}{(axt,axs;q)_\infty}\sum_{n=0}^{\infty}\sum_{m=0}^{\infty}\varphi_n(a,x)\varphi_m(a,x)\frac{t^n}{(q;q)_n}\frac{s^m}{(q;q)_m}.\ (2.10)$$

By applying Euler identity (1.4) on the terms: $1/(xst;q)_\infty$, $1/(axt;q)_\infty$ and $1/(axs;q)_\infty$:

$$\sum_{k=0}^{\infty}\frac{(xst)^k}{(q;q)_k}\sum_{n=0}^{\infty}\sum_{m=0}^{\infty}h_{n+m}(x|q)\frac{t^n}{(q;q)_n}\frac{s^m}{(q;q)_m}$$

$$=\sum_{k=0}^{\infty}\frac{(axt)^k}{(q;q)_k}\sum_{j=0}^{\infty}\frac{(axs)^j}{(q;q)_j}\sum_{n=0}^{\infty}\sum_{m=0}^{\infty}\varphi_n(a,x)\varphi_m(a,x)\frac{t^n}{(q;q)_n}\frac{s^m}{(q;q)_m}$$

$$\Rightarrow \sum_{k=0}^{\infty}\sum_{n=0}^{\infty}\sum_{m=0}^{\infty}\frac{x^k}{(q;q)_k}h_{n+m}(x|q)\frac{t^{n+k}}{(q;q)_n}\frac{s^{m+k}}{(q;q)_m}$$

$$=\sum_{k=0}^{\infty}\sum_{j=0}^{\infty}\sum_{n=0}^{\infty}\sum_{m=0}^{\infty}\frac{(ax)^k}{(q;q)_k}\frac{(ax)^j}{(q;q)_j}\varphi_n(a,x)\varphi_m(a,x)\frac{t^{n+k}}{(q;q)_n}\frac{s^{m+j}}{(q;q)_m}.$$

Set $n \to n-k$ and $m \to m-k$:

$$\sum_{k=0}^{\infty}\sum_{n=k}^{\infty}\sum_{m=k}^{\infty}\frac{x^k}{(q;q)_k}h_{n+m-2k}(x|q)\frac{t^n}{(q;q)_{n-k}}\frac{s^m}{(q;q)_{m-k}}$$

$$=\sum_{k=0}^{\infty}\sum_{j=0}^{\infty}\sum_{n=k}^{\infty}\sum_{m=j}^{\infty}\frac{(ax)^k}{(q;q)_k}\frac{(ax)^j}{(q;q)_j}\varphi_{n-k}(a,x)\varphi_{m-j}(a,x)\frac{t^n}{(q;q)_{n-k}}\frac{s^m}{(q;q)_{m-j}}.$$

The proof will be completed after comparing the coefficients of $t^n s^m$.

Notice that when we set $a=0$ in (2.9), we get the fames linearization formula of the classical Rogers-Szegö polynomials: [6, 13]:

$$h_n(x|q)\ h_m(x|q) = \sum_{k=0}^{\min\{n,m\}}\begin{bmatrix}n\\k\end{bmatrix}\begin{bmatrix}m\\k\end{bmatrix}(q;q)_k\ x^k\ h_{n+m-2k}(x|q).$$

Also, putting $m=0$ in (2.9) to obtained the following relation between the classical Rogers-Szegö polynomials $h_n(x|q)$ and the bivariate Hahn polynomials $\varphi_n(a,x)$:

$$h_n(x|q) = \sum_{k=0}^{n}\begin{bmatrix}n\\k\end{bmatrix}(ax)^k\ \varphi_{n-k}(a,x).$$

We give the inverse relation of (2.12) as follows:

$$\varphi_n(a,x) = \sum_{k=0}^{n}\begin{bmatrix}n\\k\end{bmatrix}(-1)^k q^{\binom{k}{2}}(ax)^k\ h_{n-k}(x|q).$$

Notice that, we can prove the relation (2.12) due to the generating function of the classical Rogers-Szegö polynomials (1.7) as follows:

Proof. Rewrite identity (1.7) as follows:

$$\sum_{n=0}^{\infty}h_n(x|q)\frac{t^n}{(q;q)_n}=\frac{1}{(t,xt;q)_\infty}=\frac{(axt;q)_\infty}{(t,xt;q)_\infty}\frac{1}{(axt;q)_\infty}$$

$$=\sum_{n=0}^{\infty}\varphi_n(a,x)\frac{t^n}{(q;q)_n}\sum_{k=0}^{\infty}\frac{(axt)^k}{(q;q)_k}$$

$$=\sum_{n=0}^{\infty}\sum_{k=0}^{\infty}\varphi_n(a,x)\frac{(ax)^k}{(q;q)_n(q;q)_k}\ t^{n+k}\ ;\qquad set\quad n=n-k$$

$$=\sum_{n=0}^{\infty}\sum_{k=0}^{n}\varphi_{n-k}(a,x)\frac{(ax)^k}{(q;q)_{n-k}(q;q)_k}\ t^n.$$

By comparing the coefficient of t^n in two sides, we get identity (2.12), and the proof will be finished.

Lemma 2.9 For $n,m\geq 0$, assume (2.10) is satisfied, then:

$$\sum_{k=0}^{n}\sum_{j=0}^{m}\begin{bmatrix}n\\k\end{bmatrix}\begin{bmatrix}m\\j\end{bmatrix}\ q^{\binom{k}{2}+\binom{j}{2}}(-ax)^{k+j}\ h_{n+m-k-j}(x|q)$$

$$= \sum_{k=0}^{\min\{n,m\}} \begin{bmatrix} n \\ k \end{bmatrix} \begin{bmatrix} m \\ k \end{bmatrix} (q;q)_k \; q^{\binom{k}{2}} (-x)^k \; \varphi_{n-k}(a,x)\varphi_{m-k}(a,x).$$

Proof. Rewrite identity (2.10) as follows:

$$\sum_{n=0}^{\infty}\sum_{m=0}^{\infty} h_{n+m}(x|q)\frac{t^n}{(q;q)_n}\frac{s^m}{(q;q)_m}$$

$$= \frac{(xst;q)_\infty}{(axt,axs;q)_\infty}\sum_{n=0}^{\infty}\sum_{m=0}^{\infty}\varphi_n(a,x)\varphi_m(a,x)\frac{t^n}{(q;q)_n}\frac{s^m}{(q;q)_m}.$$

Multiply it by $(axt,axs;q)_\infty$:

$$(axt,axs;q)_\infty\sum_{n=0}^{\infty}\sum_{m=0}^{\infty} h_{n+m}(x|q)\frac{t^n}{(q;q)_n}\frac{s^m}{(q;q)_m}$$

$$= (xst;q)_\infty\sum_{n=0}^{\infty}\sum_{m=0}^{\infty}\varphi_n(a,x)\varphi_m(a,x)\frac{t^n}{(q;q)_n}\frac{s^m}{(q;q)_m}.$$

Now expand $(xst;q)_\infty, (axt;q)_\infty$ and $(axs;q)_\infty$ by Euler's identity (1.5) as follows:

$$\sum_{k=0}^{\infty}\frac{(-1)^k q^{\binom{k}{2}}(axt)^k}{(q;q)_k}\sum_{j=0}^{\infty}\frac{(-1)^j q^{\binom{j}{2}}(axs)^j}{(q;q)_j}\sum_{n=0}^{\infty}\sum_{m=0}^{\infty} h_{n+m}(x|q)\frac{t^n}{(q;q)_n}\frac{s^m}{(q;q)_m}$$

$$= \sum_{k=0}^{\infty}\frac{(-1)^k q^{\binom{k}{2}}(xst)^k}{(q;q)_k}\sum_{n=0}^{\infty}\sum_{m=0}^{\infty}\varphi_n(a,x)\varphi_m(a,x)\frac{t^n}{(q;q)_n}\frac{s^m}{(q;q)_m}$$

$$\Rightarrow \sum_{n=0}^{\infty}\sum_{m=0}^{\infty}\sum_{k=0}^{\infty}\sum_{j=0}^{\infty}\frac{(-1)^{k+j}q^{\binom{k}{2}+\binom{j}{2}}(ax)^{k+j}}{(q;q)_k(q;q)_j} \; h_{n+m}(x|q)\frac{t^{n+k}}{(q,q)_n}\frac{s^{m+j}}{(q,q)_m}$$

$$= \sum_{n=0}^{\infty}\sum_{m=0}^{\infty}\sum_{k=0}^{\infty}\frac{(-1)^k \; q^{\binom{k}{2}}x^k}{(q;q)_k} \; \varphi_n(a,x)\varphi_m(a,x)\frac{t^{n+k}}{(q,q)_n}\frac{s^{m+k}}{(q,q)_m}.$$

Setting $n \to n-k$ and $m \to m-j$:

$$\Rightarrow \sum_{k=0}^{\infty}\sum_{j=0}^{\infty}\sum_{n=k}^{\infty}\sum_{m=j}^{\infty}\frac{(-1)^{k+j}q^{\binom{k}{2}+\binom{j}{2}}(ax)^{k+j}}{(q;q)_k(q;q)_j} \; h_{n+m-k-j}(x|q)\frac{t^n}{(q,q)_{n-k}}\frac{s^m}{(q,q)_{m-j}}$$

$$= \sum_{k=0}^{\infty}\sum_{n=k}^{\infty}\sum_{m=k}^{\infty}\frac{(-1)^k \; q^{k}{}_2 \; x^k}{(q;q)_k} \; \varphi_{n-k}(a,x)\varphi_{m-k}(a,x)\frac{t^n}{(q,q)_{n-k}}\frac{s^m}{(q,q)_{m-k}}.$$

Comparing the coefficients of $t^n s^m$, we get the required identity.

Setting $a = 0$ in (2.14), to get the Askey-Ismail formula of the classical Rogers-Szegö polynomials [6, 13]:

$$h_{m+n}(x|q)$$

$$= \sum_{k=0}^{\min\{m,n\}} \begin{bmatrix} n \\ k \end{bmatrix}\begin{bmatrix} m \\ k \end{bmatrix}(q;q)_k \; q^{\binom{k}{2}}(-x)^k h_{n-k}(x|q)h_{m-k}(x|q).$$

3. An Extended Identities

In this section, we introduce an extended generating function, extended Mehler's formula and extended Rogers formula for bivariate Hahn polynomials $\varphi_n(a;x)$ by using our representation (2.1) and the roles (1.15), (1.17) and (1.16) of the Cauchy operator respectively, then we give another extended identities.

Theorem 3.1 (Extended generating function for $\varphi_n(a;x)$) Assume (1.15) and (2.1) are satisfied, then:

$$\sum_{n=0}^{\infty} \varphi_{n+k}(a;x)\frac{t^n}{(q;q)_n}$$
$$= \frac{(axt;q)_\infty}{(t,xt;q)_\infty}\sum_{j=0}^{k}\begin{bmatrix}k\\ j\end{bmatrix}\ \frac{(a,t;q)_j}{(axt;q)_j}\ \ x^j\ ,$$

where $|xt|<1$.

Proof.

$$\sum_{n=0}^{\infty} \varphi_{n+k}(a;x)\frac{t^n}{(q;q)_n} = \sum_{n=0}^{\infty}\lim_{c\to 1}\ T(a,x;D_q)\{c^{n+k}\}\ \ \frac{t^n}{(q;q)_n}$$
$$= \lim_{c\to 1}\ T\big(a,x;D_q\big)\left\{c^k\ \ \sum_{n=0}^{\infty}\frac{(ct)^n}{(q;q)_n}\right\} = \lim_{c\to 1}\ T(a,x;D_q)\left\{\frac{c^k}{(ct;q)_\infty}\right\}$$
$$= \lim_{c\to 1}\left[\frac{(axt;q)_\infty}{(ct,xt;q)_\infty}\sum_{j=0}^{k}\begin{bmatrix}k\\ j\end{bmatrix}\ \frac{(a,ct;q)_j}{(axt;q)_j}\ \ x^j\ \ c^{k-j}\right] = \frac{(axt;q)_\infty}{(t,xt;q)_\infty}\sum_{j=0}^{k}\begin{bmatrix}k\\ j\end{bmatrix}\ \frac{(a,t;q)_j}{(axt;q)_j}\ \ x^j\ .$$

Setting $k=0$ in the above theorem, we get the generating function (2.2) for the bivariate Hahn polynomials $\varphi_n(a;x)$.

Theorem 3.2 (Extended Mehler's formula for $\varphi_n(a;x)$) Assume (1.17) and (2.1) are satisfied, then:

$$\sum_{n=0}^{\infty} \varphi_n(a;x)\varphi_{n+k}(b;y)\frac{t^n}{(q;q)_n}$$
$$= \frac{(axt,byt;q)_\infty}{(t,xt,yt;q)_\infty}\sum_{l=0}^{\infty}\sum_{j=0}^{k}\begin{bmatrix}k\\ j\end{bmatrix}\frac{(b,t;q)_{j+l}(xt;q)_j(a;q)_l}{(axt,byt;q)_{j+l}(q;q)_l}\ \ y^{j+l}(xt)^l, \qquad (3.2)$$

where $\max\{|yt|,|xyt|\}<1$.

Proof.

$$\sum_{n=0}^{\infty} \varphi_n(a;x)\varphi_{n+k}(b;y)\frac{t^n}{(q;q)_n} = \sum_{n=0}^{\infty}\varphi_n(a;x)\ \lim_{c\to 1}T(b,y;D_q)\{c^{n+k}\}\ \ \frac{t^n}{(q;q)_n}$$
$$= \lim_{c\to 1}T(b,y;D_q)\left\{c^k\ \ \sum_{n=0}^{\infty}\varphi_n(a;x)\frac{(ct)^n}{(q;q)_n}\right\} = \lim_{c\to 1}\ T(b,y;D_q)\left\{c^k\ \ \frac{(axct;q)_\infty}{(ct,xct;q)_\infty}\right\}$$
$$= \lim_{c\to 1}\left[\frac{(axct,byt;q)_\infty}{(ct,xct,yt;q)_\infty}\sum_{l=0}^{\infty}\sum_{j=0}^{k}\begin{bmatrix}k\\ j\end{bmatrix}\frac{(b,ct;q)_{j+l}\ \ (xct;q)_j\ \ (a;q)_l}{(axct,byt;q)_{j+l}\ \ (q;q)_l}\ \ y^{j+l}\ \ c^{k-j}\ \ (xt)^l\right]$$
$$= \frac{(axt,byt;q)_\infty}{(t,xt,yt;q)_\infty}\sum_{l=0}^{\infty}\sum_{j=0}^{k}\begin{bmatrix}k\\ j\end{bmatrix}\frac{(b,t;q)_{j+l}\ \ (xt;q)_j\ \ (a;q)_l}{(axt,byt;q)_{j+l}\ \ (q;q)_l}\ \ y^{j+l}\ \ (xt)^l\ .$$

Setting $k=0$ in the above theorem, we get Mehler's formula (2.4) for the bivariate Hahn polynomials $\varphi_n(a;x)$.

Theorem 3.3 (Extended Rogers formula for $\varphi_n(a;x)$) Assume (1.16) and (2.1) are satisfied, then:

$$\sum_{n=0}^{\infty}\sum_{m=0}^{\infty}\varphi_{n+m+k}(a;x)\ \frac{t^n}{(q;q)_n}\ \frac{s^m}{(q;q)_m}$$
$$=\frac{(axt;q)_\infty}{(t,s,xt;q)_\infty}\sum_{l=0}^{\infty}\sum_{j=0}^{k}\begin{bmatrix}k\\j\end{bmatrix}\ \frac{(a,t;q)_{j+l}\ (s;q)_j}{(axt;q)_{j+l}\ (q;q)_l}\ x^{j+l}\ s^l\ , \tag{3.3}$$

where $\max\{|xs|,|xt|\}<1$.

Proof.

$$\sum_{n=0}^{\infty}\sum_{m=0}^{\infty}\varphi_{n+m+k}(a;x)\frac{t^n}{(q;q)_n}\ \frac{s^m}{(q;q)_m}\ =\sum_{n=0}^{\infty}\sum_{m=0}^{\infty}\lim_{c\to 1}\ T(a,x;D_q)\{c^{n+m+k}\}\ \frac{t^n}{(q;q)_n}\ \frac{s^m}{(q;q)_m}$$
$$=\lim_{c\to 1}\ T(a,x;D_q)\left\{c^k\ \sum_{n=0}^{\infty}\frac{(ct)^n}{(q;q)_n}\ \sum_{m=0}^{\infty}\frac{(cs)^m}{(q;q)_m}\right\}\ =\lim_{c\to 1}\ T(a,x;D_q)\left\{\frac{c^k}{(cs,ct;q)_\infty}\right\}$$
$$=\lim_{c\to 1}\left[\frac{(axt;q)_\infty}{(ct,cs,xt;q)_\infty}\sum_{l=0}^{\infty}\sum_{j=0}^{k}\begin{bmatrix}k\\j\end{bmatrix}\ \frac{(a,ct;q)_{j+l}\ (cs;q)_j}{(axt;q)_{j+l}\ (q;q)_l}\ x^{j+l}\ s^l\ c^{k-j}\right]$$
$$=\frac{(axt;q)_\infty}{(t,s,xt;q)_\infty}\sum_{l=0}^{\infty}\sum_{j=0}^{k}\begin{bmatrix}k\\j\end{bmatrix}\ \frac{(a,t;q)_{j+l}\ (s;q)_j}{(axt;q)_{j+l}\ (q;q)_l}\ x^{j+l}\ s^l\ .$$

Setting $k=0$ in the above theorem, we get the Rogers formula (2.5) for the bivariate Hahn polynomials $\varphi_n(a;x)$.

Theorem 3.4 Assume (1.13) and (2.1) are satisfied, then:

$$\sum_{n=0}^{\infty}\sum_{m=0}^{\infty}\sum_{k=0}^{\infty}\varphi_{n+m+k}(a;x)\ \frac{t^n}{(q;q)_n}\ \frac{s^m}{(q;q)_m}\ \frac{(-1)^k q^{\binom{k}{2}}v^k}{(q;q)_k}$$
$$=\frac{(axs,v;q)_\infty}{(xs,s,t;q)_\infty}\ {}_3\phi_2\left(\begin{matrix}a,s,v/t\\axs,v\end{matrix};q,xt\right), \tag{3.4}$$

where $\max\{|s|,|t|,|xt|,|xs|\}<1$.

Proof.

$$\sum_{n=0}^{\infty}\sum_{m=0}^{\infty}\sum_{k=0}^{\infty}\varphi_{n+m+k}(a;x)\ \frac{t^n}{(q;q)_n}\ \frac{s^m}{(q;q)_m}\ \frac{(-1)^k q^{\binom{k}{2}}v^k}{(q;q)_k}$$
$$=\sum_{n=0}^{\infty}\sum_{m=0}^{\infty}\sum_{k=0}^{\infty}\lim_{c\to 1}T(a,x;D_q)\{c^{n+m+k}\}\ \frac{t^n}{(q;q)_n}\ \frac{s^m}{(q;q)_m}\ \frac{(-1)^k q^{\binom{k}{2}}v^k}{(q;q)_k}$$
$$=\lim_{c\to 1}\ T(a,x;D_q)\left\{\sum_{n=0}^{\infty}\frac{(ct)^n}{(q;q)_n}\sum_{m=0}^{\infty}\frac{(cs)^m}{(q;q)_m}\sum_{k=0}^{\infty}\frac{(-1)^k q^{\binom{k}{2}}(cv)^k}{(q;q)_k}\right\}\ =\lim_{c\to 1}\ T(a,x;D_q)\left\{\frac{(cv;q)_\infty}{(cs,ct;q)_\infty}\right\}$$
$$=\lim_{c\to 1}\left[\frac{(axs,cv;q)_\infty}{(xs,cs,ct;q)_\infty}\ {}_3\phi_2\left(\begin{matrix}a,cs,v/t\\axs,cv\end{matrix};q,xt\right)\right]\ =\frac{(axs,v;q)_\infty}{(xs,s,t;q)_\infty}\ {}_3\phi_2\left(\begin{matrix}a,s,v/t\\axs,v\end{matrix};q,xt\right).$$

Theorem 3.5 Assume (1.18) and (2.1) are satisfied, then:

$$\sum_{n=0}^{\infty}\sum_{m=0}^{\infty}\sum_{k=0}^{\infty}\varphi_{n+m+k}(a;x)\ \frac{t^n}{(q;q)_n}\ \frac{s^m}{(q;q)_m}\ \frac{v^k}{(q;q)_k}$$

$$= \frac{1}{(v,xt;q)_\infty}\sum_{j=0}^{\infty}\frac{(a;q)_k\ \ (xv)^k}{(q;q)_k}\frac{(axtq^k;q)_\infty}{(sq^k,tq^k;q)_\infty}\quad {}_2\phi_1\left(\begin{matrix}aq^k,tq^k\\ axtq^k\end{matrix};q,xs\right), \tag{3.5}$$

where $\max\{|v|,|s|,|t|,|xt|,|xs|\}<1$.

Proof.

$$\sum_{n=0}^{\infty}\sum_{m=0}^{\infty}\sum_{k=0}^{\infty}\varphi_{n+m+k}(a;x)\frac{t^n}{(q;q)_n}\ \ \frac{s^m}{(q;q)_m}\ \ \frac{v^k}{(q;q)_k}$$

$$= \lim_{c\to 1}T(a,x;D_q)\left\{\sum_{n=0}^{\infty}\frac{(ct)^n}{(q;q)_n}\sum_{m=0}^{\infty}\frac{(cs)^m}{(q;q)_m}\sum_{k=0}^{\infty}\frac{(cv)^k}{(q;q)_k}\right\}$$

$$= \lim_{c\to 1}T(a,x;D_q)\left\{\frac{1}{(cs,ct,cv;q)_\infty}\right\}$$

$$= \lim_{c\to 1}\left[\frac{1}{(cv,xt;q)_\infty}\sum_{j=0}^{\infty}\frac{(a;q)_k\ \ (xv)^k}{(q;q)_k}\frac{(axtq^k;q)_\infty}{(csq^k,ctq^k;q)_\infty}\quad {}_2\phi_1\left(\begin{matrix}aq^k,ctq^k\\ axtq^k\end{matrix};q,xs\right)\right]$$

$$= \frac{1}{(v,xt;q)_\infty}\sum_{j=0}^{\infty}\frac{(a;q)_k\ \ (xv)^k}{(q;q)_k}\frac{(axtq^k;q)_\infty}{(sq^k,tq^k;q)_\infty}\quad {}_2\phi_1\left(\begin{matrix}aq^k,tq^k\\ axtq^k\end{matrix};q,xs\right).$$

The identity (1.17) of the Cauchy operator can be rewrite as the following form:

$$T(a,b;D_q)\left\{\frac{c^n(cv;q)_\infty}{(cs,ct;q)_\infty}\right\}$$

$$= \sum_{j=0}^{n}\begin{bmatrix}n\\ j\end{bmatrix}(a;q)_j\ \ b^jc^{n-j}\frac{(absq^j,cvq^j;q)_\infty}{(bs,csq^j,ctq^j;q)_\infty}\quad {}_3\phi_2\left(\begin{matrix}aq^j,csq^j,v/t\\ absq^j,cvq^j\end{matrix};q,bt\right), \tag{3.6}$$

where $\max\{|bs|,|bt|\}<1$.

We use (3.6) to introduce the following extended identity for bivariate Hahn polynomials:

Theorem 3.6 Assume (2.1) and (3.6) are satisfied, then:

$$\sum_{k=0}^{\infty}\varphi_{m+k}(a;x)\ \ \varphi_{n+k}(b;y)\ \ \frac{t^k}{(q;q)_k}$$

$$= \sum_{j=0}^{m}\sum_{l=0}^{n}\begin{bmatrix}m\\ j\end{bmatrix}\begin{bmatrix}n\\ l\end{bmatrix}\frac{(bytq^{j+l},axtq^{j+l};q)_\infty\ \ (a;q)_j\ \ (b;q)_l\ \ x^j\ \ y^l}{(ytq^j,tq^{j+l},xtq^l;q)_\infty}\quad {}_3\phi_2\left(\begin{matrix}bq^l,tq^{j+l},aq^j\\ bytq^{j+l},axtq^{j+l}\end{matrix};q,xyt\right), \tag{3.7}$$

where $\max\{|xt|,|yt|,|xyt|\}<1$.

Proof.

$$\sum_{k=0}^{\infty}\varphi_{m+k}(a;x)\varphi_{n+k}(b;y)\frac{t^k}{(q;q)_k}\ \ = \lim_{c\to 1}T(b,y;D_q)\left\{c^n\ \ \sum_{k=0}^{\infty}\varphi_{m+k}(a;x)\ \ \frac{(ct)^k}{(q;q)_k}\right\}$$

$$= \lim_{c\to 1}\ T(b,y;D_q)\left\{c^n\ \ \frac{(axct;q)_\infty}{(ct,xct;q)_\infty}\sum_{j=0}^{m}\begin{bmatrix}m\\ j\end{bmatrix}\ \ \frac{(a,ct;q)_j}{(axct;q)_j}\ \ x^j\right\}$$

$$= \lim_{c\to 1}\left[\sum_{j=0}^{m}\begin{bmatrix}m\\ j\end{bmatrix}\ \ (a;q)_j\ \ x^j\ \ T(b,y;D_q)\left\{\frac{c^n\ \ (axctq^j;q)_\infty}{(ctq^j,xct;q)_\infty}\right\}\right]$$

$$= \lim_{c\to 1}\left[\sum_{j=0}^{m}\begin{bmatrix}m\\ j\end{bmatrix}(a;q)_j\ \ x^j\sum_{l=0}^{n}\begin{bmatrix}n\\ l\end{bmatrix}(b;q)_ly^lc^{n-l}\ \ \frac{(bytq^{j+l},axctq^{j+l};q)_\infty}{(ytq^j,ctq^{j+l},xctq^l;q)_\infty}\quad {}_3\phi_2\left(\begin{matrix}bq^l,ctq^{j+l},aq^j\\ bytq^{j+l},axctq^{j+l};q,xyt\end{matrix}\right)\right]$$

$$= \sum_{j=0}^{m}\sum_{l=0}^{n}\begin{bmatrix}m\\ j\end{bmatrix}\begin{bmatrix}n\\ l\end{bmatrix}\frac{(bytq^{j+l},axtq^{j+l};q)_\infty\ \ (a;q)_j\ \ (b;q)_l\ \ x^j\ \ y^l}{(ytq^j,tq^{j+l},xtq^l;q)_\infty}\quad {}_3\phi_2\left(\begin{matrix}bq^l,tq^{j+l},aq^j\\ bytq^{j+l},axtq^{j+l}\end{matrix};q,xyt\right).$$

Theorem 3.7 Assume (1.19) and (2.1) are satisfied, then:

$$\sum_{m=0}^{\infty}\sum_{k=0}^{\infty}\varphi_{m+k}(a;x)\ \ \varphi_{n+k}(b;y)\ \ \frac{t^m}{(q;q)_m}\ \ \frac{s^k}{(q;q)_k}$$

$$= \sum_{j=0}^{n}\begin{bmatrix}n\\ j\end{bmatrix}(b;q)_j y^j\sum_{l=0}^{\infty}\frac{(a;q)_l(xt)^l}{(q;q)_j}\frac{(axsq^{j+l},bysq^{j+l};q)_\infty}{(t,xsq^j,sq^{j+l},ysq^l;q)_\infty}\quad {}_3\phi_2\left(\begin{matrix}aq^l,sq^{j+l},bq^j\\ axsq^{j+l},bysq^{j+l}\end{matrix};q,xys\right),\qquad (3.8\ )$$

where $\max\{|t|,|xs|,|ys|,|xys|\}<1$.

Proof.

$$\sum_{m=0}^{\infty}\sum_{k=0}^{\infty}\varphi_{m+k}(a;x)\ \ \varphi_{n+k}(b;y)\ \ \frac{t^m}{(q;q)_m}\ \ \frac{s^k}{(q;q)_k}$$

$$= \lim_{c\to 1}T(a,x;D_q)\left\{\sum_{m=0}^{\infty}\frac{(ct)^m}{(q;q)_m}\ \ \sum_{k=0}^{\infty}\varphi_{n+k}(b;y)\frac{(cs)^k}{(q;q)_k}\right\}$$

$$= \lim_{c\to 1}T(a,x;D_q)\left\{\frac{1}{(ct;q)_\infty}\ \ \frac{(bycs;q)_\infty}{(cs,ycs;q)_\infty}\sum_{j=0}^{n}\begin{bmatrix}n\\ j\end{bmatrix}\ \ \frac{(b,cs;q)_j}{(bycs;q)_j}\ \ y^j\right\}$$

$$= \lim_{c\to 1}\left[\sum_{j=0}^{n}\begin{bmatrix}n\\ j\end{bmatrix}\ \ (b;q)_j\ \ y^j\ \ T(a,x;D_q)\left\{\frac{(bycsq^j;q)_\infty}{(csq^j,cys,ct;q)_\infty}\right\}\right]$$

$$= \lim_{c\to 1}\left[\sum_{j=0}^{n}\begin{bmatrix}n\\ j\end{bmatrix}(b;q)_j y^j\sum_{l=0}^{\infty}\frac{(a;q)_l(xt)^l}{(q;q)_j}\frac{(axsq^{j+l},bycsq^{j+l};q)_\infty}{(ct,xsq^j,csq^{j+l},cysq^l;q)_\infty}\quad {}_3\phi_2\left(\begin{matrix}aq^l,csq^{j+l},bq^j\\ axsq^{j+l},bycsq^{j+l}\end{matrix};q,xys\right)\right]$$

$$= \sum_{j=0}^{n}\begin{bmatrix}n\\ j\end{bmatrix}(b;q)_j y^j\sum_{l=0}^{\infty}\frac{(a;q)_l(xt)^l}{(q;q)_j}\frac{(axsq^{j+l},bysq^{j+l};q)_\infty}{(t,xsq^j,sq^{j+l},ysq^l;q)_\infty}\quad {}_3\phi_2\left(\begin{matrix}aq^l,sq^{j+l},bq^j\\ axsq^{j+l},bysq^{j+l}\end{matrix};q,xys\right).$$

Theorem 3.8 Assume (1.19) and (2.1) are satisfied, then:

$$\sum_{n=0}^{\infty}\sum_{m=0}^{\infty}\sum_{k=0}^{\infty}\varphi_{n+k}(a;x)\varphi_{m+k}(b;y)\frac{t^n}{(q;q)_n}\ \ \frac{s^m}{(q;q)_m}\frac{w^k}{(q;q)_k}$$

$$= \sum_{j=0}^{\infty}\sum_{l=0}^{\infty}\frac{(b;q)_j(ys)^j(a;q)_l(xt)^l}{(q;q)_j(q;q)_l}\frac{(axwq^{j+l},bywq^{j+l};q)_\infty}{(s,t,xwq^j,wq^{j+l},ywq^l;q)_\infty}\quad {}_3\phi_2\left(\begin{matrix}aq^l,wq^{j+l},bq^j\\ axwq^{j+l},bywq^{j+l}\end{matrix};q,xyw\right),\qquad (3.9$$

where $\max\{|t|,|ys|,|yw|,|xw|,|xyw|\}<1$.

Proof.

$$\sum_{n=0}^{\infty}\sum_{m=0}^{\infty}\sum_{k=0}^{\infty}\varphi_{n+k}(a;x)\ \ \varphi_{m+k}(b;y)\ \ \frac{t^n}{(q;q)_n}\ \ \frac{s^m}{(q;q)_m}\ \ \frac{w^k}{(q;q)_k}$$

$$= \lim_{c\to 1}\ T(a,x;D_q)\left\{\sum_{n=0}^{\infty}\frac{(ct)^n}{(q;q)_n}\ \ \sum_{m=0}^{\infty}\sum_{k=0}^{\infty}\varphi_{m+k}(b;y)\ \ \frac{s^m}{(q;q)_m}\ \ \frac{(cw)^k}{(q;q)_k}\right\}$$

$$= \lim_{c\to 1}\ T(a,x;D_q)\left\{\frac{1}{(ct;q)_\infty}\ \ \frac{(bycw;q)_\infty}{(s,cw,ycw;q)_\infty}\quad {}_2\phi_1\left(\begin{matrix}b,cw\\ bycw\end{matrix};q,ys\right)\ \right\}$$

$$= \lim_{c\to 1}\left[\sum_{j=0}^{\infty}\frac{(b;q)_j\ \ (ys)^j}{(q;q)_j(s;q)_\infty}\ \ T(a,x;D_q)\left\{\frac{(bycwq^j;q)_\infty}{(cwq^j,ycw,ct;q)_\infty}\right\}\right]$$

$$= \lim_{c\to 1}\left[\sum_{j,l=0}^{\infty}\frac{(b;q)_j(ys)^j(a;q)_l(xt)^l}{(q;q)_j(q;q)_l}\frac{(axwq^{j+l},bycwq^{j+l};q)_\infty}{(s,ct,xwq^j,cwq^{j+l},cywq^l;q)_\infty}\ \ {}_3\phi_2\left(\begin{matrix}aq^l,cwq^{j+l},bq^j\\ axwq^{j+l},bycwq^{j+l};q,xyw\end{matrix}\right)\right]$$

$$= \sum_{j=0}^{\infty}\sum_{l=0}^{\infty}\frac{(b;q)_j(ys)^j(a;q)_l(xt)^l}{(q;q)_j(q;q)_l}\frac{(axwq^{j+l},bywq^{j+l};q)_\infty}{(s,t,xwq^j,wq^{j+l},ywq^l;q)_\infty}\ \ {}_3\phi_2\left(\begin{matrix}aq^l,wq^{j+l},bq^j\\ axwq^{j+l},bywq^{j+l};q,xyw\end{matrix}\right).$$

Theorem 3.9 Assume (1.20) and (2.1) are satisfied, then:

$$\sum_{n=0}^{\infty}\sum_{m=0}^{\infty}\varphi_{n+m}(a;x)\ \ \varphi_n(b;y)\ \ \varphi_m(d;z)\ \ \frac{t^n}{(q;q)_n}\ \ \frac{s^m}{(q;q)_m}$$

$$= \frac{(axt,byt,dzs;q)_\infty}{(t,xt,yt,s,zs;q)_\infty}\sum_{l=0}^{\infty}\sum_{j=0}^{\infty}\sum_{k=0}^{\infty}\frac{(a,t;q)_{j+k+l}(yt;q)_{k+l}(s,d;q)_k(b;q)_j}{(axt,byt;q)_{j+k+l}(dzs;q)_k(q;q)_j(q;q)_k(q;q)_l}\ \ x^{j+k+l}y^jz^kt^js^{k+l}\ ,\qquad (3.$$

where $\max\{|yt|,|zs|,|xt|,|xyt|\}<1$.

Proof.

$$\sum_{n=0}^{\infty}\sum_{m=0}^{\infty}\varphi_{n+m}(a;x)\ \ \varphi_n(b;y)\ \ \varphi_m(d;z)\ \ \frac{t^n}{(q;q)_n}\ \ \frac{s^m}{(q;q)_m}$$

$$= \lim_{c\to 1}\ T(a,x;D_q)\left\{\sum_{n=0}^{\infty}\varphi_n(b;y)\ \ \frac{(ct)^n}{(q;q)_n}\ \ \sum_{m=0}^{\infty}\varphi_m(d;z)\ \ \frac{(cs)^m}{(q;q)_m}\right\}$$

$$= \lim_{c\to 1}\ T(a,x;D_q)\left\{\frac{(byct,dzcs;q)_\infty}{(yct,ct,cs,zcs;q)_\infty}\right\}$$

$$= \lim_{c\to 1}\left[\frac{(axt,byct,dzcs;q)_\infty}{(ct,xt,yct,cs,zcs;q)_\infty}\sum_{l=0}^{\infty}\sum_{j=0}^{\infty}\sum_{k=0}^{\infty}\frac{(a,ct;q)_{j+k+l}(yct;q)_{k+l}(cs,d;q)_k(b;q)_j\ \ x^{j+k+l}(yt)^j(zs)^ks^l}{(axt,byct;q)_{j+k+l}(dzcs;q)_k(q;q)_j(q;q)_k(q;q)_l}\right]$$

$$= \frac{(axt,byt,dzs;q)_\infty}{(t,xt,yt,s,zs;q)_\infty}\sum_{l=0}^{\infty}\sum_{j=0}^{\infty}\sum_{k=0}^{\infty}\frac{(a,t;q)_{j+k+l}(yt;q)_{k+l}(s,d;q)_k(b;q)_j}{(axt,byt;q)_{j+k+l}(dzs;q)_k(q;q)_j(q;q)_k(q;q)_l}\ \ x^{j+k+l}\ \ y^j\ \ z^k\ \ t^j\ \ s^{k+l}.$$

REFERENCES

- M. A. Abdlhusein, The q -Operators and Rogers-Szegö polynomials, M.SC. thesis, University of Basrah, Basrah, Iraq, (2009).
- M. A. Abdlhusein, The new application of the Cauchy operator, *Journal of Zankoy Sulaimani (JZS-A)*, **17**, (2015) 193-204.
- M. A. Abdlhusein, The Euler operator for basic hypergeometric series, *Int. J. Adv. Appl. Math. and Mech.*, **2**, (2014) 42 - 52.
- M. A. Abdlhusein, The basic and extended identities for certain q -polynomials, *Journal of college of education for pure sciences-Thiqar university*, **2**, (2012) 11-23.
- M. A. Abdlhusein, Representation of some q -series by the q -exponential operator $R(bD_q)$, *Journal of Missan researches*, **18**, (2013) 355-362.
- R. Askey and M. E. H. Ismail, A generalization of ultraspherical polynomials, In: "Studies in Pure Mathematics", P. Erdös, Ed., Birkhäuser, Boston, MA, (1983), 55–78.
- L. Carlitz and W. A. Al-Salam, Some orthogonal q-polynomials, *Math. Nachr.*, **30** (1965) 47-61.
- L.Carlitz, Generating functions for certain q -orthogonal polynomials, *Collectanea Math.*, **23** (1972) 91-104.
- J. Cao, Generalizations of certain Carlitz's trilinear and Srivastava-Agarwal type generating functions, *J. Math. Anal. Appl.*, **396** (2012) 351- 362.

- J. Cao, On Carlitz's trilinear generating functions, *Applied Mathematics and Computation* **218** (2012) 9839-9847.
- W. Y. C. Chen, H. L. Saad and L. H. Sun, An operator approach to the Al-Salam-Carlitz polynomials, *J. Math. Phys.* **51** (2010) 1-13.
- V.Y.B. Chen and N.S.S. Gu, The Cauchy operator for basic hypergeometric series, *Adv. Appl. Math.*, **41** (2008) 177–196.
- W.Y.C. Chen and Z.G. Liu, Parameter augmenting for basic hypergeometric series, II, *J. Combin. Theory*, Ser. A **80** (1997) 175–195.
- W.Y.C. Chen and Z.G. Liu, Parameter augmentation for basic hypergeometric series, I, Mathematical Essays in Honor of Gian-Carlo Rota, Eds., B. E. Sagan and R. P. Stanley, Birkhäuser, Boston, 1998, pp. 111-129.
- W.Y.C. Chen, H.L. Saad and L.H. Sun, The bivariate Rogers-Szegö polynomials, *J. Phys. A: Math. Theor.*, **40** (2007) 6071–6084.
- G. Gasper and M. Rahman, Basic Hypergeometric Series, 2nd Ed., Cambridge University Press, Cambridge, MA, 2004.
- Da-qian Lu, q-Difference equation and the Cauchy operator identities, *J. Math. Anal. Appl.*, **359**, (2009) 265-274.
- H. L. Saad and M. A. Abdlhusein, The -exponential operator and generalized Rogers-Szegö polynomials, *Journal of Advances in Mathematics*, **8** (2014) 1440–1455.
- H. L. Saad and A. A. Sukhi, Another homogeneous q-difference operator, *Applied Mathematics and Computation* **215** (2010) 4332–4339.

MANUAL AND COMPUTER-ASSISTED CYTOMORPHOMETRIC ANALYSIS OF SALIVA AND GINGIVAL SMEARS IN DIABETIC PATIENTS.

MAYADA **I**. YALDA, **S**ABRYA **N. I**BRAHEM and **G**HAZWAN F. AHMED
Faculty of Medical Sciences, Duhok University, Iraq.

(Received: September 8, 2015; Accepted for publication: December 29, 2015)

ABSTRACT

Background Cytomorphometric analysis of oral mucosa play an important role in identifying changes of the oral cavity in diabetic patients, and it's an easy method to perform on exfoliated cells of saliva and gingival mucosa.
Aim to evaluate the mucosal changes by using different methods of smear collection and measurements as well as comparing the saliva exfoliated cells or the use of cytomorphometry computer-assisted analysis.
Methods The study included 60 patients diagnosed as type II diabetes mellitus (DM), for more than 10 years, and 30 non-diabetic healthy volunteers. Papanicolaou stain was performed on their saliva and gingival cytobrush smears. The morphological features of 50 unfolded, clearly outlined epithelial cells were evaluated under light microscope from each sample. Then these cells were analyzed for the nuclear to cytoplasm ratio (N/C ratio) by using image J software computer program. In addition the background of each slide was assessed manually for inflammation.
Results This results showed that diabetic oral mucosa cells were characterized by mild increase in the N/C ratio and slight irregular nuclear membrane; however the irregular nuclear membrane was statistically insignificant. There were no differences in other nuclear features like binucleation, hyperchromatin and prominent nucleoli. The results showed statistically highly significant increase in bacteria-coated epithelial cells (BCEC) in diabetic patients, particularly in the saliva smears. The computer- assessed smears showed similar results for the N/C ratio and there was no statistical difference between the manual and computer- assessed results.
Conclusion: Oral cytomorphology changes occur in type II DM patients who showed epithelial cell degeneration and regeneration are more obvious in gingival cytobrush smears with no significance differences between the manual and the computer-assisted nuclear morphometry analysis, while BCEC and inflammation are more obvious in saliva smear.

***KEYWORDS*:** Saliva, Gingiva, Diabetes mellitus, Computer-assisted, Cytomorphometry.

INTRODUCTION

DM is a group of metabolic diseases, and one of the commonest endocrine disorders. The total number of people with DM is projected to rise from 171 million in 2000 to 366 million in 2030.[1] Type 2 DM is the commonest form of the disease, making up 90% of diabetic cases.[2] The most common oral complications in DM are xerostomia, increased incidence of dental caries, gingivitis, periodontitis, and parotid enlargement, candidiasis, lichen planus, lichenoid reactions, burning mouth syndrome, traumatic ulcers, glossodynia, neurosensory dysesthesias, irritational fibromas and taste dysfunctions.[3, 4, 5]

With advancements in the field of quantitative oral cytology and the use of cytomorphometry computer-assisted analysis, [6, 7] various parameters such as nuclear size, cell size, N/C ratio, nuclear shape, nuclear discontinuity, optical density and nuclear texture can be evaluated collectively. These parameters have been shown to be significant in the evaluation of oral lesions. [8, 9]

On cytomorphology of oral mucosa in diabetic patients, recently few published literatures were available [10-14] that gave an idea about mucosal changes by using different methods of smear collection and measurements without comparing the saliva exfoliated cells or the use of cytomorphometry computer-assisted analysis.

PATIENTS AND METHODS

This study included 60 patients, diagnosed as type II diabetic patients for more than 10 years. The patients were collected from Azadi Hospital and Diabetic center in Duhok, from 1st of April to 1st of June-2015. The control group included 30 non-diabetic, healthy volunteers, their fasting glucose level was < 120 mg/dl and/or their HbA1c < 6.5%. The cytological examination of both saliva and gingival smear was carried out in the Central lab. Of Duhok. The exclusion criteria were: smokers, alcoholic patients, patients with

systemic diseases and on long term medications and ladies who are pregnant or taking contraceptive.

The participants were asked to gargle with 5cc of tap water to remove surface debris, after that the saliva collected on a slide. A second smear collected from the attached gingiva of the lower anterior teeth of each individual using oral cytobrush (Rover Orcellex/ Netherlands) and transferred to labeled glass slides, fixed at once in 95% ethanol, then stained using the Papanicolaou technique. From each sample (saliva and gingival cytobrush smears) 50 unfolded, clearly outlined, and separated squamous cells selected manually, then photos taken for each field. The cytomorphological features examined in this study are listed in figure 1.

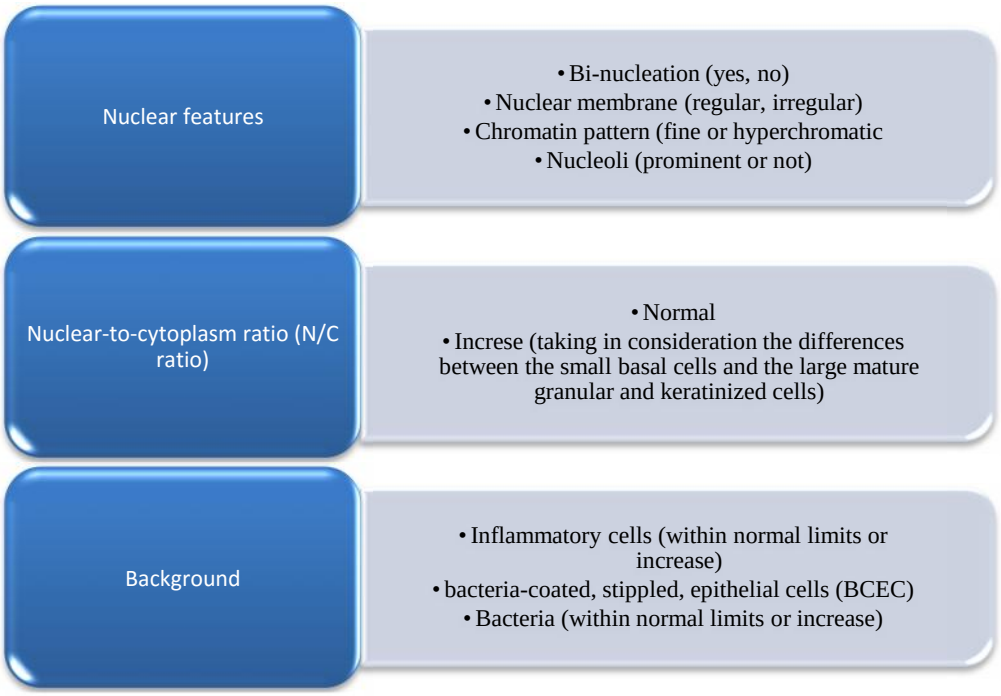

Fig.(1):- The general and nuclear cytomorphological features.

Then morphometric analysis carried out by using image J software computer program (NIH, Betheseda, USA) to assess the N/C ratio. Data analyzed by chi-square test and X^2 test using SPSS software.

RESULTS

Results of general cytomorphological examination are shown in table 1. The diabetic gingival cytobrush cells showed mild increase in the N/C ratio in 14 out of the 60 patients (23%), this increase was statistically significant. Furthermore there is a statistical highly significant increase in bacteria-coated epithelial cells (BCEC) in diabetic patients, particularly in the saliva, were more than half of the patients exhibiting these cells (53.3%). Both bacteria and inflammation were higher in salivary and gingival smears of the diabetic group (20% in saliva and 25% in gingival smears, and 25% in saliva and 21.7% in gingival smears for bacteria and inflammation respectively).

Results of nuclear features are shown in table 2. Smears of diabetic patients, especially the gingival brushcytology, show increase in cells with irregular nuclear membrane (11.7%), but this increase was statistically insignificant. There were no differences in other nuclear features like binucleation, hyper chromatin and prominent nucleoli in both types of smears and both groups. Table 3 shows comparison between manual and computer-assessed cytomorphology regarding the N/C ratio. The computer-assessed cytomorphology results were similar to that of the manual and there were no significant differences.

Table(1): -The general cytomorphological features in control (C) and diabetic mellitus (DM) group

Features		N/C ratio		Bacteria		Inflammation		BCEC	
		Normal	Increase	Normal	Increase	Normal	Increase	+	-
C (n 30)	Saliva	29	I	28	2	24	6	3	27
	%	(96.7)	(3.3)	(93.3)	(6.7)	(80)	(20)	(10)	(90)
	Brush	28	2	25	5	21	9	4	26
	%	(93.3)	(6.7)	(83.3)	(16.7)	(70)	(30)	(13.3)	(86.7)
DM (n 60)	Saliva	52	8	48	12	45	15	32	28
	%	(86.7)	(13.3)	(80)	(20)	(75)	(25)	(53.3)	(46.7)
	Brush	46	14	45	15	47	13	26	34
	%	(76.7)	(23.3)	(75)	(25)	(78.3)	(21.7)	(43.3)	(56.7)
P value*		0.035		0.209		0.784		< 0.001	

C: control group. DM: diabetics Mellitus group.
By Chi-square test: P value < 0.05 was statistically significant

Table (2):- Nuclear criteria in control and diabetics groups

Nuclear criteria	DM Patients (n:60)		Control (n:30)		P value
	Saliva	brush	Saliva	Brush	
Irregular nuclear membrane +	4 (6.7)	7 (11.7)	1 (3.3)	2 (6.7)	0.523
-	56 (93.3)	53 (88.3)	29 (96.7)	28 (93.3)	
bi- or multi nucleation +	1 (1.7)	3 (5)	0 (0)	1 (3.3)	0.520
-	59 (98.3)	57 (95)	30 (100)	29 (96.7)	
prominent nucleoli +	0 (0)	0 (0)	0 (0)	0 (0)	No prominent nucleoli
-	60 (100)	60 (100)	30 (100)	30 (100)	
Chromatin Faint	58 (96.7)	56 (93.3)	28 (93.3)	26 (86.7)	0.360
Hyper chromatic	2 (3.3)	4 (6.7)	2 (6.7)	4 (13.3)	

Table(3):- Nuclear-to-cytoplasm ratio results in manual and computer-assessed cytomorphological examination

Features		Manual assessment patients (n:60)		Computer-assessment patients (n:60)		Control(n:30)	
		Saliva	brush	Saliva	brush	Saliva	brush
N/C ratio	Normal	52	46	50	45	29	28
	%	(86.7)	(76.7)	(83.3)	(75)	(96.7)	(93.3)
	Increase	8	14	7	13	1	2
	%	(13.3)	(23.3)	(11.7)	(21.7)	(3.3)	(6.7)
P value	< 0.05	0.157		0.152		1	

*** According to X^2 test**

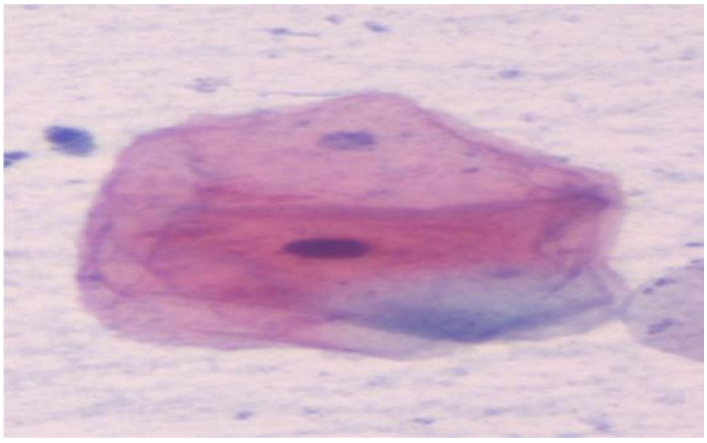

Fig. (2):-Normal Squamous cell from gingival smear of control group

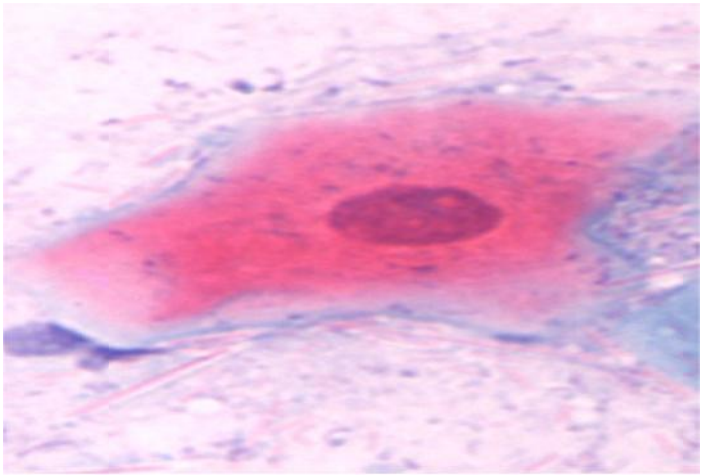

Fig.(3):- Squamous Cell from gingival brush smear with mild increase N/C ratio in diabetic patient

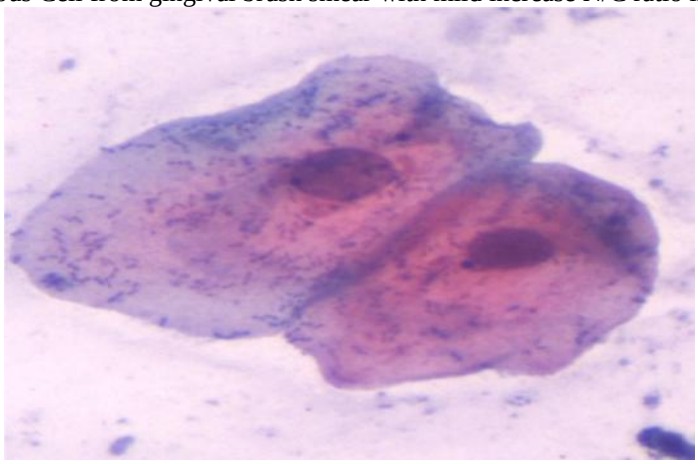

Fi.(4): -Two BCEC from gingival brush smear with mild increase N/C ratio in diabetic patient

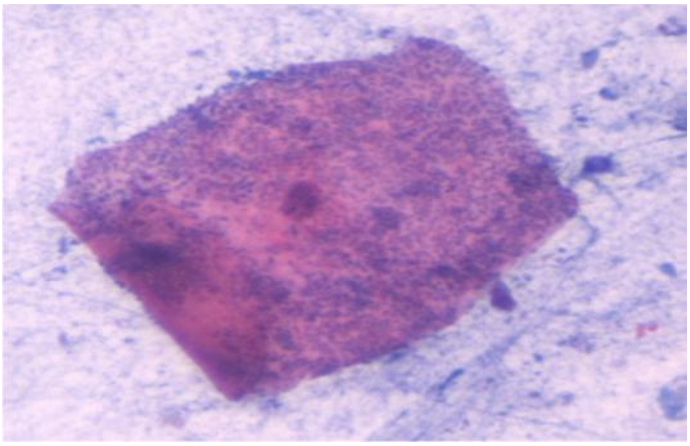

Fig.(5):- BCEC from saliva of diabetic patient with no increase in N/C ratio

DISCUSSION

Several research works have examined the effects of DM on oral mucosa, [3, 10, 11, 15, 16] some stated that the antioxidant scavengers and enzymes are depressed by elevated glucose concentration and there was excessive formation of free radicals. These noxious processes can cause serious damage to the biological structures at molecular level which can be appreciated by oral exfoliative cytology, [15, 16] but non of these studies compared the exfoliated cells of the saliva with the cytobrush cells. The current study showed variable cytomorphologic changes in the oral mucosa of diabetic patients. The results of the study indicated that changes in epithelial cells are more obvious in the gingival cytobrush smears, particularly for the N/C ratio, while inflammation and the BCEC were more obvious in the saliva. The possible explanation for the significant increase in BCEC in saliva more than the brush smear is that microorganisms, naturally found in the oral cavity, grow more rapidly in saliva of diabetic patients were alterations in saliva's composition impair immunological resistance. [17]

In this study we examined the N/C ratio and nuclear changes and the findings were similar to Alberti et al. [10] and Shareefet al. Results which showed [11] an increase in the nuclear area in type 2 diabetic patients. Contrary to the results of the previous two authors, who reported bi-nucleation in diabetic group, we did not find any bi-nucleation even after thorough examination. The possible explanations for the increase N/C ratio and nuclear changes probably related to the reduction in epithelial turnover secondary to metabolic disorders in diabetic patients. [18] Moreover, treatment with metformin had side effect that produce lacto-acidosis, [19] furthermore; diabetic patients are suffering from dry mouth (xerostomia) and atrophic changes of oral mucosa with sensory defects leading to intraoral minor trauma. [20]

The computer-assisted nuclear morphometry could be used as an additional method to assess the nuclear-cytoplasmic ration (N/C) in cytological specimens. [21] Several papers have been published on this technique, most of them are related to early detection of oral cancer. [22, 23, 24] However, with carful examination no differences were found in the results of N/C ratio between the manual and computer-assisted methods.

CONCLUSION

Oral cytomorphology changes in type II DM patients of epithelial cell degeneration and regeneration are more obvious in gingival cytobrush smears, while BCEC and inflammation are more obvious in saliva smear. Therefore, both smears are of value in examination with no significance differences between the manual and the computer-assisted nuclear morphometry analysis.

REFERENCES

- Williams's textbook of endocrinology. (12th Ed.). Philadelphia: Elsevier/Saunders. pp. 1371–1435. ISBN 978-1-4377-0324-5.
- King H, Aubert R.E. Herman WH. Global burden of diabetes, 1995-2025: Prevalence, numerical estimates, and projections. Diabetes Care. 1998; 21:1414–31
- Jajarm H.H, Mohtasham N, Rangiani A. Evaluation of oral mucosa epithelium in type II diabetic patients by an exfoliative

cytology method. J Oral Science 2008; 50(3): 335-340.
- Ship J.A. Diabetes and oral health: An overview. J Am Dent Assoc. 2003; 134: 4S-10S.
- Abate N, Chandalia M. Ethnicity, type 2 diabetes & migrant Asian Indians. Indian J Med Res. 2007; 125: 251-258.
- Patton L. L, Epstein J. B, and Kerr A. R, "Adjunctive techniques for oral cancer examination and lesion diagnosis a systematic review of the literature," Journal of the American Dental Association. 2008; vol. 139(7): 896–905.
- Mehrotra R, Hullmann M, Smeets R, Reichert T. E, and Driemel O, "Oral cytology revisited," Journal of Oral Pathology and Medicine. 2009; 38(2), 161–166.
- Ramaesh T, Mendis BR, Ratnatunga N. Diagnosis of oral premalignant and malignant lesions using cytomorphometry. Otontostomatologietropicale, 1999; 22(85):23-8
- Einstein TB, Sivapathasundharam B. Cytomorphometric analysis of the buccal mucosa of tobacco users. Indian J Dent Res. 2005; 16(2):42-46
- Alberti S, Spadella CT, Francischone TR, Assis GF, Cestari TM and Taveira LA. Exfoliative cytology of the oral mucosa in type II diabetic patients: morphology and cytomorphometry. J Oral Pathol Med, 2003; 32: 538-543.
- Shareef BT, Ang KT and Naik VR. Qualitative and quantitative exfoliative cytology of normal oral mucosa in type 2 diabetic patients. Med Oral PatolOralCirBucal. 2008; 1: 693-696.
- Jajarm HH, Mohtasham N, Rangiani A. Evaluation of oral mucosa epithelium in type II diabetic patients by an exfoliative cytology method. J. Oral Sci. 2008; 50: 335-340.
- Prasad H, Ramesh V, Balamurali PD. Morphologic and cytomorphometric analysis of exfoliated buccal mucosal cells in diabetes patients. J Cytol. 2010; 27:113-7.
- Hallikerimath S, Sapra G, Kale A, Malur PR. Cytomorphometric analysis and assessment of periodic acid schiff positivity of exfoliated cells from apparently normal buccal mucosa of type 2 diabetic patients. ActaCytol. 2011; 55:197-202.
- Caldeira E.J, Garcia P.J, Minatel E, Camilli J.A, Cagnon V.H. Morphometric analysis and ultrastructure of the epithelium of the oral mucosa in diabetic autoimmune NOD mice. Braz J Morphol Sci 2004; 21:197-205.
- A uluck A. Diabetes mellitus: An emerging risk factor for oral cancer? J Can Dent Assoc 2007; 73:501-3.
- Barchiesi F, Maracci M, Radi B, Arzeni DO, Baldassarri IO, Glacometti A, Scalise G. Point prevelance, microbiology and fluconazole susceptibility patterns of yeast isolates colonizing the oral cavities of HIV-infected patients in the era of highly active antiretroviral therapy. Journal of Antimicrobial Chemotherapy. 2002; 50: 999–1002
- Friedman EA. Advanced glycosylated end products and hyperglycemia in the pathogenesis of diabetic complications. Diabetes Care. 1999; 22:65-71.
- Haveles EB. A-Z Listing of Drugs. In: Delmar's Dental Drug Reference. The Thomson Learning, 2000; 3: 302.
- Porth CM, Gaspard KJ and Matfin G. Diabetes mellitus and the metabolic syndrome. In: Essentials of pathophysiology: diabetes mellitus and metabolic syndrome, 2nd edition, Lippincott Williams & Wilkins Philadelphia, 2007; 32: 699-723.
- Simeonov R. and Simeonova G. Computerized cytomorphometric analysis of nuclear area, nuclear perimeter and mean nuclear diameter in spontaneous canine mammary gland tumours. Veterinary Research Communications. 2007; 31(5): 553-558.
- J. A. Svirsky, Burns J. C. and J. C. Burns, "Comparison of computer-assisted brush biopsy results with follow up scalpel biopsy and histology," General Dentistry. 2002; 50(6): 500–503.
- D. Eisen. "The role of the OralCdx brush test in preventing oral cancer," Dental Assistant. 2009; 78(3): 26–29.
- Z. Delavarian, N. Mohtasham, P. Mosannen-Mozaffari, A. Pakfetrat, M.-T. Shakeri, and R. Ghafoorian-Maddah. Evaluation of the diagnostic value of a modified liquid-based cytology using OralCDx ® brush in early detection of oral potentially malignant lesions and oral cancer. Medicina Oral, Patologia Oraly Cirugia Bucal. 2010; 15(5): 671–676.